Proglacial landscape evolution across Greenland

Michael Lewis Grimes

Submitted in accordance with the requirements for the degree of Doctor of Philosophy

The University of Leeds

Faculty of Earth and Environment

School of Geography

December 2023

Declarations

The candidate confirms that the work submitted is his own. Where work has formed part of jointly-authored publications this has been included and other authors work has been indicated below. The candidate confirms that appropriate credit has been given alongside the thesis where reference has been made to the work of others.

Chapter 3 contains work from a jointly authored manuscript where Michael Grimes is the lead author. Jonathan Carrivick and Mark Smith provided advice and reviewed text, and Jonathan assisted in curating some figures. Alexis Comber provided his scripts for running the geographically distributed accuracy assessment and helped in producing some figures and descriptive text. The work in Chapter 3 is published with Scientific Reports and titled: Land cover changes across Greenland dominated by a doubling of vegetation in three decades.

Chapter 4 also contains work for a jointly authored publication, currently in review with Global and Planetary Change. Michael Grimes is the lead author. Jonathan Carrivick and Mark Smith provided advice and reviewed the text, and Jonathan assisted with some figure formatting. The title of the manuscript is: Spatial heterogeneity, terminus environment effects and acceleration in mass loss of glaciers and ice caps across Greenland.

Acknowledgements

First, I would like to extend immense thanks to my friends and supervisors Jonathan Carrivick and Mark Smith. I was incredibly fortuitous to have two people I respect and get on with so well be my mentors throughout. Their advice and contributions have been invaluable. Our extremely long-awaited fieldwork in Greenland was one of the most incredible experiences of my life. I would also like to thank Duncan Quincey for his advice on all things remote sensing, and Lex Comber for his immensely useful contributions and advice concerning landcover accuracy assessment.

Secondly, I would like to thank my partner Grace, who has supported me through the highs and lows, and sacrificed so much when I was working every weekend and evening on my PhD alongside working full-time for the past year. I would also like to thank all the friends I have made during my time at Leeds studying for my PhD. I must thank my parents for their unwavering support throughout my life, and for motivating and pushing me to achieve things I would never have considered possible. The music of Baths, Choir Boy, Mike Oldfield, and The Smiths has also been a constant bolster during late nights and early mornings in the final year of this work.

I would like to thank Groundsure, my full-time employer, who took me on and supported me with an understanding of the stresses that come with burning the candle at both ends.

Finally, I would like to thank the NERC for funding this PhD (Grant: NE/L002574/1), permitting me to undertake this research and INTERACT (agreement number 871120) for funding the fieldwork we finally undertook after the Covid Restrictions were lifted.

Abstract

Recent decades have witnessed profound environmental and landscape transformations across Greenland, largely attributable to ongoing anthropogenic climate change. Despite frequent references to these shifts in literature, the underpinnings and manifestations of such changes at a nationwide scale remain inadequately explored in academic discourse. Greenland, a critical component of global climate dynamics, presents a unique opportunity to explore and understand these rapid shifts in an environment sensitive to even the subtlest climatic perturbations.

This thesis provides a comprehensive investigation into Greenland's changing landscapes through three focused research chapters. The first chapter presents a long-term assessment of landcover changes, revealing a significant proliferation of vegetation indicative of Arctic Greening and permits a detailed assessment of the geomorphic and ecological processes driving the wider observed changes. The second chapter delves into the mass balance changes of Greenland’s peripheral glaciers and ice caps, documenting substantial ice loss and regional variations over several decades, contextualised further by considering terminus, behaviour and surface characteristics. The third chapter offers the first Greenland-wide analysis of sediment connectivity, identifying the impact of lakes on connectivity to coastlines by assessing and comparing structural and functional connectivity measures through the production of new hydrological and connectivity data.

The findings of this thesis are significant in their breadth and depth, providing a nuanced understanding of Greenland's environmental changes. The long-term assessments of landcover and glacier mass balance changes, coupled with the pioneering analysis of sediment connectivity collectively offer a detailed, multifaceted view of Greenland's transformation, underscoring the importance of such comprehensive studies in understanding and responding to Arctic climate change. A synthesised analysis of these three facets of environmental change provides a baseline assessment upon which future research into climate change in Greenland can be built.

Table of Contents

List of Figures

List of Tables

List of Abbreviations

PGIC -Peripheral Ice Caps and Glaciers

GEE – Google Earth Engine

DEM – Digital Elevation Model

LGM – Last Glacial Maximum

LIG – Last Interglacial

LIA – Little Ice Age

BP – Before present (Present: 1 January 1950)

HTM – Holocene Thermal Maximum

GrIS – Greenland Ice Sheet

ELA – Equilibrium Line Altitude

YD – Younger Dryas

NOA – North Atlantic Oscillation

AMO – Atlantic Multi-decadal Oscillation

GBI – Greenland Blocking Index

SLR –Sea Level Rise

SAR – Synthetic Aperture Radar

SLE – Sea Level Equivalent

EGC – East Greenland Current

IC – Index of Connectivity

SDR – Sediment Delivery Ratio

DACP – Dark Ages Cold Period

DOC – Dissolved Organic Carbon

POC – Particulate Organic Carbon

POM – Particulate Organic Matter

Introduction

1.1 Research Background: Unveiling the Multifaceted Dynamics of Recent Changes in Greenland's Proglacial Landscapes

The current trajectory of global climate change, marked by a noticeable upsurge in global temperatures, sea-level rise, and extreme weather events, has brought unprecedented attention to polar regions, including Greenland (Oerlemans, 1994; Holland and Bitz, 2003; Mernild et al., 2011; Graversen et al., 2011; Pittock, 2012; Masson-Delmotte et al., 2012; IPCC, 2013; Machguth et al., 2013; Bolch et al., 2013; Knight and Harrison, 2014; McMillan et al., 2016; Noël et al., 2017; Overland et al., 2019; Carrivick et al., 2019; Bollen et al., 2023). This research highlights a consistent global trend of glacier retreat (Oerlemans, 1994; Hugonnet et al., 2021), with pronounced warming and ice loss in the Arctic (Holland and Bitz, 2003; Mernild et al., 2011; Carrivick et al., 2019). Studies indicate that warming is amplified in polar regions (Holland and Bitz, 2003), significantly impacting glacier mass balance (Machguth et al., 2013; Bolch et al., 2013) and contributing to sea-level rise (Pittock, 2012). Specific findings for Greenland reveal substantial ice loss, driven by temperature increases and altered precipitation patterns (Mernild et al., 2011; Carrivick et al., 2019). Predictions suggest continued mass loss and significant future sea-level rise (Pittock, 2012; Masson-Delmotte et al., 2012), with Greenland's glaciers playing a major role (Machguth et al., 2013; Bolch et al., 2013). Recent observations confirm an accelerated ice loss (McMillan et al., 2016; Bollen et al., 2023), underscoring the broader ecological and hydrological implications for the Arctic (Knight and Harrison, 2014; Overland et al., 2019) and the urgency of addressing climate change impacts.

Greenland, while globally renowned for its expansive ice sheet, is also distinguished by its rich and varied proglacial landscape (Abermann et al., 2017; Bendixen et al., 2017; Bhatia et al., 2013; Bjørk et al., 2018a; Carrivick et al., 2022; Christiansen & Humlum, 2013; Daniels et al., 2011; Daniels & de Molenaar, 2011; Docherty et al., 2018; Hasholt et al., 2008; Hollesen et al., 2011; Jørgensen et al., 2015; Jungsberg et al., 2022; Ó Cofaigh et al., 2003; Rasmussen et al., 2018; Rennermalm et al., 2012; Westergaard-Nielsen et al., 2018). Though the climate discussions tend to focus on the ice sheet, it is increasingly apparent that a comprehensive understanding of the

proglacial landscape is crucial for grasping the full narrative of environmental transformations across Greenland.

Greenland's proglacial landscape is multifaceted, characterised by peripheral glaciers and ice caps (PGICs) distinct from the main Greenland Ice Sheet (GrIS), intertwined with a complex network of meltwater rivers and expansive gravel braidplains (Bjørk et al., 2018b; Carrivick et al., 2023; Docherty et al., 2018; Overeem et al., 2017). This variegated terrain is further punctuated by lakes and swathes of vegetation, including tundra and wetland species, set against a backdrop of barren ground constituted by unconsolidated sediment, bedrock, regolith, and other geological features (Carrivick et al., 2022; Carrivick & Tweed, 2013; Christiansen et al., 2015; Jørgensen et al., 2015; Westergaard-Nielsen et al., 2018). Notably, interspersed amidst this predominantly natural landscape are sporadic human communities, exemplifying the endurance of civilisation in such austere environments (Hamilton et al., 2000; Laidre et al., 2015; Nuttall, 2016). This marginal zone, with its unique environmental and geomorphological attributes, is pivotal in discerning the broader impacts and feedbacks of climate change. Throughout this thesis, the term proglacial is employed to delineate the diverse terrains of Greenland that exist independent of the main ice sheet.

The landscapes encompassing Greenland's proglacial areas are characterised by intricate geomorphology, both in structure/composition/character and in functional land surface dynamics. The proglacial land surfaces here serve as crucial reference points for understanding past and present climatic conditions. These landscapes, tapestries of bedrock, soils, and vegetation, hold invaluable records of environmental shifts, dating from ancient geologic epochs to the current rapid climatic transitions (Carrivick et al., 2013; Hasholt et al., 2008). Furthermore, the proglacial landscapes of Greenland house numerous peripheral glaciers and ice caps (PGIC), and proglacial catchments (Bjørk et al., 2018b). These features, although smaller in comparison to the primary ice sheet, harbour substantial significance and are more vulnerable to rapid onset climate change (Bevis et al., 2019). The meltwater from these ice caps and glaciers feeds into the global ocean system, affecting sea level rise and ocean circulation patterns via processes such as dilution and cooling (Machguth et al., 2013; Meier et al., 2007).

Proglacial catchments, with their complex hydrological networks, can influence sediment transport and nutrient cycling, which have wider implications for both local and global ecosystems. Since the 1970s and 80s, Greenland's proglacial landscape has been undergoing widespread rapid changes. These alterations, stemming from a combination of climatic and anthropogenic factors, influence regional biodiversity, albedo dynamics, and greenhouse gas fluxes (Hamilton et al., 2000; Masson-Delmotte et al., 2012; Nuttall, 2020). Such changes can instigate feedback loops, where modifications in one component of the system can inadvertently exacerbate other climatic effects (Taylor et al., 2013). However, despite the paramount importance of these areas, there remains a glaring disparity in the quantum of research focused on Greenland's ice-free periphery compared to the central ice sheet. Such a research gap not only hampers a holistic understanding of the region but also omits capturing the subtle yet vital climatic signals and feedbacks that resonate from and within the periphery. In essence, the merits of intensively studying Greenland's proglacial landscapes are manifold. By delving into the complexities of this region, we stand to gain nuanced insights into climate change repercussions, both at a regional and global scale. It is imperative that the academic and research community continues to broaden its lens, acknowledging the full spectrum of environmental changes and their multifaceted interconnections in the context of a warming Greenland.

In the forthcoming chapters, this thesis will endeavour to shed light on the environmental transitions around Greenland's proglacial zone, elucidating its significance in the grand narrative of global environmental change. This thesis presents research conducted at a national scale for all of Greenland, whilst ensuring quality by utilising relatively fine-resolution data; a notable advancement from many previous works which have typically been constrained to coarser resolution analysis (e.g. Hugonnet et al., 2021; Li et al., 2022; Raynolds et al., 2019). By assessing Greenland’s proglacial environment consistently at a national scale, one facilitates a streamlined regional comparison. Singular, smaller-scale studies, whilst valuable, often diverge in methodological approaches, yielding disparate results that may be challenging to reconcile. A standardised, large-scale study helps weave fragmented findings into a coherent tapestry, thus amplifying the efficacy and applicability of the

research and providing a benchmark against which detailed localised studies might be compared.

A salient feature of climate change in Greenland is 'Arctic Amplification'. This phenomenon, characterised by heightened warming rates in the Arctic compared to the global average, is driven by feedback loops such as diminishing ice cover, which reduces the albedo effect, thereby amplifying warming (Pithan & Mauritsen, 2014; Serreze & Barry, 2011). Greenland stands as a prominent example of this accelerated change, making it an indispensable location for climate change research. However, these dramatic environmental shifts are not isolated to physical processes alone. Greenland's indigenous population faces a tumult of socio-economic implications as a result. As landscapes transform, traditional ways of life, including hunting and fishing, are jeopardised (Nuttall, 2016). Conversely, as the melting uncovers previously inaccessible mineral-rich terrains there is an ongoing and potential future increase in external interest in resource extraction (Christiansen, 2022). This, while potentially economically beneficial, poses questions on land rights, environmental sustainability, and socio-cultural disruptions. Greenland's proglacial landscapes therefore offer vital clues on several climate feedback mechanisms. For instance:

- **Landcover Change**: The dynamic interplay of landcover components in Greenland, from shifting vegetation patterns to the expansion of barren ground resulting from ice retreat, plays a pivotal role in climate feedback mechanisms. Specifically, alterations in vegetation types, ranging from shrubs to mosses, have direct implications on the surface albedo, the measure of the surface's reflectivity (Loranty et al., 2011). Notably, the establishment and expansion of vegetation have the potential to expedite permafrost melt, releasing trapped gases and further contributing to greenhouse gas concentrations (Heijmans et al., 2022). Wetlands, with their intrinsic capacity to sequester and release methane, also emerge as significant entities in these feedback loops (Jørgensen et al., 2015). Moreover, as barren grounds increase due to ice retreat, the exposed darker surfaces can absorb more solar radiation, thereby amplifying localised warming effects. Collectively, these alterations either amplify or mitigate local warming, instigating intricate and often self-perpetuating feedback loops with profound implications for the broader climatic system.

- **Peripheral Glaciers and Ice Caps (PGIC) Change**: The rapid transformations of these smaller ice bodies have multifaceted implications for the climate system, both regionally and globally. Foremost, their shrinking mass contributes directly to sea level rise, with immediate consequences for coastal ecosystems and human settlements. Altered albedo due to these changes also comes to the fore (Petzold & Rencz, 1975); as glaciers recede, the exposed darker surfaces not only absorb more solar radiation but their surfaces also potentially play host to features like cryoconite, darkening glacier surfaces and expediting melt (Takeuchi et al., 2018). Drawing parallels from studies such as Zhang et al. (2021) in the Himalayas, it can be postulated that cryoconite, along with subglacial sediments, can expedite the export of greenhouse gases during the melting season, with strong positive methane and CO_2 fluxes. However, on the antipode, there is evidence suggesting that proglacial rivers and streams might act as a sink for atmospheric CO_2, offering a modicum of counterbalance. However, Lamarche-Gagnon et al. (2019) reported a considerable methane flux of 14.49 mmol m^{-2} d^{-1} from the Leverett Glacier proglacial river in Greenland. Additionally, the influx of freshwater into oceans from melting PGICs alters ocean salinity (Bartholomaus et al., 2016), which in turn has cascading effects on global ocean circulation patterns, potentially influencing broader climatic systems and weather patterns (Bönisch et al., 1997; Dukhovskoy et al., 2006; Rudels, 1995; Slater et al., 2020). This interconnected web of reactions and feedbacks, driven in part by changes in PGICs, underscores their pivotal role in the complex jigsaw of climate feedback mechanisms.
- **Sediment connectivity and budgets**: As Greenland undergoes pronounced environmental shifts, the interplay between increased meltwater flow and evolving landcover assumes heightened significance in the realm of sediment transportation (Bendixen et al., 2017; Overeem et al., 2017). At a local scale, these alterations have direct repercussions on ecosystems (Estrany et al., 2019; Kemper et al., 2022). Variations in sediment delivery can impact river morphology, aquatic habitats, and the structure of coastal zones (Anthony & Aagaard, 2020; Baartman et al., 2013; Obolewski et al., 2018; Pearson et al., 2020; Tan et al., 2021). More broadly, in a greening Greenland, the dynamic flux of river-entrained sediments carries with it organic matter and nutrients

(Docherty et al., 2018; Hawkings et al., 2015; Rysgaard et al., 1998). Increased nutrient delivery to marine ecosystems, such as the Arctic Ocean, can stimulate primary productivity, potentially leading to phenomena like algal blooms (Burpee et al., 2018; Meire, Meire, et al., 2016; Meire, Mortensen, et al., 2016; Rysgaard et al., 1999). While these blooms might offer short-term carbon sequestration benefits, they can also create hypoxic conditions detrimental to marine life (Rysgaard et al., 1999). Conversely, diminished sediment and nutrient delivery could compromise the marine food web, starting from the foundational phytoplankton levels. On a global scale, these changes in sediment transportation can influence carbon sequestration processes. For instance, marine sediments play a crucial role in the long-term burial of organic carbon, thereby acting as a significant sink in the global carbon cycle (Faust & Knies, 2019; Ingall & Cappellen, 1990; Sørensen et al., 2015). As sediment dynamics shift, so does the efficiency and capacity of these marine carbon sinks, potentially affecting atmospheric CO_2 concentrations and, by extension, global climate patterns (Fung et al., 2005; Heinze et al., 2015; Riebesell, Körtzinger, et al., 2009; Riebesell, Rtzinger, et al., 2009). In essence, the nuanced changes in sediment routing and connectivity in Arctic landscapes serve as both a barometer and driver of environmental change, linking local transformations to global climate feedback loops.

Therefore, to advance our understanding of climate change dynamics, a thorough examination of Greenland's entire proglacial landscape becomes indispensable. In Greenland, glaciers stand as the primary origin for the meltwater that nurtures an extensive network of proglacial rivers and streams. These freshwater systems are pivotal in transporting vital nutrients, many of which are glacier-derived. Concurrently, transformations within these proglacial ‘buffer zones’ separating the ice from the ocean, significantly modulate sediment transportation both to and within these meltwater conduits. This thesis embarks on a comprehensive endeavour to weave together the intricate narratives of landcover alterations, glacier melt dynamics, and overarching sediment connectivity. Such a synthesis is crucial for a holistic understanding of Greenland's landscape evolution. Furthermore, it is important to underscore that sediments and nutrients emanating from glaciers,

coupled with increased organic carbon from landcover transitions and changes in connectivity, can profoundly influence both terrestrial and aquatic biota. The implications of these shifts resonate not only within aquatic ecosystems but also cascade through coastal water systems, reverberating with profound consequences for local indigenous Greenlandic communities, who maintain a deeply rooted reliance upon their natural surroundings. Addressing this research gap is pivotal not only for elucidating the overarching trajectories of global environmental change but also for comprehending the consequent socio-ecological ramifications. The ensuing chapters of this thesis go some way towards addressing this imperative task, aiming to furnish a detailed and integrative analysis of Greenland's transitioning environment over the past forty years. Environmental change over this period is investigated through three primary lenses: landcover change, peripheral glacier and ice cap (PGIC) mass balance, and sediment connectivity.

1.2 Research Aim and Objectives

This thesis defines an overall aim, as well as objectives that by achieving each should realise the thesis aim.

Aim: To comprehensively analyse proglacial landscape evolution across Greenland over the past four decades, with specific emphasis on landcover alterations, glacier mass balance, and sediment connectivity.

Objectives:

1. Quantitative Analysis of Landcover Evolution:
    - To quantify changes in major landcover categories, specifically ice, water, barren ground (encompassing bedrock and sediments), and vegetation, spanning from the late 1980s to the late 2010s.
    - To explain the spatio-temporal pattern of landcover changes with respect to climatic warming.
2. Assessment of Peripheral Glacier Mass Balance:
    - To quantify changes in peripheral glaciers and ice caps (PGIC) mass balance on a national scale.
    - To assess the impact of glacier’s terminus, behaviour, and surface character on mass balance rates.

- To relate these newfound insights to previously conducted studies that were temporally and spatially limited, ensuring contextual coherence and expanded understanding.

3. National-Scale Analysis of Greenland Sediment Connectivity:
    - To establish a structural and functional sediment connectivity framework for Greenland. This will involve the generation of hydrological data at an unparalleled spatial resolution.
    - To evaluate sediment budgets within these watersheds, inferred from surface elevation changes
    - To determine the extent to which a structural metric of connectivity can predict a measured functional metric.
4. Synthesis and Implications:
    - To integrate the findings from the preceding objectives to draw conclusive insights on the proglacial landscape evolution around Greenland. Moreover, to interpret and discuss the implications of these findings for broader climatic, environmental, and socio-economic issues.

The outlined objectives are formulated to ensure that the research systematically unravels the multifaceted dynamics of Greenland's transforming periphery. Through this structured approach, the research aims to augment the existing academic corpus on Arctic landscape evolution and its wider global significance.

1.3 Overview of the Thesis Structure

The structure of this thesis is designed to provide a comprehensive understanding of Greenland's recent environmental change. After this introduction, the thesis unfolds over six distinct chapters. Chapter 2 offers a detailed exploration of Greenland's environmental change within the wider context of the Arctic, positioning the current shifts within a broader long-term and broader scientific context. This lays the groundwork for the empirical investigations in subsequent chapters. Due to the lack of an overarching methodological theme and format of each research chapter, being written initially for publication and encapsulating specific detailed overviews of the methods employed, this thesis forgoes an initial methods chapter. Chapters 3 through 5 present original research works. Chapters 3 and 4 are adapted from their

preliminary formatting as short-format research articles, which are currently in different stages of the publication process as outlined in the earlier declaration section of this thesis. As a result of their origins as individual research papers, these chapters are designed to be comprehensive in their own right, minimising the repetition of broader concepts reviewed in Chapter 2. Chapter 6 integrates the findings from the preceding chapters. It synthesises the theories, methods, and results from the earlier chapters, offering a coherent interpretation of the research before making concluding remarks, and summarising the overall contributions of the thesis.

1.4 Chapter 1 References

Abermann, J., Hansen, B., Lund, M., Wacker, S., Karami, M., & Cappelen, J. (2017). Hotspots and key periods of Greenland climate change during the past six decades. *Ambio*, *46*. https://doi.org/10.1007/s13280-016-0861-y

Anthony, E. J., & Aagaard, T. (2020). The lower shoreface: Morphodynamics and sediment connectivity with the upper shoreface and beach. In *Earth-Science Reviews* (Vol. 210). https://doi.org/10.1016/j.earscirev.2020.103334

Baartman, J. E. M., Masselink, R., Keesstra, S. D., & Temme, A. J. A. M. (2013). Linking landscape morphological complexity and sediment connectivity. *Earth Surface Processes and Landforms*, *38*(12). https://doi.org/10.1002/esp.3434

Bartholomaus, T. C., Stearns, L. A., Sutherland, D. A., Shroyer, E. L., Nash, J. D., Walker, R. T., Catania, G., Felikson, D., Carroll, D., Fried, M. J., Noël, B. P. Y., & Van Den Broeke, M. R. (2016). Contrasts in the response of adjacent fjords and glaciers to ice-sheet surface melt in West Greenland. *Annals of Glaciology*, *57*(73). https://doi.org/10.1017/aog.2016.19

Bendixen, M., Lonsmann Iversen, L., Anker Bjork, A., Elberling, B., Westergaard-Nielsen, A., Overeem, I., Barnhart, K. R., Abbas Khan, S., Box, J. E., Abermann, J., Langley, K., & Kroon, A. (2017). Delta progradation in Greenland driven by increasing glacial mass loss. *Nature*, *550*(7674), 101–104. https://doi.org/10.1038/nature23873

Bevis, M., Harig, C., Khan, S. A., Brown, A., Simons, F. J., Willis, M., Fettweis, X., Van Den Broeke, M. R., Madsen, F. B., Kendrick, E., Caccamise, D. J., Van Dam, T., Knudsen, P., & Nylen, T. (2019). Accelerating changes in ice mass within Greenland, and the ice sheet's sensitivity to atmospheric forcing. *Proceedings of the National Academy of Sciences of the United States of America*, *116*(6). https://doi.org/10.1073/pnas.1806562116

Bhatia, M.P., Kujawinski, E.B., Das, S.B., Breier, C.F., Henderson, P.B. and Charette, M.A., 2013. Greenland meltwater as a significant and potentially bioavailable source of iron to the ocean. *Nature Geoscience*, 6(4), pp.274-278.

Bjørk, A. A., Aagaard, S., Lütt, A., Khan, S. A., Box, J. E., Kjeldsen, K. K., Larsen, N. K., Korsgaard, N. J., Cappelen, J., Colgan, W. T., Machguth, H., Andresen, C. S., Peings, Y., & Kjær, K. H. (2018a). Changes in Greenland's peripheral

glaciers linked to the North Atlantic Oscillation. *Nature Climate Change*, *8*(1), 48–52. https://doi.org/10.1038/s41558-017-0029-1

Bolch, T., Sorensen, L. S., Simonsen, S. B., Molg, N., Machguth, H., Rastner, P., & Paul, F. (2013). Mass loss of Greenland's glaciers and ice caps 2003-2008 revealed from ICESat laser altimetry data. *Geophysical Research Letters*, *40*(5), 875–881. https://doi.org/10.1002/grl.50270

Bollen, K. E., Enderlin, E. M., & Muhlheim, R. (2023). Dynamic mass loss from Greenland's marine-terminating peripheral glaciers (1985–2018). *Journal of Glaciology*, *69*(273), 153–163.

Bönisch, G., Blindheim, J., Bullister, J. L., Schlosser, P., & Wallace, D. W. R. (1997). Long-term trends of temperature, salinity, density, and transient tracers in the central Greenland Sea. *Journal of Geophysical Research: Oceans*, *102*(C8). https://doi.org/10.1029/97JC00740

Burpee, B. T., Anderson, D., & Saros, J. E. (2018). Assessing ecological effects of glacial meltwater on lakes fed by the Greenland Ice Sheet: The role of nutrient subsidies and turbidity. *Arctic, Antarctic, and Alpine Research*, *50*(1). https://doi.org/10.1080/15230430.2017.1420953

Carrivick, J. L., Boston, C. M., King, O., James, W. H. M., Quincey, D. J., Smith, M. W., Grimes, M., & Evans, J. (2019). Accelerated Volume Loss in Glacier Ablation Zones of NE Greenland, Little Ice Age to Present. *Geophysical Research Letters*. https://doi.org/10.1029/2018gl081383

Carrivick, J. L., Boston, C. M., Sutherland, J. L., Pearce, D., Armstrong, H., Bjørk, A., Kjeldsen, K. K., Abermann, J., Oien, R. P., & Grimes, M. (2023). Mass loss of glaciers and ice caps across Greenland since the Little Ice Age. *Geophysical Research Letters*, *50*(10), e2023GL103950.

Carrivick, J. L., Geilhausen, M., Warburton, J., Dickson, N. E., Carver, S. J., Evans, A. J., & Brown, L. E. (2013). Contemporary geomorphological activity throughout the proglacial area of an alpine catchment. *Geomorphology*, *188*, 83–95. https://doi.org/10.1016/j.geomorph.2012.03.029

Carrivick, J. L., How, P., Lea, J. M., Sutherland, J. L., Grimes, M., Tweed, F. S., Cornford, S., Quincey, D. J., & Mallalieu, J. (2022). Ice-marginal proglacial lakes across Greenland: Present status and a possible future. *Geophysical Research Letters*, *49*(12), e2022GL099276.

Carrivick, J. L., & Tweed, F. S. (2013). Proglacial lakes: character, behaviour and geological importance. *Quaternary Science Reviews*, *78*, 34–52. https://doi.org/10.1016/j.quascirev.2013.07.028

Christiansen, F. G. (2022). Greenland mineral exploration history. *Mineral Economics*. https://doi.org/10.1007/s13563-022-00350-2

Christiansen, H. H., & Humlum, O. (2013). Glacial History and Periglacial Landforms of the Zackenberg area, Northeast Greenland: Preliminary results. *Geografisk Tidsskrift-Danish Journal of Geography*, *93*(1), 19–29. https://doi.org/10.1080/00167223.1993.10649332

Christiansen, J. R., Romero, A. J. B., Jørgensen, N. O. G., Glaring, M. A., Jørgensen, C. J., Berg, L. K., & Elberling, B. (2015). Methane fluxes and the functional

groups of methanotrophs and methanogens in a young Arctic landscape on Disko Island, West Greenland. *Biogeochemistry*, *122*(1). https://doi.org/10.1007/s10533-014-0026-7

Daniels, F. J. A., & de Molenaar, J. G. (2011). Flora and Vegetation of Tasiilaq, Formerly Angmagssalik, Southeast Greenland: A Comparison of Data Between Around 1900 and 2007. *Ambio*, *40*(6), 650–659. https://doi.org/10.1007/s13280-011-0171-3

Docherty, C. L., Riis, T., Hannah, D. M., Rosenhøj Leth, S., & Milner, A. M. (2018). Nutrient uptake controls and limitation dynamics in north-east Greenland streams. *Polar Research*, *37*(1). https://doi.org/10.1080/17518369.2018.1440107

Dukhovskoy, D., Johnson, M., & Proshutinsky, A. (2006). Arctic decadal variability from an idealized atmosphere-ice-ocean model: 2. Simulation of decadal oscillations. *Journal of Geophysical Research: Oceans*, *111*(6). https://doi.org/10.1029/2004JC002820

Estrany, J., Ruiz, M., Calsamiglia, A., Carriquí, M., García-Comendador, J., Nadal, M., Fortesa, J., López-Tarazón, J. A., Medrano, H., & Gago, J. (2019). Sediment connectivity linked to vegetation using UAVs: High-resolution imagery for ecosystem management. *Science of the Total Environment*, *671*. https://doi.org/10.1016/j.scitotenv.2019.03.399

Faust, J. C., & Knies, J. (2019). Organic Matter Sources in North Atlantic Fjord Sediments. *Geochemistry, Geophysics, Geosystems*, *20*(6). https://doi.org/10.1029/2019GC008382

Fung, I. Y., Doney, S. C., Lindsay, K., & John, J. (2005). Evolution of carbon sinks in a changing climate. *Proceedings of the National Academy of Sciences of the United States of America*, *102*(32). https://doi.org/10.1073/pnas.0504949102

Graversen, R. G., Drijfhout, S., Hazeleger, W., van de Wal, R., Bintanja, R., & Helsen, M. (2011). Greenland's contribution to global sea-level rise by the end of the 21st century. *Climate Dynamics*, *37*(7), 1427–1442. https://doi.org/10.1007/s00382-010-0918-8

Hamilton, L., Lyster, P., & Otterstad, O. (2000). Social change, ecology and climate in 20th-century Greenland. *Climatic Change*, *47*(1–2). https://doi.org/10.1023/a:1005607426021

Hasholt, B., Krüger, J., & Skjernaa, L. (2008). Landscape and sediment processes in a proglacial valley, the Mittivakkat Glacier area, Southeast Greenland. *Geografisk Tidsskrift-Danish Journal of Geography*, *108*(1), 97–110. https://doi.org/10.1080/00167223.2008.10649576

Hawkings, J. R., Wadham, J. L., Tranter, M., Lawson, E., Sole, A., Cowton, T., Tedstone, A. J., Bartholomew, I., Nienow, P., Chandler, D., & Telling, J. (2015). The effect of warming climate on nutrient and solute export from the Greenland Ice Sheet. *Geochemical Perspectives Letters*, *1*(1), 94–104. https://doi.org/10.7185/geochemlet.1510

Heijmans, M. M. P. D., Magnússon, R., Lara, M. J., Frost, G. V., Myers-Smith, I. H., van Huissteden, J., Jorgenson, M. T., Fedorov, A. N., Epstein, H. E., Lawrence,

D. M., & Limpens, J. (2022). Tundra vegetation change and impacts on permafrost. In *Nature Reviews Earth and Environment* (Vol. 3, Issue 1). https://doi.org/10.1038/s43017-021-00233-0

Heinze, C., Meyer, S., Goris, N., Anderson, L., Steinfeldt, R., Chang, N., Le Quéré, C., & Bakker, D. C. E. (2015). The ocean carbon sink - Impacts, vulnerabilities and challenges. In *Earth System Dynamics* (Vol. 6, Issue 1). https://doi.org/10.5194/esd-6-327-2015

Holland, M. M., & Bitz, C. M. (2003). Polar amplification of climate change in coupled models. *Climate Dynamics*, *21*(3–4), 221–232. https://doi.org/10.1007/s00382-003-0332-6

Hollesen, J., Elberling, B., & Jansson, P. E. (2011). Future active layer dynamics and carbon dioxide production from thawing permafrost layers in Northeast Greenland. *Global Change Biology*, *17*(2), 911–926. https://doi.org/10.1111/j.1365-2486.2010.02256.x

Hugonnet, R., McNabb, R., Berthier, E., Menounos, B., Nuth, C., Girod, L., Farinotti, D., Huss, M., Dussaillant, I., Brun, F., & Kääb, A. (2021). Accelerated global glacier mass loss in the early twenty-first century. *Nature*, *592*(7856). https://doi.org/10.1038/s41586-021-03436-z

Ingall, E. D., & Cappellen, P. Van. (1990). Relation between sedimentation rate and burial of organic phosphorus and organic carbon in marine sediments. *Geochimica et Cosmochimica Acta*, *54*(2). https://doi.org/10.1016/0016-7037(90)90326-G

IPCC. (2013). *Climate Change 2013: The Physical Science Basis. Contribution of Working Group I to the Fifth Assessment Report of the Intergovernmental Panel on Climate Change* (T. F. Stocker, D. Qin, G.-K. Plattner, M. Tignor, S. K. Allen, J. Boschung, A. Nauels, Y. Xia, V. Bex, & P. M. Midgley, Eds.). Cambridge University Press. https://doi.org/10.1017/CBO9781107415324

Jørgensen, C. J., Johansen, K. M. L., Westergaard-Nielsen, A., & Elberling, B. %J N. G. (2015). *Net regional methane sink in High Arctic soils of northeast Greenland*. *8*(1), 20–23.

Jungsberg, L., Herslund, L. B., Nilsson, K., Wang, S., Tomaškovičová, S., Madsen, K., Scheer, J., & Ingeman-Nielsen, T. (2022). Adaptive capacity to manage permafrost degradation in Northwest Greenland. *Polar Geography*, *45*(1). https://doi.org/10.1080/1088937X.2021.1995067

Kemper, J. T., Thaxton, R. D., Rathburn, S. L., Friedman, J. M., Mueller, E. R., & Scott, M. L. (2022). Sediment-ecological connectivity in a large river network. *Earth Surface Processes and Landforms*, *47*(2). https://doi.org/10.1002/esp.5277

Knight, J., & Harrison, S. (2014). Mountain Glacial and Paraglacial Environments under Global Climate Change: Lessons from the Past, Future Directions and Policy Implications. *Geografiska Annaler Series A-Physical Geography*, *96*(3), 245–264. https://doi.org/10.1111/geoa.12051

Laidre, K. L., Stern, H., Kovacs, K. M., Lowry, L., Moore, S. E., Regehr, E. V., Ferguson, S. H., Wiig, Ø., Boveng, P., Angliss, R. P., Born, E. W., Litovka, D.,

Quakenbush, L., Lydersen, C., Vongraven, D., & Ugarte, F. (2015). Arctic marine mammal population status, sea ice habitat loss, and conservation recommendations for the 21st century. *Conservation Biology*, *29*(3), 724–737. https://doi.org/10.1111/COBI.12474

Lamarche-Gagnon, G., Wadham, J. L., Sherwood Lollar, B., Arndt, S., Fietzek, P., Beaton, A. D., Tedstone, A. J., Telling, J., Bagshaw, E. A., Hawkings, J. R., Kohler, T. J., Zarsky, J. D., Mowlem, M. C., Anesio, A. M., & Stibal, M. (2019). Greenland melt drives continuous export of methane from the ice-sheet bed. *Nature*, *565*(7737). https://doi.org/10.1038/s41586-018-0800-0

Li, Z., Chao, B. F., Zhang, Z., Jiang, L., & Wang, H. (2022). Greenland Interannual Ice Mass Variations Detected by GRACE Time-Variable Gravity. *Geophysical Research Letters*, *49*(19). https://doi.org/10.1029/2022GL100551

Loranty, M. M., Goetz, S. J., & Beck, P. S. A. (2011). Tundra vegetation effects on pan-Arctic albedo. *Environmental Research Letters*, *6*(2). https://doi.org/10.1088/1748-9326/6/2/029601

Machguth, H., Rastner, P., Bolch, T., Mölg, N., Sørensen, L. S., Aðalgeirsdottir, G., van Angelen, J. H., van den Broeke, M. R., & Fettweis, X. (2013). The future sea-level rise contribution of Greenland's glaciers and ice caps. *Environmental Research Letters*, *8*(2). https://doi.org/10.1088/1748-9326/8/2/025005

Masson-Delmotte, V., Swingedouw, D., Landais, A., Seidenkrantz, M. S., Gauthier, E., Bichet, V., Massa, C., Perren, B., Jomelli, V., Adalgeirsdottir, G., Hesselbjerg Christensen, J., Arneborg, J., Bhatt, U., Walker, D. A., Elberling, B., Gillet-Chaulet, F., Ritz, C., Gallée, H., van den Broeke, M., … Vinther, B. (2012). Greenland climate change: From the past to the future. *Wiley Interdisciplinary Reviews: Climate Change*, *3*(5), 427–449. https://doi.org/10.1002/WCC.186

McMillan, M., Leeson, A., Shepherd, A., Briggs, K., Armitage, T. W. K., Hogg, A., Kuipers Munneke, P., Van Den Broeke, M., Noël, B., & van de Berg, W. J. (2016). A high-resolution record of Greenland mass balance. *Geophysical Research Letters*, *43*(13), 7002–7010.

Meier, M. F., Dyurgerov, M. B., Rick, U. K., O'Neel, S., Pfeffer, W. T., Anderson, R. S., Anderson, S. P., & Glazovsky, A. F. (2007). Glaciers dominate Eustatic sea-level rise in the 21st century. *Science*, *317*(5841), 1064–1067. https://doi.org/10.1126/science.1143906

Meire, L., Meire, P., Struyf, E., Krawczyk, D. W., Arendt, K. E., Yde, J. C., Pedersen, T. J., Hopwood, M. J., Rysgaard, S., & Meysman, F. J. R. (2016). High export of dissolved silica from the Greenland Ice Sheet. *Geophysical Research Letters*, *43*(17), 9173–9182. https://doi.org/10.1002/2016gl070191

Meire, L., Mortensen, J., Rysgaard, S., Bendtsen, J., Boone, W., Meire, P., & Meysman, F. J. R. (2016). Spring bloom dynamics in a subarctic fjord influenced by tidewater outlet glaciers (Godthabsfjord, SW Greenland). *Journal of Geophysical Research-Biogeosciences*, *121*(6), 1581–1592. https://doi.org/10.1002/2015jg003240

Mernild, S. H., Knudsen, N. T., Lipscomb, W. H., Yde, J. C., Malmros, J. K., Hasholt, B., & Jakobsen, B. H. (2011). Increasing mass loss from Greenland's

Mittivakkat Gletscher. *Cryosphere*, *5*(2), 341–348. https://doi.org/10.5194/tc-5-341-2011

Noël, B., Van De Berg, W. J., Lhermitte, S., Wouters, B., Machguth, H., Howat, I., Citterio, M., Moholdt, G., Lenaerts, J. T. M., & Van Den Broeke, M. R. (2017). A tipping point in refreezing accelerates mass loss of Greenland's glaciers and ice caps. *Nature Communications*, *8*. https://doi.org/10.1038/ncomms14730

Nuttall, M. (2016). Living in a world of movement: Human resilience to environmental instability in Greenland. In *Anthropology and Climate Change: From Encounters to Actions*. https://doi.org/10.4324/9781315434773-26

Nuttall, M. (2020). Water, ice, and climate change in northwest Greenland. *Wiley Interdisciplinary Reviews: Water*, *7*(3), e1433. https://doi.org/10.1002/WAT2.1433

Ó Cofaigh, C., Evans, D. J. A., & England, J. (2003). Ice-marginal terrestrial landsystems: sub-polar glacier margins of the Canadian and Greenland High Arctic. *Glacial Landsystems. Arnold, London*, 45–64.

Obolewski, K., Glińska-Lewczuk, K., & Bąkowska, M. (2018). From isolation to connectivity: the effect of floodplain lake restoration on sediments as habitats for macroinvertebrate communities. *Aquatic Sciences*, *80*(1). https://doi.org/10.1007/s00027-017-0556-x

Oerlemans, J. (1994). Quantifying Global Warming from the Retreat of Glaciers. *Science*, *264*(5156), 243–245. https://doi.org/DOI 10.1126/science.264.5156.243

Overeem, I., Hudson, B. D., Syvitski, J. P. M., Mikkelsen, A. B., Hasholt, B., van den Broeke, M. R., Noël, B. P. Y., & Morlighem, M. (2017). Substantial export of suspended sediment to the global oceans from glacial erosion in Greenland. *Nature Geoscience*, *10*(11), 859–863. https://doi.org/10.1038/ngeo3046

Overland, J. E., Wang, M. Y., & Box, J. E. (2019). An integrated index of recent pan-Arctic climate change. *Environmental Research Letters*, *14*(3). https://doi.org/ARTN 035006 10.1088/1748-9326/aaf665

Pearson, S. G., van Prooijen, B. C., Elias, E. P. L., Vitousek, S., & Wang, Z. B. (2020). Sediment Connectivity: A Framework for Analyzing Coastal Sediment Transport Pathways. *Journal of Geophysical Research: Earth Surface*, *125*(10). https://doi.org/10.1029/2020JF005595

Petzold, D. E., & Rencz, A. N. (1975). The Albedo of Selected Subarctic Surfaces. *Arctic and Alpine Research*, *7*(4). https://doi.org/10.2307/1550183

Pithan, F., & Mauritsen, T. (2014). Arctic amplification dominated by temperature feedbacks in contemporary climate models. *Nature Geoscience*, *7*(3), 181–184. https://doi.org/10.1038/ngeo2071

Pittock, A. B. (2012). Ten reasons why climate change may be more severe than projected. In *Sudden and Disruptive Climate Change* (pp. 26–42). Routledge.

Rasmussen, L. H., Zhang, W., Hollesen, J., Cable, S., Christiansen, H. H., Jansson, P. E., & Elberling, B. (2018). Modelling present and future permafrost thermal regimes in Northeast Greenland. *Cold Regions Science and Technology*, *146*. https://doi.org/10.1016/j.coldregions.2017.10.011

Raynolds, M. K., Walker, D. A., Balser, A., Bay, C., Campbell, M., Cherosov, M. M., Daniels, F. J. A., Eidesen, P. B., Emiokhina, K. A., Frost, G. V, Jedrzejek, B., Jorgenson, M. T., Kennedy, B. E., Kholod, S. S., Lavrinenko, I. A., Lavrinenko, O. V, Magnusson, B., Matveyeva, N. V, Metusalemsson, S., … Troeva, E. (2019). A raster version of the Circumpolar Arctic Vegetation Map (CAVM). *Remote Sensing of Environment*, *232*. https://doi.org/UNSP 111297 10.1016/j.rse.2019.111297

Rennermalm, A. K., Smith, L. C., Chu, V. W., Forster, R. R., Box, J. E., & Hagedorn, B. (2012). Proglacial river stage, discharge, and temperature datasets from the Akuliarusiarsuup Kuua River northern tributary, Southwest Greenland, 2008-2011. *Earth System Science Data*, *4*(1), 1–12. https://doi.org/10.5194/essd-4-1-2012

Riebesell, U., Körtzinger, A., & Oschlies, A. (2009). Tipping Elements in Earth Systems Special Feature: Sensitivities of marine carbon fluxes to ocean change. *Proceedings of the National Academy of Sciences of the United States of America*, *106*(49).

Riebesell, U., Rtzinger, A. K., & Oschlies, A. (2009). Sensitivities of marine carbon fluxes to ocean change. In *Proceedings of the National Academy of Sciences of the United States of America* (Vol. 106, Issue 49). https://doi.org/10.1073/pnas.0813291106

Rudels, B. (1995). The thermohaline circulation of the Arctic Ocean and the Greenland Sea. *Philosophical Transactions - Royal Society of London, A*, *352*(1699). https://doi.org/10.1098/rsta.1995.0071

Rysgaard, S., Nielsen, T. G., & Hansen, B. W. (1999). Seasonal variation in nutrients, pelagic primary production and grazing in a high-Arctic coastal marine ecosystem, Young Sound, Northeast Greenland. *Marine Ecology Progress Series*, *179*, 13–25. https://doi.org/DOI 10.3354/meps179013

Rysgaard, S., Thamdrup, B., Risgaard-Petersen, N., Fossing, H., Berg, P., Christensen, P. B., & Dalsgaard, T. (1998). Seasonal carbon and nutrient mineralization in a high-Arctic coastal marine sediment, Young Sound, Northeast Greenland. *Marine Ecology Progress Series*, *175*. https://doi.org/10.3354/meps175261

Serreze, M. C., & Barry, R. G. (2011). Processes and impacts of Arctic amplification: A research synthesis. *Global and Planetary Change*, *77*(1–2), 85–96. https://doi.org/10.1016/j.gloplacha.2011.03.004

Slater, D. A., Felikson, D., Straneo, F., Goelzer, H., Little, C. M., Morlighem, M., Fettweis, X., & Nowicki, S. (2020). Twenty-first century ocean forcing of the Greenland ice sheet for modelling of sea level contribution. In *Cryosphere* (Vol. 14, Issue 3). https://doi.org/10.5194/tc-14-985-2020

Sørensen, H. L., Meire, L., Juul-Pedersen, T., De Stigter, H. C., Meysman, F. J. R., Rysgaard, S., Thamdrup, B., & Glud, R. N. (2015). Seasonal carbon cycling in a Greenlandic fjord: An integrated pelagic and benthic study. *Marine Ecology Progress Series*, *539*. https://doi.org/10.3354/meps11503

Takeuchi, N., Sakaki, R., Uetake, J., Nagatsuka, N., Shimada, R., Niwano, M., & Aoki, T. (2018). Temporal variations of cryoconite holes and cryoconite coverage on the ablation ice surface of Qaanaaq Glacier in northwest Greenland. *Annals of Glaciology*, *59*(77), 21–30.

Tan, Z., Li, Y., Zhang, Q., Liu, X., Song, Y., Xue, C., & Lu, J. (2021). Assessing effective hydrological connectivity for floodplains with a framework integrating habitat suitability and sediment suspension behavior. *Water Research*, *201*. https://doi.org/10.1016/j.watres.2021.117253

Taylor, P. C., Cai, M., Hu, A. X., Meehl, J., Washington, W., & Zhang, G. J. (2013). A Decomposition of Feedback Contributions to Polar Warming Amplification. *Journal of Climate*, *26*(18), 7023–7043. https://doi.org/10.1175/Jcli-D-12-00696.1

Westergaard-Nielsen, A., Karami, M., Hansen, B. U., Westermann, S., & Elberling, B. (2018). Contrasting temperature trends across the ice-free part of Greenland. *Scientific Reports*, *8*(1). https://doi.org/10.1038/s41598-018-19992-w

Chapter 2: Literature Review

2.1 Introduction

In the ever-evolving scientific discourse surrounding the Arctic landscape, Greenland stands as a focal point of multifarious research, owing to its complex environmental interplays, pronounced sensitivity to climatic fluctuations, and the Greenland Ice Sheet (GrIS) which currently accounts for a terrestrial store of 7.42m sea level equivalent (Abermann et al., 2017; Bevis et al., 2019; López-Blanco et al., 2022; Masson-Delmotte et al., 2012; Oerlemans, 1991; Preece et al., 2023; Stranne et al., 2021). Since the 1980s, a period marked by significant and rapid increases in global carbon and greenhouse gas emissions (McConnell et al., 2007; Mieville et al., 2010; Mouillot et al., 2006), Greenland's landscape has undergone transformations that bear implications not only for the Arctic region but also for global ocean, geophysical and climatic systems.

This thesis aims to provide a comprehensive assessment of the environmental changes in Greenland’s ice sheet peripheral proglacial regions during the late 20th and early 21st centuries. These regions have been consistently and historically influenced by the dynamics of the expansive Greenland Ice Sheet (GrIS), which has exhibited variations in its size, both exceeding and falling short of its current extent. The accompanying literature review therefore first gives broad context and background on Greenland's long-term climate, ice sheet, and landscape transformations before assessing the region's more recent environmental shifts. This foundational context is crucial for understanding the current extent, climate, and historical exposure of the proglacial landscapes as presented here. Quaternary climate shifts which mirror those experienced today and into the future may inform a proxy for future landscape changes also witnessed over these Late Pleistocene-Holocene periods. While the research chapters herein were originally written and formatted as short-format research articles for journal publication, they are reproduced here in the format of traditional thesis chapters. Therefore, to minimise repetition, this literature review offers an overarching contextual discussion on the specified themes, whilst each individual chapter introduction provides a more succinct rationale, drawing only on the most pertinent and significant literature.

After defining the history of Greenland's proglacial areas it is important to demark the importance of and processes occurring within these landscapes. To assess the late 20th and early 21st-century landscape evolution this thesis presents a landcover change assessment and thus the second section of this literature review discusses the significance and historical context of proglacial landscapes and landcover classification and change studies, reviewing existing products within the Arctic, underscoring their importance in interpreting ecological and climatic dynamics. The second research chapter of this thesis presents peripheral glacier and ice cap (PGIC) mass balance changes and therefore, following a brief introduction to mass balance modelling, a contextual examination of existing literature assessing changes in PGIC in Greenland is presented. Finally, as the final research chapter of this thesis produces the first Greenland-wide assessment of Sediment Connectivity this review explores the concept of sediment connectivity, its theoretical underpinnings, and practical applications in mountainous and glaciated catchments. A notable gap is identified in the application of sediment connectivity assessments in the Arctic. This comprehensive review thus not only contextualises Greenland's environmental changes within a broader historical and theoretical framework but also reveals the motivation and requirement of the research conducted here.

2.2 Long-term Overview of Greenland's Peripheral Climate and Landscape

This thesis focuses on the recent landscape and climatic changes in Greenland during the late 20th and early 21st centuries. However, it is imperative to contextualise these recent developments within the broader historical framework of Greenland's climatic and landscape evolution. A concise examination of the more-distant past, particularly concerning the deglaciation processes and the subsequent exposure history of the ice-sheet-free periphery under changing climate is an important contemporary analogue. This historical perspective will elucidate the genesis and evolution of the proglacial 'buffer zone' that currently defines the outer limits of Greenland beyond the present margins of the ice sheet. Such an understanding is crucial for comprehending the baseline conditions and transformations that predate the period under investigation in this research.

2.2.1 The Ice Sheet Extent Prior to the Last Glacial Period

During the Last Interglacial (LIG) period, which spanned from approximately 130 to 116 thousand years before present (ka BP), the Earth witnessed significant climatic and sea-level changes (Vasskog et al., 2015). This period, globally corresponding to Marine Isotope Stage (MIS) 5e and known as the Eemian in Europe, was characterised by global temperatures that were approximately 1.5–2.0 °C higher than ~present (Clark & Huybers, 2009) but within the range of projected warming for the 21st century under climate change. The peak warming during this period did not occur simultaneously around the globe, and regional variations in the magnitude of seasonal temperature increases have been observed (Merz et al., 2014). Sea level reconstructions from this period, utilising probabilistic statistical approaches, indicate that global mean sea level was likely more than 6.0 m higher than present, with some studies suggesting a rise as high as 8.0–9.4 m above present levels (Dutton & Lambeck, 2012; Kopp et al., 2009; Lambeck et al., 2012). The contribution of the Greenland Ice Sheet (GrIS) to this sea-level rise during the LIG has been a topic of extensive research and debate. Modelling experiments suggest that the GrIS was between 7% and 60% smaller than its present size, contributing approximately 0.5–5.5 m to the global LIG sea-level rise (SLR) (Born & Nisancioglu, 2012; Cuffey & Marshall, 2000; Fyke et al., 2018; Letréguilly et al., 1991; Lhomme et al., 2005; Oerlemans et al., 2006; Otto-Bliesner et al., 2006; Stone et al., 2013; Tarasov & Peltier, 2003; Yau et al., 2016). These models, while varying in their estimates, underscore the sensitivity of the GrIS to climatic changes and its significant role in contributing to global sea-level fluctuations in the past and so to the future. The last interglacial saw rapid warming and associated melt, providing a potentially useful proxy for present rapid warming under anthropogenic climate change, highlighting the alarming potential retreat of the ice sheet and peripheral glaciers, and associated SLR (Brovkin et al., 2016; Landais et al., 2016). Following the LIG, the onset of the last glacial period marked a shift in the Earth's climate system, leading to the extensive glaciation known as the Last Glacial Maximum (LGM). The transition from the LIG to the LGM involved complex climatic and glacial dynamics, significantly impacting the GrIS and contributing to the shaping of its present form (S. O. Rasmussen et al., 2014; Simpson et al., 2009; Vasskog et al., 2015).

2.2.2 Greenland's Peripheral Environment During and After the Last Glacial Maximum

During the Last Glacial Maximum (LGM), the Greenland Ice Sheet (GrIS) experienced one of its most extensive glaciations (Lecavalier et al., 2014). It merged with the Innuitian ice sheet, and large ice streams discharged ice through the Nares Strait both northwards and southwards, where these ice sheets coalesced (Alley et al., 2010; England, 1999; England et al., 2006; Simon et al., 2014; Zreda et al., 1999). This formation was supported by cold temperatures and the thick sea-ice cover in the Arctic Ocean, leading to a stable cover of thick multiyear sea-ice and the formation of an extensive partly grounded ice shelf over much of the north Greenland shelf and the Lincoln Sea (Larsen et al., 2010; Möller et al., 2010; Simon et al., 2014). The interpretation of the GrIS's extent during the LGM has been revised over time, largely due to the lack of terrestrial evidence, with moraine and geomorphological evidence largely existing offshore (Arndt et al., 2015; Rignot et al., 2016; Schaffer et al., 2016; Slabon et al., 2016). The LGM extent in north east Greenland remains somewhat uncertain, with existing studies suggesting a range of maximum and minimum scenarios with an uncertainty of approximately 100 km (Evans et al., 2009; Larsen et al., 2022; Winkelmann et al., 2010). In west Greenland numerous weathering limits or 'trimlines', once thought to represent the elevation of the LGM ice sheet, are now interpreted as englacial thermal boundaries, marking a transition from warm-based ice to cold-based non-erosive ice (Kelly & Bennike, 1985; T. P. Lane et al., 2014, 2015; Roberts et al., 2013; N. E. Young & Briner, 2015). This understanding suggests that certain areas previously considered ice-free during the LGM might have been covered by cold-based non-erosive ice (Håkansson et al., 2011; Ó Cofaigh et al., 2004; Sbarra et al., 2022; Vasskog et al., 2015). Recent work by Sbarra et al. (2022) extends the LGM maximum extent to the offshore shelf break in southwest Greenland in the vicinity of Kangerlussuaq, one of the largest and most southern proglacial areas in Greenland. It can therefore be assumed that the present-day proglacial landscape exposure at most extends back to the end of the LGM.

The period following the LGM witnessed gradual deglaciation, initiated asynchronously around Greenland. The retreat of the GrIS margin from its LGM position was not a uniform process across the ice sheet. In southern Greenland, deglaciation was already underway around 19 ka BP, with a cessation of

sedimentation on the Kangerlussuaq Trough mouth fan by approximately 18 ka BP (Carlson et al., 2008, 2014; Winkelmann et al., 2010). This retreat was mainly driven by accelerated calving from floating ice shelves and break-up of ice grounded below sea level on the continental shelf (Reeh, 2017; Syvitski et al., 2001; Vasskog et al., 2015), occurring predominantly between 17 and 11.5 ka BP. A notable warming trend in the Northern Hemisphere began around 17 ka BP, which became more pronounced during the Bølling interstadial, around 14.7–14.1 ka BP (Rasmussen et al., 2006; Rosen et al., 2014). This period saw substantial temperature increases, particularly evident in the Greenland ice cores. While initial estimates based on δ18O measurements suggested a dramatic increase of around 15 °C, subsequent studies using nitrogen isotopes and isotope diffusion indicated a more moderate warming of approximately 11.1 ± 2.8 °C (Annan & Hargreaves, 2013a, 2013b; Buizert et al., 2014; Rasmussen et al., 2006).

The Younger Dryas (YD) stadial, occurring between 12.9–11.7 ka BP, marked a significant cooling event, characterised by a reorganisation of ocean and atmospheric circulation patterns in the Northern Hemisphere (Alley, 2000; Larsson et al., 2022; Z. Liu et al., 2012). This period saw a decrease in Northern Hemisphere temperatures of about 0.5–1.0 °C, with the NGRIP ice-core record from Greenland reflecting a more substantial cooling of 8.1 ± 2.6 °C relative to the preceding Bølling and Allerød interstadials (Buizert et al., 2014; Shakun et al., 2012; Vasskog et al., 2015). The Early Holocene, following the YD, was a period of significant change for the GrIS. This was the time when the ice margin first retreated onto land along most of the Greenland coast. In many areas, it retreated to its present position and beyond. Early Holocene moraine sequences in north Greenland, south east Greenland, and the Disko Bugt area in west Greenland provide evidence of the ice sheet's dynamic response to climate changes during this period (Carlson et al., 2008; Dyke et al., 2016; Hughes et al., 2012; Larsen et al., 2016).

The Middle Holocene saw further changes in the GrIS, with the ice margin in west Greenland retreating behind its Late Holocene maximum extent sometime during this period. This retreat was documented through various forms of terrestrial evidence, including exposure dates from boulders and bedrock, radiocarbon dates of basal lake sediment, and marine bivalves reworked into younger moraines (Carlson et al., 2008, 2014; Dyke et al., 2016; Graly et al., 2018; Hughes et al., 2012; Larsen et al., 2010,

2016, 2022; Levy et al., 2012; Schweinsberg et al., 2018; Vasskog et al., 2015; J. C. Young et al., 2018; N. E. Young & Briner, 2015). By the end of the Middle Holocene, the volume of the GrIS was likely somewhat smaller than it is today, with model results indicating a total mass loss of approximately 0.5 m SLE over this period (Lecavalier et al., 2013, 2014; Pedersen et al., 2011).

Throughout these periods, the GrIS's history has been intricately linked with broader climatic changes and has been a significant contributor to global sea-level variations. Its dynamic nature underscores the complexity of ice sheet systems and their sensitivity to environmental changes, offering critical insights into past climate dynamics and future projections. The ice sheet's history sets a precedent for where and how it may retreat under current and future climate conditions. GrIS retreat is intrinsically coupled with the exposure of barren ground and meltwater fluxes which have connotations for progressive landscape and geomorphic evolution of the growing proglacial areas surrounding Greenland.

2.2.3 Greenland’s Neoglacial Climate

The term "recent" in the context of Greenland's climatic history is often, and here, associated with the Neoglacial period, a phase that encapsulates significant climatic shifts, notably during and subsequent to the Little Ice Age (LIA). This period, extending from the end of the Early Holocene to the Middle Holocene Thermal Maximum (HTM) to the culmination of the LIA and spans at least the last 3500 years (Cheng et al., 2020). The HTM, with Northern Hemisphere temperatures higher than present, has been dated in Greenland to between around 8000 and 4000 years BP, depending on location and proxy type (Adamson et al., 2019; Axford et al., 2021; Briner et al., 2016; McFarlin et al., 2018). The Neoglacial is delineated by a gradual transition from relatively warmer conditions of the HTM to a markedly cooler climate regime. Neoglacial cooling was not homogenous and regionally diverged, however was most pronounced in the extratropical Northern Hemisphere (Marcott et al., 2013). A decline in summer insolation drove cooling temperatures which in turn caused changes in surface albedo linked to feedbacks from vegetation and snow/ice (Marcott et al., 2013). This cooling trend, which led to the Neoglacial period, has been traditionally divided into two distinct phases: an older Neoglacial phase, stretching from around 5000 to 950 years before present (BP), and a younger phase,

known as the LIA, from approximately 750 to 50 years BP (1900 CE) (Kjær et al., 2022).

The LIA is notably associated with reduced global temperatures and extensive glacier advances, marking significant shifts in ice margins and glacier activities in Greenland (Carrivick et al., 2023; Kjær et al., 2022). During this period, Northern Hemisphere temperature reconstructions estimated a cooling of 0.5 to 1.0 °C relative to the global mean (Briner et al., 2016; Kaufman et al., 2009; Landrum et al., 2013; Mann et al., 2008; Zhou et al., 2011). The onset of the LIA cooling varied but typically spanned between 800 – 550 yrs. BP, making it a critical period for understanding the Neoglacial glacier activity in the wider context of the past 5000 years (Kjær et al., 2022). Glacial responses during the Neoglacial were complex and somewhat asynchronous across Greenland. While glaciers generally responded to the Neoglacial cooling, their maximum extent was often delayed relative to the onset of LIA temperature cooling. For example, some studies report the maximum glacier advance occurred in the 1700s CE or by the end of the 1800s CE (Brooks et al., 2022; Khan et al., 2014; Kjær et al., 2022; Weidick et al., 2012). This delay in glacial response underscores the intricate relationships between climate change, atmospheric circulation, and glacier dynamics. Ice-core records have been pivotal in reconstructing Holocene temperature variations, with $\delta^{18}O$ and $\delta^{2}H$ isotopes in glacier ice providing high-resolution proxy records (e.g. Dansgaard et al., 1973; Johnsen et al., 2001). However, these reconstructions are not without challenges, as they are influenced by various factors, including altitude changes due to ice flow and ice-sheet elevation changes (Lecavalier et al., 2013; Malmierca-Vallet et al., 2020; Vinther et al., 2009). The records indicate pronounced melting during the HTM, decreasing markedly around 6000 BP, signalling a drop in summer temperatures and marking the beginning of a general cooling trend towards the LIA (Kjær et al., 2022).

The LIA itself consisted of two distinct cold periods, with temperature minima at 400 and 100 years. BP (1550 and 1850 CE), with temperatures 0.5 and 0.7 °C below the present, respectively. Post-LIA, temperatures peaked around 20 yrs. BP (1930 CE), marking the end of the Neoglacial period. This period saw significant atmospheric circulation changes, including a generally southward displacement and intensification of westerly circulation, influencing precipitation and snow accumulation in Greenland (Dahl-Jensen et al., 1998; Kjær et al., 2022; Meese et al.,

1994). The Neoglacial also saw varied oceanographic conditions. The East Greenland Current (EGC) played a significant role, showing a marked intensification from around 4000–3500 yrs. BP onward to the LIA (Bond et al., 2001; Perner et al., 2015; Wangner et al., 2018, 2020). Concurrently, the warm Irminger Current (IC) intensified episodically during the LIA, particularly prevalent in south/south east Greenland and likely in response to lowered solar activity and changes in atmospheric pressure systems (Andresen et al., 2017; Bond et al., 2001; Perner et al., 2015). This period of strong water mass stratification, characterised by strong EGC and IC inflow, parallels conditions recorded during earlier periods such as the Dark Ages Cold Period (DACP) (Kjær et al., 2022).

2.2.4 Post-LIA Climate Change in Greenland

Since the end of the Little Ice Age (LIA), Greenland's glacier ice-free proglacial regions have undergone significant climatic changes, markedly influencing ecosystem structure, soil carbon dynamics, and permafrost stability (Jungsberg et al., 2022; Schuur et al., 2009; Westergaard-Nielsen et al., 2018; Zimov et al., 2006). The past three decades, in particular, have been a focus of study to understand the magnitude and implications of these changes. Westergaard-Nielsen et al. (2018) characterise, utilising satellite-derived land surface temperatures (LST) and modelled air temperatures validated against observations, significant changes across Greenland's proglacial areas, noting pronounced seasonal and regional variations in temperature trends (Westergaard-Nielsen et al., 2017). The study reveals that the spatial distribution of temperature changes is not uniform across Greenland. For instance, recent temperature trends indicate significant summer warming in west Greenland, while significant spring cooling has been observed in south Greenland. Additionally, widespread autumn cooling is evident in south west and mid-Greenland (Westergaard-Nielsen et al., 2017). These findings underscore the complexity of climate dynamics in the region, highlighting the interplay between various atmospheric and oceanic drivers (Hachem et al., 2012; Urban et al., 2013). The relationship between observed temperatures and the Greenland Blocking Index (GBI) anomalies is particularly notable, with the strongest link observed in west Greenland during spring and winter (Hanna et al., 2016, 2018). This correlation suggests that fluctuations in GBI may have influenced warming trends in the 1990s, followed by a period of stable or cooler temperatures from 2000–2015 (Westergaard-Nielsen et al.,

2017). These observations align with broader trends in the Arctic region, where recent enhanced warming (Arctic amplification) has coincided with increased mean annual precipitation and interannual variability in specific areas of Greenland (Henderson et al., 2021; Preece et al., 2023; Screen & Simmonds, 2010). The implications of these temperature changes are far-reaching, especially regarding the stability and dynamics of permafrost. High-resolution temperature data is essential for evaluating ecosystem services and understanding the growing season dynamics, active layer thickness, and vulnerability of permafrost (Rasmussen et al., 2018; Westermann, Elberling, et al., 2015). Stable permafrost conditions are critical for supporting infrastructure, reducing erosion risks, and preserving carbon stocks in permafrost soils (Hollesen et al., 2011; Jungsberg et al., 2022). However, areas with warm permafrost, which have experienced recent climate warming, are considered the most vulnerable (Westergaard-Nielsen et al., 2017).

The response of proglacial landscapes to recent climate changes are extremely complex and nonlinear making prediction and modelling difficult. This research therefore aims to measure and quantify the response of the proglacial landscapes to climate warming through multi-temporal landcover classification and change analysis.

2.3 Proglacial landscapes

2.3.1 Definition and Relevance

As the GrIS and peripheral glaciers and ice caps (PGIC) retreat, the area of newly exposed ice-free landcover is increasing on the coastal fringes of Greenland. Following exposure, these areas are characterised by very active geomorphological dynamics, including rapid mass movement, widespread periglacial processes, and intense sediment redistribution (Marienfeld, 1992; Stott and Grove, 2001). Many of these processes are further enhanced by the presence, and melting, of permafrost (Hollesen et al., 2011). The vast sediment redistribution, particularly during melt seasons, can have profound effects on stream networks and meltwater routing, creating braided and even anastomosed streams in low-relief flat areas (e.g. Mink et al., 2014; Rennermalm et al., 2012). In more ice-distal ice-free areas with longer exposure times, longer-term paraglacial dynamics have altered the environment and sediment availability, such as the development of raised beaches as isostatic

readjustment outpaces eustatic sea-level rise (Bennike, 2004), and soil development allowing for the colonisation of vegetation (Daniels and de Molenaar, 2011; Daniels et al., 2011; Eichel et al., 2013). Landcover change and exposure to air, precipitation, and more marked temperature fluctuation is also known to influence numerous climate-feedback mechanisms, such as: (i) darker sediment and bedrock causing positive climatic feedback via reduced solar energy reflectance (albedo) and increased thermal retention; (ii) increased deposition of organic matter, both terrestrially and within streams and eventually fjords, as a consequence of soil formation and colonisation of vegetation in areas where sediment redistribution is common and stream networks diverge regularly; and (iii) increased/altered biogeochemical weathering and reactions coinciding with changes in microbial community composition affecting gas (e.g. CO_2, O_2, N_2O) production and sequestration rates (Barcena et al., 2011). All processes triggered by glacial retreat at various temporal and spatial scales are considered under the paraglacial concept (Ballantyne, 2002a; Ballantyne, 2002b; Mercier, 2008; Mercier and Etienne, 2008; Slaymaker, 2009; Slaymaker, 2011). Paraglacial responses are initially intense following exposure, with a gradual decline towards a '*geomorphological equilibrium*' (Ballantyne, 2008). The transition to an equilibrium state in Arctic proglacial landscapes is oft drawn in parallel to widespread vegetation expansion in these regions with climate warming (Hill & Henry, 2011; Karami et al., 2018; Myers-Smith et al., 2011; Pearson et al., 2013; Vowles & Björk, 2019). Vegetation encroachment, expansion, and establishment in proglacial Arctic landscapes have manifold impacts on geomorphological function, hillslope stability, permafrost thaw, and sediment delivery and composition (particulate and dissolved organic carbon) in rivers and streams (Daniels et al., 2011; Estrany et al., 2019; Pearson et al., 2013; Swann et al., 2010).

The importance of proglacial landscapes and their processes and paraglacial activity is highlighted by the recent apparent upsurge in research publications on the subject, with studies largely concentrated in the European Alps (e.g. Baewert and Morche, 2014; Carrivick et al., 2013; Carrivick and Heckmann, 2017; Carrivick et al., 2018; Draebing and Eichel, 2018; Eichel et al., 2018; Geilhausen et al., 2013; Goldstein et al., 2023; Heckmann et al., 2016b; Kellerer-Pirklbauer et al., 2010; Kirkbride and Deline, 2018; Knight and Harrison, 2014; Lane et al., 2017; Morche et al., 2013). By

contrast, polar regions such as Greenland have received far less attention, meaning our understanding of proglacial systems and paraglacial activity is far less developed here (Anderson et al., 2017; Carrivick et al., 2017). It is therefore one aim of this thesis to both spatially and temporally classify and categorise the proglacial areas and proglacial dynamics of the entire periphery of Greenland.

2.3.2 Monitoring Proglacial Landscape Change

In the context of Greenland's rapidly changing peripheral environment, the need for detailed monitoring of proglacial landscape changes is increasingly important. This vast and remote region, characterised by its relatively young and evolving post-glacial landscape as explored earlier in this review, presents unique challenges with unstable landscapes marked by loosely consolidated sediments and ongoing permafrost thaw. These factors necessitate a robust and adaptable approach to monitoring, especially given the logistical challenges posed by Greenland's harsh terrain and sparse population. This is where the significance of landcover classification and change assessment using remotely sensed data becomes apparent. Remote sensing technology is indispensable for overcoming the geographical and logistical barriers in Greenland and provides a continuous, comprehensive means of observing and documenting the dynamic changes in the landscape over periods of satellite coverage. Subtle variations in landcover can be identified, offering critical insights into the evolving geomorphological processes and enabling the detailed tracking of sediment redistribution, hydrological changes, glacier’s areal extent, and vegetation establishment and expansion, crucial for understanding the progression towards geomorphological stability.

2.3.2.1 Landcover classification

Spatial land cover classifications derived from spectral remotely sensed images are crucial for environmental assessment and monitoring of natural resources and change (Cingolani et al., 2004; Hansen et al., 2000; Tucker et al., 1985). Such classifications are necessary input for many hydrological, ecological and geomorphological models (Saha et al., 2011). Remotely sensed data is of particular utility in remote, vast and mountainous regions such as Greenland. Greenland’s high-latitude location and sparse population give it a unique character not especially facilitating of either field or remote research:

i. It is remote and largely inaccessible, meaning ground validation is sparse and hard to acquire.
ii. It is high latitude, meaning many potentially useful sensors mounted aboard equatorial orbiting satellites are useless due to the extremely oblique viewing angle.
iii. It is mountainous and rugged, so topographic correction is recommended but extremely computationally costly.
iv. Shadows are common due to deep and narrow valleys and steep slopes originating from the mountainous terrain and glacial erosional landforms.
v. The mountains are coupled with low sun angles for the majority of the year, amplifying shadowing in remotely sensed images.
vi. The land surface is visible for only a short time each year as the ice-free ground is covered by snow for most of the year. If this short snow-free window each year coincides with cloudy conditions, common for many regions of the Greenland coast in summer, during satellite image acquisition then quality image collection is hindered and further complex preprocessing methods are required.

Spectral landcover classification, a pivotal technique in the realm of remote sensing and geographical analysis, represents a method whereby different landcover types are identified and categorised based on their spectral signatures as captured by satellite or aerial imagery. This technology, increasingly vital in the context of environmental monitoring and land management, utilises a spectrum of classification approaches, each tailored to suit specific landcover types and analysis objectives. Predominantly, these classifications are bifurcated into three categories: unsupervised, supervised, and semi-supervised. Unsupervised classification, often the initial step in exploratory analysis, involves algorithmically grouping pixels based on their natural spectral variability without prior labelling. Conversely, supervised classification necessitates the pre-identification of 'training areas', segments of the image known to represent specific landcover types, to guide and refine the classification process. Semi-supervised classification, a synthesis of the two, merges both labelled and unlabelled data, harnessing the strengths of each approach to improve classification accuracy. These methodologies are applied variably, contingent upon the landcover type of interest. For instance, in the analysis of vegetation and phenological changes,

spectral classification can discern different types of vegetation and monitor their temporal changes, leveraging the unique spectral signatures of various plant species and their phenological states. In aquatic environments, such as rivers and lakes, spectral classification aids in delineating water bodies and detecting changes over time, a crucial component in the study of hydrological dynamics and, in proglacial catchments, glacier meltwater routing and connectivity.

The benefits of spectral landcover classifications are multifaceted. They offer a non-invasive, cost-effective means of monitoring large and inaccessible areas, providing invaluable data for environmental conservation, urban planning, and agricultural management. Moreover, these classifications facilitate change detection, enabling the identification and analysis of temporal changes in landcover, a function critical in understanding environmental dynamics and anthropogenic impacts. In the context of Arctic change, particularly within proglacial environments, spectral landcover classifications assume a role of paramount importance. The Arctic, a region experiencing rapid environmental transformations due to climate change, presents unique challenges and opportunities for landcover analysis. Proglacial areas are dynamic landscapes characterised by varied and evolving landcover types, ranging from bare ground and glacial moraines to pioneering vegetation.

Several studies have highlighted that accurate landcover data is required in the Arctic (e.g. Bartsch et al., 2016; Ottlé et al., 2013; Westermann, Østby, et al., 2015). The research presented here, focusing on Greenland's proglacial areas, seeks to elucidate the nuances of landcover types within these environments, drawing upon a rich repository of existing studies and datasets. A number of landcover products exist in the Arctic and Greenland at a number of spatial scales and resolutions, as well as at differing times.

2.3.2.2 Existing Arctic Landcover Classifications

The development of land cover mapping in Arctic and permafrost regions has significantly evolved with the increasing availability of satellite data, primarily optical. The evolution of land cover mapping in Arctic and permafrost regions has been marked by a significant transition from the initial optical satellite data explorations in the 1970s and 1980s, primarily using the Landsat series (Pearce, 1991), to the sophisticated integration of high-resolution optical and Synthetic

Aperture Radar (SAR) data. Early efforts focused on habitat mapping in Alaska and the Canadian Arctic, gradually expanding with the advent of SAR satellites like ERS-1 and Almaz (Belchansky et al., 1995; Douglas & Ovchinnikov, 1995), which brought new dimensions to tundra habitat classification, despite initial challenges in comparison to optical data. The introduction of high-resolution data, such as from the SPOT sensors (Käykhü & Pellikka, 1994; Markon & Derksen, 1994), and the development of advanced processing techniques, addressed the fine-scaled heterogeneity of the Arctic tundra vegetation (Brossard & Joly, 1994; Mosbech and Hansen, 1994), a critical factor given the region's complex dynamics.

The late 1990s and onwards saw increased use of AVHRR data for thematic applications and a growing emphasis on capturing detailed landscape features, including water bodies crucial for identifying thaw lakes associated with permafrost (Bartsch et al., 2012; Cihlar et al., 1996; Takeuchi et al., 2003; Walker, 1999). This period of technological advancement and methodological refinement, which also saw the incorporation of different polarisations from modern SAR systems (Atwood et al., 2012; S. Banks et al., 2013; S. N. Banks et al., 2014; Bartsch et al., 2012), has significantly enhanced the understanding and monitoring capabilities of these sensitive and rapidly changing regions. However, the specificity of the approaches as applied for specific monitoring of single land cover facets highlights the ongoing need for high thematic and spatial detail in Arctic land cover mappings (Bartsch et al., 2016).

The Circum-Arctic Vegetation Map (CAVM) has been a pivotal pan-Arctic dataset, providing a consistent thematic base for vegetation and ecological studies across the Arctic's diverse landscape (Walker et al., 2005). Developed primarily from NOAA-AVHRR data, the CAVM represents the first unified effort to map the Arctic with a spatial resolution of 1 km, specifically focusing on the region's unique vegetation types and permafrost features (Raynolds et al., 2019). The map, which precedes regional mappings, has been widely recognised for its utility in various scientific and environmental applications, such as the improved mapping of reindeer pastures when compared to global land cover maps (Rees & Danks, 2007). However, the CAVM's resolution and thematic content have certain limitations, particularly in distinguishing broader processes (sediment distribution, periglacial activity) in the heterogeneous Arctic. The CAVM also finds little utility in assessing land cover

changes, being a fairly modern snapshot dataset. The dataset is also pan-Arctic, and so not specifically honed and designed for application in a specific Arctic environment, such as Greenland, where vegetation types can vary significantly from those elsewhere in the Arctic. Despite these constraints, the CAVM remains a fundamental resource for understanding Arctic vegetation patterns and their implications for global climate dynamics.

WorldCover, developed by the European Space Agency using Sentinel-1 and Sentinel-2 data, offers a detailed global land cover map with a 10-meter resolution (Zanaga et al., 2021). However, despite its precision, it's not ideally suited for Arctic land cover change assessments, particularly for studying Arctic-specific proglacial processes. The primary issue lies in its thematic content, which, being designed for global applicability, lacks the specificity required to accurately capture the nuanced and complex landscape of the Arctic. This region is characterised by subtle spectral differences in sparse vegetation and barren lands, as well as distinct proglacial features, which are often not adequately distinguished in a generalist global classification system. Furthermore, the persistent cloud cover and polar darkness prevalent in the Arctic pose additional challenges for the optical sensors used by WorldCover, leading to potential data gaps and reliability issues. The Copernicus Arctic Land Cover Climate Change Initiative (CALC-2020) is a project under the European Space Agency's Climate Change Initiative program, dedicated to producing high-resolution, accurate land cover maps specifically for the Arctic region (C. Liu et al., 2023). By focusing exclusively on the Arctic, CALC-2020 addresses the unique and complex landscape of this area, utilising tailored algorithms and methodologies to capture subtle variations in land cover and monitor the rapid environmental changes due to climate change. While CALC-2020 provides invaluable data for understanding current land cover and short-term changes, its utility for longer-term change assessments may be limited. This limitation stems from the relatively short temporal coverage of the dataset, which may not capture the full extent of historical land cover dynamics or long-term trends, crucial for understanding the gradual processes and legacy effects of climate change in the Arctic.

In Greenland, land cover mapping has been an integral part of understanding and monitoring the region's ecological dynamics and permafrost characteristics. One notable study by Mosbech and Hansen (1994) compared satellite imagery and

infrared aerial photography for vegetation mapping methods in east Greenland, employing both SPOT and Landsat TM data. They emphasised the challenges of capturing the finely-scaled tundra Arctic vegetation mosaic by species using satellite data, however highlighted that broad distinction of vegetation occurrence and type were very well resolved. Despite improvements with high spatial resolution satellites, species distinction remains a challenge, particularly when mapping larger national and pan-Arctic areas. More recently, Jørgensen et al. (2015) used Landsat TM normalised difference water index composites to estimate fluxes in the Zackenberg Valley, north east Greenland, in 2015. Their work was based on a detailed earlier classification by Elberling et al. (2008), which used airborne data for soil properties analysis. This classification also served as input for soil organic carbon estimates (Palmtag et al., 2015). Jørgensen et al. (2015) found fairly low accuracy in distinguishing specific species when comparing satellite-derived results to ground validation, however, they present broader dry-tundra and wetland classifications to infer methane fluxes and find excellent accuracy.

Karami et al. (2018) addressed the challenge of the coarse resolution in large-scale land cover maps of the Arctic, which often fail to capture the intricate heterogeneity of these landscapes by mapping vegetation change over a 15-year period (2001 – 2015). They developed an innovative approach by incorporating multi-temporal Landsat-8 OLI data to produce a detailed tundra vegetation classification map for the entirety of Greenland. Their study extracted vegetation phenology from a single-year time series of 4,169 OLI scenes at a 30m resolution. They combined these phenological metrics with satellite-derived wetness and terrain information, utilising a random forest classifier to delineate land surface classes effectively. By still considering fairly broad phenological vegetation classes, they were able to achieve an impressive cross-validation accuracy of 89.25% across the area under study. Karami et al. (2018) therefore proved the efficacy of Landsat's 30m resolution for land cover change mapping in Greenland, however concentrated their analysis on 21st century change, specifically for vegetation.

These studies collectively indicate a trend towards integrating high spatial resolution and sophisticated classification techniques to address the unique and dynamic environmental characteristics of Greenland, acknowledging the region's significant role in global climate dynamics and the need for precise ecological monitoring. It

also highlights the requisite thematic detail when working at tens-of-metre resolutions and over large (regional and national) areas. Species differentiation is often problematic and, when not necessary for the research aim, may be superfluous and detrimental to overall accuracy. The research presented here therefore considered vegetation types broadly, covering dry tundra and wetland species separately as proven to be distinguishable with high accuracy using 30m data.

For tasks concerned with capturing a contemporary snapshot of landcover then the most modern data is paramount. However, when considering landcover changes in Arctic regions such as Greenland, the longer the difference between datasets to be compared the more useful and impactful the findings when considering the impacts of Arctic Amplified climate change (Serreze & Barry, 2011). These longer-duration studies are therefore restricted to the best available data at their earliest time step, where a contemporary equivalent of the same resolution and band designations exists (Poursanidis et al., 2015). As shown here, most change classifications in the Arctic are therefore restricted to fairly contemporary (1990s onwards) changes due to the lack of available high-quality data prior to this. Existing contemporary classifications as outlined above are therefore of little utility, as post-classification comparisons created using differing methods are flawed by the implausibility of matching thematic content and for change accuracy assessment (Serra et al., 2003). The earlier Landsat missions (e.g. Landsat 5) have fairly poor Arctic coverage and repeat survey times, particularly in Greenland, where traditional methods classifying single image tiles were unusable (e.g. Marshall et al., 1994). However, recent high-performance cloud-based computing, such as Google Earth Engine, has enabled image composites and mosaics to be produced, filtering through extremely large, multi-year catalogues of images to select the best quality pixels for every location. It is through leveraging this advancement that the research presented in Chapter 3 is able to extend the proglacial landcover change record for the entire proglacial area of Greenland back to the mid-1980s, covering all salient facets of landcover rather than a focussed assessment of a single landcover type.

2.4 Greenland's Peripheral Glaciers and Ice Caps

Greenland's ice sheet marginal proglacial landscapes are interspersed by tens of thousands of smaller peripheral ice caps and glaciers (PGIC). As outlined earlier in

this review, many of these PGICs were likely connected to and part of the GrIS at various stages during the quaternary and early Holocene. However, due to their current disconnected state, they are marked by unique responses to climate change when compared to the neighbouring ice sheet.

2.4.1 Glacier's Responses to Climate Fluctuations

The glacial response in Greenland, particularly during the Neoglacial period and the Little Ice Age (LIA), has been significantly influenced by atmospheric variability, with the North Atlantic Oscillation (NAO) playing a pivotal role. Peripheral glaciers and ice caps (PGICs), which account for up to 20% of the early twenty-first century (2003–2008) Greenland ice loss, provide an interesting avenue of research to understand these dynamics (Bolch et al., 2013; Colgan et al., 2015; Gardner et al., 2013). PGICs, being predominantly land-terminating, react more rapidly to climate variability due to their relatively short glacier reservoir times, leading to faster mass turnover via enhanced snow and melt fluxes (Bjørk et al., 2018). This responsiveness is evident in the varied glacial responses across east and west Greenland. For instance, most PGICs in east Greenland retreated at an average rate of 22.1 ± 6.4 m yr^{-1} from 1910 to 1932, almost twice the retreat rate of the 2000–2013 period (12.2 ± 1.8 m yr^{-1}) (Bjork et al., 2018). The NAO's influence on precipitation and, consequently, on glacier dynamics in Greenland is significant (Straneo & Heimbach, 2013). Positive phases of the NAO are associated with increased accumulation and glacier growth in east Greenland, whereas the opposite effect is observed in West Greenland (Bjørk et al., 2018; Straneo & Heimbach, 2013). This east–west asymmetry in precipitation, driven by large-scale circulation patterns, is crucial in understanding regional differences in glacial behaviour (Li et al., 2022). During the twentieth century, periods of strong winter NAO− (1962–1971) and NAO+ (1988–1995) were particularly influential (Bromwich et al., 1999; Mosley-Thompson et al., 2005). These phases indicated that the connection between NAO and regional precipitation is strongest in east Greenland, with opposite effects during strong NAO+ and NAO− phases (Bjork et al., 2018). For example, during the NAO− period of 1962–1971, there was a 9.0 ± 0.7 Gt yr^{-1} (−17.4%) deficit in annual accumulation in east Greenland, while the NAO+ period of 1988–1995 saw an additional 5.3 ± 0.4 Gt yr^{-1} (7.6%) of annual accumulation (Bjork et al., 2018). Auger et al. (2017) investigate the impact of various atmospheric and oceanic patterns on precipitation in

southern Greenland. Focussing on the influence of the North Atlantic Oscillation (NAO), Atlantic Multi-decadal Oscillation (AMO), Icelandic Low, Azores High, regional blocking patterns, and near-surface temperature and winds on precipitation patterns. The findings revealed that the correlations between precipitation and the Icelandic Low, as well as near-surface winds, were statistically more significant (with correlation coefficients ranging between 0.5 and 0.7, and a p-value < 0.05) compared to the relatively lower correlations between precipitation and the NAO or AMO climate indices. In southwest Greenland, the correlation coefficients with the NAO and AMO were 0.12 and 0.28, respectively, while in southeast Greenland, they were 0.25 and −0.07, respectively. The study also noted a prominent correlation between the recent phenomenon of Arctic amplification, characterised by enhanced warming in the Arctic, and the increase in the Greenland Blocking Index. These changes were associated with an increase in both the mean annual precipitation and its interannual variability in southwest Greenland.

NAO-driven variability, though significant at the regional scale, has a spatially compensating effect that minimises its overall influence on the ice sheet. However, as these changes increase towards the coasts, they can lead to accumulation rate changes exceeding −20% and +25%, significantly affecting peripheral glacier and ice sheet geometry (Bjork et al., 2018). The NAO's role underscores the importance of considering large-scale atmospheric variability in understanding regional changes in ice volume for both the GrIS and PGICs.

2.4.2 Post-Little Ice Age Glacier Change

Post-LIA, Greenland has experienced substantial changes in its glaciological and climatic conditions. The period following the termination of the LIA around 1900 has been marked by a significant transformation in Greenland's PGICs and the GrIS. The first two decades of the 21st century, in particular, have been the warmest since the onset of meteorological measurements in the 1780s, surpassing the previously warm 1920s–1930s by 0.2°C (Masson-Delmotte et al., 2012). The year 2010 was exceptionally warm, with surface air temperatures (SAT) at coastal stations in West Greenland being three standard deviations above the 1960–1990 climatological average, resulting in a record melt over the GrIS (Masson-Delmotte et al., 2012).

From 1990 to 2010, the GrIS lost approximately 2750 Gigatons (Gt) of ice, with a significant acceleration in the rate of mass loss (Masson-Delmotte et al., 2012). The rapid melting of Greenland's glaciers since the early 1990s, particularly those south of 70°N, has been observed through remote sensing methods such as altimetry and velocity measurements from satellites and aircraft. This marked acceleration and retreat have accounted for about 50% of the recent GrIS mass loss (Masson-Delmotte et al., 2012). In terms of Greenland's peripheral glaciers and ice caps, Carrivick et al. (2023) report a total volume loss of between 528 and 646 km^3 since the LIA termination, equating to between 449 and 549 Gt at a mean rate of 4.34 Gt yr^{-1}. This mass loss is considerably higher than the long-term mean mass balance in glacier ablation areas, which was estimated to be at least -0.18 to -0.22 m w.e. yr^{-1}. The rate of mass loss between 2000 and 2019 was three times higher, showing a significant acceleration in recent years. The greatest proportion of volume loss has come from the north east region of Greenland, although this region also contains a large proportion of the total LIA glacier area. Carrivick et al. (2023) also noted that the mean PGIC mass balance rate over the past 20 years is at least twice as negative as the LIA to 2015 mean. In the south west and north west regions, the rate has become approximately three times more negative, and in the north, the rate has become five times more negative.

The current atmospheric and oceanic warming has had large impacts on the approximately 20,000 Greenland Alpine and outlet glaciers. Since the early 1990s, the retreat of marine-terminating outlet glaciers suggests a common forcing and occurs at a rate that is one order of magnitude larger than previously documented. This retreat, likely triggered by enhanced basal melting, reduces the backforce exerted by floating ice tongues on fast marine-terminated glaciers such as Jakobshavn Isbrae, Helheim, or Kangerlussuaq glaciers, leading to an acceleration and subsequent thinning of these glaciers (Masson-Delmotte et al., 2012).

The response of Greenland’s PGIC to recent climate change is therefore complex, and both spatially and temporally heterogeneous. This thesis therefore aims to extend the geodetic measurement period for Greenland’s PGIC back to the 1980s, using a lesser applied dataset made plausible through rigorous pre-processing and analysis of the data, explored further in Chapter 4.

2.5 Sediment Connectivity

The connectivity of sediment fluxes, both within Greenland's terrestrial landscape and between its terrestrial and marine realms, provides vital insights into geomorphological processes and their evolution over time. Notably, the intensified melting of Greenland's glaciers has engendered shifts in sediment transport pathways and deposition zones. Despite this, no current published literature explicitly explores and quantifies sediment connectivity in Greenland. This segment of the literature review therefore accentuates pioneering research endeavours that have ventured to map, quantify, and interpret sediment connectivity elsewhere, with emphasis on similar mountainous glaciated landscapes. By discerning the mechanisms underpinning sediment connectivity and its alterations, and the relevance of sediment connectivity to Greenland this section aims to enhance the understanding of the approaches taken here to produce the first exploration of sediment connectivity in the Arctic.

2.5.1 Sediment Connectivity: Background

Connectivity in the context of earth science, specifically in hydrology and geomorphology, is a fundamental concept describing the degree to which different components and compartments within a landscape facilitate the transfer of water and sediment, both internally and exogenously. Borne out of early work concerning hillslope-channel-outlet coupling (Walling, 1983), it encapsulates the interconnections and interactions between various landscape components, such as landforms, channels and complex hydro-geomorphic processes which influence and control the movement and distribution of water and sediment within and out of a watershed (Heckmann et al., 2018). More specifically, sediment connectivity is conceptualised as the coherent transfer of sediment within a system, encompassing its detachment from a source, traversing through diverse geomorphic zones, and finally depositing at a sink (e.g. lakes, fjords, ocean) (Bracken et al., 2015). This concept gains particular relevance in catchment systems where sediment movement is closely and intricately linked to: i) hillslope dynamics, ii) interactions between hillslopes and channels, iii) and processes within the channels themselves (Cavalli et al., 2019; Najafi et al., 2021). Principal examples of such catchments are those with steep, poorly consolidated hillslopes closely coupled to channels, including high-

mountain, alpine catchments and recently deglaciated proglacial landscapes (Mancini & Lane, 2020). As defined in an earlier section of this review, proglacial systems are regarded as some of the most dynamic on earth, experiencing rapid adjustment and redistribution as a function of: i) glacier mass loss, ii) intermittent seasonally variable meltwater flux, iii) permafrost thaw and degradation, iv) poor sediment consolidation and vegetation establishment, v) freeze-thaw cycles (seasonal), vi) steep valley sides dominated by mass-movement processes (S. N. Lane et al., 2017; Mancini & Lane, 2020). Many of these characteristics extend beyond the defined proglacial systems in high arctic environments, such as Greenland where ice-cover dominates and surficial-ice-free distances to major outlets on coastlines and fjords are relatively short. Sediment connectivity concerns solid material transfer between distinct zones, mediated by various vectors like water, wind, and gravity (Baartman et al., 2013). Each zone encapsulates a morphologic system of landforms and a cascading system of energy and materials flow. One of the primary limitations in existing discussions on 'connectivity' is the ambiguity in its definition and application within geomorphic contexts (Heckmann et al., 2018). Sediment connectivity in a geomorphic system might manifest through physical contact between zones, material transfer across them, and barriers or sinks hindering continued transport. The granular-level processes of erosion, sediment transport, and deposition collectively forge landscape features, presenting a significant geomorphological challenge: the reconciliation of erosion rates observed at small scales with broader-scale regional and national denudation rates (Coulthard & Van De Wiel, 2017). Overcoming this challenge necessitates addressing the shortcomings of localised single-catchment studies, comprehending the continuum of sediment sources and deposition within sinks within catchments, and acknowledging the uncertainties arising from changing surface geomorphology and landcover patterns. The sediment connectivity paradigm is underpinned by two distinctive yet interconnected components, each contributing unique insights to our understanding: structural and functional connectivity (Heckmann & Vericat, 2018; Lane et al., 2017). The former encompasses the tangible, physical characteristics of the landscape that facilitate ‘potential’ sediment transport, while the latter delves into the intricate processes of soil erosion and ‘measured’ sediment movement. These two facets prove instrumental in unravelling the spatial intricacies of sediment distribution, sediment cascades, and the dynamic distribution of sediment aggradation and degradation zones, thereby mitigating

uncertainties inherent in sediment transport (Heckmann et al., 2018). In the pursuit of quantifying sediment connectivity, diverse techniques have been employed, encompassing the use of indices, pre-existing models, and graph theory. Among these, sediment connectivity indices have emerged as comprehendible, user-friendly tools for the quantitative representation of potential sediment delivery across catchment compartments (Crema & Cavalli, 2018; Lizaga et al., 2018; Zanandrea et al., 2021). However, despite the burgeoning interest and proliferation of sediment connectivity studies over the past decade, a lingering cloud of discord and ambiguity shrouds both conceptual and methodological aspects. This pertains to a multiplicity of factors, ranging from the bewildering array of indices employed for quantifying sediment connectivity, the varied methods employed to scrutinise connectivity across divergent spatiotemporal scales, and the current status of sediment connectivity research as a whole (Najafi et al., 2021).

A pivotal assessment of sediment connectivity research conducted prior to 2021 exists in Najafi et al. (2021) which constitutes a comprehensive review of 117 scholarly papers on the subject permitting their categorisation of previous research into five distinct thematic strands: (i) the development of conceptual frameworks, (ii) depiction of the spatial and temporal distribution of sediment source and sink areas, (iii) the formulation and refinement of sediment connectivity indices, (iv) the utilisation and refinement of predictive models, and (v) investigations into sediment delivery likelihood through the prism of network analysis (Najafi et al., 2021). The proportions of contributions within each category stand as follows: 8% for conceptual frameworks, 23% for spatial and temporal distribution analyses, 55% for sediment connectivity index development, 10% for model-centric explorations, and 4% for network analysis investigations. This categorisation underscores the preponderance of efforts directed towards structural-based assessments, which predominantly focus on static attributes such as an index of potential connectivity. This, however, has been to the relative neglect of functional connectivity, which accentuates the dynamism inherent in sediment transport processes across landscapes. A dominant factor determining this is the relative necessity for repeat surveys or field investigations and experiments required for functional process studies. The imperative of future research lies in the intensification of these process-based sediment connectivity studies when possible, combining structural and

functional approaches to elucidate the intricate spatiotemporal dynamics of sediment transport within watersheds. Therefore the research presented in Chapter 5 of this thesis aims to combine structural and functional connectivity assessments in Greenland, considering the predictive capability of structural indices of actual measured sediment delivery ratios.

The identification of sediment-prone regions assumes critical importance within the ambit of effective watershed management strategies. Moreover, once the sediment source areas are demarcated, elucidating the patterns of geomorphic coupling, i.e., the potential pathways for sediment transport from sources to the channel network, becomes imperative for formulating erosion and sediment management strategies. This is precisely where the concept of connectivity manifests its relevance. It embodies the degree to which a catchment enables the transit of water and sediment through its intricate web of interconnected components, thereby delineating the continuity or discontinuity of runoff and sediment pathways at any given juncture. However, a relatively under-explored dimension, particularly pertinent to regions such as Greenland, is the potential of this concept to enhance understanding among researchers and indigenous communities regarding ongoing and future sediment and nutrient fluxes to coastal waters. This understanding is vital for assessing the longevity of coastal ecosystems. It has cascading effects up the food chain, impacting the viability of fishing grounds and habitats for larger Arctic fauna, which are integral to traditional hunting practices. This aspect of sediment connectivity warrants further investigation to fully comprehend its implications for environmental sustainability and indigenous livelihoods in Arctic regions.

Regional and national scale assessments of sediment connectivity are rare, and no studies to specifically quantify connectivity exist to date in Greenland, despite the apparent importance of sediment and nutrient delivery to coastal waters. This work therefore aims to be the first in both areas, to define a nationally consistent index of connectivity for the first time in Greenland. The second section of this work then aims to test the applicability of an aggregated watershed index value in predicting functional connectivity, measured as the sediments delivery ratio for each watershed over 40 years.

2.5.2 Metrics of Sediment Connectivity

Heckmann et al. (2018) provide a comprehensive review of existing metrics to quantify and represent sediment connectivity for catchments, particularly focussing on the proliferation of indices of connectivity and their utility. Heckmann et al. (2018) distinguish between raster-based connectivity indices, approaches delineating an “effective catchment area”, and network-based indices.

Raster-based indices have emerged with advancements in GIS technology and the availability of high-quality Digital Elevation Models (DEMs), focusing on how topography influences processes like landsliding, erosion, and sediment yield (Mancini & Lane, 2020). These methods often utilise the concept of stream power (Ω) and slope-area indices, as discussed by Montgomery & Dietrich (1994) and Wilson and Gallant (2000), to model the topographic potential for erosion and deposition. Notably, the Index of Connectivity (IC) by Borselli et al. (2008) is highlighted as a GIS-based index that takes into account topography and land cover-related information, aiming to represent potential connectivity between catchment components.

The DEBAS and DENET indices, developed by Dalla Fontana and Marchi (Dalla Fontana & Marchi, 1998; Marchi & Dalla Fontana, 2005) are noted for their use in alpine environments to evaluate impedance to sediment fluxes. Walling & Zhang's (2004) GIS-based procedure finds utility for estimating lateral connectivity, similar to Jain & Tandon’s (2010) fourfold classification of connectivity. These indices collectively reflect a growing interest in the quantitative characterisation of landscape linkages, essential for understanding and managing sediment dynamics in various environments.

Of these methods, the Index of Connectivity (IC) designed by Borselli et al. (2008) has come to the forefront, with different researchers adapting it to address specific landscape features and processes. For example, refinements to the original IC involve calculating the slope angle along the direction of flow and using the D-infinity approach for a more accurate representation of divergent flow paths on hillslopes (Cavalli & Marchi, 2008; Crema & Cavalli, 2018; Tarboton, 1997). The inclusion of surface roughness as a weighting factor in IC computation (Cavalli et al., 2013; Trevisani & Cavalli, 2016) is also noted for its advantages in providing an objective

estimate that enhances the index's application. Other significant adaptations of the IC include the incorporation of rainfall erosivity factors for assessing typhoons impact on connectivity (Chartin et al., 2017), curve numbers for runoff generation potential (Kalantari et al., 2019), and the use of LiDAR data for estimating forest density (Lizaga et al., 2018). These modifications reflect the IC's flexibility in addressing different environmental conditions and the dynamic nature of connectivity. These advancements underscore the growing complexity and refinement in sediment connectivity assessment, demonstrating a trend towards more nuanced application, and context-specific approaches. The IC however offers a measure of structural connectivity, essentially representing the potential connectivity given proxy data in the form of topography and landcover.

Heckmann and Vericat (2018) explore the inference of functional sediment connectivity (actual sediment movement through and out of a system) through the computation of spatially distributed Sediment Delivery Ratios (SDRs). They demonstrate that DEMs of Difference (DoD) provide critical insights into geomorphic processes and sediment budgets by capturing the spatial pattern of elevation changes. Their approach allows for the calculation of the net sediment yield (SY) for a cell's contributing area and, when applied to the negative subset of the DoD, provides a minimum estimate of erosion (E) within the same area. The ratio of SY to E yields the SDR, which serves as a measure of functional sediment connectivity. SDRs are particularly effective in assessing functional connectivity because they represent the proportion of material eroded within a cell's contributing area that has been exported from that area (Heckmann & Vericat, 2018).

This provides a direct measure of the efficiency of sediment transfer through a catchment, reflecting the dynamic interplay between erosion and deposition processes (Vigiak et al., 2012). However, it should be noted that the SDR requires careful interpretation and further research to refine the approach when measured and represented as a spatially distributed surface. When considered in isolation for a given point, the interpretation of sediment redistribution from contributing areas is fairly sound, depending on inherent data limitations. For studying large areas, SDR can be calculated to a single point, rather than as a spatially distributed surface, vastly reducing the computational cost.

The application of SDRs offers a promising avenue for advancing our understanding of functional sediment connectivity in geomorphic systems. A small number of studies have considered IC in combination with an SDR measure, including Vigiak et al. (2012) who evaluated four metrics to define the spatially variable hillslope sediment delivery ratio (HSDR). They found the IC metric significantly enhanced the prediction of specific sediment yields, implementation is straightforward and user-friendly, and the metric is independent of scale, making it versatile across various geographical extents. They also concluded that the IC formulation is adept at incorporating landscape variables and topology, aligning well with the principles of sedimentological connectivity.

2.5.3 Connectivity in Greenland

The study of sediment connectivity in Greenland's peripheral regions marks a nascent yet crucial domain within scientific research, particularly due to the susceptibility of these areas to climate change impacts, including increased ice sheet melt and sediment transport. To date, there are no existing studies in Greenland explicitly studying sediment connectivity, either locally or nationally (Najafi et al., 2021). Sediment connectivity is vital for the dynamics of coastal ecosystems, where glacial meltwater streams transport essential nutrients from glaciers to coastal waters (Lane et al., 2017; Rysgaard et al., 1999). This seemingly straightforward process is intricate; insufficient sediment can cause nutrient deficits in fjords and coastal waters, while excessive sediment can create sediment plumes, impeding light penetration and reducing primary productivity (Cape et al., 2018; Docherty et al., 2018; Hawkings et al., 2015; Oksman et al., 2022). These effects have far-reaching implications, affecting the trophic hierarchy and the livelihoods of local indigenous communities reliant on these ecosystems (Hamilton et al., 2000; Nuttall, 2016).

A detailed examination of functional and structural sediment connectivity is essential, especially given the emerging role of proglacial lakes as sediment sinks (Carrivick & Tweed, 2013) and the "greening" trend in Greenland (Karami et al., 2018; Normand et al., 2013), where increased vegetation affects sediment dynamics (Klaar et al., 2015). The expansion of vegetation influences sediment availability, while the growth of meltwater streams due to rising temperatures can increase

sediment transport. This is further complicated by the thawing of permafrost, which potentially releases immobilised sediments and alters flow regimes(Lamoureux et al., 2014; Lewkowicz & Harris, 2005). These dynamic interactions necessitate a comprehensive approach to understanding sediment connectivity in the face of Greenland's changing landscape and climate. The research in the fifth chapter of this thesis seeks to elucidate the complex interplay of forces shaping sediment connectivity in Greenland, thereby enhancing our understanding of the relationship between climate change and geomorphological processes in this polar region.

2.6 Chapter 2 References

Abermann, J., Hansen, B., Lund, M., Wacker, S., Karami, M., & Cappelen, J. (2017). Hotspots and key periods of Greenland climate change during the past six decades. *Ambio*, *46*. https://doi.org/10.1007/s13280-016-0861-y

Adamson, K., Lane, T., Carney, M., Bishop, T., & Delaney, C. (2019). High-resolution proglacial lake records of pre-Little Ice Age glacier advance, northeast Greenland. *Boreas*, *48*(3). https://doi.org/10.1111/bor.12361

Alley, R. B. (2000). The Younger Dryas cold interval as viewed from central Greenland. *Quaternary Science Reviews*, *19*(1–5). https://doi.org/10.1016/S0277-3791(99)00062-1

Alley, R. B., Andrews, J. T., Brigham-Grette, J., Clarke, G. K. C., Cuffey, K. M., Fitzpatrick, J. J., Funder, S., Marshall, S. J., Miller, G. H., Mitrovica, J. X., Muhs, D. R., Otto-Bliesner, B. L., Polyak, L., & White, J. W. C. (2010). History of the Greenland Ice Sheet: paleoclimatic insights. *Quaternary Science Reviews*, *29*(15–16). https://doi.org/10.1016/j.quascirev.2010.02.007

Andresen, C. S., Kokfelt, U., Sicre, M. A., Knudsen, M. F., Dyke, L. M., Klein, V., Kaczmar, F., Miles, M. W., & Wangner, D. (2017). Exceptional 20th century glaciological regime of a major SE Greenland outlet glacier. *Scientific Reports*, *7*(1). https://doi.org/10.1038/s41598-017-13246-x

Annan, J. D., & Hargreaves, J. C. (2013a). A new global reconstruction of temperature changes at the Last Glacial Maximum. *Climate of the Past*, *9*(1). https://doi.org/10.5194/cp-9-367-2013

Annan, J. D., & Hargreaves, J. C. (2013b). Climate of the Past Geoscientific Instrumentation Methods and Data Systems A new global reconstruction of temperature changes at the Last Glacial Maximum. *Clim. Past*, *9*.

Arndt, J. E., Jokat, W., Dorschel, B., Myklebust, R., Dowdeswell, J. A., & Evans, J. (2015). A new bathymetry of the Northeast Greenland continental shelf: Constraints on glacial and other processes. *Geochemistry, Geophysics, Geosystems*, *16*(10). https://doi.org/10.1002/2015GC005931

Atwood, D. K., Small, D., & Gens, R. (2012). Improving PolSAR land cover classification with radiometric correction of the coherency matrix. *IEEE*

Journal of Selected Topics in Applied Earth Observations and Remote Sensing, *5*(3). https://doi.org/10.1109/JSTARS.2012.2186791

Auger, J. D., Birkel, S. D., Maasch, K. A., Mayewski, P. A., & Schuenemann, K. C. (2017). Examination of precipitation variability in southern Greenland. *Journal of Geophysical Research*, *122*(12). https://doi.org/10.1002/2016JD026377

Axford, Y., De Vernal, A., & Osterberg, E. C. (2021). Past warmth and its impacts during the holocene thermal maximum in greenland. In *Annual Review of Earth and Planetary Sciences* (Vol. 49). https://doi.org/10.1146/annurev-earth-081420-063858

Baartman, J. E. M., Masselink, R., Keesstra, S. D., & Temme, A. J. A. M. (2013). Linking landscape morphological complexity and sediment connectivity. *Earth Surface Processes and Landforms*, *38*(12). https://doi.org/10.1002/esp.3434

Banks, S. N., King, D. J., Merzouki, A., & Duffe, J. (2014). Characterizing scattering behaviour and assessing potential for classification of arctic shore and near-shore land covers with Fine Quad-Pol RADARSAT-2 data. *Canadian Journal of Remote Sensing*, *40*(4). https://doi.org/10.1080/07038992.2014.979487

Banks, S., Ullmann, T., Roth, A., Schmitt, A., Dech, S., & King, D. (2013). Classification of Arctic Coastal land covers with polarimetric SAR data. *IEEE National Radar Conference - Proceedings*. https://doi.org/10.1109/RADAR.2013.6586059

Bartsch, A., Hofler, A., Kroisleitner, C., & Trofaier, A. M. (2016). Land cover mapping in northern high latitude permafrost regions with satellite data: Achievements and remaining challenges. *Remote Sensing*, *8*(12). https://doi.org/10.3390/rs8120979

Bartsch, A., Trofaier, A. M., Hayman, G., Sabel, D., Schlaffer, S., Clark, D. B., & Blyth, E. (2012). Detection of open water dynamics with ENVISAT ASAR in support of land surface modelling at high latitudes. *Biogeosciences*, *9*(2). https://doi.org/10.5194/bg-9-703-2012

Belchansky, G. I., Ovchinnikov, G. K., Kozlenko, N. N., & Douglas, D. C. (1995). Assessment of dependence between SAR data focusing parameters and tundra habitat classification. *International Geoscience and Remote Sensing Symposium (IGARSS)*, *1*. https://doi.org/10.1109/igarss.1995.520241

Bevis, M., Harig, C., Khan, S. A., Brown, A., Simons, F. J., Willis, M., Fettweis, X., Van Den Broeke, M. R., Madsen, F. B., Kendrick, E., Caccamise, D. J., Van Dam, T., Knudsen, P., & Nylen, T. (2019). Accelerating changes in ice mass within Greenland, and the ice sheet's sensitivity to atmospheric forcing. *Proceedings of the National Academy of Sciences of the United States of America*, *116*(6). https://doi.org/10.1073/pnas.1806562116

Bjørk, A. A., Aagaard, S., Lütt, A., Khan, S. A., Box, J. E., Kjeldsen, K. K., Larsen, N. K., Korsgaard, N. J., Cappelen, J., Colgan, W. T., Machguth, H., Andresen, C. S., Peings, Y., & Kjær, K. H. (2018). Changes in Greenland's peripheral glaciers linked to the North Atlantic Oscillation. *Nature Climate Change*, *8*(1). https://doi.org/10.1038/s41558-017-0029-1

Bjørk, A. A., Kjær, K. H., Korsgaard, N. J., Khan, S. A., Kjeldsen, K. K., Andresen, C. S., Box, J. E., Larsen, N. K., & Funder, S. (2012). An aerial view of 80 years of climate-related glacier fluctuations in southeast Greenland. *Nature Geoscience*, *5*(6), 427–432. https://doi.org/10.1038/ngeo1481

Bond, G., Kromer, B., Beer, J., Muscheler, R., Evans, M. N., Showers, W., Hoffmann, S., Lotti-Bond, R., Hajdas, I., & Bonani, G. (2001). Persistent solar influence on north atlantic climate during the Holocene. *Science*, *294*(5549). https://doi.org/10.1126/science.1065680

Born, A., & Nisancioglu, K. H. (2012). Melting of Northern Greenland during the last interglaciation. *Cryosphere*, *6*(6). https://doi.org/10.5194/tc-6-1239-2012

Borselli, L., Cassi, P., & Torri, D. (2008). Prolegomena to sediment and flow connectivity in the landscape: A GIS and field numerical assessment. *Catena*, *75*(3), 268–277. https://doi.org/10.1016/j.catena.2008.07.006

Bracken, L. J., Turnbull, L., Wainwright, J., & Bogaart, P. (2015). Sediment connectivity: a framework for understanding sediment transfer at multiple scales. *Earth Surface Processes and Landforms*, *40*(2), 177–188. https://doi.org/10.1002/esp.3635

Briner, J. P., McKay, N. P., Axford, Y., Bennike, O., Bradley, R. S., de Vernal, A., Fisher, D., Francus, P., Fréchette, B., Gajewski, K., Jennings, A., Kaufman, D. S., Miller, G., Rouston, C., & Wagner, B. (2016). Holocene climate change in Arctic Canada and Greenland. In *Quaternary Science Reviews* (Vol. 147). https://doi.org/10.1016/j.quascirev.2016.02.010

Bromwich, D. H., Chen, Q. S., Li, Y., & Cullather, R. I. (1999). Precipitation over Greenland and its relation to the North Atlantic Oscillation. *Journal of Geophysical Research Atmospheres*, *104*(D18). https://doi.org/10.1029/1999JD900373

Brooks, J. P., Larocca, L. J., & Axford, Y. L. (2022). Little Ice Age climate in southernmost Greenland inferred from quantitative geospatial analyses of alpine glacier reconstructions. *Quaternary Science Reviews*, *293*. https://doi.org/10.1016/j.quascirev.2022.107701

BROSSARD, T., & JOLY, D. (1994). Probability models, remote sensing and field observation: test for mapping some plant distributions in the Kongsfjord area, Svalbard. *Polar Research*, *13*(1). https://doi.org/10.1111/j.1751-8369.1994.tb00445.x

Brovkin, V., Brücher, T., Kleinen, T., Zaehle, S., Joos, F., Roth, R., Spahni, R., Schmitt, J., Fischer, H., Leuenberger, M., Stone, E. J., Ridgwell, A., Chappellaz, J., Kehrwald, N., Barbante, C., Blunier, T., & Dahl Jensen, D. (2016). Comparative carbon cycle dynamics of the present and last interglacial. *Quaternary Science Reviews*, *137*. https://doi.org/10.1016/j.quascirev.2016.01.028

Buizert, C., Gkinis, V., Severinghaus, J. P., He, F., Lecavalier, B. S., Kindler, P., Leuenberger, M., Carlson, A. E., Vinther, B., Masson-Delmotte, V., White, J. W. C., Liu, Z., Otto-Bliesner, B., & Brook, E. J. (2014). Greenland temperature

response to climate forcing during the last deglaciation. *Science*, *345*(6201). https://doi.org/10.1126/science.1254961

Cape, M. R., Straneo, F., Beaird, N., Bundy, R. M., & Charette, M. A. (2018). Nutrient release to oceans from buoyancy-driven upwelling at Greenland tidewater glaciers. *Nature Geoscience*. https://doi.org/10.1038/s41561-018-0268-4

Carlson, A. E., Stoner, J. S., Donnelly, J. P., & Hillaire-Marcel, C. (2008). Response of the southern Greenland Ice Sheet during the last two deglaciations. *Geology*, *36*(5). https://doi.org/10.1130/G24519A.1

Carlson, A. E., Winsor, K., Ullman, D. J., Brook, E. J., Rood, D. H., Axford, Y., Legrande, A. N., Anslow, F. S., & Sinclair, G. (2014). Earliest Holocene south Greenland ice sheet retreat within its late Holocene extent. *Geophysical Research Letters*, *41*(15). https://doi.org/10.1002/2014GL060800

Carrivick, J. L., Boston, C. M., Sutherland, J. L., Pearce, D., Armstrong, H., Bjørk, A., Kjeldsen, K. K., Abermann, J., Oien, R. P., & Grimes, M. (2023). Mass loss of glaciers and ice caps across Greenland since the Little Ice Age. *Geophysical Research Letters*, *50*(10), e2023GL103950.

Carrivick, J. L., & Tweed, F. S. (2013). Proglacial lakes: character, behaviour and geological importance. *Quaternary Science Reviews*, *78*, 34–52. https://doi.org/10.1016/j.quascirev.2013.07.028

Cavalli, M., & Marchi, L. (2008). Characterisation of the surface morphology of an alpine alluvial fan using airborne LiDAR. *Natural Hazards and Earth System Sciences*, *8*(2), 323–333. https://doi.org/DOI 10.5194/nhess-8-323-2008

Cavalli, M., Trevisani, S., Comiti, F., & Marchi, L. (2013). Geomorphometric assessment of spatial sediment connectivity in small Alpine catchments. *Geomorphology*, *188*, 31–41. https://doi.org/10.1016/j.geomorph.2012.05.007

Cavalli, M., Vericat, D., & Pereira, P. (2019). Mapping water and sediment connectivity. In *Science of the Total Environment* (Vol. 673). https://doi.org/10.1016/j.scitotenv.2019.04.071

Chartin, C., Evrard, O., Laceby, J. P., Onda, Y., Ottlé, C., Lefèvre, I., & Cerdan, O. (2017). The impact of typhoons on sediment connectivity: lessons learnt from contaminated coastal catchments of the Fukushima Prefecture (Japan). *Earth Surface Processes and Landforms*, *42*(2). https://doi.org/10.1002/esp.4056

Cheng, B., Adams, J., Chen, J., Zhou, A., Zhang, Q., & W MacKay, A. (2020). Neoglacial trends in diatom dynamics from a small alpine lake in the Qinling mountains of central China. *Climate of the Past*, *16*(2). https://doi.org/10.5194/cp-16-543-2020

Cihlar, J., Ly, H., & Xiao, Q. (1996). Land cover classification with AVHRR multichannel composites in northernenvironments. *Remote Sensing of Environment*, *58*(1). https://doi.org/10.1016/0034-4257(95)00210-3

Clark, P. U., & Huybers, P. (2009). Global change: Interglacial and future sea level. In *Nature* (Vol. 462, Issue 7275). https://doi.org/10.1038/462856a

Coulthard, T. J., & Van De Wiel, M. J. (2017). Modelling long term basin scale sediment connectivity, driven by spatial land use changes. *Geomorphology*, *277*, 265–281. https://doi.org/10.1016/j.geomorph.2016.05.027

Crema, S., & Cavalli, M. (2018). SedInConnect: a stand-alone, free and open source tool for the assessment of sediment connectivity. *Computers & Geosciences*, *111*, 39–45. https://doi.org/10.1016/j.cageo.2017.10.009

Cuffey, K. M., & Marshall, S. J. (2000). Substantial contribution to sea-level rise during the last interglacial from the Greenland ice sheet. *Nature*, *404*(6778). https://doi.org/10.1038/35007053

Dahl-Jensen, D., Mosegaard, K., Gundestrup, N., Clow, G. D., Johnsen, S. J., Hansen, A. W., & Balling, N. (1998). Past temperatures directly from the Greenland Ice Sheet. *Science*, *282*(5387). https://doi.org/10.1126/science.282.5387.268

Dalla Fontana, G., & Marchi, L. (1998). GIS indicators for sediment sources study in Alpine basins. *IAHS-AISH Publication*, *248*.

Daniels, F. J. A., de Molenaar, J. G., Chytry, M., & Tichy, L. (2011). Vegetation change in Southeast Greenland? Tasiilaq revisited after 40 years. *Applied Vegetation Science*, *14*(2), 230–241. https://doi.org/10.1111/j.1654-109X.2010.01107.x

Dansgaard, W., Johnsen, S. J., Clausen, H. B., & Langway, C. C. (1973). Time scale and ice accumulation during the last 125,000 years is indicated by Greenland O18 curve. In *Geological Magazine* (Vol. 110, Issue 1). https://doi.org/10.1017/S0016756800047373

Docherty, C. L., Riis, T., Hannah, D. M., Rosenhøj Leth, S., & Milner, A. M. (2018). Nutrient uptake controls and limitation dynamics in north-east Greenland streams. *Polar Research*, *37*(1). https://doi.org/10.1080/17518369.2018.1440107

Douglas, D. C., & Ovchinnikov, G. K. (1995). Comparative Evaluation of ALMAZ, ERS-1, JERS-1, and Landsat-TM for Discriminating Wet Tundra Habitats. *Polar Record*, *31*(177). https://doi.org/10.1017/S0032247400013668

Dutton, A., & Lambeck, K. (2012). Ice volume and sea level during the last interglacial. *Science*, *337*(6091). https://doi.org/10.1126/science.1205749

Dyke, L. ~M., Hughes, A. ~L. ~C., Andresen, C. ~S., Murray, T., Hiemstra, J. ~F., & Rodés, Á. (2016). Investigating the dynamics of deglaciation in coastal areas of southeast Greenland. *EGU General Assembly Conference Abstracts*, *18*.

Elberling, B., Tamstorf, M. P., Michelsen, A., Arndal, M. F., Sigsgaard, C., Illeris, L., Bay, C., Hansen, B. U., Christensen, T. R., Hansen, E. S., Jakobsen, B. H., & Beyens, L. (2008). Soil and Plant Community-Characteristics and Dynamics at Zackenberg. In *Advances in Ecological Research* (Vol. 40). https://doi.org/10.1016/S0065-2504(07)00010-4

England, J. (1999). Coalescent Greenland and Innuitian ice during the Last Glacial Maximum: Revising the Quaternary of the Canadian High Arctic. *Quaternary Science Reviews*, *18*(3). https://doi.org/10.1016/S0277-3791(98)00070-5

England, J., Atkinson, N., Bednarski, J., Dyke, A. S., Hodgson, D. A., & Ó Cofaigh, C. (2006). The Innuitian Ice Sheet: configuration, dynamics and chronology. *Quaternary Science Reviews*, *25*(7–8). https://doi.org/10.1016/j.quascirev.2005.08.007

Estrany, J., Ruiz, M., Calsamiglia, A., Carriquí, M., García-Comendador, J., Nadal, M., Fortesa, J., López-Tarazón, J. A., Medrano, H., & Gago, J. (2019). Sediment connectivity linked to vegetation using UAVs: High-resolution imagery for ecosystem management. *Science of the Total Environment*, *671*. https://doi.org/10.1016/j.scitotenv.2019.03.399

Evans, J., Ó Cofaigh, C., Dowdeswell, J. A., & Wadhams, P. (2009). Marine geophysical evidence for former expansion and flow of the Greenland Ice Sheet across the north-east Greenland continental shelf. *Journal of Quaternary Science*, *24*(3), 279–293. https://doi.org/10.1002/jqs.1231

Fyke, J., Sergienko, O., Löfverström, M., Price, S., & Lenaerts, J. T. M. (2018). An Overview of Interactions and Feedbacks Between Ice Sheets and the Earth System. *Reviews of Geophysics*, *56*(2). https://doi.org/10.1029/2018RG000600

Goldstein, S. N., Ryan, J. C., How, P. R., Esenther, S. E., Pitcher, L. H., LeWinter, A. L., Overstreet, B. T., Kyzivat, E. D., Fayne, J. V., & Smith, L. C. (2023). Proglacial river stage derived from georectified time-lapse camera images, Inglefield Land, Northwest Greenland. *Frontiers in Earth Science*, *11*. https://doi.org/10.3389/feart.2023.960363

Graly, J. A., Corbett, L. B., Bierman, P. R., Lini, A., & Neumann, T. A. (2018). Meteoric 10Be as a tracer of subglacial processes and interglacial surface exposure in Greenland. *Quaternary Science Reviews*, *191*, 118–131. https://doi.org/10.1016/j.quascirev.2018.05.009

Hachem, S., Duguay, C. R., & Allard, M. (2012). Comparison of MODIS-derived land surface temperatures with ground surface and air temperature measurements in continuous permafrost terrain. *Cryosphere*, *6*(1). https://doi.org/10.5194/tc-6-51-2012

Håkansson, L., Briner, J. P., Aldahan, A., & Possnert, G. (2011). 10Be data from meltwater channels suggest that Jameson Land, east Greenland, was ice-covered during the last glacial maximum. *Quaternary Research*, *76*(3). https://doi.org/10.1016/j.yqres.2011.06.007

Hamilton, L., Lyster, P., & Otterstad, O. (2000). Social change, ecology and climate in 20th-century Greenland. *Climatic Change*, *47*(1–2). https://doi.org/10.1023/a:1005607426021

Hanna, E., Cropper, T. E., Hall, R. J., & Cappelen, J. (2016). Greenland Blocking Index 1851–2015: a regional climate change signal. *International Journal of Climatology*, *36*(15). https://doi.org/10.1002/joc.4673

Hanna, E., Hall, R. J., Cropper, T. E., Ballinger, T. J., Wake, L., Mote, T., & Cappelen, J. (2018). Greenland blocking index daily series 1851–2015: Analysis of changes in extremes and links with North Atlantic and UK climate variability and change. *International Journal of Climatology*, *38*(9). https://doi.org/10.1002/joc.5516

Hawkings, J. R., Wadham, J. L., Tranter, M., Lawson, E., Sole, A., Cowton, T., Tedstone, A. J., Bartholomew, I., Nienow, P., Chandler, D., & Telling, J. (2015). The effect of warming climate on nutrient and solute export from the Greenland Ice Sheet. *Geochemical Perspectives Letters*, *1*(1), 94–104. https://doi.org/10.7185/geochemlet.1510

Heckmann, T., Cavalli, M., Cerdan, O., Foerster, S., Javaux, M., Lode, E., Smetanová, A., Vericat, D., & Brardinoni, F. (2018). Indices of sediment connectivity: opportunities, challenges and limitations. *Earth-Science Reviews*, *187*, 77–108. https://doi.org/10.1016/j.earscirev.2018.08.004

Heckmann, T., & Vericat, D. (2018). Computing spatially distributed sediment delivery ratios: inferring functional sediment connectivity from repeat high-resolution digital elevation models. *Earth Surface Processes and Landforms*, *43*(7), 1547–1554. https://doi.org/10.1002/esp.4334

Henderson, G. R., Barrett, B. S., Wachowicz, L. J., Mattingly, K. S., Preece, J. R., & Mote, T. L. (2021). Local and Remote Atmospheric Circulation Drivers of Arctic Change: A Review. In *Frontiers in Earth Science* (Vol. 9). https://doi.org/10.3389/feart.2021.709896

Hill, G. B., & Henry, G. H. R. (2011). Responses of High Arctic wet sedge tundra to climate warming since 1980. *Global Change Biology*, *17*(1). https://doi.org/10.1111/j.1365-2486.2010.02244.x

Hollesen, J., Elberling, B., & Jansson, P. E. (2011). Future active layer dynamics and carbon dioxide production from thawing permafrost layers in Northeast Greenland. *Global Change Biology*, *17*(2), 911–926. https://doi.org/10.1111/j.1365-2486.2010.02256.x

Hughes, A. L. C., Rainsley, E., Murray, T., Fogwill, C. J., Schnabel, C., & Xu, S. (2012). Rapid response of Helheim Glacier, southeast Greenland, to early Holocene climate warming. *Geology*, *40*(5). https://doi.org/10.1130/G32730.1

Jain, V., & Tandon, S. K. (2010). Conceptual assessment of (dis)connectivity and its application to the Ganga River dispersal system. *Geomorphology*, *118*(3–4). https://doi.org/10.1016/j.geomorph.2010.02.002

Johnsen, S. J., Dahl-Jensen, D., Gundestrup, N., Steffensen, J. P., Clausen, H. B., Miller, H., Masson-Delmotte, V., Sveinbjörnsdottir, A. E., & White, J. (2001). Oxygen isotope and palaeotemperature records from six Greenland ice-core stations: Camp Century, Dye-3, GRIP, GISP2, Renland and NorthGRIP. *Journal of Quaternary Science*, *16*(4). https://doi.org/10.1002/jqs.622

Jørgensen, C. J., Johansen, K. M. L., Westergaard-Nielsen, A., & Elberling, B. %J N. G. (2015). *Net regional methane sink in High Arctic soils of northeast Greenland*. *8*(1), 20–23.

Jungsberg, L., Herslund, L. B., Nilsson, K., Wang, S., Tomaškovičová, S., Madsen, K., Scheer, J., & Ingeman-Nielsen, T. (2022). Adaptive capacity to manage permafrost degradation in Northwest Greenland. *Polar Geography*, *45*(1). https://doi.org/10.1080/1088937X.2021.1995067

Kalantari, Z., Ferreira, C. S. S., Koutsouris, A. J., Ahmer, A. K., Cerdà, A., & Destouni, G. (2019). Assessing flood probability for transportation

infrastructure based on catchment characteristics, sediment connectivity and remotely sensed soil moisture. *Science of the Total Environment*, *661*. https://doi.org/10.1016/j.scitotenv.2019.01.009

Karami, M., Westergaard-Nielsen, A., Normand, S., Treier, U. A., Elberling, B., & Hansen, B. U. (2018). A phenology-based approach to the classification of Arctic tundra ecosystems in Greenland. *ISPRS Journal of Photogrammetry and Remote Sensing*, *146*. https://doi.org/10.1016/j.isprsjprs.2018.11.005

Kaufman, D. S., Schneider, D. P., McKay, N. P., Ammann, C. M., Bradley, R. S., Briffa, K. R., Miller, G. H., Otto-Bliesner, B. L., Overpeck, J. T., Vinther, B. M., Abbott, M., Axford, Y., Bird, B., Birks, H. J. B., Bjune, A. E., Briner, J., Cook, T., Chipman, M., Francus, P., … Thomas, E. (2009). Recent warming reverses long-term arctic cooling. *Science*, *325*(5945). https://doi.org/10.1126/science.1173983

Käykhü, J., & Pellikka, P. (1994). Remote sensing of the impact of reindeer grazing on vegetation in northern Fennoscandia using SPOT XS data. *Polar Research*, *13*(1). https://doi.org/10.3402/polar.v13i1.6686

Kelly, M., & Bennike, O. (1985). Quaternary geology of parts of central and western North Greenland: a preliminary account. *Rapport Grønlands Geologiske Undersøgelse*, *126*. https://doi.org/10.34194/rapggu.v126.7917

Khan, S. A., Kjeldsen, K. K., Kjær, K. H., Bevan, S., Luckman, A., Bjørk, A. A., Korsgaard, N. J., Box, J. E., Van Den Broeke, M., Van Dam, T. M., & Fitzner, A. (2014). Glacier dynamics at Helheim and Kangerdlugssuaq glaciers, southeast Greenland, since the Little Ice Age. *Cryosphere*, *8*(4). https://doi.org/10.5194/tc-8-1497-2014

Kjær, K. H., Bjørk, A. A., Kjeldsen, K. K., Hansen, E. S., Andresen, C. S., Siggaard-Andersen, M. L., Khan, S. A., Søndergaard, A. S., Colgan, W., Schomacker, A., Woodroffe, S., Funder, S., Rouillard, A., Jensen, J. F., & Larsen, N. K. (2022). Glacier response to the Little Ice Age during the Neoglacial cooling in Greenland. In *Earth-Science Reviews* (Vol. 227). https://doi.org/10.1016/j.earscirev.2022.103984

Klaar, M. J., Kidd, C., Malone, E., Bartlett, R., Pinay, G., Chapin, F. S., & Milner, A. (2015). Vegetation succession in deglaciated landscapes: Implications for sediment and landscape stability. *Earth Surface Processes and Landforms*, *40*(8). https://doi.org/10.1002/esp.3691

Kopp, R. E., Simons, F. J., Mitrovica, J. X., Maloof, A. C., & Oppenheimer, M. (2009). Probabilistic assessment of sea level during the last interglacial stage. *Nature*, *462*(7275). https://doi.org/10.1038/nature08686

Lambeck, K., Purcell, A., & Dutton, A. (2012). The anatomy of interglacial sea levels: The relationship between sea levels and ice volumes during the Last Interglacial. *Earth and Planetary Science Letters*, *315–316*. https://doi.org/10.1016/j.epsl.2011.08.026

Lamoureux, S. F., Lafrenière, M. J., & Favaro, E. A. (2014). Erosion dynamics following localized permafrost slope disturbances. *Geophysical Research Letters*, *41*(15). https://doi.org/10.1002/2014GL060677

Landais, A., Masson-Delmotte, V., Capron, E., Langebroek, P. M., Bakker, P., Stone, E. J., Merz, N., Raible, C. C., Fischer, H., Orsi, A., Prié, F., Vinther, B., & Dahl-Jensen, D. (2016). How warm was Greenland during the last interglacial period? *Climate of the Past*, *12*(9). https://doi.org/10.5194/cp-12-1933-2016

Landrum, L., Otto-Bliesner, B. L., Wahl, E. R., Conley, A., Lawrence, P. J., Rosenbloom, N., & Teng, H. (2013). Last millennium climate and its variability in CCSM4. *Journal of Climate*, *26*(4). https://doi.org/10.1175/JCLI-D-11-00326.1

Lane, S. N., Bakker, M., Gabbud, C., Micheletti, N., & Saugy, J. N. (2017). Sediment export, transient landscape response and catchment-scale connectivity following rapid climate warming and Alpine glacier recession. *Geomorphology*, *277*, 210–227. https://doi.org/10.1016/j.geomorph.2016.02.015

Lane, T. P., Roberts, D. H., Rea, B. R., Cofaigh, C., & Vieli, A. (2015). Controls on bedrock bedform development beneath the Uummannaq Ice Stream onset zone, West Greenland. *Geomorphology*, *231*. https://doi.org/10.1016/j.geomorph.2014.12.019

Lane, T. P., Roberts, D. H., Rea, B. R., Cofaigh, C., Vieli, A., & Rodés, A. (2014). Controls upon the Last Glacial Maximum deglaciation of the northern Uummannaq Ice Stream System, West Greenland. *Quaternary Science Reviews*, *92*. https://doi.org/10.1016/j.quascirev.2013.09.013

Larsen, N. K., Funder, S., Linge, H., Möller, P., Schomacker, A., Fabel, D., Xu, S., & Kjær, K. H. (2016). A Younger Dryas re-advance of local glaciers in north Greenland. *Quaternary Science Reviews*, *147*. https://doi.org/10.1016/j.quascirev.2015.10.036

Larsen, N. K., Kjær, K. H., Funder, S., Möller, P., van der Meer, J. J. M., Schomacker, A., Linge, H., & Darby, D. A. (2010). Late Quaternary glaciation history of northernmost Greenland - Evidence of shelf-based ice. *Quaternary Science Reviews*, *29*(25–26). https://doi.org/10.1016/j.quascirev.2010.07.027

Larsen, N. K., Søndergaard, A. S., Levy, L. B., Strunk, A., Skov, D. S., Bjørk, A., Khan, S. A., & Olsen, J. (2022). Late glacial and Holocene glaciation history of North and Northeast Greenland. *Arctic, Antarctic, and Alpine Research*, *54*(1). https://doi.org/10.1080/15230430.2022.2094607

Larsson, S. A., Kylander, M. E., Sannel, A. B. K., & Hammarlund, D. (2022). Synchronous or Not? The Timing of the Younger Dryas and Greenland Stadial-1 Reviewed Using Tephrochronology. *Quaternary*, *5*(2). https://doi.org/10.3390/quat5020019

Lecavalier, B. S., Milne, G. A., Simpson, M. J. R., Wake, L., Huybrechts, P., Tarasov, L., Kjeldsen, K. K., Funder, S., Long, A. J., Woodroffe, S., Dyke, A. S., & Larsen, N. K. (2014). A model of Greenland ice sheet deglaciation constrained by observations of relative sea level and ice extent. *Quaternary Science Reviews*, *102*. https://doi.org/10.1016/j.quascirev.2014.07.018

Lecavalier, B. S., Milne, G. A., Vinther, B. M., Fisher, D. A., Dyke, A. S., & Simpson, M. J. R. (2013). Revised estimates of Greenland ice sheet thinning

histories based on ice-core records. *Quaternary Science Reviews*, *63*. https://doi.org/10.1016/j.quascirev.2012.11.030

Letréguilly, A., Reeh, N., & Huybrechts, P. (1991). The Greenland ice sheet through the last glacial-interglacial cycle. *Global and Planetary Change*, *4*(4). https://doi.org/10.1016/0921-8181(91)90004-G

Levy, L. B., Kelly, M. A., Howley, J. A., & Virginia, R. A. (2012). Age of the Ørkendalen moraines, Kangerlussuaq, Greenland: Constraints on the extent of the southwestern margin of the Greenland Ice Sheet during the Holocene. *Quaternary Science Reviews*, *52*. https://doi.org/10.1016/j.quascirev.2012.07.021

Lewkowicz, A. G., & Harris, C. (2005). Frequency and magnitude of active-layer detachment failures in discontinuous and continuous permafrost, northern Canada. *Permafrost and Periglacial Processes*, *16*(1), 115–130. https://doi.org/10.1002/ppp.522

Lhomme, N., Clarke, G. K. C., & Ritz, C. (2005). Global budget of water isotopes inferred from polar ice sheets. *Geophysical Research Letters*, *32*(20). https://doi.org/10.1029/2005GL023774

Li, Z., Chao, B. F., Zhang, Z., Jiang, L., & Wang, H. (2022). Greenland Interannual Ice Mass Variations Detected by GRACE Time-Variable Gravity. *Geophysical Research Letters*, *49*(19). https://doi.org/10.1029/2022GL100551

Liu, C., Xu, X., Feng, X., Cheng, X., Liu, C., & Huang, H. (2023). CALC-2020: a new baseline land cover map at 10m resolution for the circumpolar Arctic. *Earth System Science Data*, *15*(1). https://doi.org/10.5194/essd-15-133-2023

Liu, Z., Carlson, A. E., He, F., Brady, E. C., Otto-Bliesner, B. L., Briegleb, B. P., Wehrenberg, M., Clark, P. U., Wu, S., Cheng, J., Zhang, J., Noone, D., & Zhu, J. (2012). Younger dryas cooling and the greenland climate response to CO2. *Proceedings of the National Academy of Sciences of the United States of America*, *109*(28). https://doi.org/10.1073/pnas.1202183109

Lizaga, I., Quijano, L., Palazón, L., Gaspar, L., & Navas, A. (2018). Enhancing Connectivity Index to Assess the Effects of Land Use Changes in a Mediterranean Catchment. *Land Degradation and Development*, *29*(3). https://doi.org/10.1002/ldr.2676

López-Blanco, E., Langen, P. L., Williams, M., Christensen, J. H., Boberg, F., Langley, K., & Christensen, T. R. (2022). The future of tundra carbon storage in Greenland – Sensitivity to climate and plant trait changes. *Science of the Total Environment*, *846*. https://doi.org/10.1016/j.scitotenv.2022.157385

Malmierca-Vallet, I., Sime, L. C., Valdes, P. J., & Tindall, J. C. (2020). Sea ice feedbacks influence the isotopic signature of Greenland ice sheet elevation changes: Last interglacial HadCM3 simulations. *Climate of the Past*, *16*(6). https://doi.org/10.5194/cp-16-2485-2020

Mancini, D., & Lane, S. N. (2020). Changes in sediment connectivity following glacial debuttressing in an Alpine valley system. *Geomorphology*, *352*. https://doi.org/10.1016/j.geomorph.2019.106987

Mann, M. E., Zhang, Z., Hughes, M. K., Bradley, R. S., Miller, S. K., Rutherford, S., & Ni, F. (2008). Proxy-based reconstructions of hemispheric and global surface temperature variations over the past two millennia. *Proceedings of the National Academy of Sciences of the United States of America*, *105*(36). https://doi.org/10.1073/pnas.0805721105

Marchi, L., & Dalla Fontana, G. (2005). GIS morphometric indicators for the analysis of sediment dynamics in mountain basins. *Environmental Geology*, *48*(2). https://doi.org/10.1007/s00254-005-1292-4

Marcott, S. A., Shakun, J. D., Clark, P. U., & Mix, A. C. (2013). A reconstruction of regional and global temperature for the past 11,300 years. *Science*, *339*(6124). https://doi.org/10.1126/science.1228026

Markon, C. J., & Derksen, D. V. (1994). Identification of tundra land cover near Teschekpuk Lake, Alaska using SPOT satellite data. *Arctic*, *47*(3). https://doi.org/10.14430/arctic1292

Marshall, G. J., Dowdeswell, J. A., & Rees, W. G. (1994). The spatial and temporal effect of cloud cover on the acquisition of high quality landsat imagery in the European Arctic sector. *Remote Sensing of Environment*, *50*(2). https://doi.org/10.1016/0034-4257(94)90041-8

Masson-Delmotte, V., Swingedouw, D., Landais, A., Seidenkrantz, M. S., Gauthier, E., Bichet, V., Massa, C., Perren, B., Jomelli, V., Adalgeirsdottir, G., Hesselbjerg Christensen, J., Arneborg, J., Bhatt, U., Walker, D. A., Elberling, B., Gillet-Chaulet, F., Ritz, C., Gallée, H., van den Broeke, M., … Vinther, B. (2012). Greenland climate change: From the past to the future. *Wiley Interdisciplinary Reviews: Climate Change*, *3*(5), 427–449. https://doi.org/10.1002/WCC.186

McConnell, J. R., Edwards, R., Kok, G. L., Flanner, M. G., Zender, C. S., Saltzman, E. S., Banta, J. R., Pasteris, D. R., Carter, M. M., & Kahl, J. D. W. (2007). 20th-Century industrial black carbon emissions altered arctic climate forcing. *Science*, *317*(5843). https://doi.org/10.1126/science.1144856

McFarlin, J. M., Axford, Y., Osburn, M. R., Kelly, M. A., Osterberg, E. C., & Farnsworth, L. B. (2018). Pronounced summer warming in northwest Greenland during the Holocene and Last Interglacial. *Proceedings of the National Academy of Sciences of the United States of America*, *115*(25). https://doi.org/10.1073/pnas.1720420115

Meese, D. A., Gow, A. J., Grootes, P., Mayewski, P. A., Ram, M., Stuiver, M., Taylor, K. C., Waddington, E. D., & Zielinski, G. A. (1994). The accumulation record from the GISP2 core as an indicator of climate change throughout the holocene. *Science*, *266*(5191). https://doi.org/10.1126/science.266.5191.1680

Merz, N., Born, A., Raible, C. C., Fischer, H., & Stocker, T. F. (2014). Dependence of Eemian Greenland temperature reconstructions on the ice sheet topography. *Climate of the Past*, *10*(3). https://doi.org/10.5194/cp-10-1221-2014

Mieville, A., Granier, C., Liousse, C., Guillaume, B., Mouillot, F., Lamarque, J. F., Grégoire, J. M., & Pétron, G. (2010). Emissions of gases and particles from biomass burning during the 20th century using satellite data and an historical

reconstruction. *Atmospheric Environment*, *44*(11). https://doi.org/10.1016/j.atmosenv.2010.01.011

Möller, P., Larsen, N. K., Kjær, K. H., Funder, S., Schomacker, A., Linge, H., & Fabel, D. (2010). Early to middle Holocene valley glaciations on northernmost Greenland. *Quaternary Science Reviews*, *29*(25–26). https://doi.org/10.1016/j.quascirev.2010.06.044

Montgomery, D. R., & Dietrich, W. E. (1994). A physically based model for the topographic control on shallow landsliding. *Water Resources Research*, *30*(4). https://doi.org/10.1029/93WR02979

MOSBECH, A., & HANSEN, B. U. (1994). Comparison of satellite imagery and infrared aerial photography as vegetation mapping methods in an arctic study area; Jameson Land, East Greenland. *Polar Research*, *13*(1). https://doi.org/10.1111/j.1751-8369.1994.tb00444.x

Mosley-Thompson, E., Readinger, C. R., Craigmile, P., Thompson, L. G., & Calder, C. A. (2005). Regional sensitivity of Greenland precipitation to NAO variability. *Geophysical Research Letters*, *32*(24). https://doi.org/10.1029/2005GL024776

Mouillot, F., Narasimha, A., Balkanski, Y., Lamarque, J. F., & Field, C. B. (2006). Global carbon emissions from biomass burning in the 20th century. *Geophysical Research Letters*, *33*(1). https://doi.org/10.1029/2005GL024707

Myers-Smith, I. H., Hik, D. S., Kennedy, C., Cooley, D., Johnstone, J. F., Kenney, A. J., & Krebs, C. J. (2011). Expansion of canopy-forming willows over the twentieth century on Herschel Island, Yukon Territory, Canada. *Ambio*, *40*(6). https://doi.org/10.1007/s13280-011-0168-y

Najafi, S., Dragovich, D., Heckmann, T., & Sadeghi, S. H. (2021). Sediment connectivity concepts and approaches. In *Catena* (Vol. 196). https://doi.org/10.1016/j.catena.2020.104880

Normand, S., Randin, C., Ohlemüller, R., Bay, C., Høye, T. T., Kjær, E. D., Körner, C., Lischke, H., Maiorano, L., Paulsen, J., Pearman, P. B., Psomas, A., Treier, U. A., Zimmermann, N. E., & Svenning, J. C. (2013). A greener Greenland? Climatic potential and long-term constraints on future expansions of trees and shrubs. *Philosophical Transactions of the Royal Society B: Biological Sciences*, *368*(1624). https://doi.org/10.1098/rstb.2012.0479

Nuttall, M. (2016). Living in a world of movement: Human resilience to environmental instability in Greenland. In *Anthropology and Climate Change: From Encounters to Actions*. https://doi.org/10.4324/9781315434773-26

Ó Cofaigh, C., Dowdeswell, J. A., Evans, J., Kenyon, N. H., Taylor, J., Mienert, J., & Wilken, M. (2004). Timing and significance of glacially influenced mass-wasting in the submarine channels of the Greenland Basin. *Marine Geology*, *207*(1–4). https://doi.org/10.1016/j.margeo.2004.02.009

Oerlemans, J. (1991). The mass balance of the Greenland ice sheet: sensitivity to climate change as revealed by energy-balance modelling. *Holocene*, *1*(1). https://doi.org/10.1177/095968369100100106

Oerlemans, J., Dahl-Jensen, D., & Masson-Delmotte, V. (2006). Ice Sheets and Sea Level. *Science*, *313*(5790). https://doi.org/10.1126/science.313.5790.1043c

Oksman, M., Kvorning, A. B., Larsen, S. H., Kjeldsen, K. K., Mankoff, K. D., Colgan, W., Andersen, T. J., Nørgaard-Pedersen, N., Seidenkrantz, M. S., Mikkelsen, N., & Ribeiro, S. (2022). Impact of freshwater runoff from the southwest Greenland Ice Sheet on fjord productivity since the late 19th century. *Cryosphere*, *16*(6). https://doi.org/10.5194/tc-16-2471-2022

Ottlé, C., Lescure, J., Maignan, F., Poulter, B., Wang, T., & Delbart, N. %J E. S. S. D. (2013). *Use of various remote sensing land cover products for plant functional type mapping over Siberia*. *5*(2), 331.

Otto-Bliesner, B. L., Marshall, S. J., Overpeck, J. T., Miller, G. H., & Hu, A. (2006). Simulating arctic climate warmth and icefield retreat in the last interglaciation. *Science*, *311*(5768). https://doi.org/10.1126/science.1120808

Palmtag, J., Hugelius, G., Lashchinskiy, N., Tamstorf, M. P., Richter, A., Elberling, B., & Kuhry, P. (2015). Storage, landscape distribution, and burial history of soil organic matter in contrasting areas of continuous permafrost. *Arctic, Antarctic, and Alpine Research*, *47*(1). https://doi.org/10.1657/AAAR0014-027

Pearce, C. M. (1991). Mapping muskox habitat in the Canadian High Arctic with SPOT satellite data. *Arctic*, *44*(Suppl. 1). https://doi.org/10.14430/arctic1570

Pearson, R. G., Phillips, S. J., Loranty, M. M., Beck, P. S. A., Damoulas, T., Knight, S. J., & Goetz, S. J. (2013). Shifts in Arctic vegetation and associated feedbacks under climate change. *Nature Climate Change*, *3*(7). https://doi.org/10.1038/nclimate1858

Pedersen, J. B. T., Kroon, A., & Jakobsen, B. H. (2011). Holocene sea-level reconstruction in the Young Sound region, Northeast Greenland. *Journal of Quaternary Science*, *26*(2), 219–226. https://doi.org/10.1002/jqs.1449

Perner, K., Moros, M., Lloyd, J. M., Jansen, E., & Stein, R. (2015). Mid to late Holocene strengthening of the East Greenland Current linked to warm subsurface Atlantic water. *Quaternary Science Reviews*, *129*. https://doi.org/10.1016/j.quascirev.2015.10.007

Poursanidis, D., Chrysoulakis, N., & Mitraka, Z. (2015). Landsat 8 vs. Landsat 5: A comparison based on urban and peri-urbanland cover mapping. *International Journal of Applied Earth Observation and Geoinformation*, *35*(PB). https://doi.org/10.1016/j.jag.2014.09.010

Preece, J. R., Mote, T. L., Cohen, J., Wachowicz, L. J., Knox, J. A., Tedesco, M., & Kooperman, G. J. (2023). Summer atmospheric circulation over Greenland in response to Arctic amplification and diminished spring snow cover. *Nature Communications*, *14*(1). https://doi.org/10.1038/s41467-023-39466-6

Rasmussen, L. H., Zhang, W., Hollesen, J., Cable, S., Christiansen, H. H., Jansson, P. E., & Elberling, B. (2018). Modelling present and future permafrost thermal regimes in Northeast Greenland. *Cold Regions Science and Technology*, *146*. https://doi.org/10.1016/j.coldregions.2017.10.011

Rasmussen, S. O., Andersen, K. K., Svensson, A. M., Steffensen, J. P., Vinther, B. M., Clausen, H. B., Siggaard-Andersen, M. L., Johnsen, S. J., Larsen, L. B.,

Dahl-Jensen, D., Bigler, M., Röthlisberger, R., Fischer, H., Goto-Azuma, K., Hansson, M. E., & Ruth, U. (2006). A new Greenland ice core chronology for the last glacial termination. *Journal of Geophysical Research Atmospheres*, *111*(6). https://doi.org/10.1029/2005JD006079

Rasmussen, S. O., Bigler, M., Blockley, S. P., Blunier, T., Buchardt, S. L., Clausen, H. B., Cvijanovic, I., Dahl-Jensen, D., Johnsen, S. J., Fischer, H., Gkinis, V., Guillevic, M., Hoek, W. Z., Lowe, J. J., Pedro, J. B., Popp, T., Seierstad, I. K., Steffensen, J. P., Svensson, A. M., … Winstrup, M. (2014). A stratigraphic framework for abrupt climatic changes during the Last Glacial period based on three synchronized Greenland ice-core records: Refining and extending the INTIMATE event stratigraphy. *Quaternary Science Reviews*, *106*. https://doi.org/10.1016/j.quascirev.2014.09.007

Raynolds, M. K., Walker, D. A., Balser, A., Bay, C., Campbell, M., Cherosov, M. M., Daniels, F. J. A., Eidesen, P. B., Emiokhina, K. A., Frost, G. V, Jedrzejek, B., Jorgenson, M. T., Kennedy, B. E., Kholod, S. S., Lavrinenko, I. A., Lavrinenko, O. V, Magnusson, B., Matveyeva, N. V, Metusalemsson, S., … Troeva, E. (2019). A raster version of the Circumpolar Arctic Vegetation Map (CAVM). *Remote Sensing of Environment*, *232*. https://doi.org/UNSP 111297 10.1016/j.rse.2019.111297

Reeh, N. (2017). Greenland Ice Shelves and Ice Tongues. In *Springer Polar Sciences*. https://doi.org/10.1007/978-94-024-1101-0_4

Rees, W. G., & Danks, F. S. (2007). Derivation and assessment of vegetation maps for reindeer pasture analysis in Arctic European Russia. *Polar Record*, *43*(4). https://doi.org/10.1017/S0032247407006420

Rignot, E., Fenty, I., Xu, Y., Cai, C., Velicogna, I., Cofaigh, C., Dowdeswell, J. A., Weinrebe, W., Catania, G., & Duncan, D. (2016). Bathymetry data reveal glaciers vulnerable to ice-ocean interaction in Uummannaq and Vaigat glacial fjords, west Greenland. *Geophysical Research Letters*, *43*(6). https://doi.org/10.1002/2016GL067832

Roberts, D. H., Rea, B. R., Lane, T. P., Schnabel, C., & Rodés, A. (2013). New constraints on Greenland ice sheet dynamics during the last glacial cycle: Evidence from the Uummannaq ice stream system. *Journal of Geophysical Research: Earth Surface*, *118*(2). https://doi.org/10.1002/jgrf.20032

Rosen, J. L., Brook, E. J., Severinghaus, J. P., Blunier, T., Mitchell, L. E., Lee, J. E., Edwards, J. S., & Gkinis, V. (2014). An ice core record of near-synchronous global climate changes at the Bølling transition. *Nature Geoscience*, *7*(6). https://doi.org/10.1038/ngeo2147

Rysgaard, S., Nielsen, T. G., & Hansen, B. W. (1999). Seasonal variation in nutrients, pelagic primary production and grazing in a high-Arctic coastal marine ecosystem, Young Sound, Northeast Greenland. *Marine Ecology Progress Series*, *179*, 13–25. https://doi.org/DOI 10.3354/meps179013

Sbarra, C. M., Briner, J. P., Graham, B. L., Poinar, K., Thomas, E. K., & Young, N. E. (2022). Evidence for a more extensive Greenland Ice Sheet in southwestern

Greenland during the Last Glacial Maximum. *Geosphere*, *18*(4). https://doi.org/10.1130/GES02432.1

Schaffer, J., Timmermann, R., Erik Arndt, J., Savstrup Kristensen, S., Mayer, C., Morlighem, M., & Steinhage, D. (2016). A global, high-resolution data set of ice sheet topography, cavity geometry, and ocean bathymetry. *Earth System Science Data*, *8*(2). https://doi.org/10.5194/essd-8-543-2016

Schuur, E. A. G., Vogel, J. G., Crummer, K. G., Lee, H., Sickman, J. O., & Osterkamp, T. E. (2009). The effect of permafrost thaw on old carbon release and net carbon exchange from tundra. *Nature*, *459*(7246). https://doi.org/10.1038/nature08031

Schweinsberg, A. D., Briner, J. P., Miller, G. H., Lifton, N. A., Bennike, O., & Graham, B. L. (2018). Holocene mountain glacier history in the Sukkertoppen Iskappe area, southwest Greenland. *Quaternary Science Reviews*, *197*, 142–161. https://doi.org/10.1016/j.quascirev.2018.06.014

Screen, J. A., & Simmonds, I. (2010). The central role of diminishing sea ice in recent Arctic temperature amplification. *Nature*, *464*(7293), 1334–1337. https://doi.org/10.1038/nature09051

Serra, P., Pons, X., & Saurí, D. (2003). Post-classification change detection with data from different sensors: Some accuracy considerations. *International Journal of Remote Sensing*, *24*(16). https://doi.org/10.1080/0143116021000021189

Serreze, M. C., & Barry, R. G. (2011). Processes and impacts of Arctic amplification: A research synthesis. *Global and Planetary Change*, *77*(1–2), 85–96. https://doi.org/10.1016/j.gloplacha.2011.03.004

Shakun, J. D., Clark, P. U., He, F., Marcott, S. A., Mix, A. C., Liu, Z., Otto-Bliesner, B., Schmittner, A., & Bard, E. (2012). Global warming preceded by increasing carbon dioxide concentrations during the last deglaciation. *Nature*, *484*(7392). https://doi.org/10.1038/nature10915

Simon, Q., Hillaire-Marcel, C., St-Onge, G., & Andrews, J. T. (2014). North-eastern Laurentide, western Greenland and southern Innuitian ice stream dynamics during the last glacial cycle. *Journal of Quaternary Science*, *29*(1). https://doi.org/10.1002/jqs.2648

Simpson, M. J. R., Milne, G. A., Huybrechts, P., & Long, A. J. (2009). Calibrating a glaciological model of the Greenland ice sheet from the Last Glacial Maximum to present-day using field observations of relative sea level and ice extent. *Quaternary Science Reviews*, *28*(17–18). https://doi.org/10.1016/j.quascirev.2009.03.004

Slabon, P., Dorschel, B., Jokat, W., Myklebust, R., Hebbeln, D., & Gebhardt, C. (2016). Greenland ice sheet retreat history in the northeast Baffin Bay based on high-resolution bathymetry. *Quaternary Science Reviews*, *154*. https://doi.org/10.1016/j.quascirev.2016.10.022

Stone, E. J., Lunt, D. J., Annan, J. D., & Hargreaves, J. C. (2013). Quantification of the Greenland ice sheet contribution to Last Interglacial sea level rise. *Climate of the Past*, *9*(2). https://doi.org/10.5194/cp-9-621-2013

Straneo, F., & Heimbach, P. (2013). North Atlantic warming and the retreat of Greenland's outlet glaciers. In *Nature* (Vol. 504, Issue 7478). https://doi.org/10.1038/nature12854

Stranne, C., Nilsson, J., Ulfsbo, A., O'Regan, M., Coxall, H. K., Meire, L., Muchowski, J., Mayer, L. A., Brüchert, V., Fredriksson, J., Thornton, B., Chawarski, J., West, G., Weidner, E., & Jakobsson, M. (2021). The climate sensitivity of northern Greenland fjords is amplified through sea-ice damming. *Communications Earth and Environment*, *2*(1). https://doi.org/10.1038/s43247-021-00140-8

Swann, A. L., Fung, I. Y., Levis, S., Bonan, G. B., & Doney, S. C. (2010). Changes in arctic vegetation amplify high-latitude warming through the greenhouse effect. *Proceedings of the National Academy of Sciences of the United States of America*, *107*(4). https://doi.org/10.1073/pnas.0913846107

Syvitski, J. P. M., Stein, A. B., & Andrews, J. T. (2001). Icebergs and the sea floor of the East Greenland (Kangerlussuaq) continental margin. *Arctic, Antarctic, and Alpine Research*, *33*(1). https://doi.org/10.2307/1552277

Takeuchi, W., Tamura, M., & Yasuoka, Y. (2003). Estimation of methane emission from West Siberian wetland by scaling technique between NOAA AVHRR and SPOT HRV. *Remote Sensing of Environment*, *85*(1). https://doi.org/10.1016/S0034-4257(02)00183-9

Tarasov, L., & Peltier, W. R. (2003). Greenland glacial history, borehole constraints, and Eemian extent. *Journal of Geophysical Research: Solid Earth*, *108*(B3). https://doi.org/10.1029/2001jb001731

Tarboton, D. G. (1997). A new method for the determination of flow directions and upslope areas in grid digital elevation models. *Water Resources Research*, *33*(2), 309–319. https://doi.org/Doi 10.1029/96wr03137

Trevisani, S., & Cavalli, M. (2016). Topography-based flow-directional roughness: Potential and challenges. *Earth Surface Dynamics*, *4*(2). https://doi.org/10.5194/esurf-4-343-2016

Urban, M., Eberle, J., Hüttich, C., Schmullius, C., & Herold, M. (2013). Comparison of satellite-derived land surface temperature and air temperature from meteorological stations on the pan-arctic scale. *Remote Sensing*, *5*(5). https://doi.org/10.3390/rs5052348

Vasskog, K., Langebroek, P. M., Andrews, J. T., Nilsen, J. E. Ø., & Nesje, A. (2015). The Greenland Ice Sheet during the last glacial cycle: Current ice loss and contribution to sea-level rise from a palaeoclimatic perspective. In *Earth-Science Reviews* (Vol. 150). https://doi.org/10.1016/j.earscirev.2015.07.006

Vigiak, O., Borselli, L., Newham, L. T. H., McInnes, J., & Roberts, A. M. (2012). Comparison of conceptual landscape metrics to define hillslope-scale sediment delivery ratio. *Geomorphology*, *138*(1). https://doi.org/10.1016/j.geomorph.2011.08.026

Vinther, B. M., Buchardt, S. L., Clausen, H. B., Dahl-Jensen, D., Johnsen, S. J., Fisher, D. A., Koerner, R. M., Raynaud, D., Lipenkov, V., Andersen, K. K., Blunier, T., Rasmussen, S. O., Steffensen, J. P., & Svensson, A. M. (2009).

Holocene thinning of the Greenland ice sheet. *Nature*, *461*(7262). https://doi.org/10.1038/nature08355

Vowles, T., & Björk, R. G. (2019). Implications of evergreen shrub expansion in the Arctic. In *Journal of Ecology* (Vol. 107, Issue 2). https://doi.org/10.1111/1365-2745.13081

Walker, D. A. (1999). An integrated vegetation mapping approach for northern Alaska (1:4 M scale). *International Journal of Remote Sensing*, *20*(15–16). https://doi.org/10.1080/014311699211534

Walker, D. A., Raynolds, M. K., Daniëls, F. J. A., Einarsson, E., Elvebakk, A., Gould, W. A., Katenin, A. E., Kholod, S. S., Markon, C. J., & Melnikov, E. S. %J J. of V. S. (2005). *The circumpolar Arctic vegetation map*. *16*(3), 267–282.

Walling, D. E. (1983). THE SEDIMENT DELIVERY PROBLEM EX4 4RJ (Great Britain). In *Journal of Hydrology* (Vol. 65).

Walling, D. E., & Zhang, Y. (2004). Predicting slope-channel connectivity: A national-scale approach. *IAHS-AISH Publication*, *288*.

Wangner, D. J., Jennings, A. E., Vermassen, F., Dyke, L. M., Hogan, K. A., Schmidt, S., Kjær, K. H., Knudsen, M. F., & Andresen, C. S. (2018). A 2000-year record of ocean influence on Jakobshavn Isbræ calving activity, based on marine sediment cores. *Holocene*, *28*(11). https://doi.org/10.1177/0959683618788701

Wangner, D. J., Sicre, M. A., Kjeldsen, K. K., Jaeger, J. M., Bjørk, A. A., Vermassen, F., Sha, L., Kjær, K. H., Klein, V., & Andresen, C. S. (2020). Sea Surface Temperature Variability on the SE-Greenland Shelf (1796–2013 CE) and Its Influence on Thrym Glacier in Nørre Skjoldungesund. *Paleoceanography and Paleoclimatology*, *35*(3). https://doi.org/10.1029/2019PA003692

Weidick, A., Bennike, O., Citterio, M., & Nørgaard-Pedersen, N. (2012). Neoglacial and historical glacier changes around Kangersuneq fjord in southern West Greenland. *Geological Survey of Denmark and Greenland Bulletin*, *27*. https://doi.org/10.34194/geusb.v27.4694

Westergaard-Nielsen, A., Karami, M., Hansen, B. U., Westermann, S., & Elberling, B. (2018). Contrasting temperature trends across the ice-free part of Greenland. *Scientific Reports*, *8*(1). https://doi.org/10.1038/s41598-018-19992-w

Westermann, S., Elberling, B., Højlund Pedersen, S., Stendel, M., Hansen, B. U., & Liston, G. E. (2015). Future permafrost conditions along environmental gradients in Zackenberg, Greenland. *Cryosphere*, *9*(2). https://doi.org/10.5194/tc-9-719-2015

Westermann, S., Østby, T. I., Gisnås, K., Schuler, T. V, & Etzelmüller, B. %J T. C. (2015). *A ground temperature map of the North Atlantic permafrost region based on remote sensing and reanalysis data*. *9*(3), 1303–1319.

Wilson, J. P., Jilinski, P., & Gallant, J. C. (2000). Secondary Topographic Attributes. Terrain Analysis: Principles and Applications. *John Wiley and Sons. Springer*.

Winkelmann, D., Jokat, W., Jensen, L., & Schenke, H. W. (2010). Submarine end moraines on the continental shelf off NE Greenland - Implications for Lateglacial dynamics. *Quaternary Science Reviews*, *29*(9–10). https://doi.org/10.1016/j.quascirev.2010.02.002

Yau, A. M., Bender, M. L., Robinson, A., & Brook, E. J. (2016). Reconstructing the last interglacial at Summit, Greenland: Insights from GISP2. *Proceedings of the National Academy of Sciences of the United States of America*, *113*(35). https://doi.org/10.1073/pnas.1524766113

Young, J. C., Arendt, A., Hock, R., & Pettit, E. (2018). The challenge of monitoring glaciers with extreme altitudinal range: mass-balance reconstruction for Kahiltna Glacier, Alaska. *Journal of Glaciology*, *64*(243), 75–88. https://doi.org/10.1017/jog.2017.80

Young, N. E., & Briner, J. P. (2015). Holocene evolution of the western Greenland Ice Sheet: Assessing geophysical ice-sheet models with geological reconstructions of ice-margin change. In *Quaternary Science Reviews* (Vol. 114). https://doi.org/10.1016/j.quascirev.2015.01.018

Zanaga, D., Van De Kerchove, R., De Keersmaecker, W., Souverijns, N., Brockmann, C., Quast, R., Wevers, J., Grosu, A., Paccini, A., Vergnaud, S., Cartus, O., Santoro, M., Fritz, S., Georgieva, I., Lesiv, M., Carter, S., Herold, M., Linlin, L., Tsendbazar, N., … Arino, O. (2021). ESA WorldCover 10 m 2020 v100. *Meteosat Second Generation Evapotranspiration (MET)*.

Zanandrea, F., Michel, G. P., Kobiyama, M., Censi, G., & Abatti, B. H. (2021). Spatial-temporal assessment of water and sediment connectivity through a modified connectivity index in a subtropical mountainous catchment. *Catena*, *204*. https://doi.org/10.1016/j.catena.2021.105380

Zhou, T. J., Li, B., Man, W. M., Zhang, L. X., & Zhang, J. (2011). A comparison of the Medieval Warm Period, Little Ice Age and 20th century warming simulated by the FGOALS climate system model. *Chinese Science Bulletin*, *56*(28–29). https://doi.org/10.1007/s11434-011-4641-6

Zimov, S. A., Schuur, E. A. G., & Stuart Chapin, F. (2006). Permafrost and the global carbon budget. In *Science* (Vol. 312, Issue 5780). https://doi.org/10.1126/science.1128908

Zreda, M., England, J., Phillips, F., Elmore, D., & Sharma, P. (1999). Unblocking of the Nares Strait by Greenland and Ellesmere ice-sheet retreat 10,000 years ago. *Nature*, *398*(6723). https://doi.org/10.1038/18197

Chapter 3: Landcover Change around Greenland's Periphery since the late 1980s

3.1 Introduction

The Arctic has been warming at double the global mean rate since the 1970s (Chylek et al., 2009). Some of the most pronounced recent warming has been across Greenland, where mean annual air temperatures between 2007 and 2012 were 3ºC warmer compared to the 1979 to 2000 average (Mayewski et al., 2014). More extremes of temperature and precipitation are expected in the near future as Greenland's climate resilience decreases and non-linear land-climate system feedbacks develop (Overland et al., 2020), including soil development and vegetation change, land surface albedo change, and permafrost degradation. The environmental impacts of Arctic climate change are most obviously manifest in Greenland's abundant, expanding and rapidly evolving proglacial landscapes (Carrivick and Heckmann, 2018). Specifically, Greenland's PGICs are shrinking, glacier-fed lakes are expanding, permafrost lakes are draining, rivers are transporting vast amounts of sediment and aggrading and widening, and vegetation cover and species diversity are expanding, largely coincident with Arctic shrubification (Anderson et al., 2017; Overeem et al., 2017; Bamber et al., 2018; Box et al., 2018; Box et al., 2019; Teufel and Sushama, 2019; Shugar et al., 2020; Mekonnen et al., 2021).

Understanding ongoing climate-landscape interactions across Greenland is crucial for modelling Arctic climate (Hibbard et al., 2010), monitoring and managing water resources (Pekel et al., 2016), determining the health and livelihoods of Arctic societies Hjort et al., 2018), and for maximising economic development prospects (Ford and Goldhar, 2012). Specifically in Greenland, climate-landscape feedbacks include: (i) exposure of dark surfaces such as water and bedrock that have a high absorption of solar energy, i.e. a low albedo) causing increased thermal retention (Lunt et al., 2004; Mernild et al., 2015); (ii) increased deposition of organic matter, both terrestrially and within streams and eventually fjords as a consequence of warming-induced soil formation and permafrost degradation which drives further colonisation of vegetation in areas where sediment redistribution is common and stream networks diverge regularly (Lindborg et al., 2016); (iii) expedited degradation of permafrost by vegetation establishment and expansion subsequently releasing

substantial previously-stored greenhouse gases (Yi et al., 2007; Daanen et al., 2011; Mekonnen et al 2021); and (iv) increased/altered biogeochemical weathering and reactions coinciding with changes in microbial community composition driven by warming and increased moisture within the environment which affects gas (e.g. CO_2, O_2, N_2O) production and sequestration rates (Barcena et al., 2011; Musilova et al., 2017). The rates of change associated with these feedbacks are highly uncertain, not least because quantification of changing landcover in Greenland is needed to identify sensitive sites and to elucidate the driving earth surface processes.

Large-scale analyses of landcover changes have been hindered by a lack of computational power and the relative scarcity of satellite imagery prior to 2000. Previous analyses of landcover change across Greenland have either been spatially-localised (e.g. Elberling et al., 2008; Heindel et al., 2015; Palmtag et al., 2018), limited to modern 21st-century changes (e.g. Raynolds et al., 2019; Karami et al., 2018), or specialist in scope regarding the specific type of landcover observed (e.g. Jørgensen et al's (2015) study of vegetation in north east Greenland and Heindel et al.'s 2015 study of soil erosion in Kangerlussuaq. When regional analyses have been undertaken for Greenland, they have been relatively coarse (> 1 km) resolution (e.g. Loveland et al., 2000; Walker et al., 2002), which precludes analysis of important intra-catchment or 'process-form system' dynamics (cf. MacMillan and Shary, 2009), or not specifically designed for and verified in Greenland; e.g. CALC-2020 landcover map of the Arctic using multi-band Sentinel imagery (Liu et al., 2023). There has been no quantification of, or accounting for, the complex landcover responses across Greenland to accelerated atmospheric warming since the late 1980s.

Here spatiotemporal landcover change is reported between the late 1980s and 2010s across Greenland. This landcover change detection is achieved at 30 m spatial resolution, thereby permitting analysis and understanding of both inter- and intra-catchment earth surface processes that drive and explain regional landcover change patterns. This research presents a novel landcover phase change conceptual model for Greenland based on spatially-aggregated measurements of predominant inter-class changes and applies a rigorous spatially-distributed assessment of landcover change accuracy directly. These datasets have widespread application within the geosciences and more widely in land management and natural resource-based economic sectors.

3.1.1 Aim and Objectives

The overall aim of this research was to classify, for two time periods, predominant geophysical landcover classes in Greenland and quantify change in landscape composition in response to climate change. These classes, as outlined and justified in the preceding literature review, cover all salient features of proglacial systems of variable exposure: i) snow and ice, ii) (sediment-rich, flowing) meltwater, iii) freshwater (still, low suspended sediment), iv) barren ground (fine-grained/dry sediment, coarse-grained/wet sediments, and bedrock of variable weathering), v) tundra vegetation, and vi) dense/wetland vegetation. Several objectives are defined, the accomplishment of all will realise this overarching aim. The objectives of this chapter are:

1) To produce high-quality, topographically correct Landsat image mosaics for both the 1980s and late 2010s
2) To classify dominant landcover classes for both time periods
3) To quantify landcover change across Greenland's proglacial periphery between the late 1980s and late 2010s.
4) To identify, if present, a relationship between climate warming over the study period and landcover changes.

3.2 Methods

This research is concerned with all glacier ice-free proglacial land surfaces surrounding Greenland's ice sheet, as well as the margins of the ice sheet. Figure 3.1 shows the predominant areas of interest in this chapter, the glacier ice-free periphery. The entire workflow of analysis encompasses extremely rigorous image preprocessing, classification, accuracy assessment, change detection and analysis, change accuracy assessment, and finally relating changes to calculated climate warming variables. The subsequent sub-sections within this methods section will outline the methods and data in detail, justification for their application here, and some preliminary results of exploratory statistical and accuracy assessments.

Figure 3.1. Map of glacier ice-free areas (green) around Greenland's periphery.

3.2.1 Image Preprocessing

This study required the design and implementation of a rigorous pre-processing and classification workflow, leveraging Google Earth Engine (GEE) computing power to analyse imagery from two time periods; Landsat-5 Thematic Mapper (TM) for the late 1980s (July to Sept, 1986 to 1989 inclusive) and Landsat-8 Operational Land Imager (OLI) for the late 2010s (July to Sept, 2016 to 2019 inclusive). Multi-month multi-year mosaics were produced as: (i) the temporal resolution is limited by the 16-day return period for Landsat imaging, (ii) cloud cover and orographic shadowing are particularly problematic in certain regions of Greenland (Marshall et al., 1994), and (iii) there is poor Landsat coverage for the south, south west, and north west of Greenland during the late eighties (Goward et al., 2006). The pre-processing of Landsat imagery is required to produce the most accurate and highest quality image mosaic representing landcover at each point on the surface for the respective time periods and to negate many of the limitations imposed on imagery from Greenland. A rigorous Landsat image pre-processing procedure has been developed, shown in Figure 3.2. This work leverages and utilises the parallel processing power of Google Earth Engine (GEE) to conduct this pre-processing for the first time at a national scale and 30m resolution in Greenland. GEE is a cloud-based computing environment with access to a wide variety of open-source datasets, including the full archive of Landsat imagery (Gorelick et al., 2017). The large parallel computing platform enables high-resolution analysis over various spatial and temporal timescales. The entire Landsat collection is filtered temporally, spatially, and based on the cloud score before being topographically corrected using the Modified Sun-Canopy-Sensor method (cf. Soenen et al., 2005) (Figure 3.2).

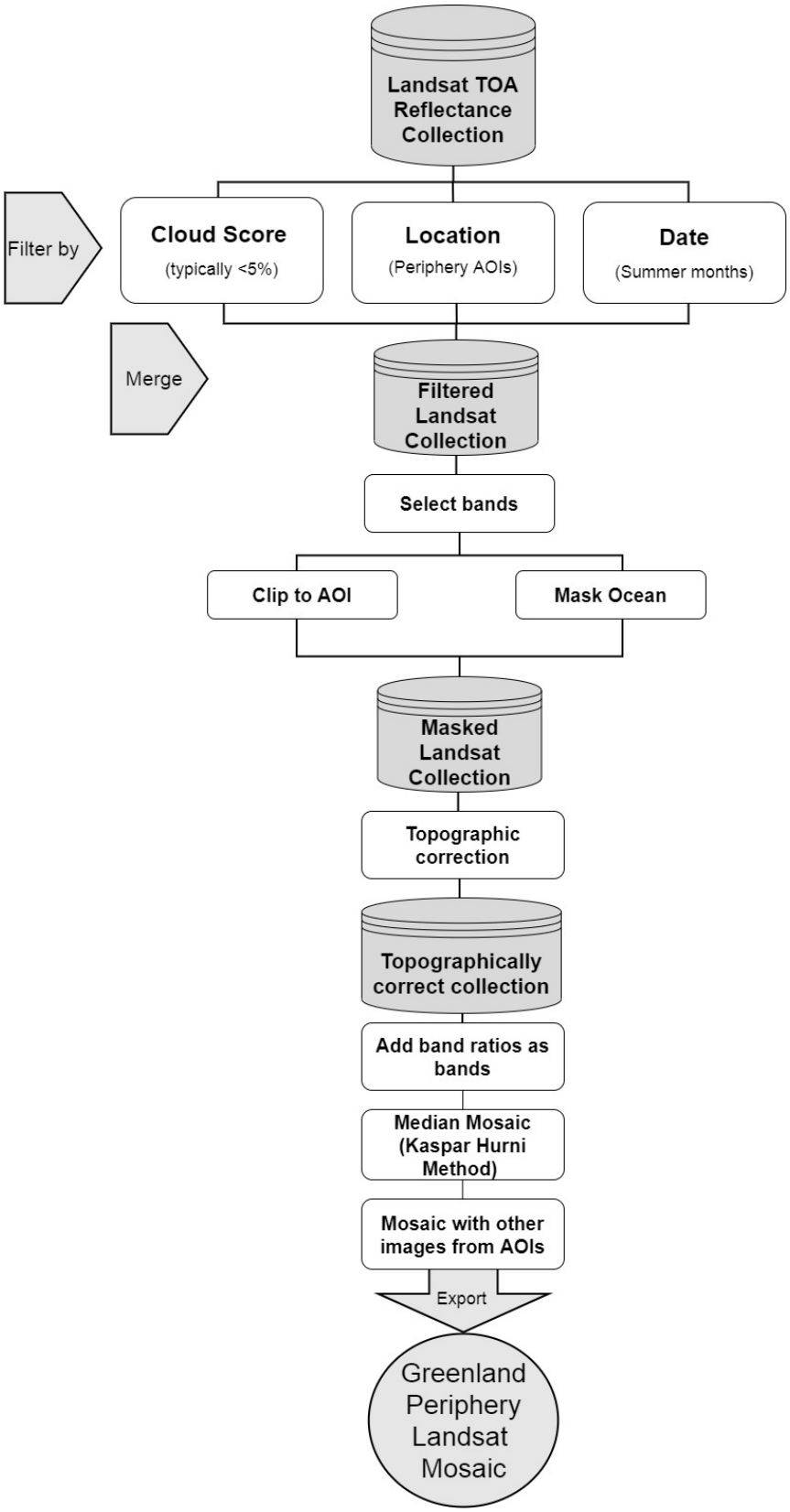

Figure 3.2 Pre-processing workflow implemented in Google Earth Engine (GEE) for Landsat imagery

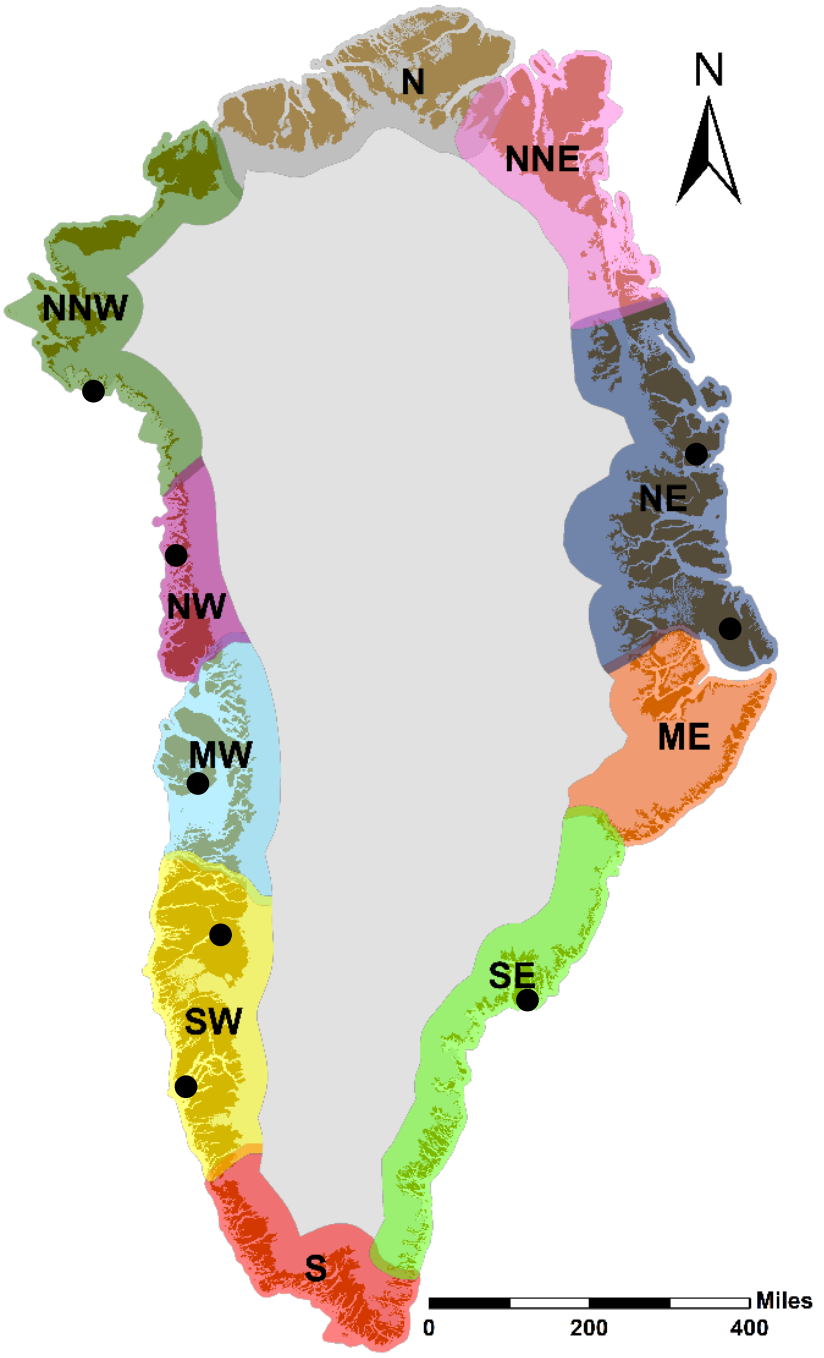

Figure 3.3. Areas of interest (AOI) referenced in the text. N = North, NNE = North-North East, NE = North East, ME = Mid-East, SE = South East, S = South, SW = South West, MW = Mid-West, NW = North West, NNW = North-North West. Black spots represent locations where accuracy assessment was conducted (Figure 3.7)

The first stage was to filter the entire Landsat-5 (1980s) and Landsat-8 (contemporary) TOA collections by date so that only summer months are considered due to lower snow cover and higher sun angles to reduce shadows. TOA products

were chosen over atmospherically corrected surface reflectance (SR) as the US Geological Survey (USGS, 2021) state the efficacy of surface reflectance correction is reduced in: (i) highly snow-covered regions, (ii) regions with low-sun angles, (iii) coastal regions where land area is small relative to adjacent ocean, (iv) areas with high cloud cover conditions, and (v) high latitude areas over 65° North (Landsat Missions). As Greenland's peripheral ice-free areas meet most/all of these criteria, SR products should not be used for analysis. Then the collection is further filtered by area, so only tiles which overlap an area of interest (AOI) are considered (Figure 3.3). Of these tiles, only images with low cloud cover over land (typically <5 %) are selected, with this information extracted from image metadata. The dimensionality of this final multi-year merged collection is reduced by only selecting 6 bands (Blue, Green, Red, NIR, SWIR1, SWIR2) in each image and creating a new image collection. The image collection is then run through a clipping function whereby each image in the collection is clipped to the area of interest (Figure 3.3). The Greenland Ice Mapping Project (GIMP) created a mask of oceans and ice through manual digitisation from Landsat -7 imagery from around the year 2000 (Howat et al., 2014). The GIMP ocean mask data is applied to remove all ocean pixels from each image in the clipped image collection.. Some manual adjustments were required as the GIMP masks are created from images collected around the year 2000 and some noise/gaps exist.

3.2.2 Topographic Correction

Misclassification from differing illumination conditions due to topographic shading and differing solar positions during image acquisition was reduced by applying a topographic correction (Soenen et al., 2005). Topographic correction is the process by which topographic effects are accounted for by alteration of cell band values based on satellite metadata (solar zenith and azimuth angles) and a digital elevation model from which aspect and slope are calculated. Topographic correction is often more important than atmospheric correction in topographically complex and high-latitude regions, vastly improving the accuracy of landcover classification in these areas (Vanonckelen et al., 2013). The Modified Sun-Canopy-Sensor Topographic Correction method, as outlined in Soenen et al. (2005) was applied to all images within the collection to account for topographic effects. Essentially, the method uses the sun-canopy-sensor (SCS) with a semi-empirical moderator to account for diffuse

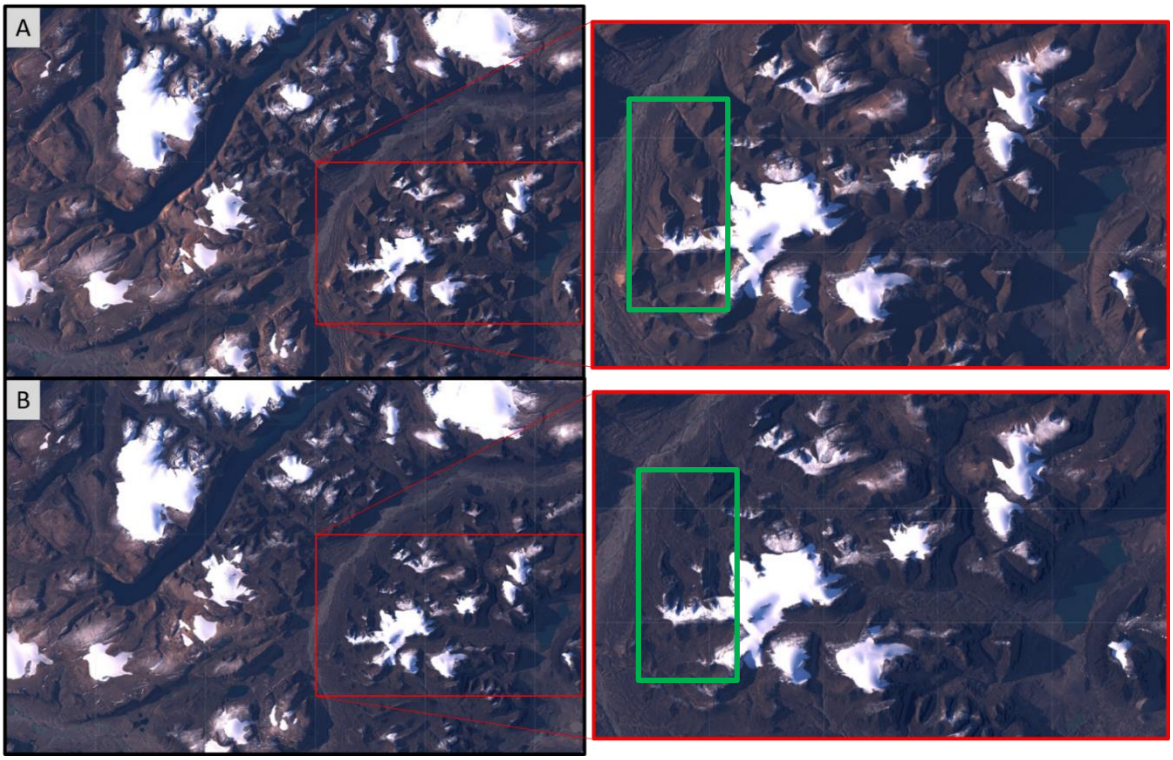

Figure 3.4 Example of pre (A) and post (B) true-colour Landsat 8 imagery (Northeast Greenland, Sermersooq Municipality). Green inset boxes highlight the removal of differences in illumination on slopes 'in pre' image (A), and how this "flattened" and removed in the 'post' image(B). As the illumination condition on the hillslopes is corrected, the same weathered surfaces are spectrally indistinct in the 'post' image (B), where before it appeared lighter when the hillslope aspect faced the sun's position and may incorrectly have been classified as a separate landcover by the classification algorithm.

radiation. Topographic corrections utilised the GIMP DEM, due to its complete spatial coverage of Greenland and its 30m resolution matching the resolution of the Landsat imagery. The source code for the topographic correction method was found in Poortinga et al. (2019); however, that was written for use on surface reflectance imagery with precise solar zenith and azimuth angles in image metadata. The code was therefore adapted here for use with TOA Landsat data through adjustments to the function for illumination condition (IC) calculation and image metadata about solar position. Due to the high computational cost, with the topographic correction algorithms applied to every cell of every band in every image within the collection, even in GEE computations timed out and memory allocations were exceeded for large areas, therefore the periphery was dissected into smaller areas with overlap. Figure 3.4 shows an example of an area in the far north east of Greenland in the Sermersooq Municipality before and after topographic correction.

3.2.3 Band Ratios and Mosaicking Procedure

Following topographic correction, a function to compute and add band ratios as bands is applied to the images in the topographically corrected collection. Band ratios were included due to their enhancement of spectral differences between bands to highlight specific landcover types, as well as to further negate the impacts of topography, aspect and shadowing (Kloiber et al., 2002). The normalised difference vegetation index (NDVI) is a well-established ratio indicator of vegetation cover (Tucker, 1979; Bannari et al., 1995). As well as effectively differentiating vegetated from non-vegetated areas, NDVI has been shown to highlight vegetation properties including leaf area, fractional vegetation cover, vegetation condition and biomass (Carlson and Ripley, 1997). The equation for the NDVI is given in equation (3.1).

$$NDVI = \frac{NIR - Red}{NIR + Red} \tag{3.1}$$

The normalised difference snow index (NDSI) finds use in discriminating snow/ice from snow and ice-free areas (Kulkarni et al., 2002; Nolin, 2010). Though high reflectance of snow and ice often leads to saturation in the visible bands of the Landsat sensors, including green (B3) used in the NDSI, this shortcoming is most pronounced at lower latitudes where incoming solar radiation is highest and resultantly so too are levels of reflected radiation over comparable surfaces (Selkowitz and Forster, 2015). The NDSI also allows for improved differentiation between snow and ice variants such as fresh/dry snow, wet snow, wet ice and bare ice (Hall and Riggs, 2011). The equation for the NDSI is given in equation (3.2).

$$NDSI = \frac{Green - SWIR}{Green + SWIR} \tag{3.2}$$

The NDWI is also included as a means to effectively delineate and enhance the presence of open water features in remotely sensed data (McFeeters, 1996). The index is designed to: (i) maximise the reflectance of water using green wavelengths (B3), (ii) minimise low reflectance of near infrared (B5) by water, and (iii) exploit the high reflectance of near infrared (B5) by vegetated and soil covered surfaces (Xu, 2006). Though oceans are masked, open water exists within the ice-free landscapes of Greenland as lakes and proglacial meltwater rivers. Many of the rivers have a strong suspended sediment content, making their visible spectral signal very similar to other features such as wet debris rich ice and saturated fine sediment facies. The NDWI improves the classifier's ability to differentiate between these features(Díaz-Delgado et al., 2006). The equation for NDWI is shown in equation (3.3).

$$NDWI = \frac{Green - NIR}{Green + NIR} \tag{3.3}$$

The derived ratios are stacked as bands with the original 6 bands and subsequently mosaicked using a spectral weighting method derived from the near-infrared band (c.f. Hurni et al., 2017). Essentially the method strives to select only the best cell at each point for mosaicking. Six bands (Blue, Green, Red, NIR, SWIR1, SWIR2) and three derived ratios (NDVI, NDSI, NDWI) were selected from the mosaic and a Principal Component Analysis (PCA) conducted to reduce data dimensionality and band inter-correlation whilst maintaining >98% original variance. Despite the computational power of GEE, the complexity and computational cost of the pre-processing regime developed here required that image preparation be broken up into smaller regions (shown in Figure 3.3) around the periphery which are subsequently mosaicked together. Hundreds of Landsat scenes are processed meaning the highest quality final mosaicked image can be produced grid cell by grid cell, and free from shadow and cloud which is most unlikely to be achieved when using whole images / individual scenes. Coverage over Greenland is excellent for the contemporary dates, and for the late eighties is relatively good but with gaps in the south and west. Areas with no or bad data (e.g. cloud, shadow) present in both the eighties and contemporary imagery are masked from both images.

3.2.4 Landcover Classification

To classify landcover based on the spectral bands and the band ratios defined above, multiple classifications were produced using variable numbers of clusters, training pixels, training regions, and using both the original and principal component analysis images of the input mosaic. Comparison of those multiple classifications against other contemporary classifications from around Greenland (see: Jørgensen et al., 2015; Carrivick et al., 2017; Karami et al., 2018) and independent Sentinel-2A (10 m resolution) and PlanetScope (3 to 5 m resolution) images permitted the determination that the best input and criteria were: K=70 clusters, 500,000 training pixels, and a PCA image of the input mosaic with the first 6 PC being selected. Unsupervised classification was used in the first instance as it removes the user's potential to target predefined purpose-driven classes which may be difficult to identify or that are presumed to be in abundance when relatively spatially sparse (Tømmervik, 2003; Hasmadi et al., 2009). The unsupervised approach is particularly useful for large, national/regional scale spatial analysis where it is unreasonable for the user to cover the entire area for validation and therefore only classes which can be well distinguished and are spectrally distinct are produced. The PCA is used to reduce the dimensionality of the input data and to remove the correlation between input bands (Abdu, 2019; Byrne et al., 1980; Comber et al., 2016; Novelli et al., 2016). This is achieved via an eigenvector analysis of the correlation matrix of input bands, whereby the axis of greatest variability between bands are identified and rotated to reduce obsolescence. The first 6 PC were then selected as the PCA indicated they contained the vast majority of significant information, over 98 % original bands variance. The best method determined for the contemporary classification was then also applied to the eighties mosaic for consistency. Both unsupervised classifications were improved by conducting semi-supervised reclassifications to remove the greatest sources of error. The main misclassifications were found between the Meltwater and Ice/snow classes and where shadows were misclassified as Freshwater. A Random Forest (RF) machine learning classifier was used in GEE to produce an ice mask, as wet ice and meltwater are largely spectrally indistinct (c.f. Breiman, 2001; Rodriguez-Galiano et al., 2012). Deep dark freshwater lakes are often misclassified as shadow, and vice versa. To reclassify misclassified freshwater as shadow, a simple slope threshold was used, whereby any cells classed as

Freshwater with a slope angle over 12 degrees (extracted from the 2m ArcticDEM Mosaic) were reclassified to Bad Data (Shadow/Cloud). The 12-degree threshold was chosen after sensitivity testing various slope angles, as it provided the best results by accounting for slightly erroneous values over water that exaggerated slope angles. Both of these methods were found to greatly improve the classification quality. The Random Forest (RF) classification workflow is outlined in Figure 3.5.

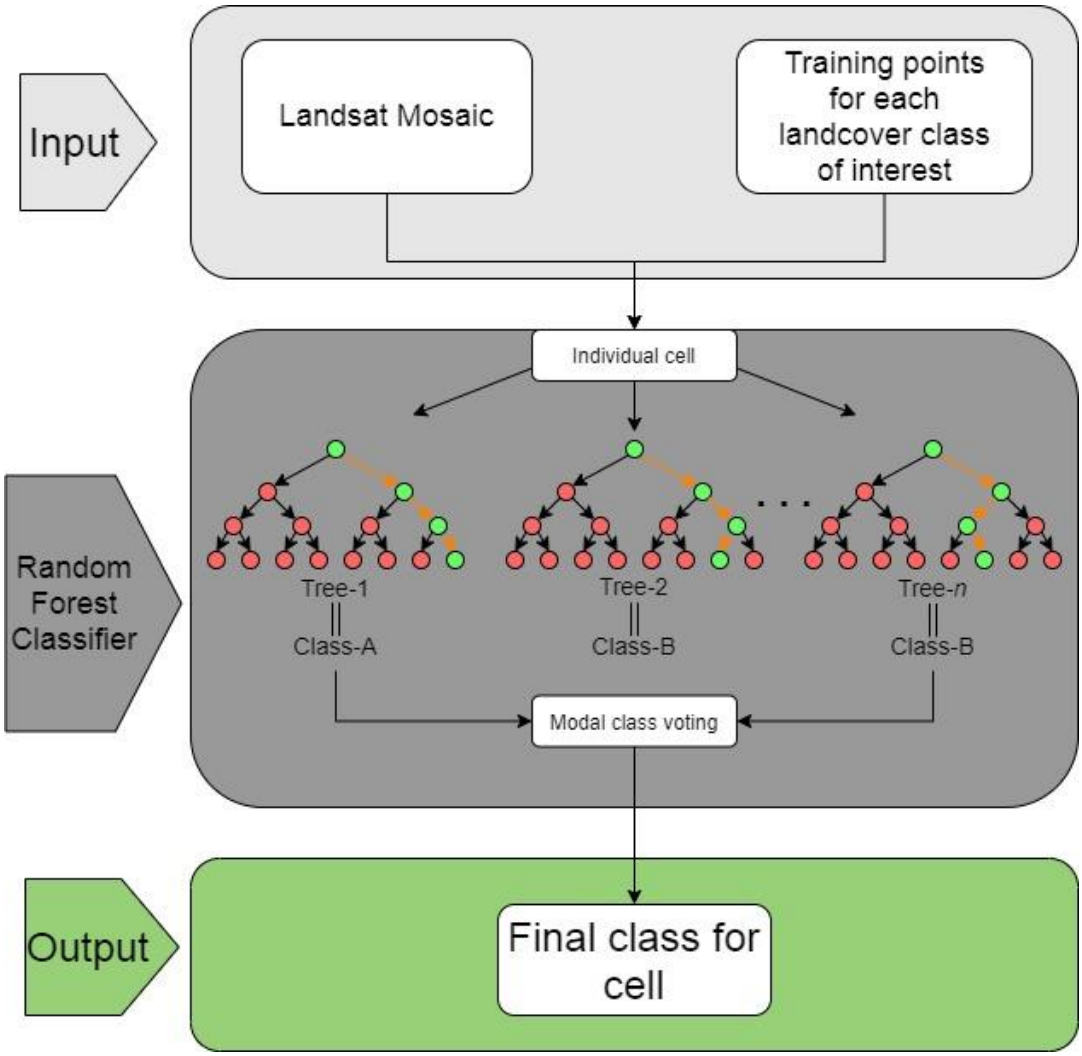

Figure 3.5 Random Forest RF classification method used for semi-supervised ice-mask production.

The final landcover classes and their descriptions, consistent for both classifications (1980s and 2010s) are given in Table 3.1 and the final contemporary landcover classification image is shown in Figure 3.6. These nine classes were chosen to represent the major landcover of the biophysical environment whilst reducing redundancy (too many classes) and maintaining accuracy (distinction between classes).

Table 3.1 Class Names and brief descriptions of class composition

Class Name	Description
Bad data	Data which does not represent the earth surface i.e. cloud covered or hidden from analysis by shadow
Snow/Ice	Snow or ice, generally the Ice Sheet or ice caps and glaciers
Meltwater	Rivers which are more ice-proximal and have higher suspended sediment (SS) concentrations
Freshwater	Deep water bodies with lower suspended sediment (SS) such as lakes which appear darker, are lower energy or stagnant, or ice distal
Coarse sediment	Generally represents scree slopes, gravel beds and larger grained (>gravel) sediment facies
Fine-grained sediment	Lighter fine grained sediment beds which may predominantly be fluvial or aeolian. May also be weathered regolith in regions predominantly underlain by sandstone/sedimentary bedrock.
Bedrock	Bedrock exposures and heavily weathered bedrock. May also include some weathered regolith
Tundra vegetation	Vegetation which is comprised of sedges, mosses, grasses, dwarf shrubs and some sparse and scattered trees.
Dense/ wet vegetation	Dense established vegetation or those in wetlands with high TWI which may be composed of forests, meadows/farmland, or those specially adapted to live in bogs, fens and wetlands i.e. hydrophytes

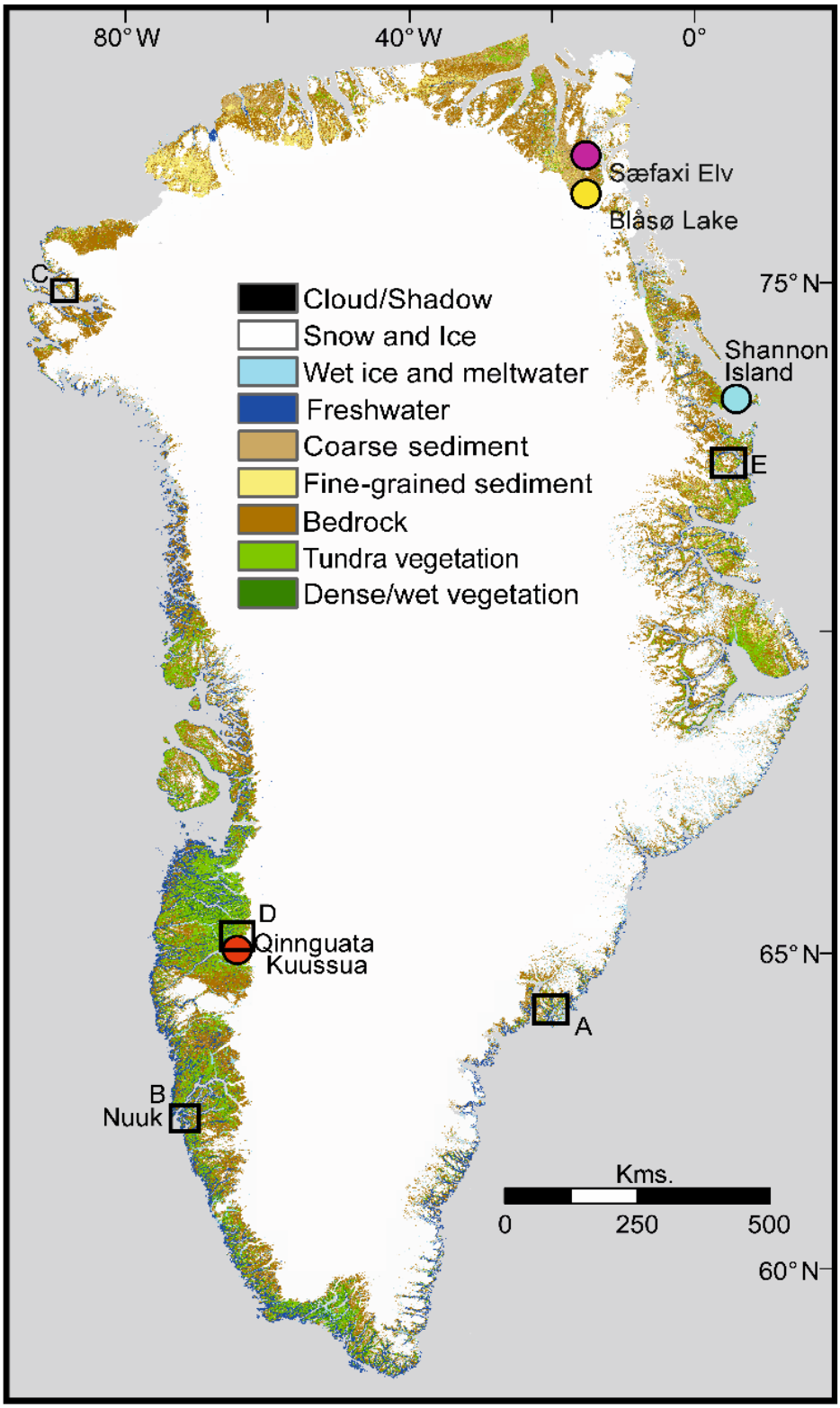

Figure 3.6 Landsat-8-derived landcover classification for the 2010s. The coloured circles and site names indicate where analysis of catchment-scale processes are highlighted in Figure 3.15, and the black squares with letters denote five locations within which are the 89 field validation points detailed in Figure 3.7.

3.2.5 Classification Accuracy Assessment

Accuracy of the contemporary classification was assessed using four band (RGB,NIR) 3 m resolution contemporary PlanetScope basemap mosaic imagery from the third quarter of 2019 (July-September) as reference (Planet Team, 2017) and a Sentinel-SA image mosaic for 2019 summer season produced in Google Earth Engine. Due to a lack of supplementary satellite imagery for the 1980s, the Landsat mosaic was used for reference alongside 2 m resolution greyscale georeferenced aerial orthophotographs, made available by the AeroDEM project (Korsgaard et al., 2016). Overall accuracy for each classification is reported to one significant figure only; 85% for the 1980s classification and 82% for the 2010s classification. Below the accuracy assessment procedure using the contemporary classification is outlined in detail. This same method was also applied to the eighties classification. Accuracy assessment was conducted for six 100 km x 100 km areas south of 76 °N shown in Figure 3.3. PlanetScope imagery is not available north of 76 °N. Stratified random sampling based on total occurrence of classes for the entirety of Greenland was used to generate 500 accuracy assessment points (AAP) distributed between the 8 landcover classes at each location. Results were then amalgamated resulting in 3,000 AAP over a total area of 60,000 km^2. The ice sheet was removed from analysis as this skewed the stratified AAP production and is largely static over the study period away from the margins. Snow and ice accuracy was therefore assessed using PGICs. A correspondence (AKA: error, confusion) matrix was produced using the 3,000 AAP and is presented both absolutely and as an expression of proportional area considering the associated error within each class, following Olofsson et al. (2013). The overall kappa coefficient is 0.781, and overall accuracy (OA) was presented as 82 %. The basic kappa coefficient however adjusts for ‘random allocation agreement’ and the validity of the adjustment has been questioned (Clifford et al., 1989; Pontius and Millones, 2011). Therefore, a stratified estimation of error was also applied following Olofsson et al. (2013) to mitigate against potential inherent measurement bias and to estimate standardised errors with quantified uncertainty based on sampling variability. The cell-count derived correspondence matrix is presented in Table 3.2.

Table 3.2 Sample counts (n_{ij}) correspondence matrix constructed from 3000 point stratified random sampling of contemporary semi-supervised classification. Classified map categories (i) are the rows and reference categories (j) are the columns. Grey shaded cells represent correct classification. W_i is the area mapped of a class ($A_{m,i}$) ÷ Total map area (A_{tot})

Class	Snow/Ice	Meltwater/ Wet Ice	Freshwater	Coarse Sediment	Fine Sediment	Bedrock	Tundra Vegetation	Dense/ Wet Vegetation	Total ($n_{i\cdot}$)	Total area (km^2)	W_i
Snow/Ice	584	23	9	0	2	0	0	0	618	254,527.32	0.206
Meltwater/ Wet Ice	16	127	12	2	3	0	0	1	161	66,214.41	0.054
Freshwater	3	11	46	2	0	0	0	2	64	26,422.66	0.021
Coarse Sediment	5	13	4	469	35	51	1	2	580	239,257.86	0.193
Fine Sediment	2	9	0	24	147	36	2	0	220	86,847.04	0.070
Bedrock	1	5	12	89	64	768	16	13	968	403,232.11	0.326
Tundra Vegetation	0	0	3	7	4	3	283	28	328	135,202.45	0.109
Dense/Wet Vegetation	0	0	0	2	1	2	9	47	61	24,989.45	0.020
Total ($n_{j\cdot}$)	611	188	86	595	256	860	311	93	3000	1,236,693.29	0.206

Table 3.3 Correspondence matrix (Table SI.2.) where cells are expressed as the estimated proportion of area ($\hat{p}_{ii}$ Classified map categories (i) are the rows and reference categories (j) are the columns.

Class	Snow/ Ice	Meltwater/ Wet Ice	Freshwater	Coarse Sediment	Fine Sediment	Bedrock	Tundra Vegetation	Dense/ Wet Vegetation	Total ($\hat{p}_{\cdot i}$)	$\hat{U}_i$	$\hat{p}_j$
Snow/ Ice	0.1945	0.0077	0.0030	0.0000	0.0007	0.0000	0.0000	0.0000	0.2058	0.9450	0.9559
Meltwater/ Wet Ice	0.0053	0.0422	0.0040	0.0007	0.0010	0.0000	0.0000	0.0003	0.0535	0.7888	0.6762
Freshwater	0.0010	0.0037	0.0154	0.0007	0.0000	0.0000	0.0000	0.0007	0.0214	0.7188	0.5347
Coarse Sediment	0.0017	0.0043	0.0013	0.1564	0.0117	0.0170	0.0003	0.0007	0.1935	0.8086	0.7885
Fine Sediment	0.0006	0.0029	0.0000	0.0077	0.0469	0.0115	0.0006	0.0000	0.0702	0.6682	0.5621
Bedrock	0.0003	0.0017	0.0040	0.0300	0.0216	0.2587	0.0054	0.0044	0.3261	0.7934	0.8956
Tundra Vegetation	0.0000	0.0000	0.0010	0.0023	0.0013	0.0010	0.0943	0.0093	0.1093	0.8628	0.9099
Dense/Wet Vegetation	0.0000	0.0000	0.0000	0.0007	0.0003	0.0007	0.0030	0.0156	0.0202	0.7705	0.5031
Total ($\hat{p}_{\cdot j}$)	0.2035	0.0625	0.0287	0.1984	0.0835	0.2889	0.1037	0.0309	1.0000	6.3560	5.8259

Table 3.2. is represented in Table 3.3 as estimators of proportional area in each cell *i,j* of the matrix, with each value being calculated using equations 3.4 through 3.7:

$$\hat{p}ij = W_i \frac{p_{ii}}{p_i} \tag{3.4}$$

$$\widehat{U_\iota} = User\ error = \frac{p_{ii}}{p_i} \tag{3.5}$$

$$\hat{p}j = Producer\ error = \frac{p_{jj}}{p_j} \tag{3.6}$$

$$\hat{O} = Overall\ accuracy = \sum_{j=1}^{8} p_{ij} = \mathbf{0.824} \tag{3.7}$$

Total proportional area accounting for stratified errors can be calculated for each class in equation 3.8:

$$\sum_{i}^{8} W_i \frac{n_{ij}}{n_i} \tag{3.8}$$

The stratified error-adjusted class estimator of area $\hat{A}_j$ is calculated in equation 3.9:

$$\widehat{A_j} = A_{tot}\hat{p}_j \tag{3.9}$$

Error margins (confidence intervals) for $\hat{A}_j$ are calculated based on sensitivity to the user's and producers' errors shown in Table 3.3 as a standard error, calculated in equation 3.10:

$$S(\widehat{p_j}) = \sqrt{\sum_{i=1}^{8} W_i^2 \frac{\frac{n_{ij}}{n_i}\left(1 - \frac{n_{ij}}{n_i}\right)}{n_i - 1}} \tag{3.10}$$

The confidence intervals expressed at a 95% error margin (z-score = 1.96) are calculated in equation 3.11:

$$\hat{A}_j = \pm 1.96 \times S(\hat{p} \cdot j) \tag{3.11}$$

The stratified area estimates for each class with a 95% confidence intervals as error margins are displayed in terms of percentage of total are in Table 3.4.

Table 3.4 Landcover class stratified area estimates and 95% error margins

Class	***Stratified 'error adjusted' areas $\hat{A}_{\cdot j}$ (km^2)***	***95% confidence interval $1.96 \times S(\hat{p}_{\cdot j})$ (km^2)***	***$\hat{A}_{\cdot j}$ %Total area***	***95% confidence interval %***
Snow/Ice	251,611.72	± 6,115.46	20.35 %	± 2.43%
Meltwater/ Wet Ice	77,243.66	± 7,408.17	6.25 %	± 9.59%
Freshwater	35,518.64	± 5,837.44	2.87 %	± 16.43%
Coarse Sediment	245,370.10	± 11,571.44	19.84 %	± 4.72%
Fine Sediment	103,243.55	± 9,859.61	8.35 %	± 9.55%
Bedrock	357,225.15	± 12,556.56	28.89 %	± 3.52%
Tundra Vegetation	128,207.33	± 6,541.80	10.37 %	± 5.10%
Dense/Wet Vegetation	38,273.15	± 5,969.91	3.09 %	± 15.60%

The overall accuracy derived using the proportional area error estimation method (Olofsson et al., 2013), is 85% for the 1980s classification and 82 % for the 2010s classification. However, the overall accuracy values are strongly affected by poor data quality within spatially-discrete sub-regions and so locally the accuracy can be much higher. A spatially distributed estimation of error and change accuracy is applied to delineate the overall and spatially distributed change accuracies between both time periods classifications, the methodology and results of which are presented in a later section of this chapter.

3.2.6 Field Validation

To further validate the contemporary classification, field validation at a spatially distributed array of 89 sites was conducted, as mapped and detailed in Figure 3.7. The sites were selected for logistical reasons (proximity to accessible field locations) and to ensure comprehensive land cover representation, especially focusing on areas where diverse land cover classes were in close proximity.Photographs of each landcover type are presented in Figure 3.8 (spanning multiple pages). Figure 3.7 shows the detail of sites where field validation was conducted, namely panels of the AeroDEM images, RGB, NGB Planet imagery, and the contemporary classification with validation points overlaid. Validation conducted in panels A – D (Figure 3.7) was collected during fieldwork in August 2022, and validation around Zackenberg in panel E was collected during August 2017. Figure 3.8 (spanning multiple pages) then

shows a series of photos collected during fieldwork with reference to landcover as classified and observed, location (Lat, Long in Decimal Degrees), and a brief description of the landcover.

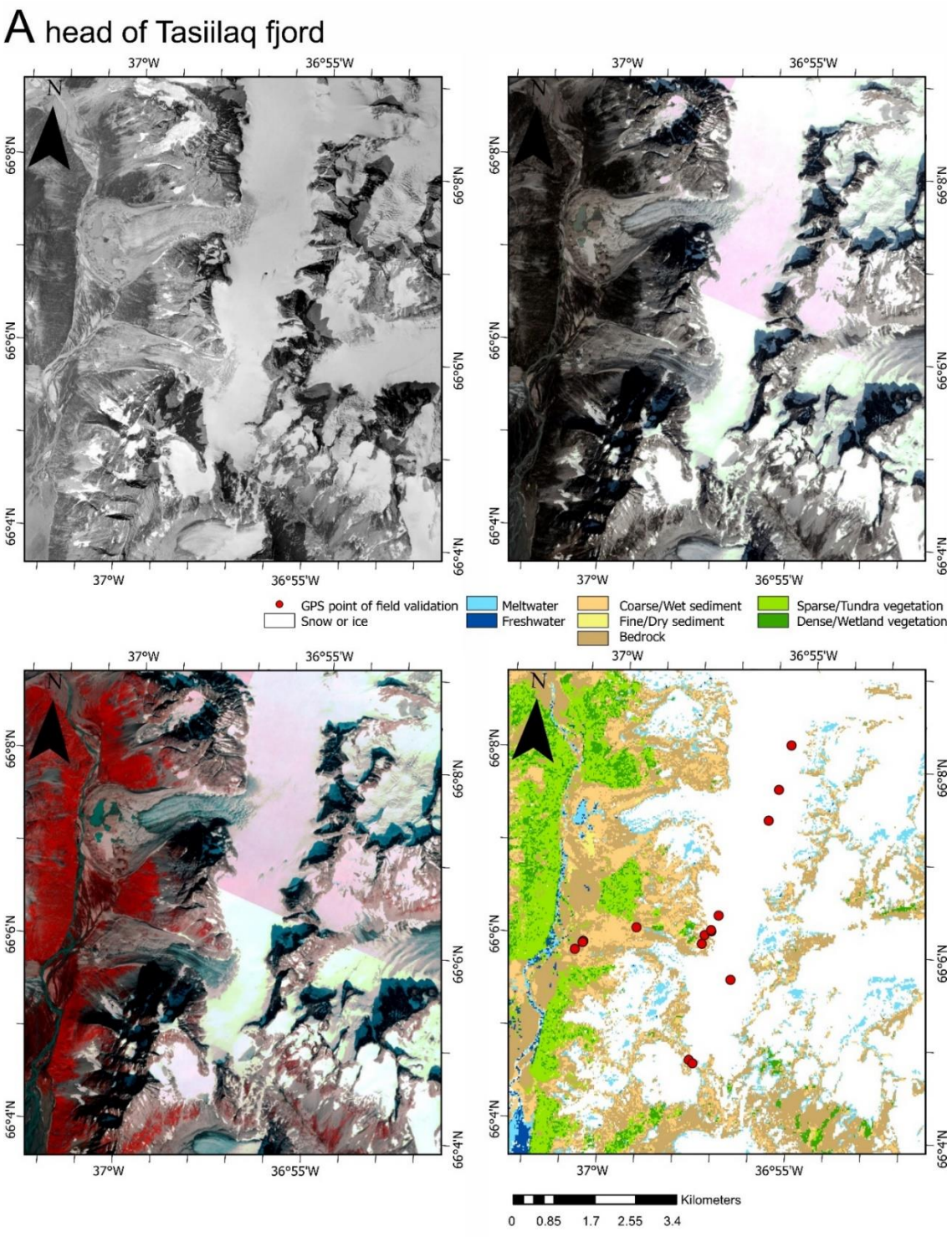

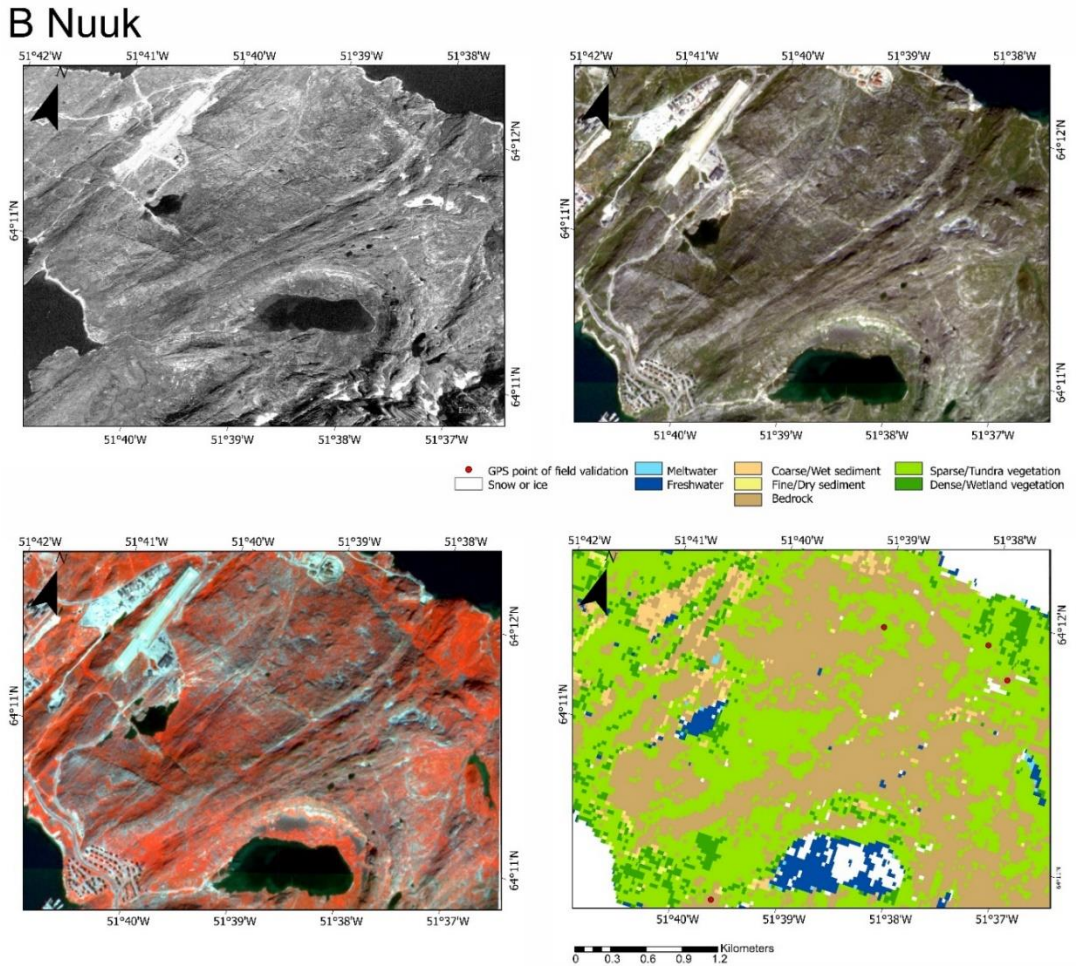
B Nuuk
51°42'W
51°41'W
51°40'W
51°39'W
51°38'W
51°37'W
64°12'N
64°11'N
GPS point of field validation
Snow or ice
Meltwater
Freshwater
Coarse/Wet sediment
Fine/Dry sediment
Bedrock
Sparse/Tundra vegetation
Dense/Wetland vegetation
Kilometers
0 0.3 0.6 0.9 1.2

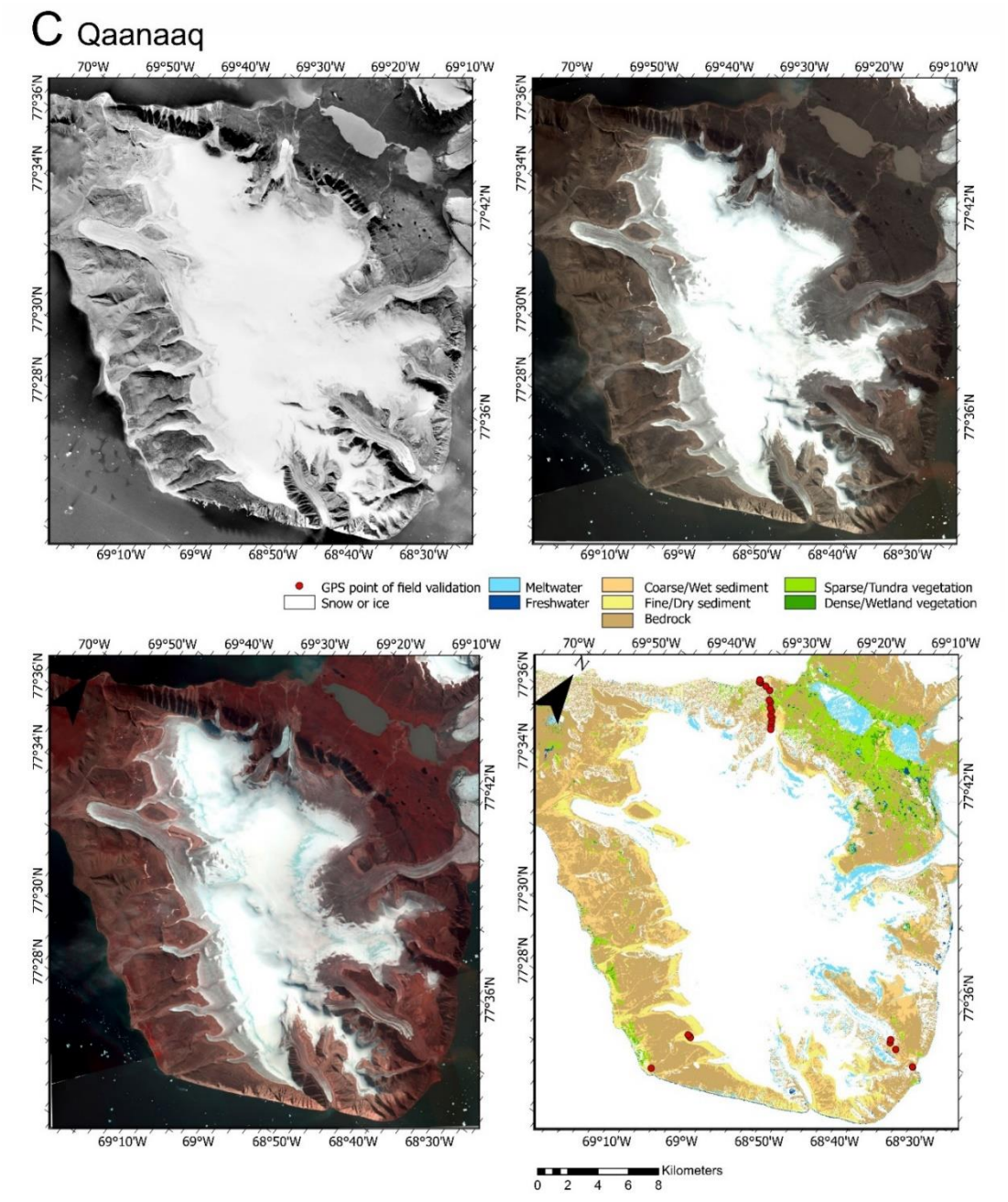
C Qaanaaq
70°W
69°50'W
69°40'W
69°30'W
69°20'W
69°10'W
77°36'N
77°34'N
77°30'N
77°28'N
77°42'N
69°10'W
69°W
68°50'W
68°40'W
68°30'W
GPS point of field validation
Snow or ice
Meltwater
Freshwater
Coarse/Wet sediment
Fine/Dry sediment
Bedrock
Sparse/Tundra vegetation
Dense/Wetland vegetation
Kilometers
0 2 4 6 8

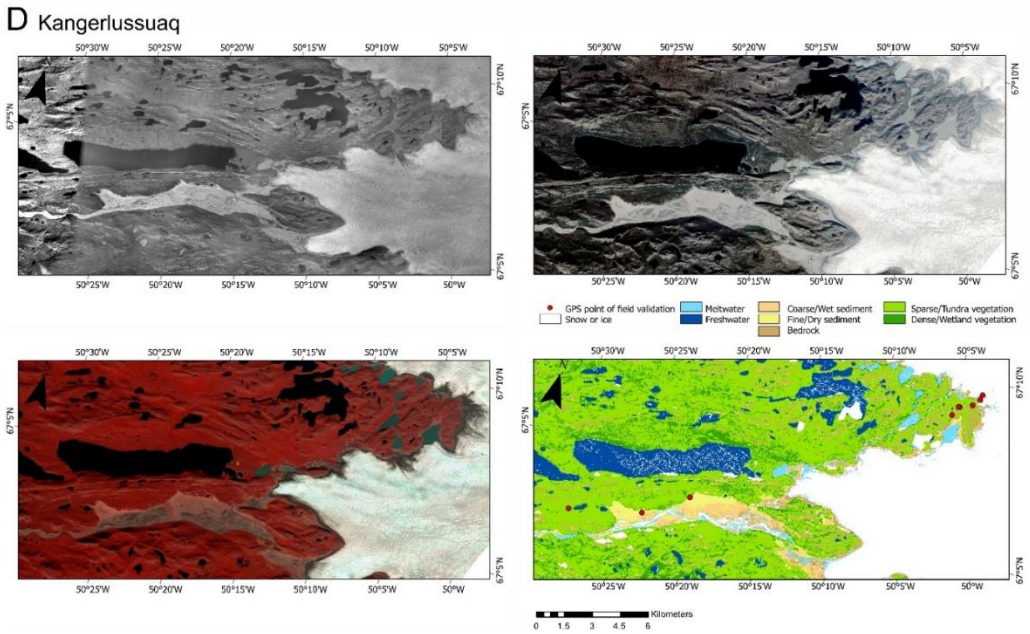
D Kangerlussuaq
50°30'W
50°25'W
50°20'W
50°15'W
50°10'W
50°5'W
50°W
67°N
67°5'N
67°10'N
GPS point of field validation
Snow or ice
Meltwater
Freshwater
Coarse/Wet sediment
Fine/Dry sediment
Bedrock
Sparse/Tundra vegetation
Dense/Wetland vegetation
Kilometers
0
1.5
3
4.5
6

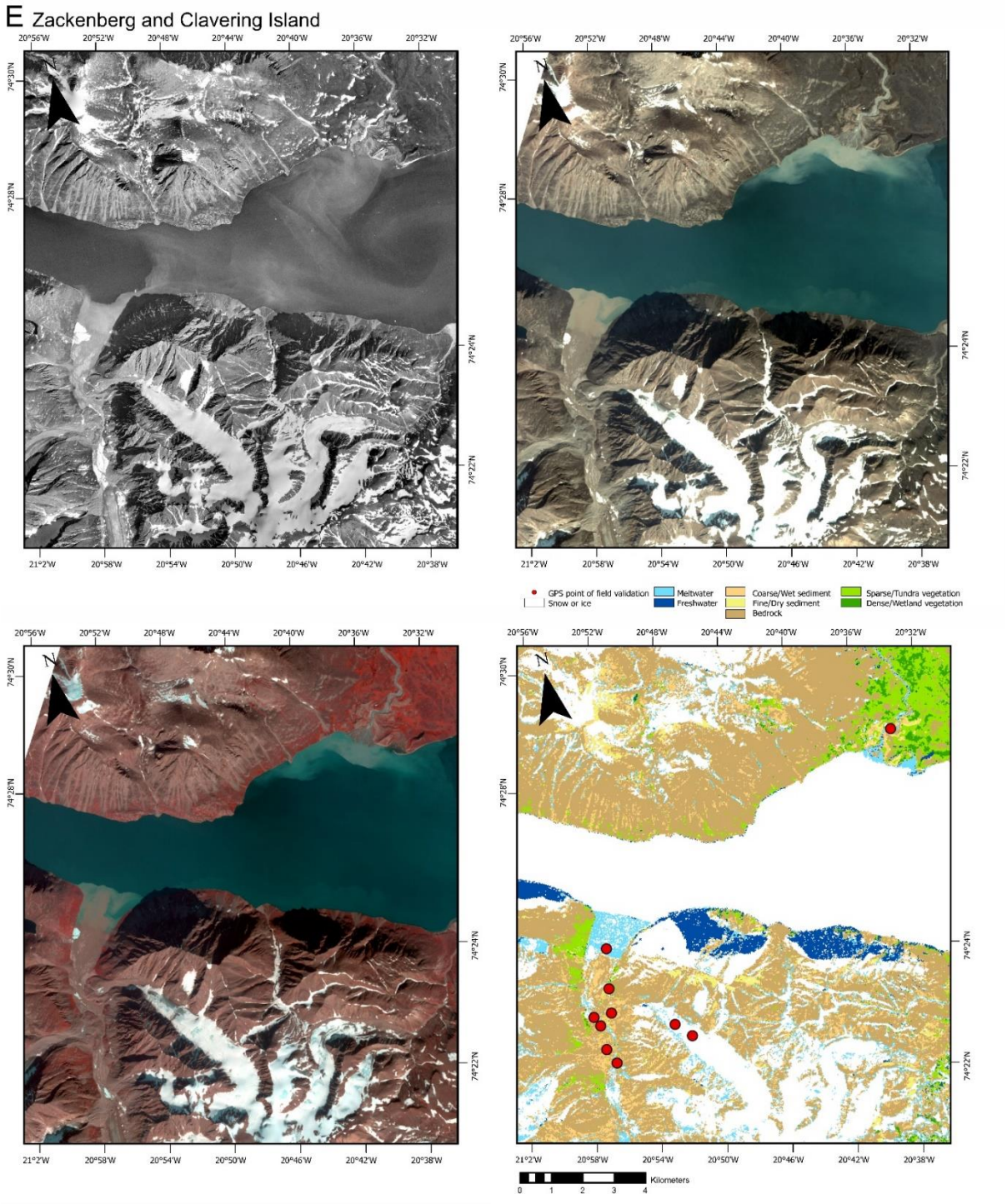

Figure 3.7 Examples of images used towards validation. 5 locations are highlighted where field observations were made (red points) as depicted in Figure 3.8. Each location is indicated in Figure 3.6. The four panels for each location comprise an aerial photograph (1980s), a RGB Planet image (2019), a NGB Planet image (2019) and the resultant landcover classification.

Panel A: Tasiilaq Mountain Hut

Lat/Long: N66.105, W -36.953

Classified: Snow/Ice

Validated: Ice

Panel B: Nuuk

Lat/Long: N64.196, W -51.625

Classified: Tundra Vegetation

Validated: Tundra Vegetation

Panel B: Nuuk

Lat/Long: N64.197, W -51.648

Classified: Tundra Vegetation

Validated: Tundra Vegetation

Panel B: Nuuk

N64.1737, W -51.654

Classified: Bedrock

Validated: Weathered Bedrock

Panel B: Nuuk

Lat/Long: N64.1739, W -51.661

Classified: Bedrock

Validated: Abraded Bedrock

Panel C: Qaanaaq

Lat/Long: N77.681, W -69.521

Classified: Tundra Vegetation

Validated: Tundra Vegetation

Panel C: Qaanaaq

Lat/Long: N77.668, W -69.457

Classified: Bedrock

Validated: Large boulders, coarse sediment

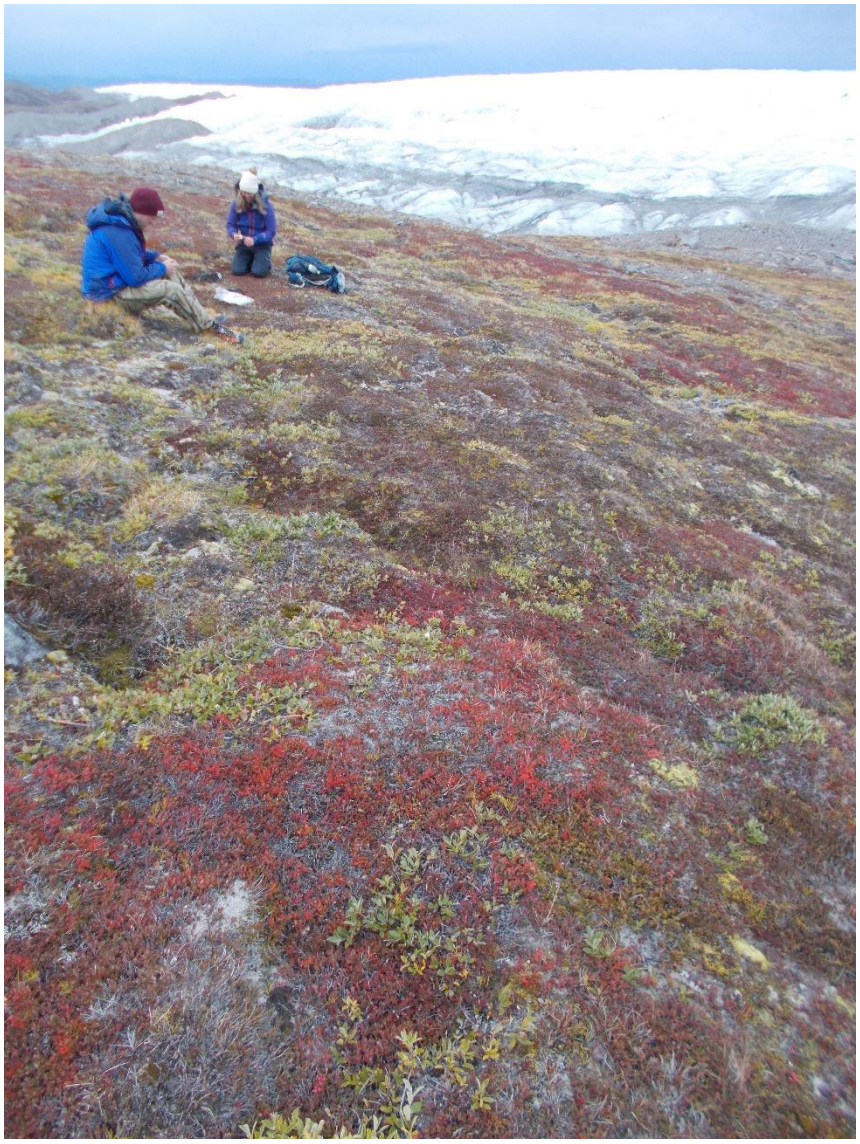

Panel D: Kangerlussuaq, Russel Glacier

Lat/Long: N 67.151, W -50.074

Classified: Tundra Vegetation

Validated: Tundra Vegetation

Panel D: Kangerlussuaq, Sandflugtdalen

Lat/Long: N 67.073, W -50.349

Classified: Fine Sediment

Validated: Fine Sediment, Sand

Panel E: Zackenberg

Lat/Long: N 74.468, W -20.589

Classified: Wetland Vegetation

Validated: Tundra vegetation on regularly flooded ground

Panel E: Clavering Island

Lat/Long: N 74.414, W -20.937

Classified: Tundra Vegetation

Validated: Tundra vegetation

Panel E: Clavering Island

Lat/Long: N 74.397, W -20.953

Classified: Coarse sediment

Validated: Coarse sediment, moraine/till

Figure 3.8 Photographs taken during field validation. Panel letters refer to panels shown in Figure 3.7.

In total, 75 of the 89 field validation points were correctly classified based on ground validation. This equates to 84% accuracy, and the confusion matrix indicated an overall Kappa coefficient of 0.81, in line with the accuracy reported from the remote validation. Misclassifications were largely proglacial moraine being classified as bedrock, and dry tundra vegetation being classified as wetland.

3.2.7 Landcover Change Areas, Error, and Confidence Intervals

The change in total coverage was simply calculated as the contemporary error-adjusted class area (contemp $\hat{A}\cdot_j$) minus the 1980s error-adjusted areas (eighties $\hat{A}\cdot_j$). Confidence intervals (CI) for changes in area are calculated as the square root of the sum-of-square error for each period, divided by the average area between the two periods. Table 3.5 shows the error adjusted areas for each period, the change area (in km^2 and percent), average area between each period, and the change confidence intervals (in km^2 and percent).

Table 3.5 Landcover class change statistics.

Class	1980s Error-adjusted Area (km^2)	Contemporary Error-adjusted Area (km^2)	Change Area (km^2)	Percent Change (%)	Change CI Area (km^2)	Change CI Percent (%)
Ice	251,611.72	280,318.82	-28,707.10	-10.24	9,766.86	3.67
Meltwater	77,243.66	67,212.65	10,031.00	14.92	10,516.63	14.56
Freshwater	35,518.64	39,854.54	-4,335.90	-10.88	8,420.79	22.34
Coarse Sediment	245,370.10	246,553.43	-1,183.34	-0.48	15,454.49	6.28
Fine Sediment	103,243.55	98,969.49	4,274.06	4.32	13,238.49	13.09
Bedrock	357,225.15	424,778.44	-67,553.29	-15.90	16,681.75	4.27
Tundra Vegetation	128,207.33	71,027.30	57,180.03	80.50	8,557.83	8.59
Wetland Vegetation	38,273.15	7,978.61	30,294.54	379.70	6,805.40	29.43
Vegetation Combined	166,480.48	79,005.91	87,474.57	110.72	15,287.54	12.45

To confirm that the accuracy of the individual classifications is reflected in the changes measured, the accuracy of changes is quantified. Using Google Earth Engine (GEE) a 64 class change map for the entirety of Greenland was produced. See Table 3.6 for a legend describing the 64 change class designations.

Table 3.6 Legend for 64 class (values from 0 – 63). From class represent the class at that location in the 1980s and the values within represent changes from that class to itself (static) and the other 7 classes. E.g. Change class value 0 = change from Snow/Ice to Snow/Ice (static), change class value 1 = change from Snow/Ice to Meltwater, change class value 8 = change from Meltwater to. Snow/Ice, change class value 62 = change from Dry tundra to Dense/wet vegetation, Etc.

64 class image values	From Class
0 - 7	Snow/Ice
8 - 15	Meltwater
16 - 23	Freshwater
24 - 31	Coarse/dark Sediment
32 - 39	Fine-grained sediment
40 - 47	Bedrock
48 - 55	Dry tundra
56 - 63	Dense/wet Vegetation

A further 3,000 AAP were randomly generated, stratified by the occurrence of each of the 64 classes in Google Earth Engine. The minimum number of points for each class was set at 5, as some classes have especially low areas which equated to less than 1 point when stratified by relative areas (e.g. class 56: Dense vegetation to

Snow/Ice). The accuracy of these changes was then assessed using the same reference data as was used for individual class accuracy assessment, i.e. Sentinel-2A mosaic and Planet imagery for contemporary, Landsat mosaic and 2 m AeroDEM orthophoto-graphs for the 1980s. The overall Kappa statistic of accuracy for the change image correspondence matrix is 0.69. Whilst conducting change class accuracy assessment it was evident that accuracy was not spatially homogenous, and misclassifications were predominantly between classes with largely similar spectral signatures and associated geomorphological process attributions. Therefore, the spatial distribution of error following class aggregation is explored as outlined in Table 3.7 and spatial distribution of change error were assessed via geographically weighted binomial regression.

Table 3.7 Change class aggregation schema. Aggregation rules: Snow/Ice has no aggregation, Meltwater and Deep Freshwater became Water, unconsolidated sediment classes and bedrock became Barren Ground, Dry Tundra vegetation and wet/dense vegetation became Vegetation. *Barren is defined as unvegetated bare earth, not perennially covered by snow, ice, or water

Aggregation class description	Aggregation class value	64 class value
Snow/Ice to Snow/Ice	1	1
Snow/Ice to Water	2	2,3
Snow/Ice to Barren* Ground	3	4,5,6
Snow/Ice to Vegetation	4	7,8
Water to Snow/Ice	5	9,17
Water to Water	6	10,11,18,19
Water to Barren* Ground	7	12,13,14,20,21,22
Water to Vegetation	8	15,16,23,24
Barren* Ground to Snow/Ice	9	25,33,41
Barren* Ground to Water	10	26,27,34,35,42,43
Barren* Ground to Barren* Ground	11	28,29,30,36,37,38,44,45,46
Barren* Ground to Vegetation	12	31,32,39,40,47,48
Vegetation to Snow/Ice	13	49,57
Vegetation to Water	14	50,51,58,59
Vegetation to Barren* Ground	15	52,53,54,60,61,62
Vegetation to Vegetation	16	55,56,63,64

Recent developments in change class accuracy assessment have proposed and explored local versions of accuracy measures (overall accuracy, user's Type I or commission error accuracy, and producer's Type II or omission error accuracy), in order to understand the spatial distribution of different levels of different types of accuracy in the study area. A series of papers have developed geographically weighted approaches to error reporting as outlined in Foody (2005) and then

developed in detail in Comber et al. (2012), Comber (2013) and Comber et al. (2017). In brief, these use a moving window or a kernel and compute a series of local correspondence matrices from which local accuracy measures are generated. Here the approach of Comber (2013) is adopted, linking the derivation of overall, user's and producer's accuracy to standard generalised, binomial regression, which can then be easily related to the spatial case via geographically weighted binomial regression. A cross tabulation of predicted against observed class is shown in Table 3.8. From this overall and class specific accuracies can be derived (Congalton 1991) as shown in Table 3.9.

Table 3.8 The cross tabulation of predicted (rows) and observed (columns).

Agg. Class	1	2	3	4	5	6	7	8	9	10	11	12	13	14	15	16
1 Snow/Ice to Snow/Ice	172	0	1	0	0	0	0	0	0	0	0	0	0	0	0	0
2 Snow/Ice to Water	35	124	8	0	0	4	0	0	0	0	1	0	0	0	0	0
3 Snow/Ice to Barren Ground	0	2	285	0	0	0	0	0	0	0	43	0	0	0	0	0
4 Snow/Ice to Vegetation	0	0	0	13	0	0	0	0	0	0	1	5	0	0	0	4
5 Water to Snow/Ice	7	0	0	0	11	9	0	0	0	0	0	0	0	0	0	0
6 Water to Water	35	4	4	0	0	260	0	0	0	0	19	0	0	0	0	0
7 Water to Barren Ground	1	0	13	0	0	7	114	0	0	0	57	0	0	0	0	0
8 Water to Vegetation	0	0	0	1	0	0	0	7	0	0	0	1	0	0	0	1
9 Barren Ground to Snow/Ice	8	1	0	0	0	0	0	0	55	5	17	2	0	0	0	0
10 Barren Ground to Water	0	0	0	0	0	2	0	0	15	134	43	5	0	0	0	0
11 Barren Ground to Barren Ground	0	0	0	0	0	0	0	0	0	1	527	21	0	0	0	0
12 Barren Ground to Vegetation	0	0	0	0	0	0	0	0	0	0	10	388	0	0	0	27
13 Vegetation to Snow/Ice	1	0	0	0	0	0	0	0	0	0	0	0	2	0	0	0
14 Vegetation to Water	0	0	0	0	0	5	0	0	0	0	2	0	0	16	0	7
16 Vegetation to Barren Ground	0	0	0	0	0	0	0	0	0	0	7	0	0	0	31	19
17 Vegetation to Vegetation	0	0	0	0	0	0	0	0	0	1	0	9	0	0	0	189

Table 3.9 Class specific User's and Producer's accuracies, with Overall and Kappa accuracies.

Agg. class	Users	Producers	Overall	Kappa
1 Snow/Ice to Snow/Ice	0.994	0.664	**0.832**	**0.808**
2 Snow/Ice to Water	0.721	0.947		
3 Snow/Ice to Barren Ground	0.864	0.916		
4 Snow/Ice to Vegetation	0.565	0.929		
5 Water to Snow/Ice	0.407	1.000		
6 Water to Water	0.807	0.906		
7 Water to Barren Ground	0.594	1.000		
8 Water to Vegetation	0.700	1.000		
9 Barren Ground to Snow/Ice	0.625	0.786		
10 Barren Ground to Water	0.673	0.950		
11 Barren Ground to Barren Ground	0.960	0.725		
12 Barren Ground to Vegetation	0.913	0.900		
13 Vegetation to Snow/Ice	0.667	1.000		
14 Vegetation to Water	0.533	1.000		
16 Vegetation to Barren Ground	0.544	1.000		
17 Vegetation to Vegetation	0.950	0.765		

The accuracy measures in Table 3.9 can be considered as a series of probabilities that are possible to generate from a logistic binomial regression (Comber 2013). Essentially, overall accuracy, can be estimated from a logistic regression model of a binomial variable indicating where predicted class equals observed class (0 otherwise), and if the result is logit transformed then the returned values provide an estimate of the probability of overall accuracy being equal to 1 (True). In a similar

way user's accuracy can be estimated from a binomial logistic model of reference data (y) against the classified data (x) and producer's accuracy from a regression model of classified data (y) against reference data (x).

Any model can be extended to the spatial case using the geographically weighted framework (see Comber et al. 2022). These use a moving kernel and compute a series of local models at different locations in the study area, using data under the kernel, but weighted by distance to the kernel centre. Here the spgwr package (Bivand et al. 2017) was used to undertake the spatial analyses of error in R, and a Gaussian kernel was used for the distance weighting.

A series of logistic regressions were undertaken to estimate the spatial distributions of the user and producer errors for each class. A few things to note:

i) the GWR analyses were undertaken over a grid of regression points spaced at 5km, covering a 20 km buffer of the sample locations.
ii) the spatial data were transformed to North America Lambert Conformal Conic projection so that distances etc. were planar.
iii) the kernel was manually set to the include nearest 15 % of the data points (i.e. 419 of 2,799 data points) in each local model.
iv) overall accuracy can be easily done this way but kappa requires a different approach (it does not directly equate to a logistic regression).

Maps for user and producer accuracy for one class have been generated (Class 12, Barren Ground to Vegetation) and these explain the per class variation in accuracy. The results of this analysis are shown in the Figures 3.9, 3.10 and 3.11.

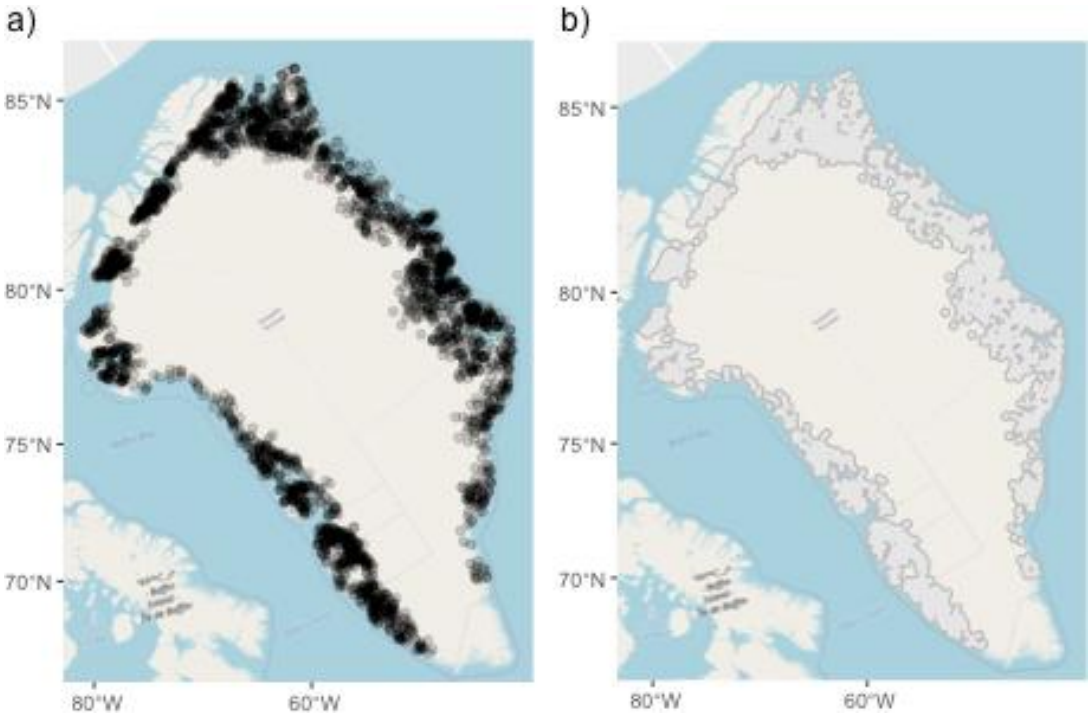

Figure 3.9 a) The validation sample locations over a Lambert Conformal Conic projection, and b) the buffered area over which a 5km grid was created for the GW models, with an OpenStreetMap backdrop © OSM contributors

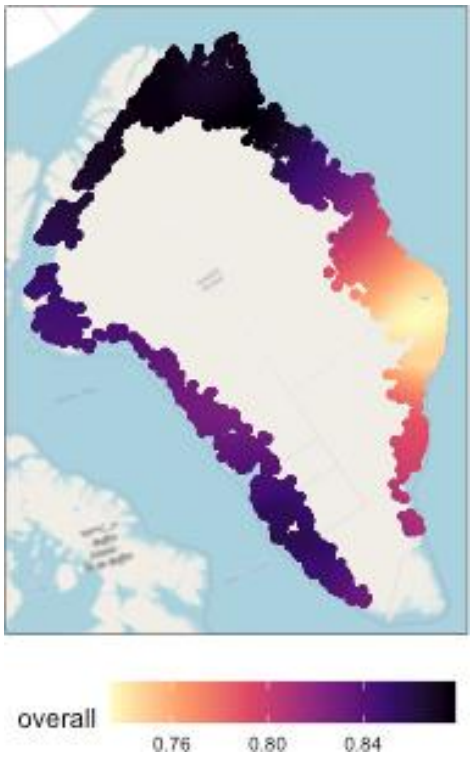

Figure 3.10 The GW overall accuracy

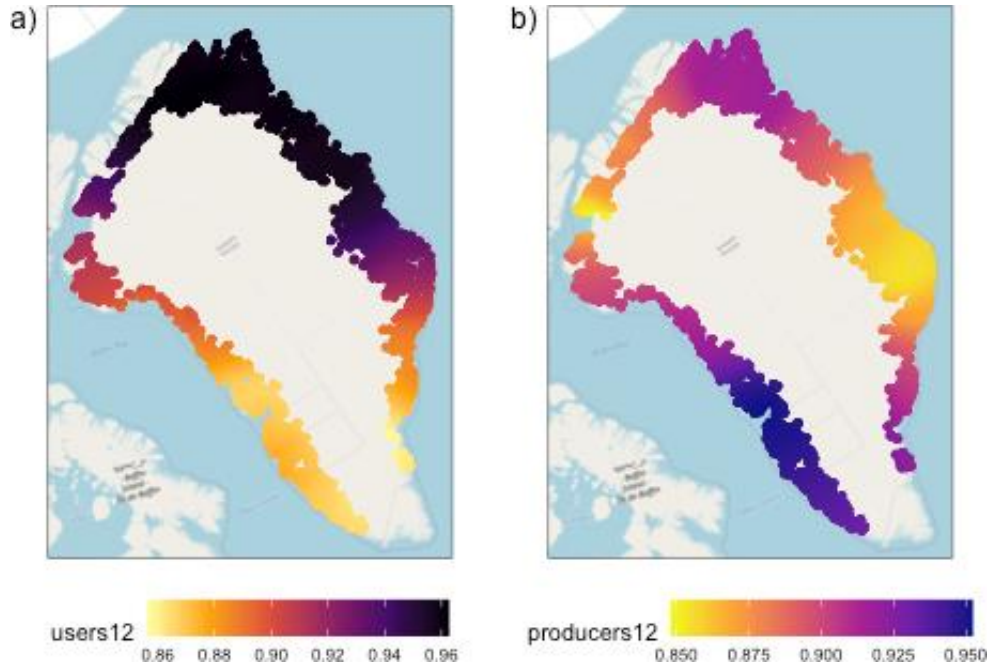

Figure 3.11 The GW user (a) and producer (b) accuracies for class 12, barren ground to vegetation

The same geographically weighted accuracy analyses were undertaken for all classes, the results of which are summarised in table 3.10 and table 3.11.

Table 3.10 Summaries of the spatial distributions of User accuracies.

	Min	**Q1**	**Median**	**Mean**	**Q3**	**Max**
users1	0.972	0.995	0.997	0.994	0.999	1.000
users2	0.583	0.652	0.705	0.724	0.780	0.877
users3	0.767	0.933	0.959	0.934	0.977	0.996
users4	0.262	0.502	0.616	0.668	0.893	1.000
users5	0.010	0.272	0.316	0.329	0.445	0.720
users6	0.568	0.729	0.833	0.794	0.858	0.940
users7	0.486	0.558	0.605	0.595	0.646	0.670
users8	0.534	0.625	0.660	0.728	0.851	0.980
users9	0.231	0.524	0.595	0.590	0.655	0.772
users10	0.544	0.667	0.676	0.670	0.691	0.741
users11	0.879	0.925	0.954	0.947	0.972	0.992
users12	0.856	0.884	0.931	0.922	0.959	0.963
users13	0.042	0.402	0.532	0.567	0.818	0.999
users14	0.460	0.508	0.525	0.534	0.544	0.725
users15	0.378	0.479	0.530	0.619	0.709	1.000
users16	0.797	0.914	0.929	0.921	0.956	0.968

Table 3.11 Summaries of the spatial distributions of Producer accuracies.

	Min	Q1	Median	Mean	Q3	Max
producers1	0.449	0.547	0.682	0.671	0.783	0.895
producers2	0.869	0.911	0.955	0.947	0.983	0.999
producers3	0.777	0.877	0.901	0.893	0.925	0.969
producers4	0.833	0.920	0.996	0.960	1.000	1.000
producers5	1.000	1.000	1.000	1.000	1.000	1.000
producers6	0.857	0.892	0.904	0.901	0.911	0.933
producers7	1.000	1.000	1.000	1.000	1.000	1.000
producers8	1.000	1.000	1.000	1.000	1.000	1.000
producers9	0.485	0.665	0.795	0.755	0.824	0.918
producers10	0.850	0.921	0.964	0.944	0.977	0.987
producers11	0.465	0.553	0.674	0.673	0.809	0.837
producers12	0.848	0.873	0.901	0.900	0.916	0.952
producers13	1.000	1.000	1.000	1.000	1.000	1.000
producers14	1.000	1.000	1.000	1.000	1.000	1.000
producers15	1.000	1.000	1.000	1.000	1.000	1.000
producers16	0.557	0.708	0.740	0.746	0.791	0.842

Figures 3.12 and 3.13 then show these accuracy surfaces mapped for all changes to compare the spatial distributions of accuracy between change classes.

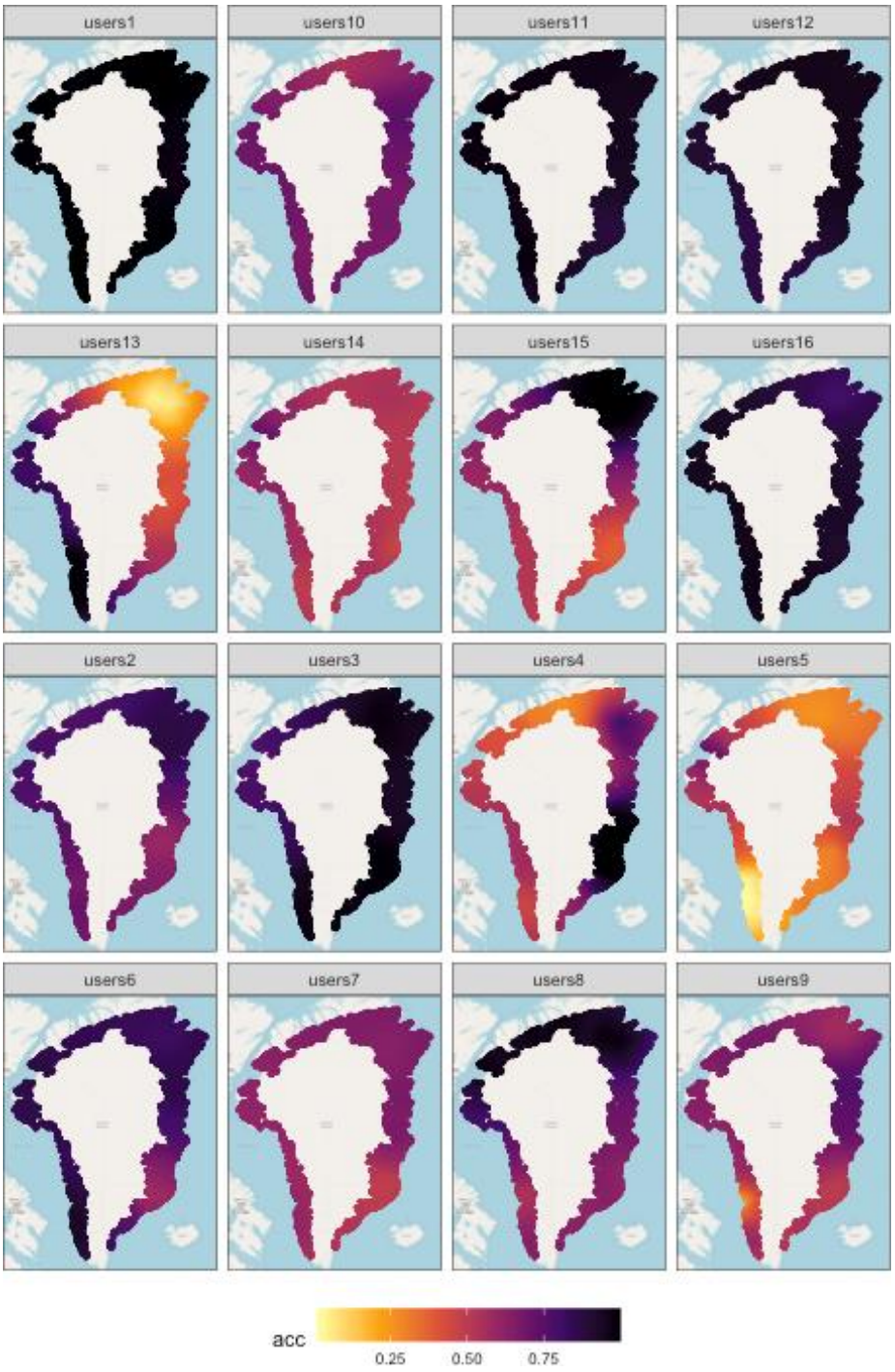

Figure 3.12 Mapped GW user accuracies

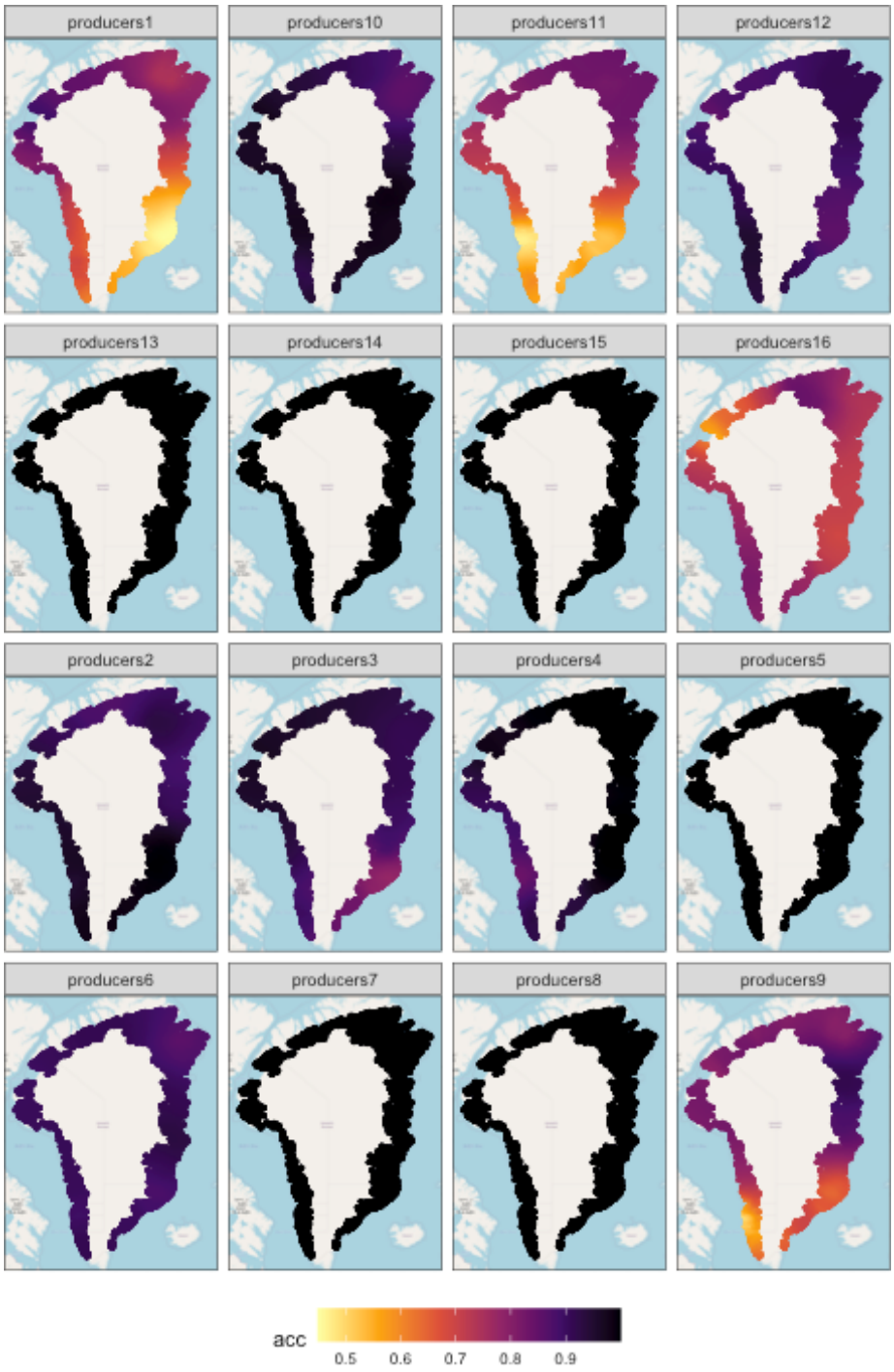

Figure 3.13 Mapped GW producer accuracies

3.2.8 Quantifying Regional Patterns of Landcover Change

To assess landcover change (LCC) at a regional/national scale across the entirety of Greenland, the 30 m resolution classifications are aggregated onto a 10 km x 10 km (100 km^2) fishnet grid, generated using ESRI's ArcMap 10.8 software. The percentage change in each landcover class within each 100 km^2 grid cell was then calculated using the Zonal Statistics as Table tool from the spatial analyst toolbox in ArcMap. To ensure that only legitimate landcover changes were measured, from both classifications any overlapping cells where one or both had a value of NoData or "Bad Data" were masked prior to calculating landcover percentages per cell. The results of this analysis are presented in the following results section of this chapter.

3.3 Results

This section presents the results of the landcover change assessments, with the implications at each level of analysis discussed in turn. Regional distributions of specific landcover change within the 10x10km^2 grid are first presented, before spatially distributed fine resolution examples of detailed landcover change are presented and analysed for four exemplar 'hot spots' of change identified within the regional mapping. This evidences the quality of the datasets produced for analysis of intra-catchment processes, leveraging and exploiting the high spatial resolution (30 m) of the landcover classifications. To understand drivers of the regional pattern of landcover changes, and due to sparse and intermittent field measurements of weather across Greenland (e.g. Box, 2002), comparisons are made between observed higher-order regional patterns of landcover change to derived Copernicus Climate Change Service (C3S) ERA5 modelled air temperature datasets (Herbach et al., 2020).

3.3.1 Regional patterns of landcover change

Overall, there has been a -28,707 km^2 ± 9,767 km^2 areal loss of the Greenland ice sheet margin and PGICs. That ice has predominantly been replaced by barren ground; bedrock and coarse sediment. As expected, detected ice loss is concentrated around the edges of present-day glacier margins, however this research reveals that it has been especially pronounced in the north and the south-west of Greenland (Figure 3.14 A) (c.f. Shepherd et al., 2020). Locally, greatest ice losses of -22 % (> 22 km^2 of a single 10 x 10 km^2 cell) are found around 77 ^oN in the west, with relatively high melt rates being observed in the mid-north-west (~ -6 % areas, 70 ^oN to 74 ^oN) and

south east (~ -8 % areas, 62 ^{o}N to 67 ^{o}N) (Figure 3.14 A). The geographically-weighted binomial regression analysis indicates that change from snow/ice accuracy was lower in the north west than other regions, although still averaging over 80 %. Ice loss is the landcover change with most marked consequences for albedo, which is a key component of surface energy balance and hence a control on micro-climate(s).

Changes in meltwater and freshwater classes have been spatially-heterogeneous, showing a slight positive correlation with latitude on both the east and west coast (Figure 3.14 B), and a negative trend for freshwater ponds and lakes (Figure 3.14 C). Across Greenland, there has been a 15 % ± 15 % (10,031 km^2 ± 10,516 km^2) increase in meltwater area, which are interpreted to represent increased river discharge and large increases in meltwater-sediment plumes in lakes and shallow parts of fjords. This increased meltwater river discharge impacts both local fjord/coastal waters in terms of sea surface temperature, salinity, suspended sediment and stratification, all of which influence marine ecosystems (Mernild et al., 2017). More widely, meltwater increase and consequent mobilisation of fluvial sediment can increase ocean freshening and impact Atlantic meridional overturning circulation (Sejr et al., 2017) besides impacting the delicate specialist marine ecosystems of the Arctic (Hawkings et al., 2015; Oliver et al., 2018).

Perhaps unexpectedly, there is a notable decrease in freshwater area of -11 % ± 22 % (-4,336 km^2 ± 8,421 km^2). However, that decreased area of freshwater is partially due to degrading permafrost and some episodic fluxes, such as from glacier lake drainages; for example.

Barren ground classes have undergone incoherent spatial changes (Figures 3.14 D, 3.14 E, 3.14 F). Notable areas with loss of bedrock and coarse/dark sediment occur in the mid/north east and mid west of Greenland (Figures 3.14 D, 3.14 F) and predominantly in ice-distal locations. The net change of coarse sediment is negligible at -0.5 % ± 6 % (-1,183 km^2 ± 15,455 km^2) but there has been a -16 % ± 4 % (-67,553 km^2 ± 16,682 km^2) loss in exposed bedrock. The latter is attributed to vegetation encroachment and growth on weathered bedrock regolith surfaces and largely via the process of shrubification due to warming temperatures (Myers-Smith et al., 2011), as studied on Disko Island, Greenland (Callaghan et all., 2011), for example, and more widely quantified herein. Indeed, losses in the sediment and bedrock classes coincide spatially with increases in both vegetation classes; dry

tundra and dense/wet vegetation (Figure 3.14 G) and these sites are also found inside the zone of highest permafrost thaw potential (Daanen et al., 2011). Exposure time since deglaciation (and prior to 1980) in these locations is sufficient (~10,000 years, Bennike and Björck, 2002) for soil and rudimentary peat development to be represented in the 1980s sediment and bedrock classes, producing optimal sites for vegetation encroachment during this study period (Romanovsky et al., 2010). Overall, loss of barren ground represents the stabilisation of land surfaces and consequently decreased sediment fluxes, which ultimately affects mineral and nutrient export to the oceans (Moreau et al., 2008; Carrivick and Tweed, 2021).

Fine sediment coverage has not significantly increased overall across Greenland; 4 % ± 13 % (4,274 km^2 ± 13,239 km^2), but locally spatially corresponds with increases in meltwater (Figures 3.14 B and 3.14 E). Fine sediment movement represents increasing sediment mobility and unstable land surfaces and is commonplace during deglaciation (cf. Carrivick and Tweed, 2021) and with thawing and drying of land. Fine sediment loss has particularly occurred in south west Greenland in the vicinity of Kangerlussuaq ~ 67 ^{o}N (Figure 3.14 E). In the same area, there has been an increase in exposure of bedrock and a negligible change in dry tundra vegetation, which is otherwise uncharacteristic in the south west (Figures 3.14 E, 3.14 F, 3.14 G). These landcover changes can be explained by expansion of deflation patches, which are proceeding at rates of ~2.5 $cm.yr^{-1}$ (Heindel et al., 2017). There is also a spatial association in south west Greenland between this aeolian erosion of fine sediment (sand and silt) and the increases in cover of vegetation. On the east coast of Greenland, fine-grained sediment has increased at 72 ^{o}N in Jameson Land and that corresponds with reduced bedrock coverage and increased coverage of meltwater with ice-loss further inland. The exposed bedrock in Jameson Land is an extensive Late Jurassic sandstone complex (Surlyk and Noe-Nygaard, 2001) and increased slope instability from permafrost degradation combined with increased glacial meltwater action and deposition has likely caused the marked increase in fine-grained sediment (Gruber and Haeberli, 2007).

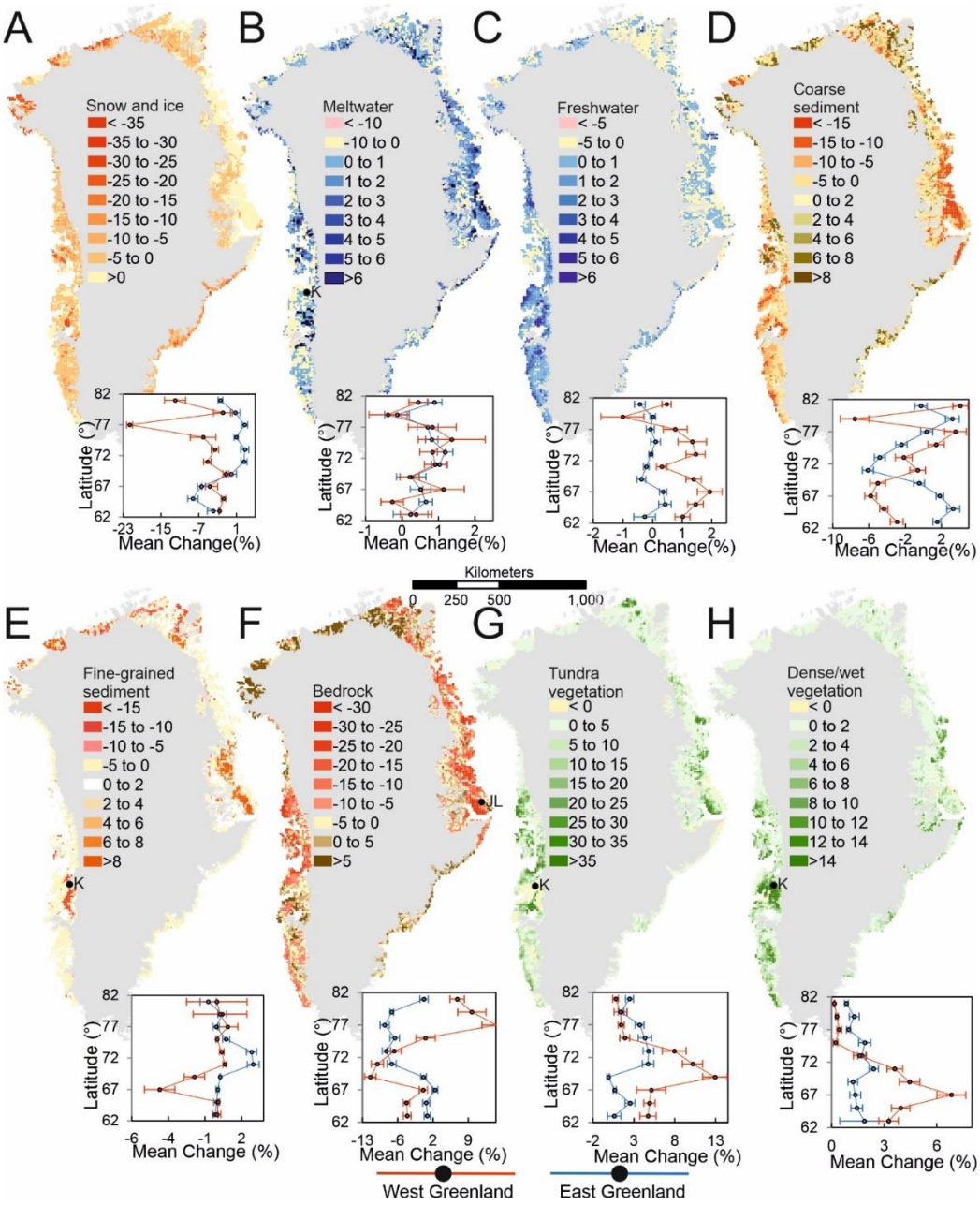

Figure 3.14 Percentage of total area change within 10 km x 10 km grid cells for each landcover class and plots of variation in average land-cover change with latitude for both east and west Greenland and 95% Confidence intervals. Labels K = Kangerlussuaq, JL = Jameson Land.

To understand drivers of the regional pattern of landcover changes, and due to sparse and intermittent field measurements of weather across Greenland (e.g. Box, 2002), the observed large-scale patterns of landcover change are compared to Copernicus Climate Change Service (C3S) ERA5 modelled air temperature datasets (Herbach et al., 2020). Intra-catchment processes were detected and analysed by exploiting the

high spatial resolution (30 m) of the landcover classifications to identify exemplar sites of landcover change types.

Both vegetation classes have in combination increased in coverage across Greenland by 111 % ± 12 % (87,475 km^2 ± 15,288 km^2). Pronounced increases in vegetation cover have occurred across the south west, east, and north east (Figure 3.14 G). The greatest increase in coverage of dense/wet vegetation has occurred in the vicinity of Kangerlussuaq in the south-west and isolated patches in the north-east (Figure 3.14 H). Most of this new dense/wet vegetation coverage can be attributed to wet heath development along receding lake shores between 1995 and 2017 (Law et al., 2018). Jørgensen et al. (2015) identify similar patterns of fenland distribution in the north-east (~2012) as those in the contemporary classification, but studies from the mid-late 20th century (Winther et al., 1950; Bay, 1994; Jakobsen, 1992) indicated far less extensive dense and wetland vegetation across the north-east, as depicted in Figure 3.14 H. Overall, changes in both vegetation cover classes show a latitudinal gradient; a pattern of increasing change with latitude to between ~63 ^{o}N and 69 ^{o}N and decreased change north of this (Figures 3.14 G, 3.14 H). Vegetation changes are especially important because they represent a stabilisation of land, introduce seasonal albedo variability and strongly affect snow retention, infiltration and overall local boundary layer (micro)climate. Moreover, vegetation development stabilises hillslopes reducing sediment and nutrient delivery to watercourses, yet simultaneously expedites permafrost degradation and introduces carbon and dissolved organic carbon and other greenhouse gases to the terrestrial (Horwath Burnham and Sletten, 2010), fluvial (Pastor et al., 2021), oceanic (Brovkin et al., 2002) and atmospheric environment (Ström et al., 2003).

3.3.2 Geomorphological Intra-catchment Processes

Using the regional maps in Figure 3.14, four locations have been identified to highlight the class changes and processes operating at the finest 30 m scale allowed by the data. These four key sites were chosen for geomorphological process analysis as they are notable regional hotspots of specific landcover change that, upon comparison of the two classifications and the change image, elucidate important geomorphological and ecological processes at the sub-catchment scale. The spatially distributed change accuracy assessment (outlined above) also allowed the selection

of sites in locations where the changes identified are most accurate. These spatially distributed sites were chosen to highlight four modes of landcover change and the associated geomorphological processes which drive this, therefore exemplifying the utility of the unprecedented 30m resolution classifications underlying the regional change maps. The same 64 class change image produced for change accuracy

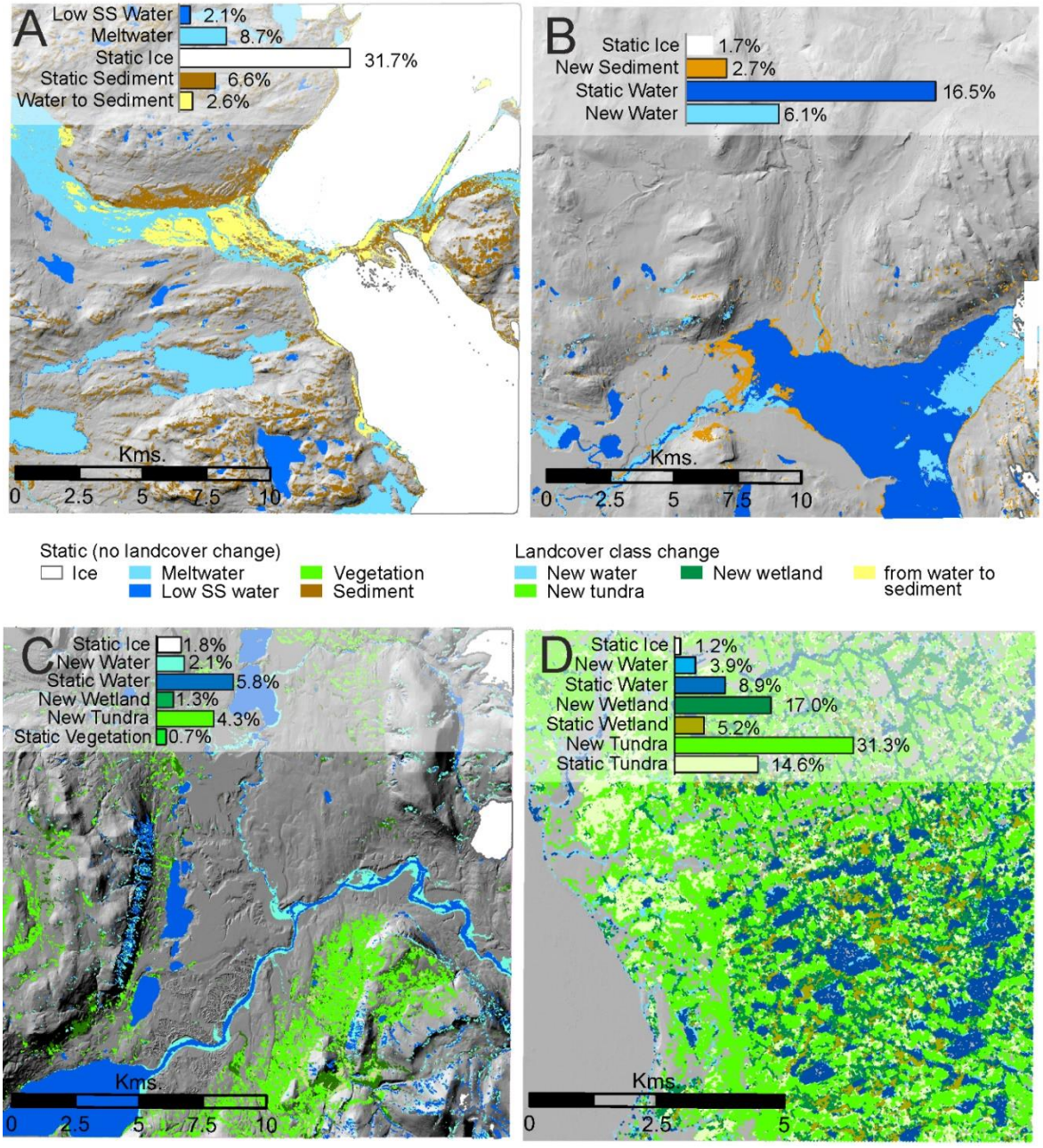

Figure 3.15 Examples of localised landcover change demonstrating geomorphological processes driving environmental evolution as seen using changes in 30 m resolution landcover data. Proglacial sedimentation (A: Qinnguata Kuussua river), delta progradation (B: Blåsø lake), increased meltwater stream size and discharge (C: Sæfaxi Elv), and vegetation and wetland growth (D: Shannon Island). SS = Suspended Sediment. Locations for sites in panels are shown in Figure 3.6.

assessment outlined above is leveraged to investigate geomorphological processes and change. Classes within the 64 class change map were reclassified to highlight geomorphological features and changes, shown in Figure 3.15.

In Figure 3.15, panel A shows the southernmost source of the Qinnguata Kuussua river in south west Greenland (Figure 3.6) where meltwater is primarily subglacially-fed and the absence of glacier surface drainage reflects low precipitation and relatively little supraglacial melt (van As et al., 2011; Ryu and Jacobson, 2012). The proglacial river braidplain is complex in planform and composition (Figure. 3.15 A) but is notable for the expansion in coverage of 3 % or ~10 km^2 of the 400 km^2 selected area of fine-grained sediment, reflecting aggradation of fluvially-transported sediment.

Figure 3.15 B evidences increased sediment flux and consequent river changes around the ice-dammed lake Blåsø in north east Greenland. There have been river channel avulsions and sedimentation across 3 % or ~11 km^2 of the 400 km^2 area and that has most obviously occurred as delta progradation. New sediment is only found around the mouths of meltwater streams (Figure 3.15 B), thereby refuting attribution to a falling lake level. Increased meltwater discharge, which is ubiquitous around Greenland (Figure 3.14 B) and the associated fluvial mobilisation of sediment is most likely to be causing the delta progradation. Where sediment supply is abundant, i.e. regions identified as presenting increasing in sediment and bare ground classes largely in proglacial landscapes (Figures 3.14 D, 3.14 E, 3.14 F), the meltwater rivers transport that sediment ultimately driving widespread progradation in lakes and fjords (Figure 3.15 B). These geomorphological processes are important because deltas considerably alter coastal and lacustrine morphodynamics, sediment delivery ratios and connectivity with knock-on implications for ecosystems dependent on nutrients present in glacigenic sediment (e.g. Hawkings et al., 2015; Bendixen et al., 2017; Hendry et al., 2019; Martin et al., 2020).

Figure 3.15 C shows the Sæfaxi Elv river which drains Centrum Lake eastward to the ocean via Hekla Sound in King Frederick VIII Land, north-east Greenland. There has been a 4 % or 16 km^2 increase in the surface area of the river over the 400 km^2 area, which can be predominantly attributed to the Greenland-wide increase in meltwater discharge (Bamber et al 2018; Mernild et al., 2017); there is a notable meltwater river area increases across Greenland of +15 % coverage, though a large proportion of this

will encompass sediment plumes into lakes and fjords, as well as some wet ice. There is also a considerable increase in both vegetation classes in this area (Figure 3.15 C), and evidences the spatial association of vegetation encroachment and growth with increased availability of freshwater sourced from melting PGICs and degrading permafrost (Rasmussen et al., 2018).

There is a near quadrupling (increase of 380 % ± 29 %, 30,295 km^2 ± 6,805 km^2) in the coverage of wet/dense vegetation across Greenland as reported here. Wetland expansion on Shannon Island, east Greenland (Figure 3.15 D) is an exemplar of widespread wetland development and expansion in east and north-east Greenland (Figure 3.14 H). Jørgensen et al. (2015) identified wetlands and fen in this region and proposed that the wetlands would continue to expand with permafrost degradation. These wetlands are likely minerotrophic, principally deriving nutrients from glacial meltwater, and constitute considerable sources of CH_4 in polar regions (Huttunen et al., 2003). Locations of wetland formation and growth in north east Greenland identified here present key sites for research to explore the poorly understood process of wetland, and peat, initiation and lateral expansion, a field at the forefront of ongoing arctic biospheric research (Walvoord and Kurylyk, 2016; Kreplin et al., 2021). Arctic wetland development has a complex and poorly understood biogeochemical connotation for greenhouse gas emission versus drawdown; Arctic wetlands are effective methane emitters (O'Connor et al., 2010), yet dry and moist arctic tundra soils in north east Greenland have been measured to draw down methane (Jørgensen et al., 2015). Expansion of vegetation and especially in wetland areas indicates but also exacerbates permafrost thaw, active layer thickening and thus emissions of greenhouse gases previously stored in these Arctic soils (Hollesen et al., 2011).

3.3.3 Association of Landcover Change with Arctic Warming

The landcover changes as quantified here are dramatic and show distinct regional patterns concerning dominant change trajectories. It has been shown that climatic warming can drive profound landcover change in Arctic environments, (as outlined in the literature review chapter of this thesis). The Arctic Amplification of climate warming drives multiple processes and feedbacks which cause transient landscape changes in Greenland, including: i) widespread glacier thinning and retreat (Chylek

et al., 2004; Khan et al., 2014; Noël et al., 2017; Straneo & Heimbach, 2013), ii) increased meltwater river discharge and sediment redistribution (e.g. Hanna et al., 2008; Mankoff et al., 2020; Rennermalm et al., 2012; Van As et al., 2014), iii) increased size and count of certain lakes (e.g. Burpee et al., 2018; Carrivick et al., 2022; Carrivick & Tweed, 2013), iv) increased active layer thickness (e.g. Hollesen et al., 2011; Lewkowicz & Harris, 2005; Schwarzkopf et al., 2023), v) degraded permafrost (e.g. Daanen et al., 2011; Jorgenson & Grosse, 2016; Zimov et al., 2006), and vi) increased vegetation growth and expansion (Daniels et al., 2011; Karami et al., 2018; Pearson et al., 2013; Swann et al., 2010). This research therefore aims to relate all of the landcover changes measured here to climate warming over the same period.

Numerous regression analyses were conducted to understand the degree to which Greenland's climate change has influenced the landcover changes observed over the thirty-year study period. Decadal and annual average summer temperature change from the European Centre for Medium-Range Weather Forecasts (ECMWF). ERA-5 monthly average dataset for summer months was correlated with the change classes, but Ordinary Least Squared (OLS) correlations were all below 0.1 and indicated a non-parametric relationship. It was therefore speculated that average increase in temperature is not a particularly useful indicator of landcover change in Greenland. This is because changes above 0˚C will produce ice melt and permafrost thawing, whereas a change (of equal magnitude) below zero will not. The magnitude of climate change, when considering landcover changes, is a less indicative measure unless a specific threshold is reached. Consider a 3˚C warming that remains below zero versus a 3˚C warming that crosses from below to above zero thereby leading to ice melt and permafrost thaw, for example. Therefore, a new set of climate warming variables were devised and calculated concerning the difference (change) in the average number of days in a year above three significant positive degrees temperature thresholds (0°C, 3°C, and 6°C) for the late 1980s and late 2010s. These thresholds were chosen for several reasons: computational and temporal efficiency, the critical importance of 0°C for positive degree days, and the fact that above 6°C, the number of days was essentially zero for many northern locations, offering less geographical distinction. These variables, termed Difference in Degree Days Above

Temperature (DDDAT) grids, were produced from ECMWF ERA5 land-hourly gridded data and prepared in Google Earth Engine.

The number of days per year were averaged where temperatures were above the three threshold values (0˚C, 3˚C, and ˚C) for the years 1986, 1987, 1988, and 1989 and the average taken of these four years to have an average Degree Days Above Threshold (DDAT) value for each threshold temperature for the late eighties. The same method was applied for the years 2016, 2017, 2018, and 2019 for the contemporary DDAT value. Differencing these grids then produced the Difference in Degree Days Above Temperature (DDDAT) grid. Zonal statistics was then used to aggregate these values to the 10 km x 10 km fishnet grids used for aggregating regional landcover change statistics. Unlike hydrological variables which, generally, cannot influence across catchment dynamics and processes, climate data is spatially non-stationary or closed, and nearby sites in space tend to have similar values of temperature/temperature change over time than would be expected by chance, with climate affecting the immediate area and those nearby by some decay factor (Yamanouchi & Takata, 2020). This inherent spatial autocorrelation in the data makes the application of classical linear and parametric tests such as OLS problematic due to the innate assumption of independently distributed error (Wang et al., 2001). In the OLS model, the variables to be related are assumed to the spatially stationary and that at each point of the study area the globally quantified relationship is constant and that the model is absolutely representative. When comparing environmental variables such as landcover change and their climatic driving variables this has been shown to rarely be the case (Propastin et al., 2008). Geographically Weighted Regression (GWR) regresses locally and allows the parameters to vary across space as a moving kernel with a set bandwidth or neighbourhood. It is incorrect to hold that for landcover types with variable responses to climate across a diverse and large spatial area a single linear model is applicable at every point (Prospatin et al., 2008; Li et al., 2010; Zhou et al., 2009; Zhao et al., 2010). Multiple studies have shown that GWR is more accurate and necessary when using climatic predictors for environmental and landscape variables, for both descriptive and predictive usage (e.g. Wang and Tenhunen, 2005; Propastin et al., 2008, and Usman et al. 2013). For a detailed description of GWR see: Brundson et al. 1996, and Fotheringham et al. 2003. Essentially each data point is weighted based on its distance from the kernel cell

within the bounds of the bandwidth (neighbourhood). The best GWR model and bandwidth may be determined from a number of model outputs and criteria. In the first order the best bandwidth and model may be determined using the Akaike Information Criterion (AIC). Lower AIC is desirable and generally reflects a closer model approximation to reality, however, involves a trade- off between goodness-of-fit and degrees-of-freedom. Fotheringham et al. (2003) defines the AIC as is shown in equation 3.12.

$$AIC = 2nlog_e(\hat{\sigma}) + nlog_e(2\pi) = \mathrm{n}\left\{\frac{n + tr(S)}{n - 2 - tr(S)}\right\} \qquad (3.12)$$

where *n* is sample size, $\hat{\sigma}$ is standard deviation of the error term (estimated), and *tr(S)* is the trace of the hat matrix as a function of bandwidth (Fotheringham et al., 2003). R^2 and adjusted R^2 are commonly used as indicators model quality so the understanding of the dependent variable based on variation in the independent(s). However, in GWR these will automatically improve towards 1 as bandwidth decreases sufficiently. AIC is adjusted for degrees of freedom and so is considered as a better indicator of GWR model quality, though R^2 is still published alongside. Spatial autocorrelation of residuals is also considered when assessing model quality, and so Moran's *I* and associated z-scores are included. Values closer to 0 of each are more desirable, yet higher values may indicate hot spots of activity outside the regional norm. The OLS results therefore supported the use of Geographically Weighted Regression (Table SI.12) OLS and GWR was conducted in ArcMap for each landcover class against the three DDDAT grids at multiple band widths (5 km, 10 km, and 20 km) as well as an AIC determined bandwidth. All OLS results indicate that GWR was necessary. Regression results are shown in Table 3.12 (spanning multiple pages).

Table 3.12 Ordinary Least Squares (OLS) and Geographically Weighted Regression (GWR) results for every class against the three Difference in Degree Day Above Temperature Grids (DDDAT). Bold and underlined values represent best (highest R^2 and lowest AIC) regression results per class and DDDAT.

Landcover Class (Dependent Variable)	DDDAT Grid	Regression model	R^2	Adjusted R^2	AIC	Morans *I* autocorrelation of residuals (z-score)
Snow/Ice	0˚C	Global OLS	0.005	0.005	50,597.28	0.5 (112.8)
		GWR bandwidth 50 km	0.58	0.55	36,425.37	0.18(38.3)

		GWR bandwidth 100 km	0.43	0.43	37,722.43	0.32 (68.3)
		GWR bandwidth AIC determined(33 km)	0.67	0.63	35,610	0.08 (18.7)
	3˚C	Global OLS	0.005	0.005	40,599.15	0.53 (113.7)
		GWR bandwidth 50 km	0.57	0.54	36,553.13	0.21(43.6)
		GWR bandwidth 100 km	0.43	0.42	37,773.14	0.33(70.1)
		GWR bandwidth AIC determined (31 km)	0.67	0.63	35,630.04	0.1 (21.4)
	6˚C	Global OLS	0.023	0.023	40,497.39	0.52 (111.75)
		GWR bandwidth 50 km	0.58	0.55	36,398.40	0.19(40.5)
		GWR bandwidth 100 km	0.41	0.40	37,930.84	0.34(71.5)
		GWR bandwidth AIC determined (29 km)	**0.69**	**0.65**	**35,348.05**	**0.06 (13.4)**
Meltwater	0˚C	Global OLS	0.000	0.000	26,663.54	0.23(48.7)
		GWR bandwidth 50 km	0.19	0.14	25,955.45	0.10(20.3)
		GWR bandwidth 100 km	0.09	0.07	26,318.84	0.17(35.1)
		GWR bandwidth AIC determined(32km)	0.30	0.21	25,641.99	0.03(7.3)
	3˚C	Global OLS	0.002	0.002	26,654.54	0.23(48.9
		GWR bandwidth 50 km	0.21	0.16	25,854.65	0.09(18.1)
		GWR bandwidth 100 km	0.10	0.08	26,239.56	0.16(33.4)
		GWR bandwidth AIC determined(31km)	0.32	0.24	25,524.29	0.02(4.7)
	6˚C	Global OLS	0.000	0.000	26,663.21	0.23(48.5)
		GWR bandwidth 50 km	0.19	0.15	25,880.75	0.09(19.8)
		GWR bandwidth 100 km	0.09	0.08	26,280.54	0.16(34.9)
		GWR bandwidth AIC determined(29km)	**0.33**	**0.24**	**25,462.50**	**0.02(3.9)**
Freshwater	0˚C	Global OLS	0.002	0.002	22,565.73	0.36(77.2)
		GWR bandwidth 50 km	0.38	0.34	20,453.23	0.12(25.3)
		GWR bandwidth 100 km	0.24	0.22	21,275.31	0.20(42.5)
		GWR bandwidth AIC determined(32km)	0.47	0.41	19,997.55	0.05(10.1)
	3˚C	Global OLS	0.003	0.003	22,560.7	0.36(76.6)
		GWR bandwidth 50 km	0.35	0.31	20,716.15	0.14(28.9)
		GWR bandwidth 100 km	0.23	0.21	21,340.74	0.21(44.0)
		GWR bandwidth AIC determined(31km)	0.47	0.41	20,078.58	0.05(11.2)
	6˚C	Global OLS	0.038	0.038	22,371.67	0.33(69.7)
		GWR bandwidth 50 km	0.34	0.31	20,736.15	0.12(26.4)

		GWR bandwidth 100 km	0.21	0.2	21,405.21	0.2(42.9)
		GWR bandwidth AIC determined(29km)	**0.49**	**0.42**	**19,943.43**	**0.03(6.6)**
Coarse Sediment	0˚C	Global OLS	0.002	0.002	36,584.89	0.56(118.4)
		GWR bandwidth 50 km	0.49	0.46	33,393.42	0.20(42.7)
		GWR bandwidth 100 km	0.35	0.34	34,400.79	0.34(71.7)
		GWR bandwidth AIC determined(32km)	0.59	0.55	32,638.55	0.11(22.6)
	3˚C	Global OLS	0.007	0.007	36,559.23	0.56(117.5)
		GWR bandwidth 50 km	0.51	0.48	33,240.38	0.19(40.8)
		GWR bandwidth 100 km	0.37	0.36	34,245.79	0.33(68.8)
		GWR bandwidth AIC determined(31km)	0.61	0.57	32,414.13	0.09(19.1)
	6˚C	Global OLS	0.005	0.005	36,570.56	0.56(118.5)
		GWR bandwidth 50 km	0.50	0.48	33,248.29	0.20(41.6)
		GWR bandwidth 100 km	0.37	0.36	34,286.52	0.34(71.0)
		GWR bandwidth AIC determined(29km)	**0.62**	**0.57**	**32,335.74**	**0.07(15.8)**
Fine-grained Sediment	0˚C	Global OLS	0.008	0.008	33,198.79	0.45(94.6)
		GWR bandwidth 50 km	0.35	0.32	31,337.99	0.18(39.0)
		GWR bandwidth 100 km	0.21	0.20	32,114.55	0.29(60.8)
		GWR bandwidth AIC determined(32km)	0.47	0.41	30,728.22	0.09(20.9)
	3˚C	Global OLS	0.003	0.002	33,227.9	0.45(95.9)
		GWR bandwidth 50 km	0.35	0.31	31,358.15	0.19(40.0)
		GWR bandwidth 100 km	0.20	0.19	32,192.42	0.30(63.1)
		GWR bandwidth AIC determined(31km)	0.48	0.41	30,695.59	0.09(19.7)
	6˚C	Global OLS	0.005	0.005	33,213.46	0.45(95.5)
		GWR bandwidth 50 km	0.35	0.31	31,388.73	0.19(40.4)
		GWR bandwidth 100 km	0.21	0.19	32,513.16	0.30(62.9)
		GWR bandwidth AIC determined(29km)	**0.50**	**0.43**	**30,510.02**	**0.07(15.7)**
Bedrock	0˚C	Global OLS	0.003	0.003	40,722.53	0.56(118.9)
		GWR bandwidth 50 km	0.58	0.55	36,548.43	0.18(38.4)
		GWR bandwidth 100 km	0.44	0.43	37,802.57	0.33(70.0)
		GWR bandwidth AIC determined(32km)	0.66	0.62	35,832.20	0.08(17.9)
	3˚C	Global OLS	0.000	0.000	40,738.89	0.57(119.8)
		GWR bandwidth 50 km	0.58	0.56	36,462.45	0.18(38.9)

		GWR bandwidth 100 km	0.45	0.44	37,690.69	0.32(69.4)
		GWR bandwidth AIC determined(31km)	0.68	0.64	35,610.95	0.07(15.8)
	6˚C	Global OLS	0.000	0.000	40,737.03	0.57(119.9)
		GWR bandwidth 50 km	0.58	0.56	36,459.76	0.17(36.7)
		GWR bandwidth 100 km	0.43	0.42	37,866.89	0.34(70.9)
		GWR bandwidth AIC determined(29km)	**0.69**	**0.65**	**35,585.63**	**0.05(11.4)**
Dry Tundra	0˚C	Global OLS	0.002	0.002	37,989.99	0.59(124.1)
		GWR bandwidth 50 km	0.50	0.47	34,710.29	0.28(59.9)
		GWR bandwidth 100 km	0.28	0.27	36,386.68	0.45(94.9)
		GWR bandwidth AIC determined(32km)	0.62	0.58	33,619.47	0.16(33.2)
	3˚C	Global OLS	0.003	0.003	37,983.55	0.59(123.9)
		GWR bandwidth 50 km	0.49	0.46	34,833.01	0.29(62.5)
		GWR bandwidth 100 km	0.27	0.26	36,432.33	0.45(96.7)
		GWR bandwidth AIC determined(31km)	0.64	0.60	33,497.23	0.15(32.2)
	6˚C	Global OLS	0.017	0.017	37,909.40	0.58(122.9)
		GWR bandwidth 50 km	0.52	0.50	34,439.45	0.26(55.6)
		GWR bandwidth 100 km	0.29	0.27	36,296.88	0.45(94.5)
		GWR bandwidth AIC determined(29km)	**0.67**	**0.63**	**33,087.02**	**0.11(22.6)**
Dense/wet Vegetation	0˚C	Global OLS	0.001	0.001	29,311.42	0.57(121.6)
		GWR bandwidth 50 km	0.49	0.46	26,113.14	0.22(46.8)
		GWR bandwidth 100 km	0.34	0.33	27,265.46	0.36(75.8)
		GWR bandwidth AIC determined(32km)	0.60	0.55	25,253.33	0.11(23.6)
	3˚C	Global OLS	0.017	0.017	29,226.08	0.56(118.4)
		GWR bandwidth 50 km	0.50	0.47	26,047.58	0.22(45.6)
		GWR bandwidth 100 km	0.34	0.33	27,204.55	0.35(75.1)
		GWR bandwidth AIC determined(31km)	0.61	0.57	25,168.41	0.09(20.1)
	6˚C	Global OLS	0.058	0.058	28,998.04	0.54(113.8)
		GWR bandwidth 50 km	0.50	0.47	26,005.77	0.21(44.9)
		GWR bandwidth 100 km	0.35	0.34	27,165.78	0.35(73.9)
		GWR bandwidth AIC determined(29km)	**0.63**	**0.58**	**25,031.95**	**0.07(16.9)**

Comparing the landcover change grids to the Difference in Degree Days Above Temperature grids (between 1980s and 2010s) on a grid cell by grid cell basis, the lowest R^2 and Akaike information criterion values are shown for the two water and the fine sediment classes. The highest R^2 and Akaike information criterion correlations however are found for the vegetation, bedrock and ice classes, suggesting a close association between these types of landcover change and climate change across Greenland. This is not unsurprising, as increased temperatures most directly cause ice melt, which in turn exposes areas of bare bedrock. These bare rock surfaces have a lower albedo, feeding increased localised warming and so exacerbated melt (Bergstrom et al., 2020; Gunnarsson et al., 2023). Similarly, vegetation has been well documented to expand and proliferate under higher positive (^{o}C) temperatures, particularly evident in the Arctic (e.g. Blok et al., 2011; Jia et al., 2009; Karami et al., 2018; Kelsey et al., 2021).

Specifically, and most interestingly, the highest R^2 and Akaike information criterion values across all land cover classes are found for the difference in the number of days above the 6°C threshold. This suggests that both historically and progressively, future land cover change is likely to be marked and accelerated in regions where the number of days per year above this 6°C threshold are increasing most rapidly. It is acknowledged that the optimal threshold may lie between 3°C and 6°C, but exploring this further was not feasible within the remit of this work and remains an interesting avenue for future research. Crucially, this work identifies that it is not simply where temperatures are set to rise most rapidly but along a posed change gradient in Greenland where the number of warm days per year, are increasing and transient responses to this shift are most marked.

3.4 Discussion: A model of changing landcover across Greenland

The findings of this chapter are multifarious and reveal complex landcover transitions at multiple scales across Greenland. Nationally, ice loss from the Greenland Ice Sheet and from glaciers and ice caps has increased since the 1980s and consequently the proglacial parts of Greenland have expanded rapidly. The loss of ice represents considerable contributions to global sea level rise and ocean freshening (Rignot et al., 2011) and will also control river discharge and associated sediment plumes in fjords affecting coastal ecosystems (e.g. Rysgaard et al., 2011). These

patterns of ice cover loss are corroborated by Mouginot et al. (2019) who reported glacier mass balance from the 1972 to 2018, finding particularly high increases in ice flux (almost 100 %) and cumulative loss (~150 Gt) from basins in mid/north west Greenland.

Beside the loss of ice cover (-28,707 km2 ± 9,767 km^2) over the past 30 years, in Greenland's transient proglacial landscapes, there has been a doubling in total areal coverage of vegetation (111 % ± 13 %), a quadrupling in wetlands coverage (380 % ± 29 %), increased meltwater (15 % ± 15 %), decreased bare bedrock (-16 % ± 4 %) and increased coverage of fine unconsolidated sediment (4 % ± 13 %). The meltwater changes (Figure 3.14 B) observed are corroborated by findings from Mernild et al. (2017), who found increasing runoff trends for 80 % of Greenland's catchments between 1979 and 2014 with relatively high runoff in the south-west and north-east, as identified in Figure 3.14 B. Similarly, freshwater lake decreases in Greenland have been observed elsewhere. Finger-Higgens et al. (2019) reported a 2 % decrease in lake area (15 % for smaller ponds) in west Greenland, and Carrivick and Quincey (2014) and How et al. (2021) both show changes in lakes adjacent to ice-margins.

The regional distributions of these individual class changes have been revealed and the implications already discussed concerning the locations of vegetation and wetland expansion coincident with barren ground loss. Moreover, further to these individual class changes, this work quantifies inter-class transitions specifically, revealing where specific classes are transitioning, and how these transitions are manifest. This allows the identification of 'hot spots' of specific change, such as meltwater to sediment classes which has been found to reveal delta progradation, an example of which revealed by this work has already found utility in wider literature, published in (Carrivick & Tweed, 2021). Moreover, as shown in figure 3.15 A, braidplain expansion and altered river morphology resulting from sediment aggradation which has far reaching implications. Terrestrial sediment deposition and anastomosing may reflect reduced energy and so reduced nutrient conveyance marine ecosystems (Makaske, 2001). However, as sand reserves are depleted globally and demand increases (e.g. urban expansion, infrastructural improvements, coastal protection), Greenland may be poised to exploit this widespread phenomenon

(4 % increase in fine sediment across Greenland) to become a leading global aggregate exporter for sustainable economic independence (Bendixen et al., 2001).

Landcover change is shown to be most strongly associated with the difference in the number of positive degree days, especially above 6^{o}C between the 1980s and the present day. Specifically, regions where the change in the number of days reaching and exceeding this threshold are most closely correlated with all landcover changes, highlighting the importance of climate transition rather than warming in driving landcover change in Greenland. Contrastingly, absolute temperature increase has a negligible association with landcover change. These landcover changes reported and discussed regionally in this chapter represent rapid and intense widespread geomorphological and process activity locally in Greenland. These localised geomorphological, hydrological and ecological processes and formations are investigated and discussed with pertinent examples in the results and discussions section of this chapter. The widespread changes and local processes revealed through changing landcover have profound consequences for land surface albedo, greenhouse gas emissions, landscape stability and sediment delivery, and biogeochemical processes. This overall discussion therefore seeks to amalgamate the regional patterns of class change with the specific inter-class transitions and associated processes in light of increasing days over 6^{o}C shown and discussed in this chapter into a conceptual transition model, shown in Figure 3.16.

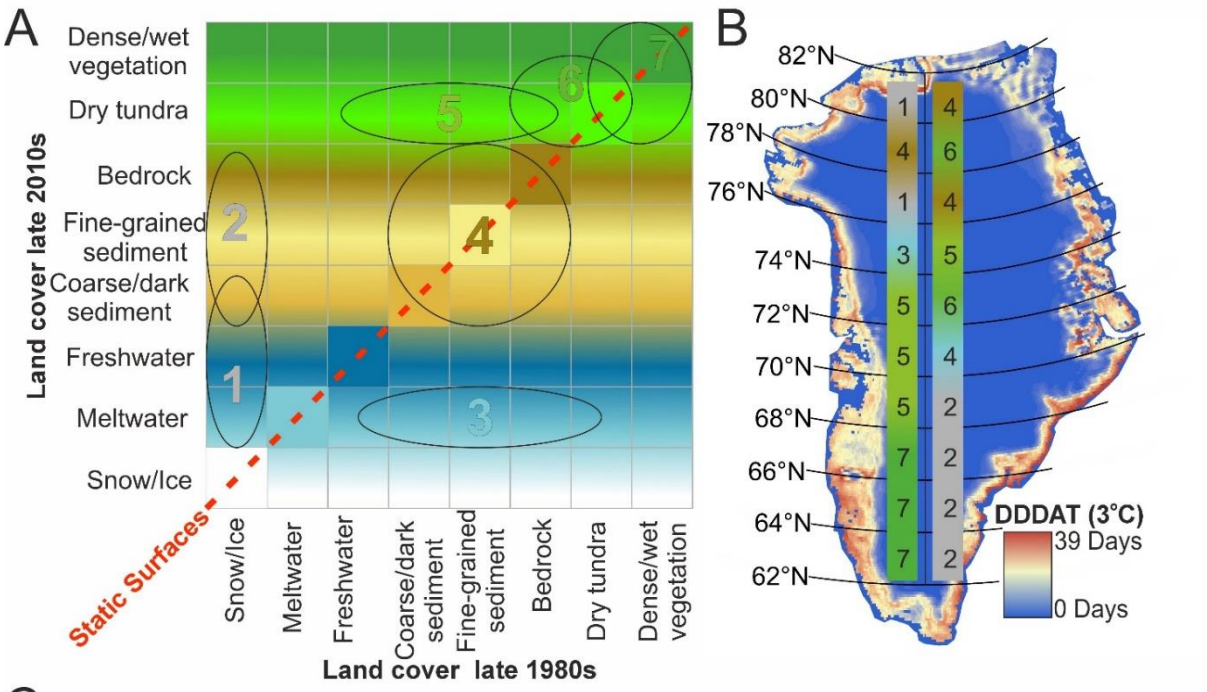

C

Phase		Description
1	Ice sheet retreat	Ice loss replaced by till (sediment) and exposed bedrock, yet relatively subdued topography results in low intensity of paraglacial activity.
2	Ice retreat topographically controlled	Ice retreat in steep mountainous areas producing relatively high hillslope activity and meltwater across valley floors.
3	Meltwater discharge hotspots	Zones where meltwater coverage is high. Sediment flux is high and vegetation encroachment in a few places, therefore cross-over with phases 4 and 5.
4	Periglacial sediment cascades	Sediment cascades dominate transient ice free landscape dynamics. Landcover change is primarily within sediment and bedrock classes.
5	Tundra vegetation colonisation	Tundra encroachment on weathered bedrock and sediment surfaces dominates the landcover change signal, moderate sediment fluxes.
6	Tundra colonisation and wetland vegetation hotspots	As well as tundra vegetation encroachment, wetlands develop often coinciding with relatively high meltwater and freshwater coverage increases.
7	Vegetation established	Vegetation already dominates landcover and is becoming more dense. Some wetland development. Sediment fluxes are relatively low. Relative stability of proglacial areas and areas of human population

Figure 3.16 Land cover change model 1980s to 2010s for Greenland, illustrating numbered predominant landcover inter-class changes on a common trajectory reflecting increasing landscape stability with time; i.e. phases (A). Panel B shows degree day difference air temperature (DDDAT) mapped and with east and west coast latitudinal transects of numbered predominant landcover inter-class change in each latitudinal band. Numbered inter-class changes are detailed in the table (C).

The conceptual transition model of landcover phase changes across Greenland utilises the 64-class change grid as referenced previously (Table 3.6). This was dissected into 20 distinct regions, with 10 latitudinal bands of 2 degrees each, split between east and west (see Figure 3.16). For each of these latitudinal bands an 8x8 matrix was produced of class transitions, with each cell of the matrix showing cell counts for each transition, and the diagonals being static, i.e. no change. These cell counts were then converted into area (km^2) and percentage of each matrix, both

considering and excluding static landcover cells (Appendix A: Figure 7.1 and 7.2). These matrices were then colour coded by proportion of that matrix each cell represents (Appendix A: Figure 7.1), and then again but comparing that transition cell against the same transition cell in each of the other matrices (Appendix A: Figure 7.2). Essentially, the predominant inter-class landcover changes were defined per latitudinal band and separately for the east and west coasts.

Notably, there is a distinct difference in the latitudinal pattern of the predominant landcover inter-class changes per latitudinal band between the east and west of Greenland, evident in both Figure 3.14 and 3.16 B. The size of proglacial areas is far larger in the south west than in the south east, and the topographic relief is generally more subdued in the west compared to the alpine east and so accommodating of regolith and tundra vegetation establishment (Bonow et al., 2014; Medvedev et al., 2013). Moreover, the two coasts have experienced different climatic change (Box, 2002) (See literature review chapter), in terms of temperature and precipitation; the east is influenced by variability in North Atlantic Oscillation and the Atlantic Meridional Overturning Circulation (Driesschaert et al., 2007; Swingedouw et al., 2022).

The model, and the relationship between landcover changes and the difference in degree days above 6^{o}C, illustrates that higher air temperatures are producing more suitable conditions for vegetation expansion and growth (Myers-Smith et al., 2011). Vegetation cover is perhaps the most profound landcover change quantified in this chapter because it has considerable feedback effects on the climate system (Normand et al., 2013). For example, the newly-established and enlarging wetlands and fens in phase 6 regions of the north east of Greenland are associated with considerable methanogenesis (Kotsyurbenko et al., 2019), but that is potentially partially offset by long-term carbon storage via peat accretion (Ovenden, 1990). Field observations combined with mapping indicate widespread shrubification in Greenland, whereby the “greening” of the Arctic is largely manifest in the proliferation of shrub tundra species (Myers-Smith et al., 2020). There is substantial vegetation areal expansion and growth in regions of critical permafrost thaw (phases 5 and 6, Figure 3.16). That expansion can be interpreted as a manifestation of increased air temperature warming ground surfaces exacerbating and compounding permafrost thaw (Schuur et al., 2015). Permafrost thaw impacts a suite of human and economic activity; Greenland’s

infrastructure has been forced onto challenging ground underlain by thick poorly consolidated glacigenic sediment and permafrost (Daanen et al., 2011) with economic development, localised population growth and increased tourism that all have environmental consequences (c.f. Arnaut and Lidman, 2021). This analysis can therefore be interpreted to reveal a positive feedback between permafrost degradation and vegetation encroachment that will likely increase exponentially, threatening both local communities and infrastructure (Hjort et al.,2018). These land cover feedbacks, especially for landscape parts in phases 5 through 7 (Figure 3.16), therefore warrant policymakers' attention for a range of purposes, including local infrastructure planning, community adaptation strategies, regional environmental management, and global climate policy formulation. Addressing these changes at multiple scales will help mitigate the impacts on local communities, support sustainable development, and contribute to broader efforts to manage climate change.

3.5 Conclusions

In conclusion, this chapter has provided a detailed and comprehensive analysis of landcover changes in Greenland over the last four decades, offering critical insights into the complex dynamics at play in the Arctic environment. By employing high-resolution Landsat image mosaics and a rigorous methodological framework, the study has successfully quantified and classified the profound transformations occurring around Greenland's periphery, highlighting the significant environmental implications of these changes.

The research has underscored the significant influence of a warming Arctic on land cover transitions, highlighting how increasing temperatures drive changes in vegetation and other land cover types. However, it has also elucidated the relatively poor utility of relying solely on simple average temperature change trends for predicting and influencing these complex changes. This indicates a need for more nuanced and detailed climate models that can better account for the various factors and feedback mechanisms involved in Arctic land cover dynamics. Instead, specific thresholds in temperature are highlighted, specifically 6^{o}C, with regions increasing most rapidly in the number of $\geq$6^{o}C days seeing the highest responses manifest in landcover transitions. This warming trend has precipitated a series of consequential environmental responses: the retreat of glaciers and ice caps, expansion of glacier-

fed and permafrost lakes, alterations in sediment transport dynamics, and a marked increase in vegetation cover and diversity. These changes, indicative of broader Arctic shrubification processes, reflect the sensitivity of Greenland's ecosystems to climatic perturbations and underscore the region's role as a barometer for wider Arctic and global environmental change.

Central to this study is the development of a novel landcover phase change conceptual model, which has facilitated a nuanced understanding of the predominant inter-class changes. This model, combined with a spatially-distributed assessment of landcover change accuracy, has allowed for an unprecedented level of detail and accuracy in mapping and interpreting landcover dynamics in Greenland transitioning from the late 20th into the early 21st century. The integration of topographic corrections and the use of advanced image preprocessing techniques have further enhanced the fidelity and robustness of the landcover classifications produced, and the output datasets might find widespread utility in geomorphological, hydrological, ecological and societal studies in Greenland. The findings from this research are sobering, illustrating not just localised environmental shifts but also their broader implications for climate feedback mechanisms. The expansion of vegetation and the associated decrease in albedo, the release of greenhouse gases from melting permafrost, and the altered biogeochemical cycles are all indicative of the complex feedback loops that are both a response to and a driver of further climate change. These transformations have far-reaching implications for local and global climate systems, water resources management, and biodiversity conservation. Moreover, the study's meticulous approach to accuracy assessment, employing both field validation and remote sensing techniques, ensures that the findings are robust and reliable. The detailed spatial analysis of change, coupled with the quantification of confidence intervals and error margins, provides a comprehensive and credible account of landcover dynamics, setting a high standard for future research in the field.

In light of these findings, it is evident that the changes occurring in Greenland's landcover are a microcosm of the broader, more dramatic transformations taking place in the rapidly changing Arctic. The insights gained from this study are invaluable for informing climate change mitigation and adaptation strategies, guiding policy decisions, and shaping the direction of future research. As the Arctic continues to warm at an accelerated pace, understanding and monitoring these

landcover changes will be crucial for predicting and mitigating the broader impacts of climate change. Thus, this chapter not only provides a detailed account of past and present changes but also forms a critical foundation for future endeavours aimed at safeguarding the Arctic and the planet's environmental future.

In summary, this study has identified, quantified and summarised regional, inter-catchment and intra-catchment landcover changes across Greenland between the late 1980s and the late 2010s. This spatiotemporal coverage has enabled proposal of a conceptual model of landcover phase change and the association of that landcover change with climate. Specifically, where the difference in degree days is > 6^{o}C, then there is increased ice sheet and glacier mass loss, increased meltwater production and increased sediment mobility. Overall, the rapid changes in landcover across Greenland requires repeated monitoring to identify change trajectories and to refine understanding, which will directly benefit human and economic development. For the geosciences, feedbacks of landcover with climate must be considered when modelling and projecting climate, the Greenland Ice Sheet, PGIC evolution, meltwater runoff, sediment yield and habitat and ecological community changes.

3.6 Chapter 3 References

Abdu, H. A. (2019). Classification accuracy and trend assessments of land cover-land use changes from principal components of land satellite images. International Journal of Remote Sensing, 40(4). https://doi.org/10.1080/01431161.2018.1524587

Anderson, N.J., Saros, J.E., Bullard, J.E., Cahoon, S.M., McGowan, S., Bagshaw, E.A., Barry, C.D., Bindler, R., Burpee, B.T., Carrivick, J.L. and Fowler, R.A. (2017). The Arctic in the twenty-first century: Changing biogeochemical linkages across a paraglacial landscape of Greenland. BioScience, 67(2), pp.118-133.

Arnaut, J. and Lidman, J. (2021). Environmental sustainability and economic growth in Greenland: testing the environmental Kuznets curve. Sustainability, 13(3), pp.1228.

Bamber, J.L., Westaway, R.M., Marzeion, B. and Wouters, B. (2018). The land ice contribution to sea level during the satellite era. Environmental Research Letters, 13(6), pp.063008. Bannari, A., Morin, D., Bonn, F. & Huete, A. R. 1995. A review of vegetation indices. Remote Sensing Reviews, 13, 95-120.

Bárcena, T.G., Finster, K.W. and Yde, J.C. (2011). Spatial patterns of soil development, methane oxidation, and methanotrophic diversity along a receding glacier forefield, Southeast Greenland. Arctic, Antarctic, and Alpine Research, 43(2), pp.178-188.

Bay, C. (1994), March. Review of vegetation mapping in Greenland. In Circumpolar Arctic Vegetation Mapping Workshop.

Bendixen, M., Lønsmann Iversen, L., Anker Bjørk, A., Elberling, B., Westergaard-Nielsen, A., Overeem, I., Barnhart, K.R., Abbas Khan, S., Box, J.E., Abermann, J. and Langley, K. (2017). Delta progradation in Greenland driven by increasing glacial mass loss. Nature, 550(7674), pp.101-104.

Bennike, O. and Björck, S. (2002). Chronology of the last recession of the Greenland Ice Sheet. Journal of Quaternary Science: Published for the Quaternary Research Association, 17(3), pp.211-219.

Bergstrom, A., Gooseff, M. N., Myers, M., Doran, pp. T., & Cross, J. M. (2020). The seasonal evolution of albedo across glaciers and the surrounding landscape of Taylor Valley, Antarctica. Cryosphere, 14(3). https://doi.org/10.5194/tc-14-769-2020

Bivand, Roger, Danlin Yu, Tomoki Nakaya, Miquel-Angel Garcia-Lopez, and Maintainer Roger Bivand. (2017). "Package 'Spgwr'." R Software Package.

Blok, D., Schaepman-Strub, G., Bartholomeus, H., Heijmans, M. M. pp. D., Maximov, T. C., & Berendse, F. (2011). The response of Arctic vegetation to the summer climate: Relation between shrub cover, NDVI, surface albedo and temperature. Environmental Research Letters, 6(3). https://doi.org/10.1088/1748-9326/6/3/035502

Bonow, J. M., Japsen, pp., & Nielsen, T. F. D. (2014). High-level landscapes along the margin of southern East Greenland-A record of tectonic uplift and incision after breakup in the NE Atlantic. Global and Planetary Change, 116. https://doi.org/10.1016/j.gloplacha.2014.01.010

Box, J.E. (2002). Survey of Greenland instrumental temperature records: 1873–2001. International Journal of Climatology: A Journal of the Royal Meteorological Society, 22(15), pp.1829-1847.

Box, J.E., Colgan, W.T., Christensen, T.R., Schmidt, N.M., Lund, M., Parmentier, F.J.W., Brown, R., Bhatt, U.S., Euskirchen, E.S., Romanovsky, V.E. and Walsh, J.E. (2019). Key indicators of Arctic climate change: 1971–2017. Environmental Research Letters, 14(4), pp.045010.

Box, J.E., Colgan, W.T., Wouters, B., Burgess, D.O., O'Neel, S., Thomson, L.I. and Mernild, S.H. (2018). Global sea-level contribution from Arctic land ice: 1971–2017. Environmental Research Letters, 13(12), pp.125012.

Breiman, L. (2001). Random forests. Machine learning, 45(1), pp.5-32.

Brovkin, V., Bendtsen, J., Claussen, M., Ganopolski, A., Kubatzki, C., Petoukhov, V. and Andreev, A. (2002). Carbon cycle, vegetation, and climate dynamics in the Holocene: Experiments with the CLIMBER-2 model. Global Biogeochemical Cycles, 16(4), pp.86-1.

Brunsdon, C., Fotheringham, A.S. and Charlton, M.E. (1996). Geographically weighted regression: a method for exploring spatial nonstationarity. Geographical analysis, 28(4), pp.281-298.

Burpee, B. T., Anderson, D., & Saros, J. E. (2018). Assessing ecological effects of glacial meltwater on lakes fed by the Greenland Ice Sheet: The role of

nutrient subsidies and turbidity. Arctic, Antarctic, and Alpine Research, 50(1). https://doi.org/10.1080/15230430.2017.1420953

Byrne, G. F., Crapper, pp. F., & Mayo, K. K. (1980). Monitoring land-cover change by principal component analysis of multitemporal landsat data. Remote Sensing of Environment, 10(3). https://doi.org/10.1016/0034-4257(80)90021-8

Callaghan, T.V., Christensen, T.R. and Jantze, E.J. (2011). Plant and vegetation dynamics on Disko Island, West Greenland: snapshots separated by over 40 years. Ambio, 40, pp.624-637.

Carlson, T.N. and Ripley, D.A. (1997). On the relation between NDVI, fractional vegetation cover, and leaf area index. Remote sensing of Environment, 62(3), pp.241-252.

Carrivick, J. L., & Tweed, F. S. (2013). Proglacial lakes: character, behaviour and geological importance. Quaternary Science Reviews, 78, 34–52. https://doi.org/10.1016/j.quascirev.2013.07.028

Carrivick, J. L., & Tweed, F. S. (2021). Deglaciation controls on sediment yield: Towards capturing spatio-temporal variability. In Earth-Science Reviews (Vol. 221). https://doi.org/10.1016/j.earscirev.2021.103809

Carrivick, J. L., How, pp., Lea, J. M., Sutherland, J. L., Grimes, M., Tweed, F. S., Cornford, S., Quincey, D. J., & Mallalieu, J. (2022). Ice-marginal proglacial lakes across Greenland: Present status and a possible future. Geophysical Research Letters, 49(12), e2022GL099276.

Carrivick, J. L., Yde, J., Russell, A. J., Quincey, D. J., Ingeman-Nielsen, T. & Mallalieu, J. (2017). Ice-margin and meltwater dynamics during the mid-Holocene in the Kangerlussuaq area of west Greenland. Boreas, 46, 369-387.

Carrivick, J.L. and Heckmann, T. (2017). Short-term geomorphological evolution of proglacial systems. Geomorphology, 287, pp.3-28.

Carrivick, J.L. and Quincey, D.J. (2014). Progressive increase in number and volume of ice-marginal lakes on the western margin of the Greenland Ice Sheet. Global and Planetary Change, 116, pp.156-163.

Carrivick, J.L. and Tweed, F.S. (2021). Deglaciation controls on sediment yield: Towards capturing spatio-temporal variability. Earth-Science Reviews, 221, pp.103809.

Chylek, P., Box, J.E. and Lesins, G., 2004. Global warming and the Greenland ice sheet. *Climatic Change*, 63(1), pp. 201-221.

Chylek, pp., Folland, C.K., Lesins, G., Dubey, M.K. and Wang, M. (2009). Arctic air temperature change amplification and the Atlantic Multidecadal Oscillation. Geophysical Research Letters, 36(14), pp. 1-5.

Clifford, pp., Richardson, S. and Hemon, D., (1989). Assessing the significance of the correlation between two spatial processes. Biometrics, pp.123-134.

Cohen, W. B. & Goward, S. N. 2004. Landsat's role in ecological applications of remote sensing. Bioscience, 54, pp. 535-545.

Comber, A.J., Harris, P. and Tsutsumida, N., 2016. Improving land cover classification using input variables derived from a geographically weighted

principal components analysis. ISPRS Journal of Photogrammetry and Remote Sensing, 119, pp.347-360.

Comber, A.J., 2013. Geographically weighted methods for estimating local surfaces of overall, user and producer accuracies. Remote Sensing Letters, 4(4), pp.373-380.

Comber, A., Callaghan, M., Harris, P., Lu, B., Malleson, N. and Brunsdon, C., 2022. Gwverse: a template for a new generic geographically weighted R package. Geographical Analysis, 54(3), pp.685-709.

Comber, A., Brunsdon, C., Charlton, M. and Harris, P., 2017. Geographically weighted correspondence matrices for local error reporting and change analyses: mapping the spatial distribution of errors and change. Remote Sensing Letters, 8(3), pp.234-243.

Comber, A., Fisher, P., Brunsdon, C. and Khmag, A., 2012. Spatial analysis of remote sensing image classification accuracy. Remote Sensing of Environment, 127, pp.237-246.

Congalton, Russell G. (1991). “A Review of Assessing the Accuracy of Classifications of Remotely Sensed Data.” Remote Sensing of Environment 37 (1): 35–46.

Daanen, R. pp., Ingeman-Nielsen, T., Marchenko, S. S., Romanovsky, V. E., Foged, N., Stendel, M., Christensen, J. H., & Hornbech Svendsen, K. (2011). Permafrost degradation risk zone assessment using simulation models. Cryosphere, 5(4). https://doi.org/10.5194/tc-5-1043-2011

Daniels, F. J. A., de Molenaar, J. G., Chytry, M., & Tichy, L. (2011). Vegetation change in Southeast Greenland? Tasiilaq revisited after 40 years. Applied Vegetation Science, 14(2), 230–241. https://doi.org/10.1111/j.1654-109X.2010.01107.x

Diaz-Delgado, R., Bustamante, J., Aragones, D. and Pacios, F., 2006. Determining Water Body Characteristics of Doana Shallow Marshes Through Remote Sensing. In: 2006 IEEE International Symposium on Geoscience and Remote Sensing. Denver, CO, USA, 2006, pp. 3662-3663.

Driesschaert, E., Fichefet, T., Goosse, H., Huybrechts, pp., Janssens, I., Mouchet, A., Munhoven, G., Brovkin, V., & Weber, S. L. (2007). Modeling the influence of Greenland ice sheet melting on the Atlantic meridional overturning circulation during the next millennia. Geophysical Research Letters, 34(10). https://doi.org/10.1029/2007gl029516

Elberling, B., Tamstorf, M.P., Michelsen, A., Arndal, M.F., Sigsgaard, C., Illeris, L., Bay, C., Hansen, B.U., Christensen, T.R., Hansen, E.S. and Jakobsen, B.H., (2008). Soil and plant community-characteristics and dynamics at Zackenberg. Advances in ecological research, 40, pp.223-248.

Finger Higgens, R.A., Chipman, J.W., Lutz, D.A., Culler, L.E., Virginia, R.A. and Ogden, L.A. (2019). Changing lake dynamics indicate a drier Arctic in Western Greenland. Journal of Geophysical Research: Biogeosciences, 124(4), pp.870-883.

Foody, G.M. (2002). Status of land cover classification accuracy assessment. Remote Sensing of Environment, 80(1), pp.185-201.

Foody, G.M. (2004). Thematic map comparison. Photogrammetric Engineering & Remote Sensing, 70(5), pp.627-633.

Foody, GM. (2005). “Local Characterization of Thematic Classification Accuracy Through Spatially Constrained Confusion Matrices.” International Journal of Remote Sensing 26 (6): 1217–28.

Ford, J.D. and Goldhar, C. (2012). Climate change vulnerability and adaptation in resource dependent communities: a case study from West Greenland. Climate Research, 54(2), pp.181-196.

Fotheringham, A.S., Brunsdon, C. and Charlton, M. (2003). Geographically weighted regression: the analysis of spatially varying relationships. John Wiley & Sons.

Gorelick, N., Hancher, M., Dixon, M., Ilyushchenko, S., Thau, D. & Moore, R. (2017). Google Earth Engine: Planetary-scale geospatial analysis for everyone. Remote Sensing of Environment, 202, 18-27.

Goward, S., Arvidson, T., Williams, D., Faundeen, J., Irons, J. and Franks, S. (2006). Historical record of Landsat global coverage. Photogrammetric Engineering & Remote Sensing, 72(10), pp.1155-1169.

Gruber, S. and Haeberli, W. (2007). Permafrost in steep bedrock slopes and its temperature-related destabilization following climate change. Journal of Geophysical Research: Earth Surface, 112(F2).

Gunnarsson, A., Gardarsson, S. M., & Pálsson, F. (2023). Modeling of surface energy balance for Icelandic glaciers using remote-sensing albedo. Cryosphere, 17(9). https://doi.org/10.5194/tc-17-3955-2023

Hall, D. K. & Riggs, G. A. (2011). Normalized-Difference Snow Index (NDSI). In: Singh, V. pp., Singh, pp. & Haritashya, U. K. (eds.) Encyclopedia of Snow, Ice and Glaciers. Dordrecht: Springer Netherlands.

Hanna, E., Huybrechts, pp., Steffen, K., Cappelen, J., Huff, R., Shuman, C., Irvine-Fynn, T., Wise, S., & Griffiths, M. (2008). Increased runoff from melt from the Greenland Ice Sheet: A response to global warming. Journal of Climate, 21(2). https://doi.org/10.1175/2007JCLI1964.1

Hasmadi, M., Pakhriazad, H.Z. and Shahrin, M.F. (2009). Evaluating supervised and unsu-pervised techniques for land cover mapping using remote sensing data. Geografia: Malaysian Journal of Society and Space, 5(1), pp.1-10.

Hawkings, J.R., Wadham, J.L., Tranter, M., Lawson, E., Sole, A., Cowton, T., Tedstone, A.J., Bartholomew, I., Niewnow, pp., Chandler, D. and Telling, J. (2015). The effect of warming climate on nutrient and solute export from the Greenland Ice Sheet. Geochemical Perspectives Letters.

Heindel, R.C., Chipman, J.W. and Virginia, R.A. (2015). The spatial distribution and ecological impacts of aeolian soil erosion in Kangerlussuaq, West Greenland. Annals of the Association of American Geographers, 105(5), pp.875-890.

Heindel, R.C., Culler, L.E. and Virginia, R.A. (2017). Rates and processes of aeolian soil erosion in West Greenland. The Holocene, 27(9), pp.1281-1290.

Hendry, K.R., Huvenne, V.A., Robinson, L.F., Annett, A., Badger, M., Jacobel, A.W., Ng, H.C., Opher, J., Pickering, R.A., Taylor, M.L. and Bates, S.L. (2019). The biogeochemical impact of glacial meltwater from Southwest Greenland. Progress in Oceanography, 176, pp.102126.

Hersbach, H., Bell, B., Berrisford, pp., Hirahara, S., Horányi, A., Muñoz-Sabater, J., Nicolas, J., Peubey, C., Radu, R., Schepers, D. and Simmons, A. (2020). The ERA5 global reanalysis. Quarterly Journal of the Royal Meteorological Society, 146(730), pp.1999-2049.

Hibbard, K., Janetos, A., van Vuuren, D.P., Pongratz, J., Rose, S.K., Betts, R., Herold, M. and Feddema, J.J. (2010). Research priorities in land use and land-cover change for the Earth system and integrated assessment modelling. *International Journal of Climatology*, 30(13), pp.2118-2128.

Hjort, J., Karjalainen, O., Aalto, J., Westermann, S., Romanovsky, V.E., Nelson, F.E., Etzelmüller, B. and Luoto, M. (2018). Degrading permafrost puts Arctic infrastructure at risk by mid-century. *Nature Communications*, 9(1), pp.5147.

Hollesen, J., Elberling, B., & Jansson, pp. E. (2011). Future active layer dynamics and carbon dioxide production from thawing permafrost layers in Northeast Greenland. *Global Change Biology*, 17(2), 911–926. https://doi.org/10.1111/j.1365-2486.2010.02256.x

Horwath Burnham, J. and Sletten, R.S. (2010). Spatial distribution of soil organic carbon in northwest Greenland and underestimates of high Arctic carbon stores. *Global Biogeochemical Cycles*, 24(3). pp. 1-14

How, pp., Messerli, A., Mätzler, E., Santoro, M., Wiesmann, A., Caduff, R., Langley, K., Bojesen, M.H., Paul, F., Kääb, A. and Carrivick, J.L. (2021). Greenland-wide inventory of ice marginal lakes using a multi-method approach. *Scientific Reports*, 11(1), pp.4481.

Howat, I. M., Negrete, A. & Smith, B. E. (2014). The Greenland Ice Mapping Project (GIMP) land classification and surface elevation data sets. Cryosphere, 8, 1509-1518.

Hurni, K., Heinimann, A., & Würsch, L. (2017). Google Earth Engine Image Pre-processing Tool: Background and Methods. Available from: https://www.cde.unibe.ch/e65013/e542846/e707304/e707386/e707390/CDE_Pre-processingTool-UserGuide_eng.pdf . Date: 09/12/2021.

Huttunen, J.T., Nykänen, H., Turunen, J. and Martikainen, pp.J. (2003). Methane emissions from natural peatlands in the northern boreal zone in Finland, Fennoscandia. *Atmospheric Environment*, 37(1), pp.147-151.

Jakobsen, B.H. (1992). Preliminary studies of soils in North-East Greenland between 74 and 75 northern latitude. Geografisk Tidsskrift, 92, pp.111-115.

Jia, G. J., Epstein, H. E., & Walker, D. A. (2009). Vegetation greening in the canadian arctic related to decadal warming. Journal of Environmental Monitoring, 11(12). https://doi.org/10.1039/b911677j

Jørgensen, C.J., Johansen, K.M.L., Westergaard-Nielsen, A. and Elberling, B. (2015). Net regional methane sink in High Arctic soils of northeast Greenland. Nature Geoscience, 8(1), pp.20-23.

Jørgenson, M. T., & Grosse, G. (2016). Remote Sensing of Landscape Change in Permafrost Regions. Permafrost and Periglacial Processes, 27(4), 324–338. https://doi.org/10.1002/ppp.1914

Joshi, pp. K., Ghosh, A., Chakraborty, A., Sharma, R. & Joshi, A. (2013). Landsat again - continuing remote sensing, monitoring, mapping and measuring. Current Science, 105, 761-763.

Karami, M., Westergaard-Nielsen, A., Normand, S., Treier, U. A., Elberling, B., & Hansen, B. U. (2018). A phenology-based approach to the classification of Arctic tundra ecosystems in Greenland. ISPRS Journal of Photogrammetry and Remote Sensing, 146. https://doi.org/10.1016/j.isprsjprs.2018.11.005

Kelsey, K. C., Pedersen, S. H., Leffler, A. J., Sexton, J. O., Feng, M., & Welker, J. M. (2021). Winter snow and spring temperature have differential effects on vegetation phenology and productivity across Arctic plant communities. Global Change Biology, 27(8). https://doi.org/10.1111/gcb.15505

Khan, S. A., Kjeldsen, K. K., Kjær, K. H., Bevan, S., Luckman, A., Bjørk, A. A., Korsgaard, N. J., Box, J. E., Van Den Broeke, M., Van Dam, T. M., & Fitzner, A. (2014). Glacier dynamics at Helheim and Kangerdlugssuaq glaciers, southeast Greenland, since the Little Ice Age. Cryosphere, 8(4). https://doi.org/10.5194/tc-8-1497-2014

Kloiber, S. N., Brezonik, pp. L., Olmanson, L. G. & Bauer, M. E. (2002). A procedure for regional lake water clarity assessment using Landsat multispectral data. Remote Sensing of Environment, 82, 38-47.

Korsgaard, N.J., Nuth, C., Khan, S.A., Kjeldsen, K.K., Bjørk, A.A., Schomacker, A. and Kjær, K.H. (2016). Digital elevation model and orthophotographs of Greenland based on aerial photographs from 1978–1987. Scientific Data, 3(1), pp.1-15.

Kotsyurbenko, O.R., Glagolev, M.V., Merkel, A.Y., Sabrekov, A.F. and Terentieva, I.E. (2019). Methanogenesis in soils, wetlands, and peat. Biogenesis of Hydrocarbons, pp.211-228. Kulkarni, A. V., Mathur, pp., Rathore, B. pp., Alex, S., Thakur, N. & Kumar, M. 2002. Effect of global warming on snow ablation pattern in the Himalaya. Current Science, 83, 120-123.

Landsat missions. Landsat Missions | U.S. Geological Survey Available at: https://www.usgs.gov/landsat-missions. (Accessed: 20th June 2021)

Law, A.C., Nobajas, A. and Sangonzalo, R. (2018). Heterogeneous changes in the surface area of lakes in the Kangerlussuaq area of southwestern Greenland between 1995 and 2017. Arctic, Antarctic, and Alpine Research, 50(1), pp.S100027.

Lewkowicz, A. G., & Harris, C. (2005). Frequency and magnitude of active-layer detachment failures in discontinuous and continuous permafrost, northern Canada. Permafrost and Periglacial Processes, 16(1), 115–130. https://doi.org/10.1002/ppp.522

Li, S., Zhao, Z., Miaomiao, X. and Wang, Y. (2010). Investigating spatial non-stationary and scale-dependent relationships between urban surface

temperature and environmental factors using geographically weighted regression. Environmental Modelling & Software, 25(12), pp.1789-1800.

Lindborg, T., Rydberg, J., Tröjbom, M., Berglund, S., Johansson, E., Löfgren, A., Saetre, pp., Nordén, S., Sohlenius, G., Andersson, E. and Petrone, J. (2016). Biogeochemical data from terrestrial and aquatic ecosystems in a periglacial catchment, West Greenland. Earth System Science Data, 8(2), pp.439-459.

Liu, C., Xu, X., Feng, X., Cheng, X., Liu, C. and Huang, H., 2022. CALC-2020: a new baseline land cover map at 10 m resolution for the circumpolar Arctic. *Earth System Science Data Discussions*, *2022*, pp.1-28.

Loveland, T.R., Reed, B.C., Brown, J.F., Ohlen, D.O., Zhu, Z., Yang, L.W.M.J. and Merchant, J.W. (2000). Development of a global land cover characteristics database and IGBP DISCover from 1 km AVHRR data. International journal of remote sensing, 21(6-7), pp.1303-1330.

Lunt, D.J., de Noblet-Ducoudre, N. and Charbit, S. (2004). Effects of a melted Greenland ice sheet on climate, vegetation, and the cryosphere. Climate Dynamics, 23, pp.679-694.

MacMillan, R.A. and Shary, pp.A. (2009). Landforms and landform elements in geomorphometry. *Developments in Soil Science*, 33, pp.227-254.

Makaske, B. (2001). Anastomosing rivers: a review of their classification, origin and sedimentary products. Earth-Science Reviews, 53(3-4), pp.149-196.

Mankoff, K. D., Noël, B., Fettweis, X., Ahlstrøm, A. pp., Colgan, W., Kondo, K., Langley, K., Sugiyama, S., Van As, D., & Fausto, R. S. (2020). Greenland liquid water discharge from 1958 through 2019. Earth System Science Data, 12(4). https://doi.org/10.5194/essd-12-2811-2020

Marshall, G.J., Dowdeswell, J.A. and Rees, W.G., 1994. The spatial and temporal effect of cloud cover on the acquisition of high quality Landsat imagery in the European Arctic sector. Remote Sensing of Environment, 50(2), pp.149-160.

Martin, J.B., Pain, A.J., Martin, E.E., Rahman, S. and Ackerman, pp. (2020). Comparisons of nutrients exported from Greenlandic glacial and deglaciated watersheds. Global Biogeochemical Cycles, 34(12), pp.e2020GB006661.

Mayewski, pp.A., Sneed, S.B., Birkel, S.D., Kurbatov, A.V. and Maasch, K.A. (2014). Holocene warming marked by abrupt onset of longer summers and reduced storm frequency around Greenland. Journal of Quaternary Science, 29(1), pp.99-104.

Mcfeeters, S. K. (1996). The use of the normalized difference water index (NDWI) in the delineation of open water features. International Journal of Remote Sensing, 17, 1425-1432.

Medvedev, S., Souche, A., & Hartz, E. H. (2013). Influence of ice sheet and glacial erosion on passive margins of Greenland. Geomorphology, 193. https://doi.org/10.1016/j.geomorph.2013.03.029

Mekonnen, Z.A., Riley, W.J., Berner, L.T., Bouskill, N.J., Torn, M.S., Iwahana, G., Breen, A.L., Myers-Smith, I.H., Criado, M.G., Liu, Y. and Euskirchen, E.S., (2021). Arctic tundra shrubification: a review of mechanisms and impacts on

ecosystem carbon balance. Environmental Research Letters, 16(5), pp.053001.

Mernild, S.H., Knudsen, N.T., Yde, J.C. and Malmros, J.K. (2015), April. Detailed spatiotemporal albedo observations at Greenland's Mittivakkat Gletscher. In EGU General Assembly Conference Abstracts (p. 2643).

Mernild, S.H., Liston, G.E., Beckerman, A.P. and Yde, J.C. (2017). Reconstruction of the Greenland Ice Sheet surface mass balance and the spatiotemporal distribution of freshwater runoff from Greenland to surrounding seas. The Cryosphere Discussions, 2017, pp.1-50.

Moreau, M., Mercier, D., Laffly, D. and Roussel, E. (2008). Impacts of recent paraglacial dynamics on plant colonization: A case study on Midtre Lovénbreen foreland, Spitsbergen (79 N). Geomorphology, 95(1-2), pp.48-60.

Mouginot, J., Rignot, E., Bjørk, A.A., Van den Broeke, M., Millan, R., Morlighem, M., Noël, B., Scheuchl, B. and Wood, M. (2019). Forty-six years of Greenland Ice Sheet mass balance from 1972 to 2018. Proceedings of the national academy of sciences, 116(19), pp.9239-9244.

Musilova, M., Tranter, M., Wadham, J., Telling, J., Tedstone, A. and Anesio, A.M., (2017). Microbially driven export of labile organic carbon from the Greenland ice sheet. Nature Geoscience, 10(5), pp.360-365.

Myers-Smith, I.H., Forbes, B.C., Wilmking, M., Hallinger, M., Lantz, T., Blok, D., Tape, K.D., Macias-Fauria, M., Sass-Klaassen, U., Lévesque, E. and Boudreau, S. (2011). Shrub expansion in tundra ecosystems: dynamics, impacts and research priorities. Environmental Research Letters, 6(4), pp.045509.

Myers-Smith, I.H., Kerby, J.T., Phoenix, G.K., Bjerke, J.W., Epstein, H.E., Assmann, J.J., John, C., Andreu-Hayles, L., Angers-Blondin, S., Beck, pp.S. and Berner, L.T. (2020). Complexity revealed in the greening of the Arctic. Nature Climate Change, 10(2), pp.106-117.

Noël, B., Van De Berg, W. J., Lhermitte, S., Wouters, B., Machguth, H., Howat, I., Citterio, M., Moholdt, G., Lenaerts, J. T. M., & Van Den Broeke, M. R. (2017). A tipping point in refreezing accelerates mass loss of Greenland's glaciers and ice caps. Nature Communications, 8. https://doi.org/10.1038/ncomms14730

Nolin, A. W. (2010). Recent advances in remote sensing of seasonal snow. Journal of Glaciology, 56, 1141-1150.

Normand, S., Randin, C., Ohlemüller, R., Bay, C., Høye, T.T., Kjær, E.D., Körner, C., Lischke, H., Maiorano, L., Paulsen, J. and Pearman, pp.B. (2013). A greener Greenland? Climatic potential and long-term constraints on future expansions of trees and shrubs. Philosophical Transactions of the Royal Society B: Biological Sciences, 368(1624), pp.20120479.

Novelli, A., Tarantino, E., Caradonna, G., Apollonio, C., Balacco, G., & Piccinni, F. (2016). Improving the ANN classification accuracy of landsat data through spectral indices and linear transformations (PCA and TCT) Aimed at LU/LC

Monitoring of a River Basin. Lecture Notes in Computer Science (Including Subseries Lecture Notes in Artificial Intelligence and Lecture Notes in Bioinformatics), 9787. https://doi.org/10.1007/978-3-319-42108-7_32

O'Connor, F.M., Boucher, O., Gedney, N., Jones, C.D., Folberth, G.A., Coppell, R., Friedlingstein, pp., Collins, W.J., Chappellaz, J., Ridley, J. and Johnson, C.E., (2010). Possible role of wetlands, permafrost, and methane hydrates in the methane cycle under future climate change: A review. Reviews of Geophysics, 48(4).

Oliver, H., Luo, H., Castelao, R.M., van Dijken, G.L., Mattingly, K.S., Rosen, J.J., Mote, T.L., Arrigo, K.R., Rennermalm, Å.K., Tedesco, M. and Yager, pp.L., (2018). Exploring the potential impact of Greenland meltwater on stratification, photosynthetically active radiation, and primary production in the Labrador Sea. Journal of Geophysical Research: Oceans, 123(4), pp.2570-2591.

Olofsson, pp., Foody, G.M., Stehman, S.V. and Woodcock, C.E., (2013). Making better use of accuracy data in land change studies: Estimating accuracy and area and quantifying uncertainty using stratified estimation. Remote sensing of environment, 129, pp.122-131.

Ovenden, L., 1990. Peat accumulation in northern wetlands. Quaternary research, 33(3), pp.377-386.

Overeem, I., Hudson, B.D., Syvitski, J.P., Mikkelsen, A.B., Hasholt, B., Van Den Broeke, M.R., Noël, B.P.Y. and Morlighem, M.J.N.G., (2017). Substantial export of suspended sediment to the global oceans from glacial erosion in Greenland. Nature Geoscience, 10(11), pp.859-863.

Overland, J.E. (2020). Less climatic resilience in the Arctic. Weather and Climate Extremes, 30, pp.100275.

Palmtag, J., Cable, S., Christiansen, H.H., Hugelius, G. and Kuhry, pp., (2018). Landform partitioning and estimates of deep storage of soil organic matter in Zackenberg, Greenland. The Cryosphere, 12(5), pp.1735-1744.

Pastor, A., Skovsholt, L.J., Christoffersen, K.S., Wu, N. and Riis, T. (2021). Geomorphology and vegetation drive hydrochemistry changes in two Northeast Greenland streams. Hydrological Processes, 35(10), pp.e14369.

Pearson, R. G., Phillips, S. J., Loranty, M. M., Beck, pp. S. A., Damoulas, T., Knight, S. J., & Goetz, S. J. (2013). Shifts in Arctic vegetation and associated feedbacks under climate change. Nature Climate Change, 3(7). https://doi.org/10.1038/nclimate1858

Pekel, J.F., Cottam, A., Gorelick, N. and Belward, A.S. (2016). High-resolution mapping of global surface water and its long-term changes. Nature, 540(7633), pp.418-422.

Planet Team. (2017). Planet Lab. Available at: https://www.planet.com/ (Accessed: 01/06/2022).

Pontius Jr, R.G. and Millones, M., (2011). Death to Kappa: birth of quantity disagreement and allocation disagreement for accuracy assessment. International Journal of Remote Sensing, 32(15), pp.4407-4429.

Pontius Jr, Robert Gilmore, and Alí Santacruz. (2014). “Quantity, Exchange, and Shift Components of Difference in a Square Contingency Table.” International Journal of Remote Sensing 35 (21): 7543–54.

Pontius Jr, Robert Gilmore, and Marco Millones. (2011). “Death to Kappa: Birth of Quantity Disagreement and Allocation Disagreement for Accuracy Assessment.” International Journal of Remote Sensing 32 (15): 4407–29.

Poortinga, A., Tenneson, K., Shapiro, A., Nquyen, Q., San Aung, K., Chishtie, F. & Saah, D. (2019). Mapping Plantations in Myanmar by Fusing Landsat-8, Sentinel-2 and Sentinel-1 Data along with Systematic Error Quantification. Remote Sensing, 11

Propastin, pp., Kappas, M. and Erasmi, S. (2008). Application of geographically weighted regression to investigate the impact of scale on prediction uncertainty by modelling relationship between vegetation and climate. International journal of spatial data infrastructures research, 3(3), pp.73-94.

Rasmussen, L.H., Zhang, W., Hollesen, J., Cable, S., Christiansen, H.H., Jansson, pp.E. and Elberling, B. (2018). Modelling present and future permafrost thermal regimes in Northeast Greenland. Cold Regions Science and Technology, 146, pp.199-213.

Raynolds, M.K., Walker, D.A., Balser, A., Bay, C., Campbell, M., Cherosov, M.M., Daniëls, F.J., Eidesen, pp.B., Ermokhina, K.A., Frost, G.V. and Jedrzejek, B., (2019). A raster version of the Circumpolar Arctic Vegetation Map (CAVM). Remote Sensing of Environment, 232, pp.111297.

Rennermalm, A. K., Smith, L. C., Chu, V. W., Forster, R. R., Box, J. E., & Hagedorn, B. (2012). Proglacial river stage, discharge, and temperature datasets from the Akuliarusiarsuup Kuua River northern tributary, Southwest Greenland, 2008-2011. Earth System Science Data, 4(1), 1–12. https://doi.org/10.5194/essd-4-1-2012

Rignot, E., Velicogna, I., van den Broeke, M.R., Monaghan, A. and Lenaerts, J.T., (2011). Acceleration of the contribution of the Greenland and Antarctic ice sheets to sea level rise. Geophysical research letters, 38(5).

Rodriguez-Galiano, V. F., Ghimire, B., Rogan, J., Chica-Olmo, M. & Rigol-Sanchez, J. pp. (2012). An assessment of the effectiveness of a random forest classifier for land-cover classification. Isprs Journal of Photogrammetry and Remote Sensing, 67, 93-104.

Romanovsky, V.E., Smith, S.L. and Christiansen, H.H. (2010). Permafrost thermal state in the polar Northern Hemisphere during the international polar year 2007–2009: a synthesis. Permafrost and Periglacial processes, 21(2), pp.106-116.

Rysgaard, S., Nielsen, T.G. and Hansen, B.W. (1999). Seasonal variation in nutrients, pelagic primary production and grazing in a high-Arctic coastal marine ecosystem, Young Sound, Northeast Greenland. Marine Ecology Progress Series, 179, pp.13-25.

Ryu, J.S. and Jacobson, A.D. (2012). CO2 evasion from the Greenland Ice Sheet: A new carbon-climate feedback. Chemical Geology, 320, pp.80-95.

Schuur, E.A., McGuire, A.D., Schädel, C., Grosse, G., Harden, J.W., Hayes, D.J., Hugelius, G., Koven, C.D., Kuhry, pp., Lawrence, D.M. and Natali, S.M., (2015). Climate change and the permafrost carbon feedback. Nature, 520(7546), pp.171-179.

Schwarzkopf, K., Seitz, S., Fritz, M., Scholten, T., & Kühn, pp. (2023). Ice wedge polygon stability on steep slopes in West Greenland related to temperature and moisture dynamics of the active layer. Permafrost and Periglacial Processes, 34(2). https://doi.org/10.1002/ppp.2181

Sejr, M.K., Stedmon, C.A., Bendtsen, J., Abermann, J., Juul-Pedersen, T., Mortensen, J. and Rysgaard, S., 2017. Evidence of local and regional freshening of Northeast Greenland coastal waters. Scientific Reports, 7(1), pp.13183.

Selkowitz, D. & Forster, R. (2015). An Automated Approach for Mapping Persistent Ice and Snow Cover over High Latitude Regions. Remote Sensing, 8.

Shepherd, A. et al(IMBIE Team), 2020. Mass balance of the Greenland Ice Sheet from 1992 to 2018. *Nature* **579**, 233-239

Shugar, D.H., Burr, A., Haritashya, U.K., Kargel, J.S., Watson, C.S., Kennedy, M.C., Bevington, A.R., Betts, R.A., Harrison, S. and Strattman, K., 2020. Rapid worldwide growth of glacial lakes since (1990). Nature Climate Change, 10(10), pp.939-945.

Soenen, S. A., Peddle, D. R. & Coburn, C. A. (2005). SCS+C: A modified sun-canopy-sensor topographic correction in forested terrain. *IEEE Trans. Geosci. Remote Sens*. **43**, 2148-2159.

Straneo, F., & Heimbach, pp. (2013). North Atlantic warming and the retreat of Greenland's outlet glaciers. In Nature (Vol. 504, Issue 7478). https://doi.org/10.1038/nature12854

Ström, L., Ekberg, A., Mastepanov, M. and Røjle Christensen, T. (2003). The effect of vascular plants on carbon turnover and methane emissions from a tundra wetland. Global Change Biology, 9(8), pp.1185-1192.

Surlyk, F.I.N.N. and Noe-Nygaard, N.A.N.N.A., (2001). Sand remobilisation and intrusion in the Upper Jurassic Hareelv Formation of East Greenland. Bulletin of the Geological Society of Denmark, 48, pp.169-188.

Swann, A. L., Fung, I. Y., Levis, S., Bonan, G. B., & Doney, S. C. (2010). Changes in arctic vegetation amplify high-latitude warming through the greenhouse effect. Proceedings of the National Academy of Sciences of the United States of America, 107(4). https://doi.org/10.1073/pnas.0913846107

Swingedouw, D., Houssais, M. N., Herbaut, C., Blaizot, A. C., Devilliers, M., & Deshayes, J. (2022). AMOC Recent and Future Trends: A Crucial Role for Oceanic Resolution and Greenland Melting? Frontiers in Climate, 4. https://doi.org/10.3389/fclim.2022.838310

Teufel, B. and Sushama, L. (2019). Abrupt changes across the Arctic permafrost region endanger northern development. Nature Climate Change, 9(11), pp.858-862.

Tømmervik, H., Høgda, K.A. and Solheim, I. (2003). Monitoring vegetation changes in Pasvik (Norway) and Pechenga in Kola Peninsula (Russia) using multitemporal Landsat MSS/TM data. Remote sensing of Environment, 85(3), pp.370-388.

Tucker, C. J., Grant, D. M. & Dykstra, J. D. (2004). NASA's global orthorectified landsat data set. Photogrammetric Engineering and Remote Sensing, 70, 313-322.

Tucker, C.J. (1979). Red and photographic infrared linear combinations for monitoring vegetation. Remote sensing of Environment, 8(2), pp.127-150.

USGS. (2019). Landsat Surface Reflectance [Online]. Available: https://www.usgs.gov/land-resources/nli/landsat/landsat-surface-reflectance?qt-science_support_page_related_con=1#qt-science_support_page_related_con [Accessed 29 July 2021]

Usman, U., Yelwa, S.A., Gulumbe, S.U., Danbaba, A. and Nir, R. (2013). Modelling relationship between NDVI and climatic variables using geographically weighted regression. Journal of Mathematical Sciences and Applications, 1(2), pp.24-28.

Van As, D., Andersen, M. L., Petersen, D., Fettweis, X., Van Angelen, J. H., Lenaerts, J. T. M., Van Den Broeke, M. R., Lea, J. M., Bøggild, C. E., & Ahlstrøm, A. pp. (2014). Increasing meltwater discharge from the Nuuk region of the Greenland ice sheet and implications for mass balance (1960–2012). Journal of Glaciology, 60(220), 314–322.

van As, D., Hubbard, A., Hasholt, B., Mikkelsen, A.B., van den Broeke, M. and Fausto, R.S., (2011). Surface mass budget and meltwater discharge from the Kangerlussuaq sector of the Greenland ice sheet during record-warm year 2010. Cryosphere Discussion, 5, pp.2319-2347.

Vanonckelen, S., Lhermitte, S. & Van Rompaey, A. (2013). The effect of atmospheric and topographic correction methods on land cover classification accuracy. International Journal of Applied Earth Observation and Geoinformation, 24, 9-21.

Walker, D.A., Gould, W.A. and RAYNOLDS, M., (2002). The Circumpolar Arctic Vegetation Map: AVHRR-derived base maps, environmental controls, and integrated mapping procedures. int. j. remote sensing, vol. 23, no. 21,: 4551–4570.

Walvoord, M.A. and Kurylyk, B.L. (2016). Hydrologic impacts of thawing permafrost—A review. Vadose Zone Journal, 15(6).

Wang, J., Price, K. pp. and pp. M. Rich. (2001). Spatial patterns of NDVI in response to precipitation and temperature in the central Great Plains. International Journal of Remote Sensing, 22: 3827-3844.

Wang, Q., Ni, J. and Tenhunen, J. (2005). Application of a geographically-weighted regression analysis to estimate net primary production of Chinese forest ecosystems. Global ecology and biogeography, 14(4), pp.379-393.

Winther, pp.C., Troelsen, J., Holmen, K., Johnsen, pp., Fristrup, B. and Knuth, E., (1950). A Preliminary Account of the Danish Pearyland Expedition, 1948-9. Arctic, 3(1), pp.2-13.

Wulder, M.A., White, J.C., Goward, S.N., Masek, J.G., Irons, J.R., Herold, M., Cohen, W.B., Loveland, T.R. and Woodcock, C.E. (2008). Landsat continuity: Issues and opportunities for land cover monitoring. Remote Sensing of Environment, 112(3), pp.955-969.

Xu, H. (2006). Modification of normalised difference water index (NDWI) to enhance open water features in remotely sensed imagery. International Journal of Remote Sensing, 27, 3025-3033.

Yamanouchi, T., & Takata, K. (2020). Rapid change of the Arctic climate system and its global influences - Overview of GRENE Arctic climate change research project (2011–2016). In Polar Science (Vol. 25). https://doi.org/10.1016/j.polar.2020.100548

Yi, S., Woo, M.K. and Arain, M.A. (2007). Impacts of peat and vegetation on permafrost degradation under climate warming. Geophysical Research Letters, 34(16).

Zhao, N., Yang, Y. and Zhou, X. (2010). Application of geographically weighted regression in estimating the effect of climate and site conditions on vegetation distribution in Haihe Catchment, China. Plant Ecology, 209(2), pp.349-359.

Zhou, H., Wang, J.A., Wan, J. and Jia, H., (2010). Resilience to natural hazards: a geographic perspective. Natural hazards, 53(1), pp.21-41.

Zimov, S. A., Schuur, E. A. G., & Stuart Chapin, F. (2006). Permafrost and the global carbon budget. In Science (Vol. 312, Issue 5780). https://doi.org/10.1126/science.1128908

Chapter 4: Greenland's Peripheral glacier and ice cap (PGIC) change over the past 40 years

4.1 Introduction

Near ubiquitously across the globe, climate change is manifest in a warming trend and an increase in the magnitude and frequency of abrupt and disruptive climate shifts (Knox, 1993; Pittock, 2012; Russo et al., 2014). These climate shifts are occurring fastest in Arctic regions, part of the widespread phenomena known as the Arctic amplification of clime change (Serreze and Barry, 2011; (Pithan & Mauritsen, 2014) Zemp et al., 2015; Taylor et al., 2022). This climate warming across the Arctic has been measured at double the global mean rate since the 1970s (Holland and Blitz, 2003; Chylek et al., 2009; Screen and Simmons, 2010a; Screen and Simmons, 2010b; Pithan and Mauritsen, 2014). Within the scope of increasing Arctic warming in the late 20th and early 21st century, Greenland stands out as a notable 'hotspot', and has experienced especially pronounced warming (Preece et al., 2023). Mean annual air temperatures in Greenland from 2007 to 2012 were 3^{o}C higher than the 1979 to 2000 baseline global average (Mayewski et al., 2014). However, though still trending upwards, more recently the rate of warming has apparently decreased with only a diminished rising trend since 2000 as reported in Hanna et al. (2021). The influence of these climate shifts has already been explored in relation to Greenland's environmental change in the preceding chapter of this thesis, where increasing occurrence of 'warm' days ≥6^{o}C across Greenland have driven widespread change in nearly all facets of Greenland's physical landscape. One landcover type which was evidenced to be very closely correlated with warming temperatures was snow and ice, with the areal extent of this class, and so glacier areas, reducing substantially over the past few decades. Glacier thinning and retreat in response to rising air temperatures is well documented, globally and in Greenland, though the preponderance of Greenlandic research has focussed on the GrIS as opposed to the peripheral glaciers and ice caps.

Greenland's peripheral glaciers and ice caps (PGICs) are changing rapidly in response to climate warming and respective landscape feedbacks in Greenland (Bjørk et al., 2018; Leclercq et al., 2012; Machguth et al., 2013). PGICs represent only ~5 % of the ice-covered surface area in Greenland which equates to just ~ 0.5 %

of the volume (or ~39mm sea-level equivalent) of the Greenland Ice Sheet (GrIS) (Hanna et al., 2021). However, despite this apparent diminished relevance, Greenland's PGICs are reported to be three to four times more sensitive to ongoing atmospheric climate warming when compared to the neighbouring GrIS (Rastner et al., 2012; Fettweis et al., 2013; Goelzer et al., 2013; Machguth et al., 2013). PGICs were measured to have contributed between 14 % and 20 % of the total ice loss from Greenland between October 2003 and March 2008 (Bjørk et al., 2012; Bolch et al., 2013). However, there is considerable regional variability in the absolute amount and rate of change of glacier mass loss across Greenland, a phenomenon identified previously as requiring further scrutiny (Hugonnet et al., 2021; Khan et al., 2022). Hugonnet et al. (2021) noted that, between 2000 and 2020, the north and west of Greenland emerged as particular hotspots of negative mean glacier elevation change and mass loss (-10.6 and -11.9 Gt yr^{-1} respectively). Similarly, Khan et al.'s (2022) study of early 21st-century peripheral glacier changes in Greenland found most recently the north, north east and north west have had the most negative mass balance, with mass balance rates becoming more negative and accelerating in terms of mass loss throughout the 21st century, somewhat contrary to the trend of decreased warming.

There is consensus that mass loss and contributions from the ice sheet to global sea levels have been considerable, with a marked acceleration from the 80s/90s to the present. The IMBIE team reported that in all the GrIS lost ~3,902±342 billion tonnes of ice between the early 90s and 2018 (Shepherd et al., 2019). This equates to an average sea level rise of 10.8 ± 0.9 millimetres over that time. However, associated with their increased sensitivity to climate change and relatively high mass loss compared to the GrIS, Greenland PGICs are presently contributing a disproportionately high volume of meltwater to surrounding oceans and to global sea level rise (Noel et al., 2017). Marzeion et al. (2012) modelled global glacier surface mass balance forced with observed monthly precipitation and temperature data and estimated an increased volume loss of PGIC in Greenland seven to eight times greater than the GrIS between 1902 and 2009. Many post-LIA mass balance change and retreat studies of individual PGIC and regions have indicated substantial variability in Glacier sensitivity and spatio-temporal evolution in response to climate change (Moon et al., 2014). Many areas exhibit pronounced and accelerated mass

loss and retreat (e.g. north east Greenland (Carrivick et al., 2019), Mittivakkat Glacier (Mernild et al., 2011a), Kangerlussuaq (Mernild et al., 2011b)) whereas others show stability and apparent equilibrium (e.g. Flade Isblink, Northern Greenland (Rinne et al., 2011)). Carrivick et al. (2019) report a dramatic acceleration in volume loss from north east Greenland's PGIC throughout the 20th century following the LIA, based on the mapped moraine limits and modelled glacier surface elevation changes. These results were extended to a Greenland-wide study, which echoed the ubiquitous retreat of Greenland's PGIC since the LIA (Carrivick et al., 2023). Annual rates of mass loss increased from an average of 2.61 ± 0.52 km^3/year between 1910 and 1980 to an average rate of 3.22 ± 0.64 km^3/year between 1980 and 2014, an increase of ~23%.

This documented heightened sensitivity of Greenland's PGICs to atmospheric climate warming when compared to the GrIS is largely a function of: (i) predominantly terrestrial termini that are (more) sensitive to atmospheric warming (than marine termini that already have low basal friction) (Carrivick et al., 2023); (ii) short reservoir times and faster mass turnover (Bolch et al., 2013; Machguth et al., 2013; Bintanja and Selten, 2014); and (iii) smaller surface area (generally < 5 km^2) existing at elevations lower than the elevation of the majority of the GrIS (Raper and Braithwaite, 2006; Pfeffer et al., 2014; Bjørk et al., 2018). Moreover, runoff from Greenland PGICs affects local Greenlandic fjord water quality and circulation, which has consequences for the primary production and marine ecosystems (Hopwood et al., 2020; Krisch et al., 2020). Glacier meltwater effectively evacuates glacigenic sediments and nutrients (Bhatia et al., 2013; Böning et al., 2016; Burpee et al., 2018), debutressed material from hillslopes (where well connected) (Mancini & Lane, 2020; Micheletti & Lane, 2016), as well as organic carbon from wetlands and degrading permafrost (Schuur et al., 2009). Glacier meltwater is extremely important to Greenland's coastal ecosystems as it is rich in mineral, nutrient, and organic matter which effectively improves productivity as a source of silica, nitrogen, iron, and phosphorous (see: Beaton et al., 2017; Bhatia et al., 2013; Hatton et al., 2019; Hawkings et al., 2016; Hawkings et al., 2015; Wadham et al., 2016).

Despite the disproportionate contribution of PGICs to Greenland's net runoff and meltwater discharge to local and global oceans, and the societal importance of said runoff, previous studies examining geometric and mass changes of Greenland PGICs

have been either spatially or temporally restricted (Bjørk et al., 2018; Bolch et al., 2013; Hugonnet et al., 2021; Noël et al., 2017). Longer-term late-Holocene studies are unable to utilise directly measured glacier surfaces for geodetic analysis due to the lack of satellite data, and so have relied on modelled changes based on extents quantified from moraine limits linked to the Little Ice Age (e.g. Carrivick et al., 2019, 2023). Spatially-localised studies extending into the 20th century include those for Holm Land north east Greenland between 1978 and 2014 (von Albedyl et al., 2020), for Disko Island in west Greenland between1985 and 2015 (Huber et al., 2020), and for Prudhoe Land northwest Greenland between 1985 and 2018 (Wang et al., 2021). These studies all leveraged the AeroDEM elevation data of Korsgaard et al. (2016), which provides surface elevations for all of Greenland's periphery for dates between 1978 and 1987(depending on the region). The AeroDEM data permits longer-term geodetic study of glacier surface elevation change but suffers from some quality issues which require processing which has largely restricted prior widespread application. National and multi-regional studies of geodetic changes to Greenland PGICs (Hugonnet et al., 2021; Khan et al., 2022) have been temporally limited by the availability of suitable coverage satellite-derived elevation datasets which allow relatively simple widespread application; ASTER launched in 1999, SRTM launched in 2000, ICESat launched in 2003, TerraSAR-X launched in 2007, TanDEM-X launched in 2010, which mostly cover the last few decades only. Their analysis has also been at relatively coarse resolutions (e.g. 100m for Hugonnet et al., 2021) due to the global scale of their analysis and the computation cost and complexity of the analysis. There is, therefore, an apparent niche in literature for a longer term, nationally consistent, late 20th- to early 21st-century study of Greenland's PGIC derived from the, as yet, not widely applied AeroDEM dataset to extend the direct geodetic measurement record.

The aim of this study is to determine PGIC mass changes over a multi-decadal timescale. The research utilises the aforementioned AeroDEM (1978-1985), as well as the Greenland GIMP DEM (~2006) and the ArcticDEM mosaic (2016). To achieve this aim a number of objectives were defined:

i) To identify temporal trends of PGIC mass balance in Greenland

ii) To identify any spatial patterns of PGIC mass balance change over time

iii) To analyse glacier's morphometric properties over time and space to identify glacier groups and anomalies.

iv) Based on the above three objectives, suggest controls on PGIC mass loss, key to informing projections of PGIC evolution.

4.2 Data and Methods

Three multi-temporal elevation datasets are utilised in this research to quantify glacier surface elevation and mass balance for the PGIC around all of Greenland's ice sheet-free periphery. This section will introduce these datasets before detailing the methodological approach applied to process and analyse glacier changes. Each elevation dataset was pre-processed before statistics were amalgamated for RGI glacier ablation areas for each period. From this, the glacier's overall mass balance is calculated for three time periods, and assessed based on location, type and morphology. This study defines three time periods, determined by elevation data, over which glacier mass balance is assessed. These are termed *T0* (~1978-87 to 2016), *T1* (~1980 to 2006) and *T2* (2006 to 2016).

4.2.1 Datasets

4.2.1.1 AeroDEM

The earliest of the three elevation datasets used is the AeroDEM (Korsgaard et al., 2016), derived from aerial imagery taken between 1978 and 1987. AeroDEM elevation data, orthorectified 8-bit greyscale image files, and the associated reliability mask (Korsgaard et al., 2016) were mosaiced based on their collection years (1978, 1981, 1985, and 1987; Figure 4.1) in ESRI's ArcMap software. The AeroDEM dataset from Korsgaard et al. (2016) was employed in this study to represent the glacier surfaces of various regions in Greenland during different years: 1978 (predominantly covering north and northeast Greenland), 1981 (predominantly covering southeast Greenland), 1985 (predominantly covering all of west Greenland), and 1987 (predominantly covering central east Greenland), as shown in Figure 4.1. These 25m digital elevation models (DEMs) were generated using around 3500 vertical aerial photographs acquired by the National Cadastre and Survey of Denmark, as well as the Danish Geodata Agency. The DEM and orthophotographs were generated using the SOCET SET digital photogrammetric application and the NGATE module, with a focus on precision and reliability.

To ensure accuracy, Korsgaard et al. (2016) utilised an extensive network of reference coordinates (approximately 21,500) for aero-triangulation of the aerial photograph archive. The resulting DEMs exhibited horizontal and vertical accuracies of 10 m and 6 m, respectively. The impacts of these absolute inaccuracies are reduced and partially negated in this research by conducting co-registration and differencing, where relative elevation changes between DEMs are measured and quantified relative to one another. The quality of the AeroDEM is influenced by the spectral contrast of surfaces; therefore, areas with low surface contrast, such as snow-covered glacier accumulation zones, regularly contain some erroneous data (Korsgaard et al., 2016; Goetz & Brenning, 2019).

This quality concern has minimal impact on this research, as the analysis is restricted to directly comparing measured glacier surface elevation changes in their ablation zones. These zones were typically devoid of snow cover during the aerial photograph acquisition, and higher contrast exists within the ice (as debris cover and dirty/clean ice) and between the ice and proglacial land surfaces (e.g., Pope & Rees, 2014). Moreover, the elevation data is filtered using the AeroDEM reliability mask dataset provided alongside the elevation data and each cell's respective Figure of Merit (FOM) Value. The FOM is a numerical value ranging from 0 to 100, assigned during the terrain extraction process. The FOM can convey one of three meanings for each measured point: it can serve as an error flag, indicating uncertainty in the automatic measurement; it can signify a successful or accurate measurement; or it can act as an edit flag, indicating the type of editing applied (e.g., lake-filled, interpolated). Korsgaard et al (2016) provide a full table alongside their publication indicating the relationship between FOM values and their interpretations.

FOM values equal to or greater than 40 indicate successful automatic correlation. These higher FOM values are directly proportional to the correlation coefficient, whereby larger numbers indicate a more precise measurement. To summarise the FOM table, interpolated values fall within the range of 2 to 21; manually edited or LIDAR points (which are not present in the AeroDEM reliability mask) range from 22 to 38; the value 39 represents posts that did not automatically correlate but may still represent accurate surfaces post-processing; and finally, posts that did automatically correlate receive values ranging from 40 to 99, with increasing quality of correlation in this range. Here, values over 22 are considered to be of high enough

quality, following Huber et al.'s (2020) similar work with this data restricted to the vicinity of Disko Island. This conclusion is supported by a visual inspection of data quality in the range 22-40 for multiple glacier ablation areas and because this data undergoes a second stage of outlier filtering in this research post-co-registration, following the empirical 3 sigma rule and outlined in a later section of this chapter.

The AeroDEM elevation data, along with the orthorectified 8-bit greyscale image files and the reliability mask, were obtained from the following source: https://www.nodc.noaa.gov/archive/arc0088/0145405/. After download, the DEM and orthoimage tiles were mosaiced based on their respective collection years (1978, 1981, 1985, and 1987). Additionally, the data was reprojected into EPSG:5938 (WGS 84 / EPSG Greenland Polar Stereographic) for consistency. The AeroDEM elevation data was then resampled from 25m to 30m to correspond with the lowest native resolution of the three input elevation datasets. Bilinear interpolation was selected as the resampling method for AeroDEM elevation data due to several compelling reasons, particularly suited to the characteristics of glacier surfaces. Firstly, the relatively minor changes in resolution inherent in this study necessitate a method that smoothly transitions between data points without introducing significant artefacts or distortions. Bilinear interpolation, known for its simplicity and efficiency, is particularly adept at providing a good balance between computational load and interpolation accuracy, a critical factor in large-scale or high-resolution datasets (Smith et al., 2004; Shi et al., 2014). Additionally, the consistent and low slope angles commonly found across glacier surfaces are well-accommodated by bilinear interpolation. This method assumes a linear change between points, which aligns closely with the gradual and uniform terrain gradients of glaciers, thereby minimising the introduction of errors or exaggerations in slope and aspect (Nuth and Kääb, 2011). In environments where topographic complexity is low, as is the case on glacier surfaces, bilinear interpolation is particularly effective in maintaining the integrity and realism of the surface representation. Furthermore, the lack of topographic complexity on glacier surfaces further justifies the use of bilinear interpolation. In areas devoid of abrupt elevation changes or intricate geomorphological features, the risk of creating misleading or inaccurate surface representations is significantly reduced. Bilinear interpolation, by nature, is well-suited to these conditions as it provides a smooth surface fit that reflects the gentle

undulations and broad, sweeping features typical of Greenland's glacial surfaces (Seehaus et al., 2020). Bilinear interpolation is also underpinned by its widespread acceptance and validation in previous studies. The referenced works collectively endorse its application in similar contexts, providing a strong empirical foundation for its selection (Smith et al., 2004; Nuth and Kääb, 2011; Shi et al., 2014; Seehaus et al., 2020).

4.2.1.2 GIMP DEM

To measure accelerations in glacier changes, an intermediary elevation dataset is required, from which pre- and post-elevation and mass balance rates can be calculated and increasing/decreasing rates determined. The DEM used for 2006 is GIMP (Howat et al., 2015) (version 1, 30m horizontal resolution). This data was sourced, processed in, and exported from Google Earth Engine. GIMP DEM is generated by the Greenland Ice Mapping Project (GIMP) and provided by the National Snow and Ice Data Centre (NSIDC). Specifically, this work utilises the GIMP1 DEM, created by combining the ASTER global digital elevation model (GDEM) (Tachikawa et al., 2011), the SPIRIT DEM (SPOT 5 Stereoscopic survey of Polar Ice: Reference Images and Topographies) (Korona et al., 2009), and the Bamber DEM (Scambos & Haran, 2002), which was improved using AVHRR photoclinometry (PEB DEM) (Howat et al., 2014; Scambos & Fahnestock, 1998; Xing et al., 2020). The data were calibrated based on the average of Geoscience Laser Altimeter System (GLAS) data collected between 2003 and 2009 (Thomas et al., 2005). The temporal scope of GIMP1 therefore spans from 2003 to 2009, and thus this work adopts the central date of 2006 for this DEM, with temporal inaccuracy considered in the subsequent uncertainty assessment section of this chapter. To achieve high resolution and accuracy, the GIMP DEM integrates the PEB DEM with topographic maps generated through high-quality photogrammetry along the edges. Furthermore, it incorporates ICESat laser altimetry data to capture all land elevations (Schutz et al., 2005). The integration of the PEB DEM, topographic maps, and ICESat laser altimetry data enables the GIMP DEM to achieve a relatively high accuracy, however it is important to note that the GIMP DEM exhibits the lowest accuracy among the DEMs as they are employed in this research. Although efforts have been made to filter and fill erroneous values in the dataset (Xing et al., 2020),

the details regarding the quantification of this process remain unclear. Xing et al. (2020) find GIMP1 to have a Root Mean Squared Error (RMSE) of 2.39m.

4.2.1.3 ArcticDEM

The ArcticDEM is the most recent elevation dataset utilised here. In its native form, the 2m ArcticDEM mosaic, specifically centred on the year 2016, is resampled to 30m for use here. For consistency and given the benefits of use in glacier surface elevation interpolation as outlined above, bilinear interpolation is applied for resampling. The ArcticDEM is produced from high-quality sub-meter stereo imagery, using petascale computing capabilities and open-source photogrammetry software (Morin et al., 2016). ArcticDEM is produced by the U.S. National Geospatial Intelligence Agency (NGA) and a team led by the U.S. National Science Foundation funded Polar Geospatial Centre. Stereo imagery from Digital Globe's WorldView 1, WorldView 2, and WorldView-3 satellites is harnessed along with the Ohio State University's Surface Extraction with TIN-based Search-space Minimisation (SETSM) software to generate a comprehensive and extremely high-resolution (2m) elevation model of the Arctic region (Noh & Howat, 2017). Xing et al. (2020) find ArcticDEM in Greenland to be the highest accuracy of the DEMs they considered (GIMP1, GIMP2, TanDEMX, and ArcticDEM), with an RMSE standard deviation over multiple years of only 0.14 m, and when corrected to ICESat elevations reports a vertical accuracy of ~0.1m (Candela et al., 2017; Shiggins et al., 2023).

The three DEMs outlined above were projected to EPSG:5938 (WGS 84 / EPSG Greenland Polar Stereographic) and clipped (using ESRI ArcMap software) to the footprints dictated by the AeroDEM times of capture prior to co-registration (Figure 4.1). Glacier surface elevation and mass balance change statistics are calculated over glacier's ablation areas, and so a reliable dataset of glacier outlines was required.

4.2.1.4 Glacier Outlines

Glacier outlines were obtained from the Randolph Glacier Inventory (RGI), specifically utilising the RGI v6.0 outlines (RGI Consortium, 2017), which depict the PGIC extent circa 2001. These were primarily based on the inventory compiled by Rastner et al. (2012) for the majority of PGICs and supplemented by Howat et al. (2014) for regions extending beyond ~81° N. Exclusion criteria based on RGI glacier's attributes were applied to ensure accuracy and relevancy, with glaciers

exhibiting a connectedness greater than 1 (connectedness to the GrIS) omitted from the analysis. Furthermore, glaciers categorised under the 'Form' attribute as either 2

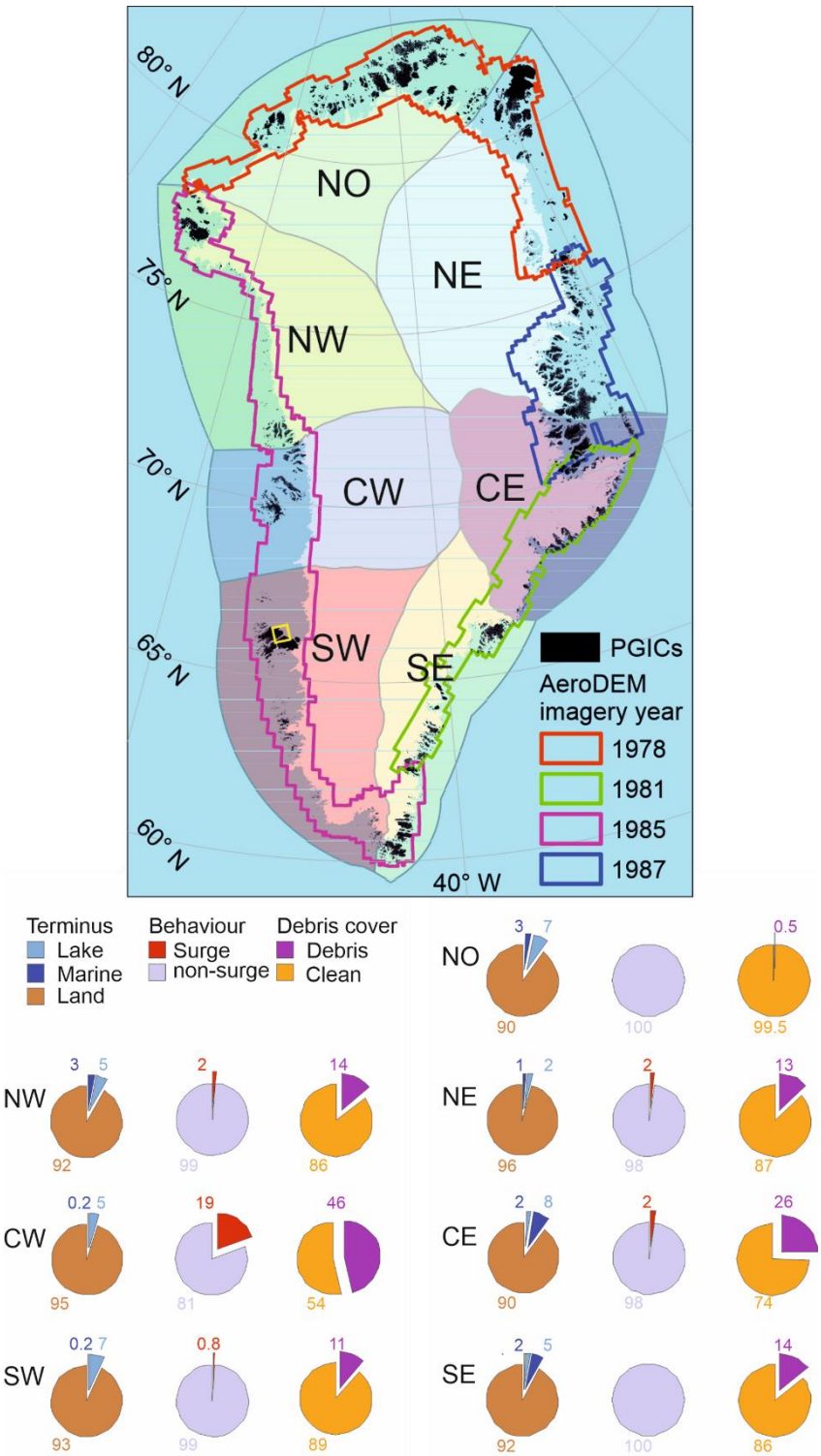

Figure 4.1 Location of peripheral glaciers and ice caps across Greenland and AeroDEM data coverage by year. Pie charts indicate percentage of glaciers within each region categorised by terminus, behaviour and surface type. Yellow extent box in south west Greenland shows the location of Figure 4.2.

(perennial snowfield) or 3 (seasonal snowfield) were also disregarded, as the focus was exclusively on continuous glacier cover.

The adoption of static glacier outlines, rather than temporally adjusting extents to align with the relevant DEMs years was strategic, with the aim to minimise the introduction of uncertainty from variable input data, particularly at the national scale. The requisite multi-temporal classification process required to generate the tens of thousands of multi-temporal outlines would introduce its own uncertainties. These uncertainties may vary significantly, ranging from 1 to 10 meters, contingent upon the reference imagery employed. This range of uncertainty is considerably larger than that introduced by the Digital Elevation Models (DEMs) being differenced, as highlighted by Zekollari et al. (2022). This approach reflects a calculated decision to balance the need for precise data representation against the inherent variability in large-scale geographical analyses.

4.2.2 Methods

Building upon the foundational data described, this study progresses to conduct comprehensive mass balance calculations for all of Greenland's PGIC. The subsequent section will outline the methodologies employed, detailing the delineation of ablation areas, co-registration, DEM differencing, void filling, and glacier filtering and aggregation procedures. Additionally, a thorough error and uncertainty assessment is conducted. These methods are essential for defining regional patterns of mass balance and changing rates, thereby facilitating a nuanced understanding of the spatial, temporal and morphological dynamics governing Greenland's PGIC. Figure 4.1 below shows all of Greenland's PGIC considered in this research. Regions are defined based on the IMBIE (2019) ice sheet drainage basin outlines and labelled: NO = North, NE = North East, CE = Central East, SE = South East, SW = South West, CW = Central West, NW = North West. Pie charts (labelled by region) reflect the percentage of glaciers as defined by the three morphometric variables studied here: Terminus (Lake, Marine, Land), Behaviour (Surge, Non-surge), and Surface cover (Debris, Clean) (Figure 4.1).

4.2.2.1 Ablation Area Delineation

The Next Generation Automated Terrain Extraction (NGATE) module within the SOCET SET digital photogrammetric application used to extract the AeroDEM

elevation data from aerial photographs relies on identifying and matching features between multiple overlapping images to triangulate and calculate the precise 3D coordinates of points on the ground (Korsgaard et al., 2016). Contrast in these images is crucial because it allows for the distinct identification of features across different photographs (Tommaselli & Berveglieri, 2018). High contrast ensures that the same points can be accurately matched between images, leading to reliable and precise elevation measurements. In areas with low contrast, such as snow and ice-covered accumulation zones, distinguishing these features becomes more challenging, affecting the accuracy and reliability of the elevation data extracted through such photogrammetric techniques. To address low-contrast areas, typical of snow-covered PGIC accumulation areas, two strategies were employed in AeroDEM to extract elevations in these regions: a standard adaptive strategy and a low-contrast strategy. The latter is particularly useful for sampling heights in areas where contrast is low, such as accumulation zones on glaciers. The low contrast of snow-covered accumulation areas necessitated Korsgaard et al. (2016) to conduct widespread interpolation in these regions and thus large artefacts and steep elevation irregularities are common within the glacier accumulation areas, both systematic and random. Conversely, glacier ablation areas are generally well-defined, with high-quality elevation extraction meaning they are mostly devoid of the accumulation area discrepancies. This is due to numerous ablation area characteristics which produce pronounced contrast in these areas from increased surface texture caused by glacier steepening, folding and crevassing, and higher contrast between bare ice, debris-rich folia, snow, crevasses and adjacent ice-free terrains.

While focused studies like that of Huber et al. (2020) managed to pinpoint locations with 'better' resolution in accumulation zones, extensive filtering and significant void filling were still imperative. Consequently, in this comprehensive study encompassing all PGIC, elevation changes are exclusively quantified over ablation areas, operating under the premise that mass loss above the Equilibrium Line Altitude (ELA) is insubstantial. This supposition is justified due to the relative stability and less dynamic nature of the accumulation areas compared to the ablation zones, making the estimated changes herein conservative minimum rates.
Ablation areas were defined by intersecting a glacier-specific ELA with the RGI glacier outline. Glacier-specific equilibrium line altitudes (ELAs) were defined using

an automated Area Altitude Balance Ratio (AABR) tool (Pellitero et al., 2015) as modified and developed to produce ablation areas automatically for thousands of glaciers in several world regions (Carrivick et al., 2019; Carrivick et al., 2020; Lee et al., 2021; Carrivick et al., 2022; Carrivick et al., 2023). The scripts were run using the contemporary ArcticDEM as the input DEM and the RGI outlines to define ablation areas. This approach assumes that present-day ELA elevations represent the maximum over the study period, ensuring that the identified ablation zones encompass all regions of mass loss throughout the duration. In this study, a balance ratio (BR) of 2.24 is used as suggested to be representative of high-latitude glaciers (Rea, 2009); however, it must be noted that the value is based only on a small sample of glaciers. The few Greenland PGICs with direct measurements of mass balance have a wide range of BR values as reported by Machguth et al. (2016). Therefore, acknowledging this uncertainty in glacier-specific ELAs, the results are reported for large spatial aggregations of glaciers rather than for individual PGICs. This aggregation process is outlined below.

4.2.2.2 DEM Co-registration

Co-registration is an indispensable step in the process of differencing Digital Elevation Models (DEMs) for studies of glacier surface elevation change. The precision of elevation change measurements is paramount in glaciological studies, as even minor inaccuracies can lead to significant errors in assessing glacier volume and mass balance changes (Nuth & Kääb, 2011). Misalignments between DEMs, often due to satellite orbital inaccuracies, sensor geometry, or terrain-induced errors, can introduce systematic biases that overshadow the real changes occurring on a glacier's surface (Li et al., 2022). Co-registration adjusts for these positional discrepancies, ensuring that the elevation differences observed are solely attributable to physical changes in the glacier, rather than artefacts of data misalignment (Nuth & Kääb, 2011). This process is critical for deriving accurate rates of glacier thinning or thickening, which are essential parameters in understanding glacier dynamics, predicting future sea-level rise, and assessing regional water resources (Shean et al., 2016). Without meticulous co-registration, studies risk systematically underestimating or overestimating the elevation changes measured. DEMS were coregistered per AeroDEM year area (see Figure 4.1), using the Nuth and Kääb (2011) method. The Nuth and Kääb (2011) method represents a sophisticated

approach for the co-registration of Digital Elevation Models (DEMs), crucial for accurate glacial and topographical change detection. Central to this methodology is the identification and correction of systematic offsets in three-dimensional space. By scrutinising stable, non-glacial terrain across temporally different DEMs, the method first quantifies misalignments in the horizontal (X and Y axes) and vertical (Z-axis) planes. Utilising an iterative least-squares matching technique, Nuth and Kääb's approach refines the offset corrections by minimising the sum of the squared differences between the stable terrain elevations of the DEMs under comparison. This process is particularly adept at isolating and rectifying biases introduced by satellite orbital drift, sensor misalignment, and terrain-induced parallax errors. This ensures that any change detected in the glacier areas is due to actual glacial movement or melting, not misalignment of the data. As the process is iterative, often involving refinement to minimise the offset and ensure the best possible alignment. The precision and reliability of this method have rendered it a standard in the field of remote sensing and glaciology, providing a robust foundation for studies focused on understanding and quantifying changes in glacier volume and elevation over time (Nuth & Kääb, 2011).

Co-registration was conducted by implementing the semi-automatic DEMcoreg python scripts of David Shean (https://pypi.org/project/demcoreg/), adapted from and designed for the NASA AMES pipeline for the processing of large terrain datasets (Shean et al., 2016, Beyer et al., 2018). The NASA AMES Stereo Pipeline (ASP) is a specialised software suite designed for processing stereo imagery to produce highly accurate Digital Elevation Models (DEMs). Developed by the Intelligent Robotics Group at the NASA AMES Research Centre, this toolset leverages automated algorithms for stereo correlation, sub-pixel refinement, and triangulation of image pairs from various satellite and aerial platforms.

These scripts have been deployed within a Linux-based environment, operational on a high-performance computing (HPC) system at the University of Leeds. The substantial random access memory (RAM) provided by the HPC is imperative for processing extensive datasets. Co-registration procedures have been meticulously applied, with both the AeroDEM and GIMP DEM aligned to the ArcticDEM. This alignment is crucial for maintaining the exclusion of non-static surfaces, achieved by masking glaciers using the RGI outlines, thereby ensuring better precision. The

strategic choice of aligning both DEMs to ArcticDEM ensures uniformity in application and mitigates the potential compounding and propagation of errors and inaccuracies that sequential co-registration might introduce. For instance, a scenario where the GIMP DEM is first coregistered to the ArcticDEM, followed by the AeroDEM being aligned to the already coregistered GIMP DEM. Subsequent to the co-registration, two DEMs of Difference (DoDs) are generated: one illustrating the elevation difference between ArcticDEM and AeroDEM (denoted as *T0*), and the other depicting the variation between ArcticDEM and GIMP (represented as *T2*). The elevation changes between AeroDEM and GIMP (*T1*) are subsequently deduced by calculating the disparity between these two DoDs (*T0* and *T2*). Maps and plots showing the detailed results of co-registration are presented in Figure 7.3, Appendix B. Co-registration results over static surfaces, such as the normalised median absolute deviation (NMAD) and standard deviation (SD - σ), are utilised in the accuracy and uncertainty assessments, outlined in a subsequent section.

4.2.2.3 DEM Differencing and Filtering

DEMs of difference (DoDs) which were produced from co-registration were standardised so that losses in elevation corresponded to minus values, and vice versa. DoDs were then clipped to the delineated ablation areas. As stated previously, some artefacts of interpolation exist over poorly resolved areas of the AeroDEM. Accordingly, Korsgaard et al. (2016) provide a reliability mask reflecting the mode of elevation extraction for each cell of the AeroDEM as outlined earlier. Though Korsgaard et al. (2016) recommend the removal of areas with reliability values <40, interrogation of the data indicated acceptable quality for areas within the 22 to 39 range over ablation areas therefore, following Huber et al. (2020) who conducted a similar plausibility check in west Greenland, areas with reliability >22 are included in the analysis, masking areas with a reliability score <22. Glaciers 82.6º north and on small east coast islands were removed from analysis due to the poor quality of the GIMP DEM in these regions.

Histograms of elevation changes for the AeroDEM to ArcticDEM and GIMP DEM to Arctic DEM DoDs demonstrated that elevation changes are normally distributed (though not perfectly) and so to remove erroneous values elevation changes per glacier were re-ranged to within 3 standard deviations of the local (per ablation area)

mean (preserving 99.7% of data) per AeroDEM timescale region following empirical three sigma rule. The empirical 3-sigma rule is a preferred method for filtering erroneous values in glacier surface elevation change data due to its robust statistical foundation and practical effectiveness (Rounce et al., 2020). Approximately 99.73% of values fall within three standard deviations from the mean in a normal distribution, making this rule an effective filter for identifying statistically improbable outliers likely caused by measurement errors or noise.

Zonal statistics were calculated using ablation areas as polygon data and the prepared DEMs as input (erroneous values yet to be removed). The zonal mean and zonal standard deviation were calculated for each ablation area and raster layers of each produced per ablation area. The zonal standard deviation rasters were then multiplied by 3 to reflect 3 standard deviations (3SD) of each glacier's specific mean elevation change. The three standard deviations raster was added and subtracted from the zonal mean raster to produce upper 3SD and lower 3SD rasters. Any values in each glacier ablation area DoD that fell outside the local upper and lower 3SD range were subsequently masked. This process was iterated numerous times until DoD's mean and standard deviation changes were below 0.01, usually on the fourth iteration.

With D as the input ablation area DoD, μ as the mean of D, σ the standard deviation of D, and Δ the change in mean or standard deviation (initialised to a value greater than 0.01). While $\Delta > 0.01$: calculate the current mean ($\mu\_current = mean(D)$) and standard deviation ($\sigma\_current = std(D)$). Then define the lower and upper bounds based on the 3-sigma rule ($L = \mu\_current - 3 * \sigma\_current$ and $U = \mu\_current + 3 * \sigma\_current$). Outliers are then removed from D using equation 4.1 below.

$$D = \{x \in D \mid L \leq x \leq U\} \tag{4.1}$$

The new mean and standard deviation of D are then calculated (μ_new and σ_new), before the change (Δ) is calculated as in equation 4.2.

$$\Delta = max(|\mu\_new - \mu\_current|, |\sigma\_new\ \sigma\_current|) \tag{4.2}$$

The process is repeated iteratively per glacier until Δ (the maximum change in mean or standard deviation between iterations) is less than 0.01.

Due to reliability masking and recursive three-sigma rule filtering, gaps and holes were introduced into the DoDs. In order to quantify elevation change across the entire area these voids must be interpolated to 'fill' the gaps with reasonable values based on local elevation changes. Interpolation of gaps and voids in the DEMs and DoDs is commonplace and widely applied, however, the exact mode of interpolation void filling is not standardised (McNabb et al., 2017; 2019). When interpolating elevation changes for surface elevation change measurement it is generally accepted that post differencing interpolation is best, and so following studies such as McNabb et al. (2017), Huber et al. (2020) and SeeHaus et al. (2020) void filling was conducted post-differencing. Post-differencing void filling reduces error/uncertainty propagation introduced by differencing of separately estimated surfaces. Moreover, for many of Greenland's PGIC, the absolute magnitude of surface elevation changes is considerably lower than differences in glacier surface elevations, particularly in steep ablation areas in mountain regions, therefore interpolated surfaces are less complex and the magnitude of variability in reconstructed surfaces is lower (See Haus et al., 2020). Due to the large spatial scale of analysis, and relatively fine 30m resolution applied here, interpolating only the difference surfaces also reduces the number of times the algorithms must be run and so too the computational cost and time for void filling.

4.2.2.4 Void Filling and Filtering

To analyse metrics of volume and mass loss for glaciers, interpolation is required to fill voids and gaps present over ablation areas in the two DoDs (*T0* and *T2*) from pre-existing "no data" areas in the precursor DEMs and introduced here by pre-processing to remove erroneous pixels and low-quality acquisition data. Here a two-part approach is applied to fill voids, applied in ESRI's ArcMap software, utilising the elevation void filling method, following previous works such as Magnusson (2016) and Albedyll et al. (2018). In the first instance for small voids, these are replaced by calculating the average of surrounding cells (in eight directions) and applying a plane fitting algorithm. For larger voids and those where the error associated with the plane fitting exceeds the threshold (four times the resolution), a

more complex inverse distance weighted (IDW) algorithm is applied. IDW is a deterministic multivariate interpolation that computes a weighted average to fill gaps with no values outside the range of input 'real' data. It is assumed that elevation changes are predominantly controlled by elevation (temperature and precipitation) and local glacier conditions (thermal regime, hypsometry). Therefore, the void filling was altered to preferentially weight cells within similar elevation bands (determined from ArcticDEM) every 50m in elevation up glacier from the terminus. Moreover, only cells within a given glacier's margin (determined from RGI outlines) were used for void filling on a given ablation area, this ensured only on-ice differences were used and cells with the most similar topographic and geographic setting were preferentially considered for void filling. Rather than specifying a maximum void size threshold, ablation areas whose cumulative voids exceeded 50% of the total ablation area were removed from the analysis. As only ablation areas are considered, percentage void areas were kept to a minimum when compared to voids for entire glacier areas in AeroDEM, and < 3% of ablation areas (proportionately less than 0.1% total ablation area in m^2) had gaps exceeding 50% of their area. The average elevation change was calculated per-glacier pre- and post-void filling, as well as per interpolated area. Where interpolated average elevation change fell outside 1 standard deviation of the pre-interpolated mean, glaciers were masked. However, only very small ablation areas with single digits of cells covering them exceeded this and would subsequently be masked regardless, as outlined below.

Figure 4.2 shows examples of the three time periods' DoDs for ablation areas of a selection of outlet glaciers on the northeast of the Maniitsoq ice cap, south west Greenland, with the location indicated by the yellow extent box in Figure 4.1. Elevation changes are shown in m yr^{-1}, and a notable acceleration can be seen in terminus acceleration for a number of the glaciers, particularly the large glacier in the north of the image and all of the small piedmont lobes in the valley between the two ice caps in the south west of the panels (Figure 4.2B, C).

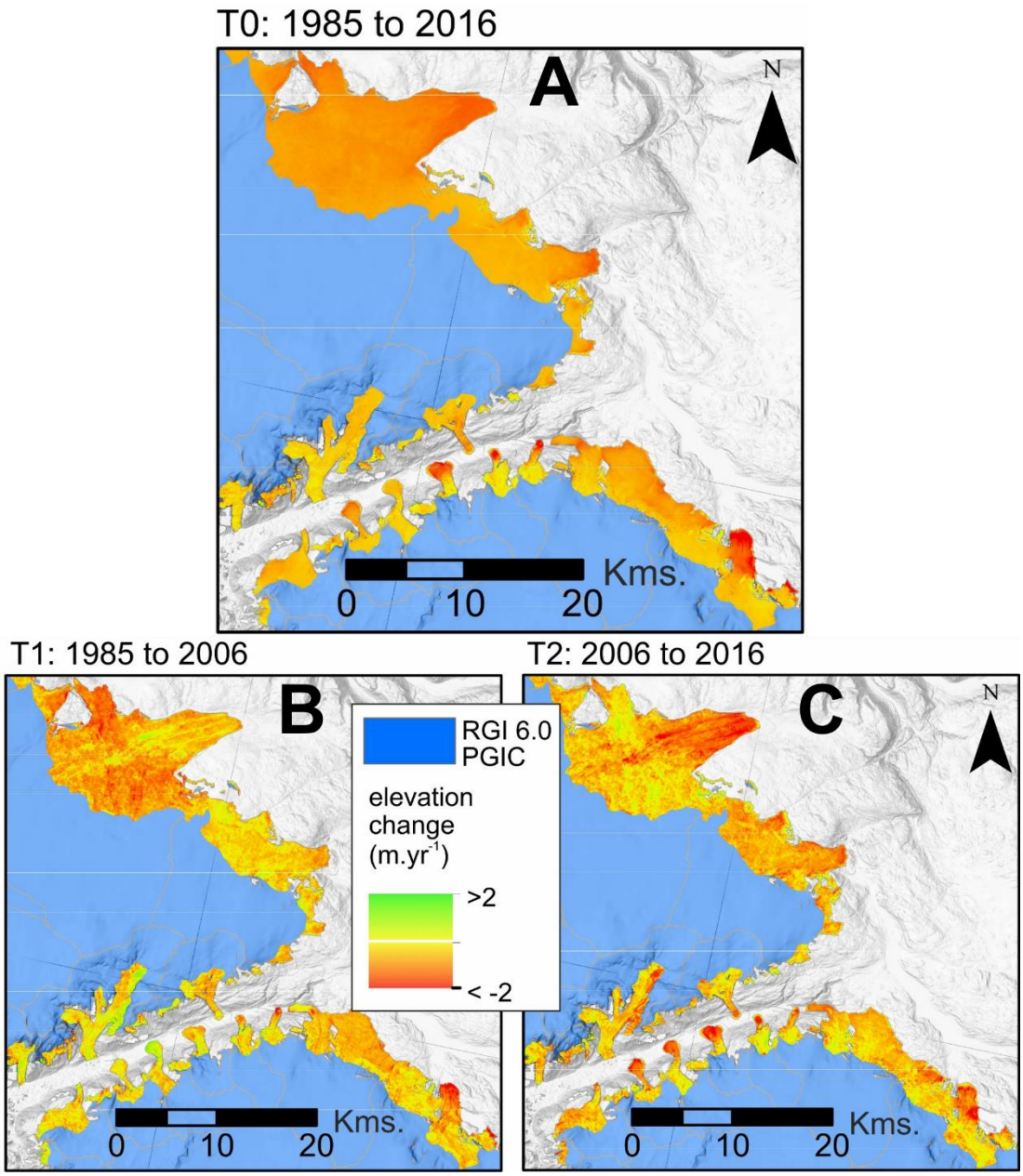

Figure 4.2 Example of accelerated surface elevation changes for outlet glacier on the north east of the Maniitsoq ice cap, south west Greenland (shown by yellow extent box in Figure 1). A) Changes over the entire study period *T0,* B) changes for *T1* (1985 – 2006), changes for *T2* (2006 – 2016). Blue areas represent ice cap accumulation zones, while green-yellow-red gradients indicate elevation changes over ablation areas. The semi-transparent grayscale ArcticDEM 2m hillshade is overlaid, with black/white grayscale regions depicting off-ice areas, including an ice-free valley dissecting the tiles from the bottom left diagonally upward to the right.

4.2.2.5 Statistical Aggregation and Grouping of Glaciers

Among the total 17,334 Greenland Glaciers documented in RGI version 6.0 (meeting the exclusion criteria outlined earlier), all glaciers with an area less than 1 km² were excluded. This exclusion criterion was based on the observation that such glaciers exhibited an average ablation area equivalent to less than three 30m grid cells (0.0027 km²). Consequently, the number of retained glaciers was reduced from 17,334 to 6,149, comprising less than 36% of the original dataset population. However, this reduction in the glacier population had a relatively minor impact on the overall glacier area, which was slightly reduced to 83,312 km^2 from 86,783 km2. Therefore, the relatively drastic reduction in glacier number preserved a significant proportion of the entire glacier area, encompassing over 96% and 99% of the total glacier area and ablation areas, respectively. This strategic curation of the dataset ensures the preservation of critical statistical representation while mitigating the influence of smaller, less statistically robust glaciers more prone to anomalous mass balance calculations with erroneous data, though this is largely handled via the quality filtering employed.

Localised DEM errors were also mitigated, and hence glacier-specific uncertainties, by aggregating the results onto a 500 km^2 hexagonal tessellated vector grid, as well as reporting statistics on aggregate by overarching region and glacier type. Using a hexagonal grid for aggregating spatial statistics, such as glacier mass balance changes, offers several advantages over a rectangular grid. Hexagons reduce edge effects, providing more uniform spatial relationships due to each cell's equal distance to its six neighbours, making them a natural choice for representing irregular glacier shapes. This arrangement is not only more efficient for data storage but also handles curvature more effectively, making it apt for the geospatial analysis conducted here. Hexagonal grids also present a visually appealing representation and ensure balanced neighbours, enhancing the overall quality of spatial statistics (Figure 4.2).

As in Lee et al. (2021), six mutually exclusive groupings of glacier by terminus type are considered (lake, marine, and land) and debris cover (clean and debris), which for Greenland GICs are: i) lake-clean (n = 169, 2.7%), ii) lake-debris (n = 61, 1%), iii) marine-clean (n = 153, 2.5%), iv) marine-debris (n = 42, 0.7%), v) land-clean (n = 4761, 77.4%), and vi) land-debris (963, 15.7%) (Figure 4.1). Debris cover was taken

from Herreid and Pellicciotti (2020), terminus type was determined from intersecting glacier outlines with lakes and the coastline after Carrivick et al. (2022), and surge status was determined from Lovell et al. (2023). Surge glaciers were considered in the analysis; however, results were skewed by the duration of this study and the timing of surge events. This is explored further in the chapter discussion.

4.2.2.6 Calculation of Volume, Mass, and Mass Balance Change

Void-filled DoDs were converted to volume change (ΔV, m^3) by summing all elevation change cells (Δh, m^2) and multiplying by the cell size for each glacier ablation area. Void-filled surface elevation changes in metres for ablation areas were converted to volume change in metres cubed per ablation area (ΔV) by summing all elevation change cells (Δh) and multiplying by the cell size ($900m^2$), as shown in equation 4.3.

$$\Delta V = \sum \Delta h \times 900m^2 \tag{4.3}$$

Rate of volume change per year per ablation area ($\Delta V/\Delta t$) for *T0*, *T1* and *T2* was calculated by dividing the total volume change (ΔV) by the respective duration (*ti-tj*). Duration of *T2* was constant however *T0* and *T1* durations varied depending on the initial AeroDEM year. This is shown in equation 4.4.

$$\frac{\Delta V}{\Delta t} = \Delta V \div \left(\frac{tj}{ti}\right) \tag{4.4}$$

Volume change was converted to mass change (kg^3) by multiplying volume change by the density of glacier ice (ρ). Here, ice density is assumed to be $850kg/m^3$ following the recommendations of Huss (2013) as this research assesses change for time periods far exceeding 5 years, and reports significant volume change exceeding 0. Moreover, when scaling to the entire glacier area the mass balance assumes the presence of a significant firn area. The total surface mass change (Δm) per glacier is then calculated as shown in equation 4.5.

$$\Delta m = \Delta V \cdot \rho \tag{4.5}$$

To estimate total glacier surface mass balance from the ablation area estimates, as outlined earlier this work conservatively assumes negligible volume change above the contemporary ELA (calculated from ArcticDEM). This assumption presumes

higher altitudes above the ELA rarely experience positive degree days and so are largely protected from warming temperatures, but not from continued precipitation to maintain surface elevation and mass transfer. To calculate mass balance over entire glacier areas following this assumption, summed ablation area elevation and volume change statistics were copied to their parent glacier within the RGI, with some glaciers having multiple ablation areas output by the ablation area tool.

Surface mass balance (B_{sfc}) is reported as total mass balance (ΔM), assuming basal melt is negligible for high artic PGIC, and is calculated in metres water equivalent per year (m w.e / yr^{-1}), calculated as mass change (m) divided by total glacier surface area in m^2 (s) divided by duration in years (ΔT). As 1kg of liquid water has a thickness of 1mm when spread evenly over $1m^2$, results are divided by 1000 to convert mm w.e / yr^{-1} to m w.e / yr^{-1}. Glacier mass balance is therefore calculated as shown in equation 4.6.

$$\Delta M = \frac{(m/s)\ /\Delta T}{1000} \tag{4.6}$$

When aggregated to a Greenland wide scale, mass changes are converted to the Sea Level Equivalent (SLE in mm or 10^{-3}) which is calculate as equation 4.7.

$$\mathrm{SLE(mm)} = \mathrm{M(Gt)} \cdot (1/361.8) \tag{4.7}$$

With an assumed global ocean coverage of 3.618 x 108 km^2, and an understanding that a 1 mm rise in sea level requires 10^{-3} m^3 input of terrestrially stored water for each square metre of the ocean surface, or 10^{-12} Gt. As 1 Gt of ice is equal to $1km^2$ of water, 361.8 Gt of ice will raise sea levels by 1mm.

4.2.2.7 Accuracy and Uncertainty Assessment

Analysing geodetic changes only within glacier ablation areas via the use of an automated AABR tool enables us to make Greenland-wide inter-regional comparisons with large numbers of glaciers. However, this approach does also mean that for specific individual glaciers some small parts of an accumulation area (in addition to the ablation area) could be included, whilst for other glaciers the full ablation area might not be included in the elevation change analysis. Additionally,

whilst down-wasting probably dominates the mass loss geometric signal over terminus recession, it can be expected that glaciers have become smaller during this study period, and so using a fixed (RGI_v6 outline) geometry for the elevation change analysis will likely slightly underestimate mass loss. Therefore, the spatial patterns and temporal trends identified are considered to be robust, and the quantification of mass balance is most likely a minimum estimate.

Random and systematic error and uncertainty in the calculated elevation changes are introduced in three forms: i) error within the static DEMs introduced during acquisition (i.e. shadow, clouds, sensor instability, poor ground illumination conditions) and preparation (georeferencing inaccuracy and pre-processing such as void filling and interpolation); ii) processing errors introduced by imperfect alignment during co-registration and resampling from native to lower resolutions; and iii) temporal uncertainty due to the imprecise dates (assigned to the GIMP and ArcticDEM DEMs). The random and systematic uncertainty is calculated in the surface elevation measurement by calculating the Normalised Median Absolute Deviation (NMAD), standard deviation, and mean of elevation changes over off-ice surfaces considered to be static over the study period (static bedrock determined from landcover change). As some surfaces determined to be static likely weren't during the study, these errors are likely overestimated here. To quantify the overall uncertainty associated with mass balance calculations $\sigma_{\Delta M}$, the random and systematic errors are accounted for in the elevation change measurements $\sigma_{\Delta h}$ and combined with temporal uncertainty $\sigma_{\Delta t}$ (from imprecise DEM acquisition dates), area uncertainty σ_A (from inaccuracies in the glacier outlines), and the density uncertainty σ_ρ associated with the constant standard bulk density estimate used of 850 kg m^{-3}. These four-uncertainty metrics ($\sigma_{\Delta h}$, $\sigma_{\Delta t}$, σ_A, and σ_ρ) are combined by substituting each into the mass balance formula as calculated per difference DEM to then calculate per glacier and regional mass balance uncertainty.

Systematic errors arising from misalignment are substantially mitigated through co-registration, where post-co-registration misalignments over static surfaces are found to be orders of magnitude smaller than the DEM resolution, thus deemed negligible (refer to Appendix B, Figure 7.3). In this approach, both AeroDEM and GIMP are coregistered to ArcticDEM (the dataset with the highest horizontal accuracy), effectively minimising the error propagation that arises from inconsistent co-

registration. Furthermore, by excluding all glaciers with surface areas less than 1 km², the common guideline suggesting spatial autocorrelation of error for distances 500 m apart is rendered inapplicable (Rolstad et al., 2009). Consequently, it is assumed that spatial error is not spatially correlated, enhancing the robustness and reliability of the elevation change data derived from the study.

Mass balance uncertainty is calculated per glacier following Shean et al. (2020) who followed well-established methodologies for geodetic analyses (e.g. Fischer et al., 2015; Berthier et al., 2016; Brun et al., 2017; Menounos et al., 2019). Glacier elevation change (dH) error $\sigma_{\Delta h}$ was assessed by calculating the mean, standard deviation, median and normalised median absolute deviation (NMAD) per pixel in areas outside of 1 km buffer zones around the RGI_v6.0 glacier margins, and 2 km around the IMBIE ice sheet outline. Elevation changes are excluded in the uncertainty assessments within this buffer as the RGI_v6.0 glacier margins are dated to circa 2001, and the IMBIE ice sheet margin is circa 2004 (Zwally et al., 2012), yet the *T0* DoDs extend back to 1978 and thus non-static areas of ice change will therefore exist around the ice margin datasets used. DoD's were filtered following the empirical (3 sigma) rule; for each DoD the random error $\sigma_{\frac{dh}{dt}\,random}$ is calculated as the combined root-mean-square-error of the normalised median absolute deviation (NMAD) and standard deviation of off-ice surface elevation changes over time $\frac{dh}{dt}$. The remaining systematic error $\sigma_{\frac{dh}{dt}\,systematic}$ is computed as the mean elevation change over time $\mu_{\frac{dh}{dt}}$ producing the total elevation change uncertainty as shown in equation 4.8.

$$\sigma_{\Delta h} = \sqrt{\sigma_{\frac{dh}{dt}\,random}^{\,2} + \sigma_{\frac{dh}{dt}\,systematic}^{\,2}} \tag{4.8}$$

The standard deviation and NMAD are multiplied by the number of pixels in the ablation area of each glacier, then multiplied by the cell size (900m) then divided by change in time to calculate $\frac{dh}{dt}$ per glacier so as to scale up rates to entire RGI glacier area (*A*) in total uncertainty calculations, as conducted in calculating per glacier mass balance. Elevation change uncertainty is combined with three other uncertainty metrics, temporal uncertainty $\sigma_{\Delta t}$ (from imprecise DEM acquisition dates), area uncertainty σ_A (from inaccuracies in the glacier outlines), and the density uncertainty σ_ρ associated with the constant standard bulk density estimate used of 850 kg m^{-3}.

Temporal uncertainty was assessed as the percentage of potential variability around the central date associated with each input DEM. For example, the date range for the ArcticDEM version used is 2015 to 2017, so a 3-year temporal coverage centred on 2016. The actual duration of the difference DEM is multiplied by the uncertainty percentage. Thus for 1978 AeroDEM differenced from ArcticDEM, the total duration is 38 years (dt) with a temporal uncertainty of 3 years or 7.9%, therefore temporal uncertainty $\sigma_t = dt \cdot 0.079$. Substituting σ_t into the total elevation change over time as $\sigma_{\Delta t} = \frac{dh}{\sigma_t}$.

The RGI area uncertainty for Greenland's periphery is cited as 5 % (Pfeffer et al., 2014) However, as only glaciers > 1km^2 are considered here the error is likely even lower (as outlined in Pfeffer et al., 2014), however the more conservative value of 5% is adopted ($\sigma_A = 0.05 \cdot A$).

Following Huss (2013), an error of 7.1% is assumed with the density assumption of 850kg m^{-3}, therefore a density uncertainty of $\sigma_\rho = 60\ kg\ m^{-3}$ is applied here.

These four error components ($\sigma_{\Delta h}$, $\sigma_{\Delta t}$, σ_A, and σ_ρ) are combined to calculate total mass balance uncertainty $\sigma_{\Delta M}$ per DoD as shown in equation 4.9.

$$\sigma_{\Delta M} = \sqrt{((\sigma_{\Delta h} \cdot \rho) \div A)^2 + ((\sigma_{\Delta t} \cdot \rho) \div A)^2 + ((\frac{dh}{dt} \cdot \rho) \div \sigma_A)^2 + ((\frac{dh}{dt} \cdot \sigma_\rho A)^2} \qquad (4.9)$$

This is converted to metres water equivalent per year (m w.e. yr^{-1}) and is used to calculate per glacier and aggregate regional mass balance uncertainty and confidence margins. Table 4.1 shown the error metrics calculated per AeroDEM region and time period (*T0, T1, and T2*) in this research.

Table 4.1 Metrics used per region for random and systematic elevation difference uncertainty

DEM of Difference	**Mean** m w.e. yr^{-1}	**Standard Deviation** m w.e. yr^{-1}	**NMAD** m w.e. yr^{-1}
T0 1978	0.34	6.13	3.62
T0 1981	-0.12	7.45	0.51
T0 1985	2.05	6.62	1.98
T0 1987	0.45	5.44	2.14
T1 1978	0.80	7.10	3.15
T1 1981	0.24	8.45	0.66
T1 1985	1.57	8.12	1.88
T1 1987	0.29	5.92	2.06
T2 1978	1.25	8.07	2.68
T2 1981	0.60	9.45	0.82
T2 1985	1.09	9.62	1.78
T2 1987	0.13	6.39	1.98

4.2.2.8 Sample significance testing

The Wilcoxon test was selected to compare regional glaciers' mass balance distributions, which exhibit a mix of normal and non-normal types. The Wilcoxon test, a non-parametric statistical method, is well-suited for this analysis because it does not assume normality, making it robust for comparing distributions that may not follow a normal distribution. This method is particularly advantageous given the diverse nature of the data. Parametric tests, such as the paired t-test, assume that differences between paired observations are normally distributed. This assumption can lead to inaccuracies when dealing with non-normal distributions. In contrast, the Wilcoxon test is based on ranks rather than raw data, which makes it more robust and reliable for this type of data. This robustness is essential for ensuring the validity of the comparative analysis. The regions under investigation have significantly varying populations, with the number of glaciers ranging from 410 in the northwest to 1900 in the northeast. The Wilcoxon test was preferred because it makes fewer assumptions regarding sample size and the central limit theorem, allowing for valid comparisons despite the heterogeneous sample sizes across different regions.

Although generalised linear models (GLMs) were considered, they are primarily used to examine the relationship between a dependent variable and multiple independent variables, accommodating various error distributions. The application of GLMs in this context would necessitate specifying an appropriate link function and error structure, which could introduce unnecessary complexity and potential biases. Given that the primary objective was to compare the central tendency of mass balance rates across distinct regions, as well as to distinguish differences between glaciers grouped by debris cover, terminus type, and surge status, the Wilcoxon test was deemed more suitable.

Significance testing was conducted using R. The R base package includes the function pairwise.wilcox.test to perform the Wilcoxon rank sum test between all pairs of samples in a study. A common method to represent significance in pairwise comparisons is the use of letters: samples sharing a letter are not significantly different from each other, whereas samples not sharing letters are significantly different. The multcompView package in R can take a square matrix of p-values and

return letters for all samples. Since pairwise.wilcox.test returns a triangular matrix, a custom function, tri.to.squ, was written to convert this output into a suitable input for the multcompLetters function of the multcompView package. This approach allowed for the easy plotting of distributions as box plots with the corresponding significance letters added as text, providing a clear visual representation of the results. Where box plots in figures show significance letters for plots, those plots which share letters are not significantly distinct from one another.

The Wilcoxon test, with its robustness to non-normal distributions and minimal assumptions, provided a more straightforward and reliable means of comparing the medians of mass balance rates. This method ensured the integrity and interpretability of the results, making it the optimal choice for this research. The added complexity and potential biases of GLMs were avoided, affirming the appropriateness of the Wilcoxon test for this study's comparative analysis of mass balance rates across Greenland's regions.

4.3 Results

Following data processing and uncertainty assessment, this section outlines the results of national and regional mass balance differences over the entire study period (*T0)* and by region, as well as notable hotspots of accelerated mass loss between the two dissecting time periods (*T1* and *T2*). Subsequently, changes are reported regionally by the terminus type (lake, terrestrial, marine), behaviour (surge, non-surge), and surface character (debris, non-debris).

4.3.1 Regional Patterns of Volume and Mass Change

In total, this research finds that Greenland’s PGICs lost at least 276 Gt of ice, equating to 0.76 mm sea level rise equivalent between the late 1970s and 2015, i.e., during T0 (total study period). Overall, all regions around Greenland were found to exhibit negative mass balance rates, and the Greenland-wide PGIC median mass balance during T0 was -0.1 ± 0.02 m w.e. yr^{-1}. Figure 4.3 shows box plots of mass balance per region over T0. Values on top of the x-axis are the sample medians, and red letters above the plots reflect the Wilcoxon post-hoc pairwise letter codes comparing distributions' significance.

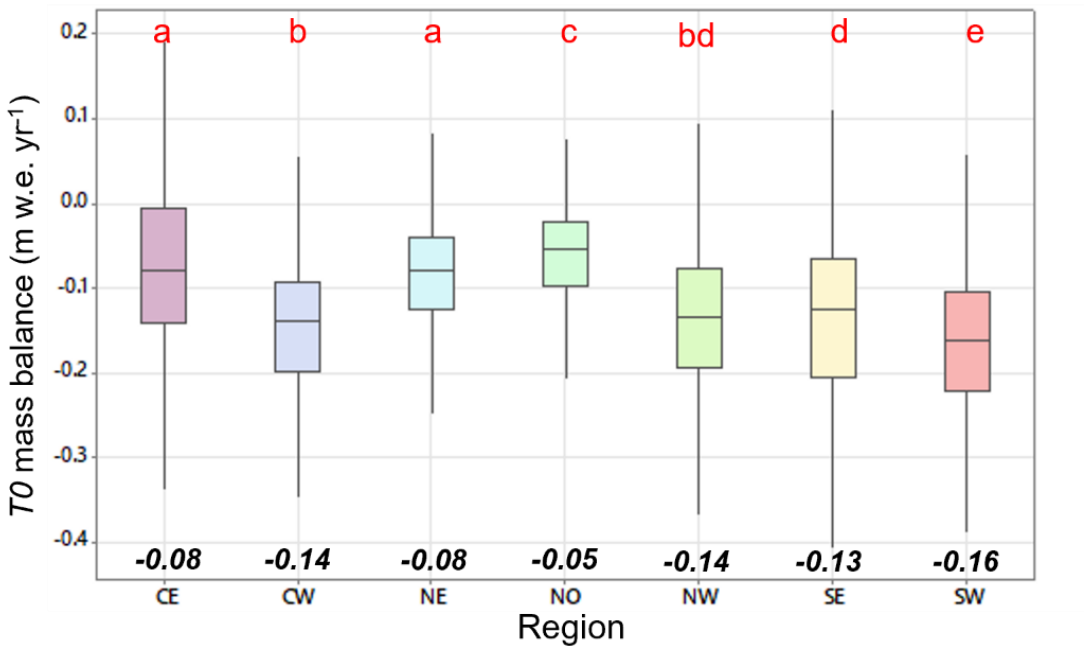

Figure 4.3 Boxplots of *T0* mass balance by region with Wilcoxon pairwise alphabetical codes of statistical difference above box 'whiskers' in red and plot medians in bold atop the x-axis.

PGICs on the west of Greenland have experienced more negative mass balances than those on the east (Figure 4.3). Over the entire study period (*T0*), the mean mass balance is more negative on both coasts at lower latitudes, with mass balance becoming less negative on both coastlines trending northward. Accordingly, north Greenland exhibits the least negative median mass balance over *T0* at -0.05 ± 0.02 m w.e. yr^{-1} (Figure 4.3). This is relatively closely followed by the north east and central east of Greenland, both with a rate of -0.08 ± 0.02 m w.e. yr^{-1}, followed by the south east with -0.13 ± 0.03 m w.e. yr^{-1} (Figure 4.3). Interestingly, the south east is the only region in the east of Greenland where the *T0* PGIC mass balance (-0.13 ± 0.03 m w.e. yr^{-1}) is lower than the reported Greenland wide average rate over the same period (-0.10 ± 0.02 m w.e. yr^{-1}). Post-hoc Wilcoxon test results for *T0* show that all regions have statistically significant differences in mass balance except the adjacent north and central east areas (Figure 4.3).

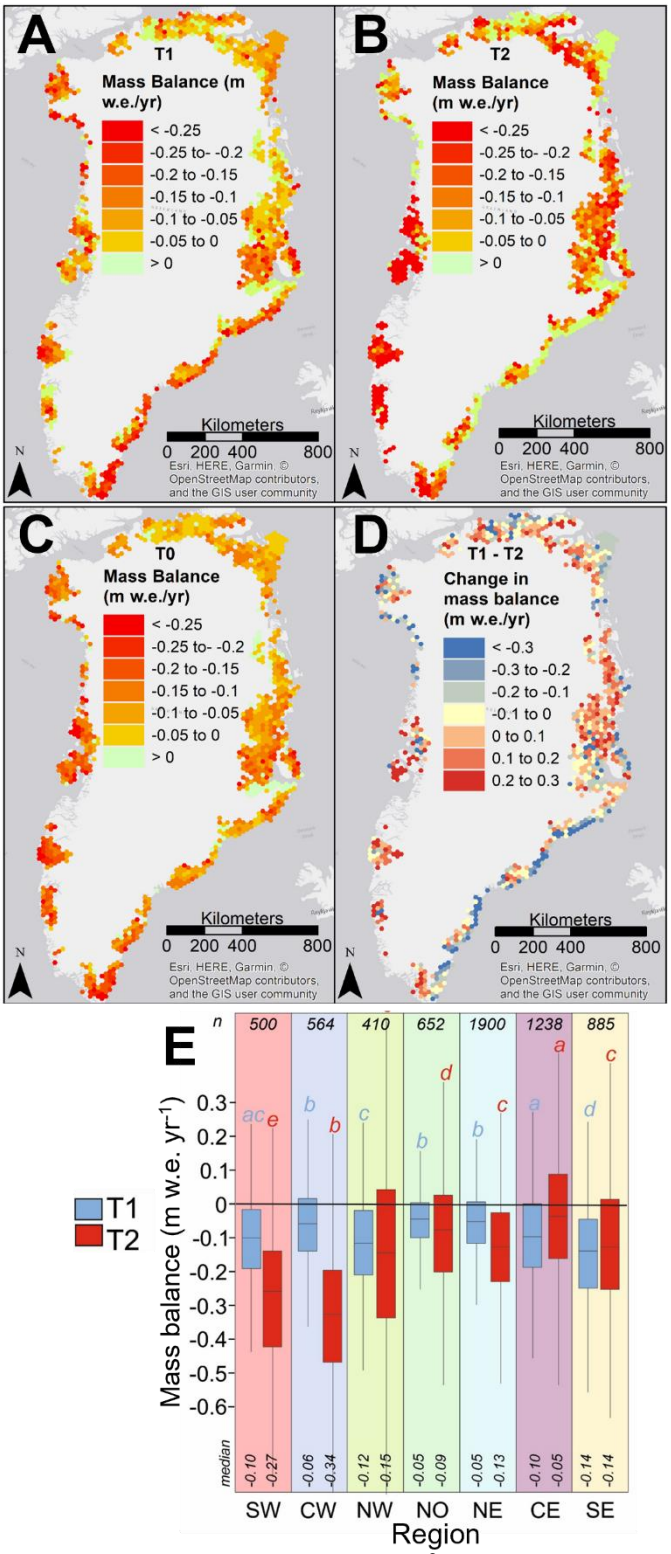

Figure 4.4 A, B and C: Tessellation (500 km^2) hexagon grids mean mass balance during *T1* (1978/81/85/87 – 2006), *T2* (2006 – 2016) and *T0* (1978/81/85/87 – 2016) respectively as labelled. D: Difference between each hex grid cell's *T1* and *T2* mass balance. Panel E: Box plots per region comparing *T1* and *T2* mass balance with Wilcoxon pairwise alphabetical codes of statistical difference above

Figure 4.4 shows maps of the distribution of mass balance rates for *T0, T1* and *T2*, with mass balance represented as averages for each 500km^2 hex grid cell (Figure 4.4 A, B, C). The difference between the *T1* and *T2* mean mass balance per hex cell is shown in Figure 4.4D, highlighting areas of acceleration (more negative) mass balance in shades of red and less negative in shades of blue. As Figure 4.4D shows *T1* rate minus *T2* rate for each hex cell, more positive values correspond to values becoming more negative in *T2*. For example, -0.1 minus -0.4 gives a value in Figure 4.4D of 0.3, reflected by a dark red hex cell. Figure 4.4E shows box plots per region comparing the *T1* and *T2* mass balance. The maps show that particular hotspots of negative glacier mass balance exist in the west and south, whereas similar latitudes on the east show fairly stable rates in *T0* and *T2* (Figure 4.4B and C). Conversely, the *T*1 mass balance distribution is the opposite in the south, with particularly highly negative mass loss rates (<-0.2) identified in the south east where the same latitude shows more stable rates > -0.1 in the west (Figure 4.4A). The north of Greenland across all time periods is fairly stable, with notably high mass loss rates in the north east (<-0.2) during *T2*. Accordingly, Figure 4.4D shows hot spots of acceleration of mass balance in the south west and central east where rates have become more negative, whereas the south east has shown a notable decrease in mass loss (Figure 4.4D). Regionally, mass loss accelerated between *T1* and *T2* for all regions except within the south and central east regions (Figure 4.4E). West Greenland's PGICs had the greatest changes in mass balance, with a 2.7 times increase in mass loss from -0.10 to -0.27 m w.e. yr^{-1} in the south west and a 5.6 times increase from -0.06 to -0.34 m w.e. yr^{-1} in the central west (Figure 4.4E). Figure 4.2 shows examples of glaciers in the south west where this acceleration in loss is very apparent in the annual surface change rates.

4.3.2 Variations by Terminus Environment, Behaviour and Surface Characteristics

As well as considering all glaciers together per region, each glacier were also assigned a value relating to its terminus type, behaviour and surface category, and mass balance trends are explored for combinations of the above nationally and per region. Mass balance during *T0* was found to vary by glacier terminus type and surface character. Figure 4.5 shows box plots for each of the six terminus-surface character combinations for all of Greenland and per region, with total counts of glaciers (n) shown above plots and median values above the x-axis. In order, from

most negative to least by median, the terminus-surface character combinations mass balance are: lake-debris (-0.15 ± 0.02 m w.e. yr^{-1}), marine-debris (-0.13 ± 0.02 m w.e. yr^{-1}), lake-clean (-0.12 ± 0.02 m w.e. yr^{-1}), land-debris (-0.11 ± 0.02 m w.e. yr^{-1}), land-clean (-0.09 ± 0.02 m w.e. yr^{-1}), and marine-clean (-0.07 ± 0.02 m w.e. yr^{-1}) (Figure 4.5).

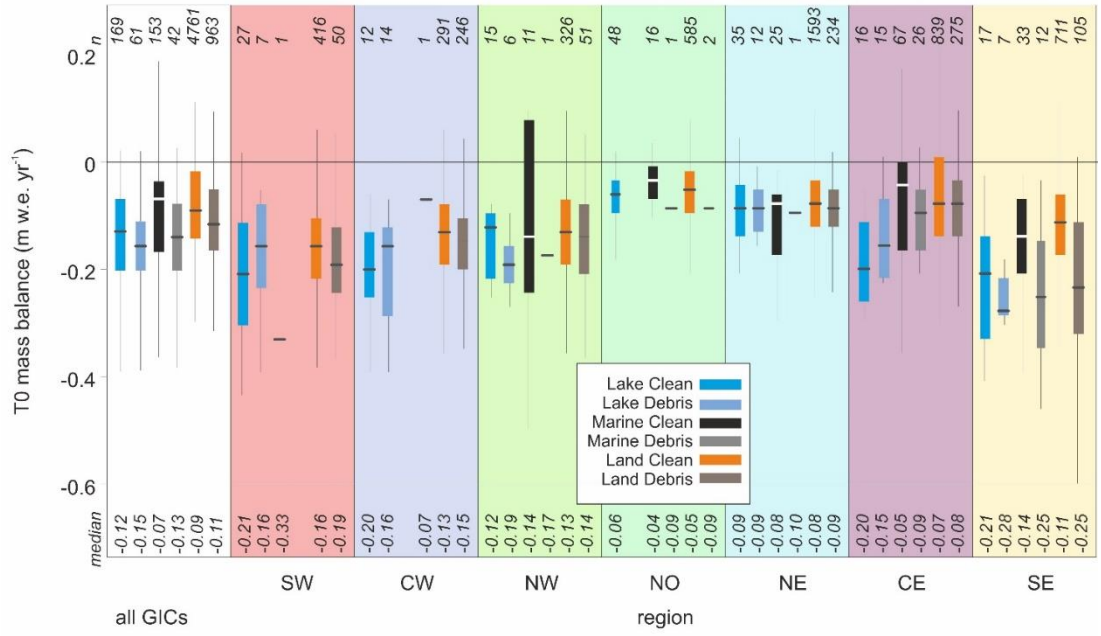

Figure 4.5 Variation of mass balance with terminus type and surface character. Counts (n) of glacier type per region are shown above each chart, and median mass balance values shown at the bottom. Note: some regions do not contain any glaciers in these categories and some categories contain too few glaciers to calculate an inter-quartile ranges.

Debris covered Greenlandic PGICs tend to have a more negative mass balance for all regions and nationally when compared to their clean counterparts as shown by the pairwise-comparison alphabetical codes in Figure 4.5. Moreover, water-terminating (lake and marine) PGICs tend to have a more negative mass balance than their land terminating counterparts, regionally and nationally (Figure 4.5). Glaciers terminating in lakes have the most negative mass balances, more-so than those terminating in oceans (Figure 4.5). Water-terminating glaciers across Greenland also have more variation (a higher inter-quartile range) in their mass balance than land-terminating glaciers (Figure 4.5). The groups with the most negative mass balances (where $n > 4$) are found in the south east region with three of these groups being water-terminating

and the lowest being debris covered: lake-debris (-0.28 ± 0.03 m w.e. yr^{-1}), marine-debris (-0.25 ± 0.03 m w.e. yr^{-1}), land-debris (-0.23 ± 0.03 m w.e. yr^{-1}), and lake-clean (-0.21 ± 0.03 m w.e. yr^{-1}). The fifth lowest mass balance of any group is for clean lake-terminating glaciers in south west Greenland (-0.21 ± 0.03 m w.e. yr^{-1}). Taken together, these results suggest strongly that mass balance of Greenland's PGICs is controlled by the compounding influences of latitude and terminus environment, and to a lesser extent by glacier surface character, the connotations of which are explored in the later discussion.

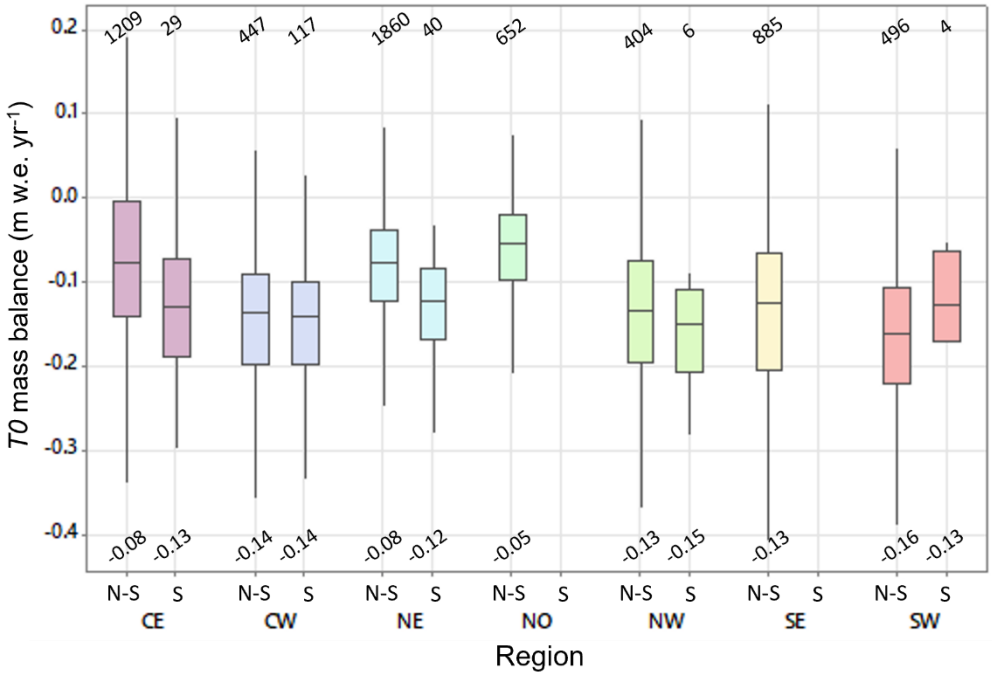

Figure 4.6 Plots of *T0* mass balance for surge-type glaciers regionally. On the x-axis N-S is non-surge and S is surge. Median values are shown above the x-axis, and number of glaciers (n) above the plots.

Regional surge-type glacier results are shown in Figure 4.6. Surge-type PGICs (n = 96, i.e. 0.015 % of total) in Greenland are found predominantly within a west and an east cluster, and during 1985 to 2019 surge activity has apparently transitioned from being focussed in the west to the east according to recent work of Lovell et al. (2023). Surge-type PGICs, in this research, had a more negative mass balance than their non-surging counterparts for all regions (where surge glaciers exist) except the south west (Figure 4.6). In the central and north east, non-surging glaciers had median mass balances of -0.07 ± 0.03 m w.e. yr^{-1} and -0.07 ± 0.02 m w.e. yr^{-1}, respectively, whereas surge type glaciers in those regions have a median mass

balance of -0.13 ± 0.03 m w.e. yr^{-1} and -0.12 ± 0.02 m w.e. yr^{-1}, respectively. In the north and central west, the rates are far more similar to one another than in the east, with non-surge type glaciers having a median mass balance in the north west of -0.13 ± 0.03 m w.e. yr^{-1} compared to -0.15 ± 0.03 m w.e. yr^{-1} for surge type. In the central west both surge and non-surge type glaciers have median mass balance of -0.14 ± 0.03 m w.e. yr^{-1}. In the south west, surge type glaciers have a median mass balance of -0.12 ± 0.03 m w.e. yr^{-1}, whereas surge type median mass balance of -0.16 ± 0.03 m w.e. yr^{-1}.

4.4 Discussion

In this chapter, detailed analyses of the mass balance and subsequent changes in Greenland's peripheral glaciers and ice caps (PGIC) were presented, based on extrapolated mass balance rates from well-resolved ablation areas. The results, articulated by region and categorised by glacier type, provide a nuanced understanding of the dynamic responses of these ice bodies within a changing climate on a Greenland-wide scale. This approach removes erroneous accumulation area values but introduces some uncertainty due to the reliance on extrapolated ablation area metrics and estimated equilibrium line altitudes (ELAs). The initial section of this discussion delves into the intricate relationship between mass balance and glacier typology, examining how factors such as terminus environment (lake, marine, terrestrial), surface condition (clean or debris-covered), and dynamic behaviour (surge or non-surge) influence the stability and mass evolution of glaciers. It is important to note that only glacier ablation areas were considered in this study, as accumulation areas contained erroneous values. This assumption of zero melt for accumulation areas means that the mass balance statistics presented are very conservative minimums. This comprehensive analysis sheds light on the heterogeneity of glacier responses and underscores the complex interplay between physical characteristics, spatial distribution and climatic forces. Following this, the subsequent section of the discussion situates the findings within the broader scientific context, comparing the observed rates with those documented in the literature over various temporal scales. While the estimates presented are conservative minimums, the relative rates and temporal resolution provide valuable and insightful results, enhancing our understanding of Greenlandic glacier dynamics. This comparative approach not only validates the study but also contributes to a deeper understanding

of the regional and global trends in glacier mass balance, offering valuable insights into the past, present, and potential future.

4.4.1 Relationship Between Mass Balance and Glacier Type

Lake terminating glaciers, of the three terminus types considered, were found to have the most impact on mass balance, driving the most negative mass balance rates indicating exacerbated mass loss (Figure 4.5). Lake-terminating glaciers have been found to have enhanced terminus recession, ice surface velocity and more negative mass balance than their land-terminating counterparts in several ice sheet and alpine settings (King et al., 2018; King et al., 2019; Proonk et al., 2021; Mallalieu et al., 2021) owing to a series of thermo-mechanical feedbacks and interactions between lakes and glaciers (Carrivick et al., 2020a; Carrivick et al., 2020b; Sutherland et al., 2020). The time-scale over which these lake effects on glaciers persist depends on local topography; the shape and size of the lake, as well as ice dynamics. This work adds to this discourse, showing that for PGIC in Greenland over a ~40 year period lakes have had a significant impact on mass balance rates, statistically significant from terrestrial (and marine) where for most regions lakes are seen to increase mass loss and affect accelerating rates.

The marine signal in this research is less distinct, and somewhat contrary to traditional thinking regarding marine forcing and its effect on mass balance. Marine-terminating glaciers have multiple forcings that expedite calving and mass loss in excess of climate forcing alone (van As et al., 2014; Rignot et al., 2015; McMillan et al., 2016). However, this research finds that marine-terminating glaciers have amongst the least negative mass balance of all the glacier type groupings considered (Figure 4.5). It is postulated that this unexpected finding can be explained by the location of the PGICs in this study. Of all the marine terminating glaciers studied here, 84 % are located in eastern Greenland where other research has reported evidence of increasing glacier mass (Hugonnet et al., 2021; Sørensen et al., 2018), and deceleration of mass loss has occurred since 1999 to 2018 (Khan et al., 2022). This work also reports consistently less-negative mass balance in the east, and in the vicinity of most marine terminating glaciers, as well as a deceleration in mass balance decrease between *T1* and *T2* (Figures 4.3 and 4.4).

Many glaciers worldwide accrue thick insulating debris cover sourced from rockfall from steep valley sides and that thick debris insulates underlying ice from melt (Nakawo & Rana, 1999). This is particularly the case for mountain glaciers in regions such as the European Alps (e.g. Azzoni et al., 2018; Fleischer et al., 2021), the Himalaya (e.g. Harrison et al., 2021; Pellicciotti et al., 2015; Pratap et al., 2015; Zhang, Gu, et al., 2022; Zhang, Liu, et al., 2022), and the Southern Alps of New Zealand (Brook et al., 2013; Hagg et al., 2014; Kirkbride & Warren, 1999; Reznichenko et al., 2010). However, debris cover on Greenland's PGICs is more limited in extent, being present on just 2.4 % of total glacier area (Scherler et al., 2018). Furthermore, based on interrogation of satellite imagery, it is suggested here that debris on Greenland PGICs is mostly composed of relatively thin veneers of aeolian-derived material, cryoconite (Takeuchi et al., 2018), ogive-bands (Atherton, 1963; Echelmeyer et al., 1991; Reznichenko et al., 2010), surficial glacifluvial sediment (Seguinot et al., 2020; Yang et al., 2016), and melt out till (Yde and Knudsen, 2005), due to a lack of steep valley sides to supply coarse rockfall material in many areas, or due to exceptionally hard bedrock in others (Henriksen et al., 2009). Such thin debris cover lowers surface albedo and facilitates the transmission of heat to the glacier surface, expediting melt and thus explaining the enhanced mass loss reported for debris-covered Greenland PGICs (Figure 4.5). It is acknowledged that the debris cover on some glaciers could have changed during the study period, and that the properties of supraglacial debris on Greenland's PGICs are almost unknown, whereas a few studies have detailed the surface composition of parts of the GrIS (Bøggild et al., 2010; Ryan et al., 2018).

Surge-type glaciers are a unique subset of glaciers characterised by their cyclical nature of quiescent and active phases (Clarke et al., 1986; Sevestre & Benn, 2015). During their active phase, surge-type glaciers exhibit a rapid 'surge' in ice movement and redistribution of their mass to lower elevations. This can lead to a temporary gain of mass in their ablation areas, leading to an expectation of positive mass balance in these zones when measurement periods cover a surge phase (e.g. Dowdeswell et al., 1995). However, the findings of this study are contrasting to this expectation. It is observed here that glaciers classified as surge type are, in fact, associated with a more negative mass balance compared to their non-surge counterparts for nearly all region's PGIC in Greenland (Figure 4.6). This surprising revelation suggests that the

glaciers in question may have surged prior to the initial observation period of this study (*T1*), spanning from the late 1970s to 2006. This has led to subsequent rapid mass loss in their ablation zones during the study period (Truffer et al., 2021). Specifically, in central western Greenland, out of the 63 glaciers identified as surge-type, only 11 showed evidence of surge-type elevation profile changes between 1985 and 2012 (Huber et al., 2020). Conversely, the observed pattern in the south-west region implies a more recent occurrence of these surges. This complex interplay between expectation and reality adds a nuanced layer to understandings of glacier dynamics, particularly in the context of surge-type PGIC.

4.4.2 Comparison with Existing Reported Rates of PGIC Mass Balance

The mass balance rates reported in this research are placed into context against a longer estimated rate since the Little Ice Age (LIA) and a more recent study covering multiple time periods since 2000, shown in Figure 4.7. While these comparisons are based on extrapolated ablation area metrics and are therefore conservative estimates, they still provide a justified comparative assessment. This approach allows for a meaningful evaluation of relative rates and trends over time Nationally, the *T0* mass balance for Greenland's PGICs as reported here is slightly less negative than the rate since the Little Ice Age (LIA) as reported by Carrivick et al. (2023) and less negative within all regions than for rates calculated since the year 2000 as reported by

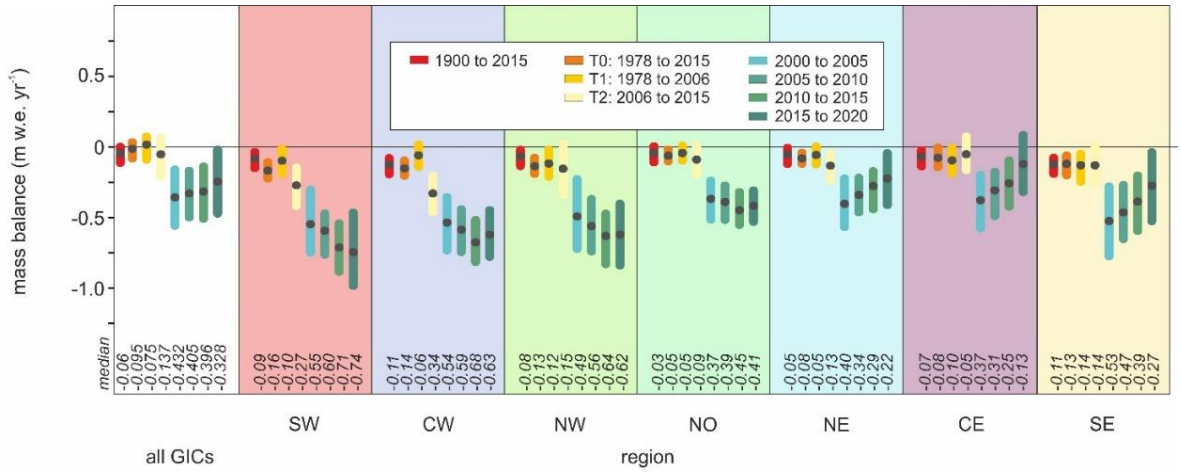

Figure 4.7 Comparison between the *T0*, *T1* and *T2* estimates of glacier-wide mass balance made here and existing Greenland-wide and per region rates that have been reconstructed since the Little Ice Age termination (year 1900) by Carrivick et al. (2023) and for four time periods since 2000 by Hugonnet et al. (2021)

Hugonnet et al. (2021) (Figure 4.7). There has therefore been a net acceleration of mass loss from Greenland's PGICs not only since the LIA (Carrivick et al., 2023) but most especially since the late 1970s and before 2000 (Figure 4.7).

The most recent rate of Greenland-wide mass loss (2015 to 2020), calculated from the elevation change data provided alongside Hugonnet et al. (2021) seems to be approaching the longer-term mean (Figure 4.7), which suggests that mass loss must have been much less negative, and perhaps even a positive mass balance for many PGICs in the 1980s and 1990s (Figures 4.4E and 4.7), which is plausible given that the GrIS was more or less in state of balance during the 1970s (Rignot et al., 2008) and during the 1990s (Shepherd et al.,2020). However, there is considerable variability in mass loss rates through time across Greenland as reported here. PGIC mass balance has become progressively less negative in the south east, central east, and north east regions (Figure 4.4D) since the year 2000, whereas since the 1980s it has become progressively more negative in the western regions (Figure 4.7).

These findings of an east-west asynchrony across Greenland in PGIC mass loss support those of other remote-sensing-based studies (e.g. Sørensen et al., 2018; Hugonnet et al., 2020; Khan et al., 2022). However, this research considers a substantially longer time-frame and reveals greater complexity by region and by glacier type than those before. The few direct field measurements of glacier mass balance from Greenland's PGIC also show differences between glaciers on the west and east of Greenland (see Machguth et al., 2016). These glacier responses are predominantly linked to temperature-precipitation trends and asynchrony between Greenland's east and west, which are often manifest opposite between the two coastlines with the east of Greenland experiencing particularly high precipitation when west Greenland is largely devoid, and vice-versa (Box, 2002). Bjørk et al. (2018) conducted a comprehensive study mapping the length fluctuations of approximately 350 peripheral glaciers and ice caps in East and West Greenland since 1890, finding recent rates of retreat were 12.2 meters per year in east Greenland and 16.6 meters per year in west Greenland, second only to the rapid changes observed during the early 20th century's post-Little Ice Age period. These findings of increased mass loss for western PGIC are mirrored in the findings reported here. Bjørk et al. (2018) established a link between regional changes in ice volume, as indicated by glacier length, and variations in precipitation patterns connected to the

North Atlantic Oscillation (NAO), notably an east-west asymmetry. During positive phases of the NAO, accumulation and, consequently, glacier growth increased in east Greenland, while the opposite was true for west Greenland. Future projections indicating a trend towards more positive NAO phases suggests that eastern peripheral glaciers may maintain relative stability, while western glaciers are likely to continue their decline. This mirrors the findings presented here, where more recently eastern PGIC have shown less negative mass balance and accordingly an inferred deceleration in mass loss and relative stability (Figures 4.4 and 4.7).

Table 4.1 presents this study's *T0* mass balance estimate for Greenland in the context of other works covering various time periods from the start of the 20th century to 2020.

Table 4.2 Comparison of GIC mass balance across Greenland by time period.

Time period	Duration (years)	Mass Balance m w.e. yr^{-1}	Method	Study
1900 to 2015	115	-0.06	modelled	Carrivick et al. (2023)
1958 to 1997	39	-0.14	modelled	Noël et al. (2017)
1978 to 2016	37	-0.30	geodetic	This study *T0* ablation areas
2003 to 2008	5	-0.31	geodetic	Bolch et al. (2013)
2003 to 2009	6	-0.43 ± 0.13	gravimetric	Colgan et al., (2015)
2000 to 2020	20	-0.40	geodetic	Hugonnet et al. (2021)
2003 to 2009	6	-0.42	geodetic	Gardner et al. (2013)
1997 to 2015	18	-0.44	modelled	Noël et al. (2017)
1985 to 2012	27	-0.45	geodetic	Huber et al. (2020) (*extrapolated)
2006 to 2016	10	-0.57	geodetic	Zemp et al. (2019)

It is apparent that glacier mass balance is generally less negative when longer time periods of study are considered (Table 4.1). For example, the 37-year study period presented here has a net geodetic mass balance of 0.3 m w.e yr^{-1} for ablation areas, which is less negative than the mass balance calculated from studies focussing on shorter and more recent time periods (Table 4.1). The least negative rate in Table 4.1 is that reported by Noël et al. (2017) who report a rate of -0.14 m w.e. yr^{-1} for the 39-year time period 1958 to 1997. Contrastingly, they report -0.44 m w.e. yr^{-1} for the 18-year time period of 1997 to 2015, which is almost as negative as the extrapolation of Huber et al. (2020) and the geodetic calculation of Zemp et al., 2019 for the 10-year time period 2006 to 2016 (Table 4.1).

The results presented here should assist with refinement of global glacier evolution models (Marzeion et al., 2012; Huss et al., 2015; Rounce et al., 2023), which rely on calibration utilising data for baseline time periods before projecting into the future. Greenland's population of PGIC pose problems for numerical models due to data gaps and relatively widespread model failure (e.g. 20 % of total glacier surface area, Table 2 of Marzeion et al., 2012) leading to likely bias, or systematic error and hence relatively high uncertainty in model results across this region (Marzeion et al., 2020). Moreover, PGIC are associated with larger uncertainties when considered in numerical models due to their higher sensitivity but poorly constrained responses to various factors such as their terminus environment and surface debris cover, addressed principally by this work's consideration of various glacier types in isolation and combined regionally around Greenland's entire periphery.

4.5 Conclusions

This work presents the first Greenland-wide surface elevation changes of PGICs at 30 m resolution between the late 1970s and 2015. All 6149 glaciers larger than 1 km^2 and not connected to the ice sheet are considered, accounting for > 96 % of Greenland's PGIC ablation area, and 99 % of all PGIC area when considering accumulation areas. By restricting the analysis to glacier ablation areas, the research maintained high accuracy in the measured and produced elevation change datasets. However, this approach necessitated the assumption that there was no mass loss above the estimated equilibrium lines, making the estimates a conservative minimum.

Overall, this work finds that Greenland PGICs have experienced annual mass loss in their ablation areas of -8.5 ± 1.53 Gt yr^{-1}, equating to -0.0003 Gt yr^{-1} per km^2 for *T0*; covering the late 1970s to 2015. Extrapolating this value to permit glacier-wide statistics produces an estimate of mass balance for *T0* of -0.10 ± 0.02 m w.e. yr^{-1}. These findings support a growing body of research identifying an acceleration in mass loss from Greenland PGICs during the late 20th/early 21st century. However, these Greenland-wide values hide considerable spatio-temporal heterogeneity measured here. Quantified glacier mass balance rates are reported to be most negative in southern Greenland and becoming less negative towards the north up to 2015. Some glaciers in some regions are found to in fact experienced positive mass

balances (Figure 4.7). Glaciers in west Greenland have had significantly more negative mass balances since the late 1970s than those in the east. Furthermore, glaciers in east Greenland have had a decelerating mass loss since the year 2000 whereas the mass loss of western glaciers has continued to accelerate since the 1980s. Therefore, the Greenland-wide signal of mass loss up to 2015 was apparently dominated by glaciers in the east (Figure 4.7). This work also finds that lake-terminating glaciers and those with debris cover have experienced the most negative mass balance rates in most regions compared to those that are marine- or land-terminating and to those with clean ice surfaces (Figures 4.5 and 4.6). These controls of glacier type on mass loss underpin and suggest that glacier evolution models should consider incorporating terminus environment and surface characteristics to refine projections of mass loss and sea level contributions from Greenland and throughout the Arctic.

The quantification of the spatially heterogeneous rates of mass loss across Greenland reported here should be useful for understanding climate change across the region, given that PGICs are relatively sensitive to climate change (in comparison to the GrIS), and given that weather station records and river runoff records across Greenland are extremely sparsely distributed and do not tend to extend back more than a few decades at most. Glacier mass loss and consequent meltwater production has implications for proglacial fluvial dynamics, hydrological and sediment connectivity and hence for freshwater, sediment/mineral and nutrient export to the oceans. On a local scale, these factors affect indigenous communities' sustainability, economically-important salmon behaviour, and economically-important hydropower and sand mining, for example. More widely, meltwater from Greenland PGICs will produce freshening of Arctic oceans that could have complex implications for coastal biodiversity, and they will remain an important contribution to global sea level rise. The spatial distribution of Greenlandic PGIC's mass loss, and the temporal accelerations and decelerations, therefore inform on the dynamics of proglacial systems, which may be more sensitive to rapid transient change dominated by exposed glacier sediments and fluctuating discharge. When paired with the growing occurrence of proglacial lakes, effective sediment and nutrient sinks, rapid glacier melt has serious connotations for sediment and nutrient connectivity through Greenland's proglacial systems and into coastal waters.

4.6 Chapter 4 References

Atherton, D. (1963). Comparisons of Ogive Systems Under Various Regimes. Journal of Glaciology, 4(35). https://doi.org/10.3189/s0022143000028082

Azzoni, R.S., Fugazza, D., Zerboni, A., Senese, A., D'Agata, C., Maragno, D., Carzaniga, A., Cernuschi, M. and Diolaiuti, G.A., 2018. Evaluating high-resolution remote sensing data for reconstructing the recent evolution of supra glacial debris: A study in the Central Alps (Stelvio Park, Italy). *Progress in Physical Geography: Earth and Environment*, 42(1), pp.3-23.

Beyer, R.A., Alexandrov, O. and McMichael, S. 2018. The Ames Stereo Pipeline: NASA's open source software for deriving and processing terrain data. Earth and Space Science. 5(9), pp.537–548.

Bhatia, M.P., Kujawinski, E.B., Das, S.B., Breier, C.F., Henderson, P.B. and Charette, M.A., 2013. Greenland meltwater as a significant and potentially bioavailable source of iron to the ocean. *Nature Geoscience*, 6(4), pp.274-278.

Bintanja, R. and Selten, F.M., 2014. Future increases in Arctic precipitation linked to local evaporation and sea-ice retreat. *Nature*, 509(7501), pp.479-482.

Bjørk, A. A., Aagaard, S., Lütt, A., Khan, S. A., Box, J. E., Kjeldsen, K. K., Larsen, N. K., Korsgaard, N. J., Cappelen, J., Colgan, W. T., Machguth, H., Andresen, C. S., Peings, Y., & Kjær, K. H. (2018). Changes in Greenland's peripheral glaciers linked to the North Atlantic Oscillation. Nature Climate Change, 8(1), 48–52. https://doi.org/10.1038/s41558-017-0029-1

Bjørk, A.A., Kjær, K.H., Korsgaard, N.J., Khan, S.A., Kjeldsen, K.K., Andresen, C.S., Box, J.E., Larsen, N.K. and Fun-der, S. 2012. An aerial view of 80 years of climate-related glacier fluctuations in southeast Green-land. Nature Geo-science. 5(6), pp.427–432.

Bøggild, C.E., Brandt, R.E., Brown, K.J. and Warren, S.G. 2010. The ablation zone in northeast Greenland: ice types, albedos and impurities. Journal of Glaciology. 56(195), pp.101–113.

Bolch, T., Sorensen, L. S., Simonsen, S. B., Molg, N., Machguth, H., Rastner, P., & Paul, F. (2013). Mass loss of Greenland's glaciers and ice caps 2003-2008 revealed from ICESat laser altimetry data. Geophysical Research Letters, 40(5), 875–881. https://doi.org/10.1002/grl.50270

Bollen, K.E., Enderlin, E.M. and Muhlheim, R. 2023. Dynamic mass loss from Greenland's marine-terminating peripheral glaciers (1985–2018). Journal of Glaciology. 69(273), pp.153–163.

Böning, C. W., Behrens, E., Biastoch, A., Getzlaff, K., & Bamber, J. L. %J N. G. (2016). Emerging impact of Greenland meltwater on deepwater formation in the North Atlantic Ocean. 9(7), 523.

Box, J.E. 2002. Survey of Greenland instrumental temperature records: 1873-2001. International Journal of Climatology. 22(15).

Brook, M.S., Hagg, W. and Winkler, S., 2013. Debris cover and surface melt at a temperate maritime alpine glacier: Franz Josef Glacier, New Zealand. *New Zealand Journal of Geology and Geophysics*, 56(1), pp.27-38.

Burpee, B.T., Anderson, D. and Saros, J.E., 2018. Assessing ecological effects of glacial meltwater on lakes fed by the Greenland Ice Sheet: The role of nutrient subsidies and turbidity. Arctic, antarctic, and alpine research, 50(1), p.S100019.

Candela, S.G., Howat, I., Noh, M.-J., Porter, C.C. and Morin, P.J. 2017. ArcticDEM validation and accuracy assessment In: AGU fall meeting abstracts, pp.C51A-0951.

Carrivick, J.L., Boston, C.M., King, O., James, W.H., Quincey, D.J., Smith, M.W., Grimes, M. and Evans, J., 2019. Accelerated volume loss in glacier ablation zones of NE Greenland, Little Ice Age to present. *Geophysical Research Letters*, 46(3), pp.1476-1484.

Carrivick, J. L., Boston, C. M., Sutherland, J. L., Pearce, D., Armstrong, H., Bjørk, A., Kjeldsen, K. K., Abermann, J., Oien, R. P., & Grimes, M. (2023). Mass loss of glaciers and ice caps across Greenland since the Little Ice Age. Geophysical Research Letters, 50(10), e2023GL103950.

Carrivick, J. L., How, P., Lea, J. M., Sutherland, J. L., Grimes, M., Tweed, F. S., Cornford, S., Quincey, D. J., & Mallalieu, J. (2022). Ice-marginal proglacial lakes across Greenland: Present status and a possible future. Geophysical Research Letters, 49(12), e2022GL099276.

Carrivick, J.L., Boston, C.M., King, O., James, W.H.M., Quincey, D.J., Smith, M.W., Grimes, M. and Evans, J. 2019. Accelerated Volume Loss in Glacier Ablation Zones of NE Greenland, Little Ice Age to Present. Geophysical Research Letters. 46(3), 1476-1484.

Carrivick, J.L., Boston, C.M., Sutherland, J.L., Pearce, D., Armstrong, H., Bjørk, A., Kjeldsen, K.K., Abermann, J., Oien, R.P. and Grimes, M. 2023. Mass loss of glaciers and ice caps across Greenland since the Little Ice Age. Geophysical Research Letters. 50(10), e2023GL103950.

Carrivick, J.L., How, P., Lea, J.M., Sutherland, J.L., Grimes, M., Tweed, F.S., Cornford, S., Quincey, D.J. and Mallalieu, J. 2022. Ice-marginal proglacial lakes across Greenland: Present status and a possible future. Geophysical Research Letters. 49(12), e2022GL099276.

Carrivick, J.L., James, W.H., Grimes, M., Sutherland, J.L. and Lorrey, A.M., 2020. Ice thickness and volume changes across the Southern Alps, New Zealand, from the little ice age to present. Scientific Reports, 10(1), p.13392.

Carrivick, J.L., Sutherland, J.L., Huss, M., Purdie, H., Stringer, C.D., Grimes, M., James, W.H. and Lorrey, A.M., 2022. Coincident evolution of glaciers and ice-marginal proglacial lakes across the Southern Alps, New Zealand: Past, present and future. Global and Planetary Change, 211, p.103792.

Carrivick, J.L., Tweed, F.S., Sutherland, J.L. and Mallalieu, J., 2020b. Toward numerical modelling of interactions between ice-marginal proglacial lakes and glaciers. Frontiers in Earth Science, p.500.

Chylek, P., Folland, C.K., Lesins, G., Dubey, M.K. and Wang, M.Y. 2009. Arctic air temperature change amplification and the Atlantic Multidecadal Oscillation. Geophysical Research Letters. 36(14). L14801

Clarke, G. K. C., Schmok, J. P., Ommanney, C. S. L., & Collins, S. G. (1986). Characteristics of surge-type glaciers. Journal of Geophysical Research: Solid Earth, 91(B7). https://doi.org/10.1029/jb091ib07p07165

Colgan, W., Abdalati, W., Citterio, M., Csatho, B., Fettweis, X., Luthcke, S., Moholdt, G., Simonsen, S.B. and Stober, M., 2015. Hybrid glacier Inventory, Gravimetry and Altimetry (HIGA) mass balance product for Greenland and the Canadian Arctic. Remote Sensing of Environment, 168, pp.24-39.

Dowdeswell, J. A., Hodgkins, R., Nuttall, A. -M, Hagen, J. O., & Hamilton, G. S. (1995). Mass balance change as a control on the frequency and occurrence of glacier surges in Svalbard, Norwegian High Arctic. Geophysical Research Letters, 22(21). https://doi.org/10.1029/95GL02821

Echelmeyer, K., Clarke, T. S., & Harrison, W. D. (1991). Surficial glaciology of Jakobshavns Isbrae, West Greenland: part I. Surface morphology. Journal of Glaciology, 37(127). https://doi.org/10.1017/S0022143000005803

Fettweis, X., Franco, B., Tedesco, M., van Angelen, J.H., Lenaerts, J.T.M., van den Broeke, M.R. and Gallee, H. 2013. Estimating the Greenland ice sheet surface mass balance contribution to future sea level rise using the re-gional atmospheric climate model MAR. Cryosphere. 7(2), pp.469–489.

Fettweis, X., Hanna, E., Gallee, H., Huybrechts, P. and Erpicum, M. 2008. Estimation of the Greenland ice sheet surface mass balance for the 20th and 21st centuries. Cryosphere. 2(2), pp.117–129.

Fleischer, F., Otto, J. C., Junker, R. R., & Hölbling, D. (2021). Evolution of debris cover on glaciers of the Eastern Alps, Austria, between 1996 and 2015. Earth Surface Processes and Landforms, 46(9). https://doi.org/10.1002/esp.5065

Gardner, A.S., Moholdt, G., Cogley, J.G., Wouters, B., Arendt, A.A., Wahr, J., Berthier, E., Hock, R., Pfeffer, W.T., Kaser, G., Ligtenberg, S.R.M., Bolch, T., Sharp, M.J., Hagen, J.O., van den Broeke, M.R. and Paul, F. 2013. A Reconciled Estimate of Glacier Contributions to Sea Level Rise: 2003 to 2009. Science. 340(6134), pp.852–857.

Goelzer, H., Huybrechts, P., Furst, J.J., Nick, F.M., Andersen, M.L., Edwards, T.L., Fettweis, X., Payne, A.J. and Shannon, S. 2013. Sensitivity of Greenland ice sheet projections to model formulations. Journal of Glaci-ology. 59(216), pp.733–749.

Goetz, J., & Brenning, A. (2019). Quantifying Uncertainties in Snow Depth Mapping From Structure From Motion Photogrammetry in an Alpine Area. Water Resources Research, 55(9). https://doi.org/10.1029/2019WR025251

Hagg, W., Brook, M., Mayer, C., & Winkler, S. (2014). A short-term field experiment on sub-debris melt at the highly maritime Franz Josef Glacier, Southern Alps, New Zealand. Journal of Hydrology, 53(2).

Hanna, E., Cappelen, J., Fettweis, X., Mernild, S.H., Mote, T.L., Mottram, R., Steffen, K., Ballinger, T.J. and Hall, R.J., 2021. Greenland surface air temperature changes from 1981 to 2019 and implications for ice-sheet melt and mass-balance change. International Journal of Climatology, 41, pp.E1336-E1352.

Harrison, S., Jones, D., Anderson, K., Shannon, S., & Betts, R. A. (2021). Is ice in the Himalayas more resilient to climate change than we thought? Geografiska Annaler, Series A: Physical Geography, 103(1). https://doi.org/10.1080/04353676.2021.1888202

Henriksen, N., Higgins, A.K., Kalsbeek, F. and Pulvertaft, T.C.R., 2009. Greenland from Archaean to Quaternary. Descriptive text to the 1995 Geological map of Greenland, 1: 2 500 000. GEUS Bulletin, 18, pp.1-126. https://doi.org/10.34194/geusb.v18.4993

Herreid, S., & Pellicciotti, F. (2020). The state of rock debris covering Earth's glaciers. Nature Geoscience, 13(9), pp. 621–627.

Holland, M.M. and Bitz, C.M. 2003. Polar amplification of climate change in coupled models. Climate Dynam-ics. 21(3–4), pp.221–232.

Hopwood, M.J., Carroll, D., Dunse, T., Hodson, A., Holding, J.M., Iriarte, J.L., Ribeiro, S., Achterberg, E.P., Can-toni, C. and Carlson, D.F. 2020. How does glacier discharge affect marine biogeochemistry and primary production in the Arctic? The Cryosphere. 14(4), pp.1347–1383.

Howat, I. M., Negrete, A., & Smith, B. E. (2014). The Greenland Ice Mapping Project (GIMP) land classification and surface elevation data sets. Cryosphere, 8(4), 1509–1518. https://doi.org/10.5194/tc-8-1509-2014

Howat, I., Negrete, A. and Smith, B. (2015). MEaSUREs Greenland ice mapping project (GIMP) digital elevation model, version 1. Cryosphere. 8, pp.1509–1518.

Howat, I.M., Negrete, A. and Smith, B.E. (2014). The Greenland Ice Mapping Project (GIMP) land classification and surface elevation data sets. Cryosphere. 8(4), pp.1509–1518.

Huber, J., McNabb, R. and Zemp, M. (2020). Elevation changes of west-central Greenland glaciers from 1985 to 2012 from remote sensing. Frontiers in Earth Science. 8, p.35.

Hugonnet, R., McNabb, R., Berthier, E., Menounos, B., Nuth, C., Girod, L., Farinotti, D., Huss, M., Dussaillant, I., Brun, F., & Kääb, A. (2021). Accelerated global glacier mass loss in the early twenty-first century. Nature, 592(7856). https://doi.org/10.1038/s41586-021-03436-z

Huss, M. (2013). Density assumptions for converting geodetic glacier volume change to mass change. The Cryosphere. 7(3), pp.877–887.

Huss, M. and Hock, R., (2015). A new model for global glacier change and sea-level rise. Frontiers in Earth Science, 3, p.54.

Khan, S.A., Colgan, W., Neumann, T.A., Van Den Broeke, M.R., Brunt, K.M., Noël, B., Bamber, J.L., Hassan, J. and Bjørk, A.A., (2022). Accelerating ice loss from peripheral glaciers in North Greenland. Geophysical Research Letters, 49(12), p.e2022GL098915.

King, O., Bhattacharya, A., Bhambri, R. and Bolch, T., (2019). Glacial lakes exacerbate Himalayan glacier mass loss. Scientific Reports, 9(1), p.18145.

King, O., Dehecq, A., Quincey, D. and Carrivick, J., (2018). Contrasting geometric and dynamic evolution of lake and land-terminating glaciers in the central Himalaya. Global and Planetary Change, 167, pp.46-60.

Kirkbride, M. P., & Warren, C. R. (1999). Tasman Glacier, New Zealand: 20th-century thinning and predicted calving retreat. Global and Planetary Change, 22(1–4). https://doi.org/10.1016/S0921-8181(99)00021-1

Knox, J.C. (1993). Large Increases in Flood Magnitude in Response to Modest Changes in Climate. Nature. 361(6411), pp.430–432.

Korona, J., Berthier, E., Bernard, M., Rémy, F., & Thouvenot, E. (2009). SPIRIT. SPOT 5 stereoscopic survey of Polar Ice: Reference Images and Topographies during the fourth International Polar Year (2007-2009). ISPRS Journal of Photogrammetry and Remote Sensing, 64(2). https://doi.org/10.1016/j.isprsjprs.2008.10.005

Korsgaard, N.J., Nuth, C., Khan, S.A., Kjeldsen, K.K., Bjørk, A.A., Schomacker, A. and Kjær, K.H., 2016. Digital elevation model and orthophotographs of Greenland based on aerial photographs from 1978–1987. Scientific Data, 3(1), pp.1-15.

Krisch, S., Browning, T.J., Graeve, M., Ludwichowski, K.U., Lodeiro, P., Hopwood, M.J., Roig, S., Yong, J.C., Kanzow, T. and Achterberg, E.P. (2020). The influence of Arctic Fe and Atlantic fixed N on summertime primary production in Fram Strait, North Greenland Sea. Scientific Reports. 10(1).

Leclercq, P. W., Weidick, A., Paul, F., Bolch, T., Citterio, M., & Oerlemans, J. (2012). Brief communication “Historical glacier length changes in West Greenland.” Cryosphere, 6(6), 1339–1343. https://doi.org/10.5194/tc-6-1339-2012

Lee, E., Carrivick, J. L., Quincey, D. J., Cook, S. J., James, W. H. M., & Brown, L. E. (2021). Accelerated mass loss of Himalayan glaciers since the Little Ice Age. Scientific Reports, 11(1), 24284.

Lovell, H., Carrivick, J.L., King, O., Yde, J.C., Boston, C.M., Małecki, J. and Sutherland, J.L. (2023). Surge-type glaciers in Kalaallit Nunaat (Greenland): distribution, temporal patterns and climatic controls. Journal of Glaciology.

Machguth, H., Rastner, P., Bolch, T., Mölg, N., Sørensen, L. S., Aðalgeirsdottir, G., van Angelen, J. H., van den Broeke, M. R., & Fettweis, X. (2013). The future sea-level rise contribution of Greenland’s glaciers and ice caps. Environmental Research Letters, 8(2). https://doi.org/10.1088/1748-9326/8/2/025005

Machguth, H., Thomsen, H.H., Weidick, A., Ahlstrøm, A.P., Abermann, J., Andersen, M.L., Andersen, S.B., Bjørk, A.A., Box, J.E. and Braithwaite, R.J. (2016). Greenland surface mass-balance observations from the ice-sheet ablation area and local glaciers. Journal of Glaciology. 62(235), pp.861–887.

Magnússon, E., Muñoz-Cobo Belart, J., Pálsson, F., Ágústsson, H. and Crochet, P. (2016). Geodetic mass balance record with rigorous uncertainty estimates deduced from aerial photographs and lidar data–Case study from Drangajökull ice cap, NW Iceland. The Cryosphere. 10(1), pp.159–177.

Mallalieu, J., Carrivick, J.L., Quincey, D.J. and Raby, C.L., (2021). Ice-marginal lakes associated with enhanced re-cession of the Greenland Ice Sheet. Global and Planetary Change, 202, p.103503.

Mancini, D., & Lane, S. N. (2020). Changes in sediment connectivity following glacial debuttressing in an Alpine valley system. Geomorphology, 352. https://doi.org/10.1016/j.geomorph.2019.106987

Marzeion, B., Hock, R., Anderson, B., Bliss, A., Champollion, N., Fujita, K., Huss, M., Immerzeel, W.W., Kraaijen-brink, P., Malles, J.H. and Maussion, F., (2020). Partitioning the uncertainty of ensemble projections of global glacier mass change. Earth's Future, 8(7), p.e2019EF001470.

Marzeion, B., Jarosch, A.H. and Hofer, M., (2012). Past and future sea-level change from the surface mass balance of glaciers. The Cryosphere, 6(6), pp.1295-1322.

Mayewski, P.A., Sneed, S.B., Birkel, S.D., Kurbatov, A. V and Maasch, K.A. (2014). Holocene warming marked by abrupt onset of longer summers and reduced storm frequency around Greenland. Journal of Quaternary Science. 29(1), pp.99–104.

McMillan, M., Leeson, A., Shepherd, A., Briggs, K., Armitage, T.W.K., Hogg, A., Kuipers Munneke, P., Van Den Broeke, M., Noël, B. and van de Berg, W.J. (2016). A high-resolution record of Greenland mass balance. Geophysical Research Letters. 43(13), pp.7002–7010.

McNabb, R., Nuth, C., Kääb, A. and Girod, L. (2017). The effects of void handling on geodetic mass balances In: EGU General Assembly Conference Abstracts., p.7570.

McNabb, R., Nuth, C., Kääb, A. and Girod, L. (2019). Sensitivity of glacier volume change estimation to DEM void interpolation. The Cryosphere. 13(3), pp.895–910.

Micheletti, N., & Lane, S. N. (2016). Water yield and sediment export in small, partially glaciated Alpine watersheds in a warming climate. Water Resources Research, 52(6). https://doi.org/10.1002/2016WR018774

Morin, P., Porter, C., Cloutier, M., Howat, I., Noh, M.-J., Willis, M., Bates, B., Willamson, C., & Peterman, K. (2016). ArcticDEM; A Publically Available, High Resolution Elevation Model of the Arctic. Geophysical Research Abstracts, 18.

Nakawo, M., & Rana, B. (1999). Estimate of ablation rate of glacier ice under a supraglacial debris layer. Geografiska Annaler, Series A: Physical Geography, 81(4). https://doi.org/10.1111/j.0435-3676.1999.00097.x

Noël, B., Van De Berg, W. J., Lhermitte, S., Wouters, B., Machguth, H., Howat, I., Citterio, M., Moholdt, G., Lenaerts, J. T. M., & Van Den Broeke, M. R. (2017). A tipping point in refreezing accelerates mass loss of Greenland's glaciers and ice caps. Nature Communications, 8. https://doi.org/10.1038/ncomms14730

Noh, M. J., & Howat, I. M. (2017). The Surface Extraction from TIN based Search-space Minimization (SETSM) algorithm. ISPRS Journal of Photogrammetry and Remote Sensing, 129. https://doi.org/10.1016/j.isprsjprs.2017.04.019

Nuth, C. and Kääb, A. (2011). Co-registration and bias corrections of satellite elevation data sets for quantifying glacier thickness change. The Cryosphere. 5(1), pp.271–290.

Pellicciotti, F., Stephan, C., Miles, E., Herreid, S., Immerzeel, W. W., & Bolch, T. (2015). Mass-balance changes of the debris-covered glaciers in the Langtang Himal, Nepal, from 1974 to 1999. Journal of Glaciology, 61(226). https://doi.org/10.3189/2015JoG13J237

Pellitero, R., Rea, B.R., Spagnolo, M., Bakke, J., Hughes, P., Ivy-Ochs, S., Lukas, S. and Ribolini, A. (2015). A GIS tool for automatic calculation of glacier equilibrium-line altitudes. Computers & Geosciences. 82, pp.55–62.

Pfeffer, W.T., Arendt, A.A., Bliss, A., Bolch, T., Cogley, J.G., Gardner, A.S., Hagen, J.O., Hock, R., Kaser, G., Kienholz, C., Miles, E.S., Moholdt, G., Molg, N., Paul, F., Radic, V., Rastner, P., Raup, B.H., Rich, J., Sharp, M.J., Ande-assen, L.M., Bajracharya, S., Barrand, N.E., Beedle, M.J., Berthier, E., Bhambri, R., Brown, I., Burgess, D.O., Burgess, E.W., Cawkwell, F., Chinn, T., Copland, L., Cullen, N.J., Davies, B., De Angelis, H., Fountain, A.G., Frey, H., Giffen, B.A., Glasser, N.F., Gurney, S.D., Hagg, W., Hall, D.K., Haritashya, U.K., Hartmann, G., Herreid, S., Howat, I., Jiskoot, H., Khromova, T.E., Klein, A., Kohler, J., Konig, M., Kriegel, D., Kutuzov, S., Lavrentiev, I., Le Bris, R., Li, X., Manley, W.F., Mayer, C., Menounos, B., Mercer, A., Mool, P., Negrete, A., Nosenko, G., Nuth, C., Osmonov, A., Pettersson, R., Racoviteanu, A., Ranzi, R., Sarikaya, M.A., Schneider, C., Sigurdsson, O., Sirguey, P., Stokes, C.R., Wheate, R., Wolken, G.J., Wu, L.Z., Wyatt, F.R. and Consortium, R. 2014. The Randolph Glacier Inventory: a globally complete inventory of glaciers. Journal of Glaciology. 60(221), pp.537–552.

Pithan, F., & Mauritsen, T. (2014). Arctic amplification dominated by temperature feedbacks in contemporary climate models. Nature Geoscience, 7(3), 181–184. https://doi.org/10.1038/ngeo2071

Pittock, A.B. (2012). Ten reasons why climate change may be more severe than projected In: Sudden and Disrup-tive Climate Change. Routledge, pp.26–42.

Pope, A., & Rees, W. G. (2014). Impact of spatial, spectral, and radiometric properties of multispectral imagers on glacier surface classification. Remote Sensing of Environment, 141. https://doi.org/10.1016/j.rse.2013.08.028

Pratap, B., Dobhal, D. P., Mehta, M., & Bhambri, R. (2015). Influence of debris cover and altitude on glacier surface melting: A case study on Dokriani Glacier, central Himalaya, India. Annals of Glaciology, 56(70). https://doi.org/10.3189/2015AoG70A971

Preece, J.R., Mote, T.L., Cohen, J., Wachowicz, L.J., Knox, J.A., Tedesco, M. and Kooperman, G.J. (2023). Summer atmospheric circulation over Greenland in response to Arctic amplification and diminished spring snow cover. Nature Communications, 14(1), p.3759.

Pronk, J.B., Bolch, T., King, O., Wouters, B. and Benn, D.I., (2021). Contrasting surface velocities between lake-and land-terminating glaciers in the Himalayan region. The Cryosphere, 15(12), pp.5577-5599.

Raper, S.C. and Braithwaite, R.J. (2006). Low sea level rise projections from mountain glaciers and icecaps un-der global warming. Nature. 439(7074), pp.311–313.

Rastner, P., Bolch, T., Molg, N., Machguth, H., Le Bris, R. and Paul, F. (2012). The first complete inventory of the local glaciers and ice caps on Greenland. Cryosphere. 6(6), pp.1483–1495.

Rea, B.R. (2009). Defining modern day Area-Altitude Balance Ratios (AABRs) and their use in glacier-climate re-constructions. Quaternary Science Reviews. 28(3–4), pp.237–248.

Reznichenko, N., Davies, T., Shulmeister, J., & McSaveney, M. (2010). Effects of debris on ice-surface melting rates: An experimental study. Journal of Glaciology, 56(197). https://doi.org/10.3189/002214310792447725

RGI Consortium. (2017). Randolph Glacier Inventory – A Dataset of Global Glacier Outlines: Version 6.0: Technical Report, Global Land Ice Measurements from Space. Colorado, USA.

Rignot, E., Box, J.E., Burgess, E. and Hanna, E. (2008). Mass balance of the Greenland ice sheet from 1958 to 2007. Geophysical Research Letters. 35(20).

Rignot, E., Fenty, I., Xu, Y., Cai, C. and Kemp, C. (2015). Undercutting of marine-terminating glaciers in West Greenland. Geophysical Research Letters. 42(14), pp.5909–5917.

Rolstad, C., Haug, T., & Denby, B. (2009). Spatially integrated geodetic glacier mass balance and its uncertainty based on geostatistical analysis: Application to the western Svartisen ice cap, Norway. Journal of Glaciology, 55(192). https://doi.org/10.3189/002214309789470950

Rounce, D. R., Khurana, T., Short, M. B., Hock, R., Shean, D. E., & Brinkerhoff, D. J. (2020). Quantifying parameter uncertainty in a large-scale glacier evolution model using Bayesian inference: Application to High Mountain Asia. Journal of Glaciology, 66(256). https://doi.org/10.1017/jog.2019.91

Rounce, D.R., Hock, R., Maussion, F., Hugonnet, R., Kochtitzky, W., Huss, M., Berthier, E., Brinkerhoff, D., Com-pagno, L., Copland, L. and Farinotti, D., (2023). Global glacier change in the 21st century: Every increase in tempera-ture matters. Science, 379(6627), pp.78-83.

Russo, S., Dosio, A., Graversen, R.G., Sillmann, J., Carrao, H., Dunbar, M.B., Singleton, A., Montagna, P., Bar-bola, P. and Vogt, J. V (2014). Magnitude of extreme heat waves in present climate and their projection in a warming world. Journal of Geophysical Research-Atmospheres. 119(22), pp.12500–12512.

Ryan, J.C., Hubbard, A., Stibal, M., Irvine-Fynn, T.D., Cook, J., Smith, L.C., Cameron, K. and Box, J. (2018). Dark zone of the Greenland Ice Sheet

controlled by distributed biologically-active impurities. Nature communications. 9(1), p.1065.

Scambos, T. A., & Fahnestock, M. A. (1998). Improving digital elevation models over ice sheets using AVHRR-based photoclinometry. Journal of Glaciology, 44(146). https://doi.org/10.1017/S0022143000002392

Scambos, T. A., & Haran, T. (2002). An image-enhanced DEM of the Greenland ice sheet. Annals of Glaciology, 34. https://doi.org/10.3189/172756402781817969

Scherler, D., Wulf, H. and Gorelick, N. (2018). Global assessment of supraglacial debris-cover extents. Geophysical Research Letters. 45(21), pp.11–798.

Schutz, B. E., Zwally, H. J., Shuman, C. A., Hancock, D., & DiMarzio, J. P. (2005). Overview of the ICESat mission. In Geophysical Research Letters (Vol. 32, Issue 21). https://doi.org/10.1029/2005GL024009

Schuur, E. A. G., Vogel, J. G., Crummer, K. G., Lee, H., Sickman, J. O., & Osterkamp, T. E. (2009). The effect of permafrost thaw on old carbon release and net carbon exchange from tundra. Nature, 459(7246). https://doi.org/10.1038/nature08031

Screen, J.A. and Simmonds, I. (2010a). Increasing fall-winter energy loss from the Arctic Ocean and its role in Arctic temperature amplification. Geophysical Research Letters. 37.

Screen, J.A. and Simmonds, I. (2010b). The central role of diminishing sea ice in recent Arctic temperature amplification. Nature. 464(7293), pp.1334–1337.

Seehaus, T., Morgenshtern, V.I., Hübner, F., Bänsch, E. and Braun, M.H. (2020). Novel techniques for void filling in glacier elevation change data sets. Remote Sensing. 12(23), p.3917.

Seguinot, J., Funk, M., Bauder, A., Wyder, T., Senn, C., & Sugiyama, S. (2020). Englacial Warming Indicates Deep Crevassing in Bowdoin Glacier, Greenland. Frontiers in Earth Science, 8. https://doi.org/10.3389/feart.2020.00065

Serreze, M.C. and Barry, R.G. (2011). Processes and impacts of Arctic amplification: A research synthesis. Global and Planetary Change. 77(1–2), pp.85–96.

Sevestre, H., & Benn, D. I. (2015). Climatic and geometric controls on the global distribution of surge-type glaciers: Implications for a unifying model of surging. Journal of Glaciology, 61(228). https://doi.org/10.3189/2015JoG14J136

Shean, D. E., Alexandrov, O., Moratto, Z. M., Smith, B. E., Joughin, I. R., Porter, C., & Morin, P. (2016). An automated, open-source pipeline for mass production of digital elevation models (DEMs) from very-high-resolution commercial stereo satellite imagery. ISPRS Journal of Photogrammetry and Remote Sensing, 116, 101–117. https://doi.org/10.1016/j.isprsjprs.2016.03.012

Shean, D. E., Bhushan, S., Montesano, P., Rounce, D. R., Arendt, A., & Osmanoglu, B. (2020). A Systematic, Regional Assessment of High Mountain Asia Glacier Mass Balance. Frontiers in Earth Science, 7. https://doi.org/10.3389/feart.2019.00363

Shepherd, A., Ivins, E., Rignot, E., Smith, B., van den Broeke, M., Velicogna, I., Whitehouse, P., Briggs, K., Joughin, I., Krinner, G., Nowicki, S., Payne, T., Scambos, T., Schlegel, N., A, G., Agosta, C., Ahlstrøm, A., Babonis, G., Barletta, V.R., Bjørk, A.A., Blazquez, A., Bonin, J., Colgan, W., Csatho, B., Cullather, R., Eng-dahl, M.E., Felikson, D., Fettweis, X., Forsberg, R., Hogg, A.E., Gallee, H., Gardner, A., Gilbert, L., Gour-melen, N., Groh, A., Gunter, B., Hanna, E., Harig, C., Helm, V., Horvath, A., Horwath, M., Khan, S., Kjeld-sen, K.K., Konrad, H., Langen, P.L., Lecavalier, B., Loomis, B., Luthcke, S., McMillan, M., Melini, D., Mernild, S., Mohajerani, Y., Moore, P., Mottram, R., Mouginot, J., Moyano, G., Muir, A., Nagler, T., Nield, G., Nilsson, J., Noël, B., Otosaka, I., Pattle, M.E., Peltier, W.R., Pie, N., Riet-broek, R., Rott, H., Sandberg Sørensen, L., Sasgen, I., Save, H., Scheuchl, B., Schrama, E., Schröder, L., Seo, K.W., Si-monsen, S.B., Slater, T., Spada, G., Sutterley, T., Talpe, M., Tarasov, L., van de Berg, W.J., van der Wal, W., van Wessem, M., Vishwakarma, B.D., Wiese, D., Wilton, D., Wagner, T., Wouters, B. and Wuite, J. (2020). Mass balance of the Greenland Ice Sheet from 1992 to 2018. Nature. 579(7798).

Shi, W., Wang, B. and Tian, Y. (2014). Accuracy analysis of digital elevation model relating to spatial resolution and terrain slope by bilinear interpolation. Mathematical Geosciences. 46, pp.445–481.

Shiggins, C.J., Lea, J.M. and Brough, S. (2023). Automated ArcticDEM iceberg detection tool: insights into area and volume distributions, and their potential application to satellite imagery and modelling of glacier–iceberg–ocean systems. The Cryosphere. 17(1), pp.15–32.

Smith, S.L., Holland, D.A. and Longley, P.A. (2004). The importance of understanding error in lidar digital eleva-tion models. International Archives of the Photogrammetry, Remote Sensing and Spatial Information Sciences. 35, pp.996–1001.

Sørensen, L.S., Simonsen, S.B., Forsberg, R., Khvorostovsky, K., Meister, R. and Engdahl, M.E. (2018). 25 years of elevation changes of the Greenland Ice Sheet from ERS, Envisat, and CryoSat-2 radar altimetry. Earth and Planetary Science Letters. 495, pp.234–241.

Sutherland, J.L., Carrivick, J.L., Gandy, N., Shulmeister, J., Quincey, D.J. and Cornford, S.L., (2020). Proglacial lakes control glacier geometry and behavior during recession. Geophysical Research Letters, 47(19), p.e2020GL088865.

Tachikawa, T., Kaku, M., Iwasaki, A., Gesch, D., Oimoen, M., Zhang, Z., Danielson, J., Krieger, T., Curtis, B., Haase, J., Abrams, M., Crippen, R., & Carabajal, C. (2011). ASTER global digital elevation model version 2 – summary of validation results. Archive Center and the Joint Japan-US ASTER Science Team.

Takeuchi, N., Sakaki, R., Uetake, J., Nagatsuka, N., Shimada, R., Niwano, M. and Aoki, T. (2018). Temporal variations of cryoconite holes and cryoconite

coverage on the ablation ice surface of Qaanaaq Glacier in northwest Greenland. Annals of Glaciology. 59(77), pp.21–30.

Taylor, P. C., Boeke, R. C., Boisvert, L. N., Feldl, N., Henry, M., Huang, Y., Langen, P. L., Liu, W., Pithan, F., Sejas, S. A., & Tan, I. (2022). Process Drivers, Inter-Model Spread, and the Path Forward: A Review of Amplified Arctic Warming. In Frontiers in Earth Science (Vol. 9). https://doi.org/10.3389/feart.2021.758361

Thomas, R., Frederick, E., Krabill, W., Manizade, S., Martin, C., & Mason, A. (2005). Elevation changes on the Greenland ice sheet from comparison of aircraft and ICESat laser-altimeter data. Annals of Glaciology, 42. https://doi.org/10.3189/172756405781813050

Tommaselli, A. M. G., & Berveglieri, A. (2018). Measuring photogrammetric control targets in low contrast images. Boletim de Ciencias Geodesicas, 24(2). https://doi.org/10.1590/S1982-21702018000200012

Truffer, M., Kääb, A., Harrison, W.D., Osipova, G.B., Nosenko, G.A., Espizua, L., Gilbert, A., Fischer, L., Huggel, C. and Burns, P.A.C. (2021). Glacier surges In: Snow and ice-related hazards, risks, and disasters. Elsevier, pp.417–466.

Van As, D., Andersen, M.L., Petersen, D., Fettweis, X., Van Angelen, J.H., Lenaerts, J.T.M., Van Den Broeke, M.R., Lea, J.M., Bøggild, C.E. and Ahlstrøm, A.P. (2014). Increasing meltwater discharge from the Nuuk region of the Greenland ice sheet and implications for mass balance (1960–2012). Journal of Glaciology. 60(220), pp.314–322.

von Albedyll, L., Machguth, H., Nussbaumer, S.U. and Zemp, M. (2018). Elevation changes of the Holm Land Ice Cap, northeast Greenland, from 1978 to 2012–2015, derived from high-resolution digital elevation models. Arctic, Antarctic, and Alpine Research. 50(1).

Wang, Y., Sugiyama, S. and Bjørk, A.A. (2021). Surface elevation change of glaciers along the coast of Prudhoe land, northwestern Greenland from 1985 to 2018. Journal of Geophysical Research: Earth Surface. 126(11), e2020JF006038.

Xing, Z., Chi, Z., Yang, Y., Chen, S., Huang, H., Cheng, X., & Hui, F. (2020). Accuracy evaluation of four Greenland digital elevation models (Dems) and assessment of river network extraction. Remote Sensing, 12(20), 3429.

Yang, K., Smith, L. C., Chu, V. W., Pitcher, L. H., Gleason, C. J., Rennermalm, A. K., & Li, M. (2016). Fluvial morphometry of supraglacial river networks on the Southwest Greenland ice sheet. GIScience and Remote Sensing. https://doi.org/10.1080/15481603.2016.1162345

Yde, J.C. and Knudsen, N.T. (2005). Observations of debris-rich naled associated with a major glacier surge event, Disko Island, West Greenland. Permafrost and Periglacial Processes. 16(4), pp.319–325.

Zemp, M., Frey, H., Gartner-Roer, I., Nussbaumer, S.U., Hoelzle, M., Paul, F., Haeberli, W., Denzinger, F., Ahlstrom, A.P., Anderson, B., Bajracharya, S., Baroni, C., Braun, L.N., Caceres, B.E., Casassa, G., Cobos, G., Davila, L.R., Granados, H.D., Demuth, M.N., Espizua, L., Fischer, A., Fujita, K., Gadek, B., Ghazanfar, A., Hagen, J.O., Holmlund, P., Karimi, N., Li, Z.Q., Pelto, M.,

Pitte, P., Popovnin, V. V, Portocarrero, C.A., Prinz, R., Sangewar, C. V, Severskiy, I., Sigurosson, O., Soruco, A., Usubaliev, R., Vincent, C. and Correspondents, W.N. (2015). Historically unprecedented glob-al glacier decline in the early 21st century. Jour-nal of Glaciology. 61(228), pp.745-+.

Zemp, M., Huss, M., Thibert, E., Eckert, N., McNabb, R., Huber, J., Barandun, M., Machguth, H., Nussbaumer, S.U. and Gärtner-Roer, I. (2019). Global glacier mass changes and their contributions to sea-level rise from 1961 to 2016. Nature. 568(7752), pp.382–386.

Zemp, M., Huss, M., Thibert, E., Eckert, N., McNabb, R., Huber, J., Barandun, M., Machguth, H., Nussbaumer, S. U., & Gärtner-Roer, I. (2019). Global glacier mass changes and their contributions to sea-level rise from 1961 to 2016. Nature, 568(7752), 382–386.

Zhang, Y., Gu, J., Liu, S., Wang, X., Jiang, Z., Wei, J., & Zheng, Y. (2022). Spatial pattern of the debris-cover effect and its role in the Hindu Kush-Pamir-Karakoram-Himalaya glaciers. Journal of Hydrology, 615. https://doi.org/10.1016/j.jhydrol.2022.128613

Zhang, Y., Liu, S., & Wang, X. (2022). Debris-cover effect in the Tibetan Plateau and surroundings：a review. In Journal of Glaciology and Geocryology (Vol. 44, Issue 3). https://doi.org/10.7522/j.issn.1000-0240.2022.0086

Chapter 5: A Greenland-wide Assessment of Sediment Connectivity

5.1 Introduction and Aim

High mountain and Arctic regions are particularly prone to ongoing climate change, with ramifications and nonlinear landscape responses being widespread yet poorly constrained (e.g. Haeberli et al., 1999; Masson-Delmotte et al., 2012; Knight and Harrison, 2014; Bach et al., 2018; Box et al., 2019). The two preceding chapters of this thesis have specifically identified and measured the manifest landscape responses to late 20th and early 21st-century climate change in Greenland. Chapter 3 quantified widespread sediment redistribution, vegetation expansion, meltwater stream and lake changes, and diminishing ice extent in response to increases in positive degree days over the past ~40 years. Chapter 4 specifically measured trends in glacier volume loss, with PGIC experiencing ubiquitous decreases in mass balance, with regional variability.

A common theme associated with glacier retreat is landscape instability and growing proglacial regions, marked by glacier debuttressing and steep, poorly-consolidated slopes and sediment accumulations. These accumulations and the establishment of vegetation over time and with increasing temperatures, synchronous with underlying permafrost thaw, produce complex yet largely unquantified paraglacial processes and responses which are widespread and have important implications for sediment cascades to coastal waters (Ballantyne, 2002a; Mercier, 2008). Paraglacial processes are characterised by widespread sediment reworking, mass movements during 'extreme' events, and fluvial reworking in bifurcating and anastomosing streams, leading to a transient landscape (Ballantyne, 2002b; Mercier and Etienne, 2008; Lane et al., 2017). These processes are considered temporary, culminating in a stable or equilibrium state, a phase many of Greenland’s lower latitude ice-distal landscapes may be approaching with permafrost degradation in periglacial-dominated environments (Slaymaker, 2009; Daanen et al., 2011; Slaymaker, 2011; Christiansen and Humlum, 2013). Periglacial-dominated landscapes, which are interspersed with and fringe the paraglacial zone, frequently feature established vegetation and are shaped by seasonal freeze-thaw geomorphic processes and landforms that often determine hillslope sediment availability (Knight and Harrison, 2009; Matsuoka, 2010; Christiansen and Humlum, 2013; Johansson et al., 2015).

The extent, composition, and glacial stability within Greenland’s paraglacial zone (considering PGIC to be within the longer-term GrIS proglacial/paraglacial sphere) has

been effectively established within the preceding research chapters of this thesis. However, there are very few studies of the transient landscape response with specific reference to sediment export around Greenland. There is good reason to expect that glacier recession could increase basin-scale sediment connectivity as: sediment becomes less dependent on glacier surface transport; proglacial streams are more able to migrate laterally than subglacial streams and so access sediment for transport, and; glacier debuttressing aids the development of gullies that can dissect moraines and so aid hillslope to proglacial zone connectivity (Carrivick and Heckmann, 2017; Mancini and Lane, 2020). However, Greenlandic proglacial lake formation and expansion is identified within this thesis and in the wider literature, which acts to essentially starve downstream rivers of suspended particulate sediment and nutrients sourced from upstream (Carrivick and Tweed, 2013; Bracken et al., 2015; Fowler et al., 2020; Carrivick et al., 2022). An assessment of potential (structural) and measured (functional) connectivity of sediments from the various sediment-source compartments of Greenland's proglacial catchments (e.g. glaciers, moraines, hillslopes, braidplains, etc) perfectly accompanies the precursor research on these catchment's composition and glacier changes.

The investigation of sediment connectivity in the peripheral regions of Greenland represents a frontier in scientific exploration. It not only addresses the gaps in current research but also holds profound implications for the ecological integrity of coastal ecosystems and the well-being of indigenous communities (Rysgaard et al., 1998; Rysgaard et al., 1999; Hamilton et al., 2000). The interplay of sediment dynamics, nutrient cycling, and ecosystem responses underscores the complexity of this issue and necessitates a rigorous assessment of national connectivity to discern relative hot (and cold) spots for connectivity to Fjords (Oksman et al., 2022). This chapter contributes to the body of knowledge by producing useful connectivity datasets and assessing the relative connectivity of watersheds. The influence of lakes on watersheds' structural connectivity is of paramount concern. No assessments of connectivity exist within Greenland, and existing research is dominated by local-scale assessments (Najafi et al., 2021). These catchment-scale studies, which produce connectivity indices with fine-resolution data, often provide little utility for assessing the relative connectivity of catchments compared to others within a range or region (Heckmann et al., 2018). Conducting a nationally consistent assessment of structural connectivity will allow for a reliable evaluation of the relative connectivity of catchments and the impacts of lakes,

thereby determining potential changes in sediment flux to coastal waters with progressed glacier retreat.

Aim: To produce the first nationally consistent index of connectivity for Greenland and to assess its utility in predicting catchment sediment delivery ratios.

To realise this aim, the objectives were:

i) To produce the finest resolution to date hydrological datasets consistently to define all of Greenland's peripheral watersheds draining to coastal outlets.
ii) To produce a novel landcover-topography weighted, spatially distributed index of connectivity for all of Greenland's periphery, considering lakes passively and as sediment sinks.
iii) To examine the impact of expanding lakes on structural sediment connectivity around Greenland.
iv) To assess the utility of the national-scale index of connectivity in predicting computed watershed scale sediment delivery ratios over the past ~40 years.

In pursuit of these objectives, this chapter explores the spatial patterns of connectivity across Greenland, emphasizing the measurable impact of lake occurrence on structural connectivity within watersheds. By calculating the index of connectivity with and without considering lakes as sinks, the research evaluates the role of expanding lakes on sediment connectivity. Additionally, the chapter investigates the potential of a national structural index of connectivity to serve as a predictor for catchment-scale sediment delivery ratios (SDRs), thereby assessing its utility as a predictive tool for understanding sediment dynamics over the past four decades. This comprehensive approach aims to provide a deeper understanding of the interrelationships between landcover, topography, and hydrological connectivity in Greenland's evolving landscape.

5.2 Methods

5.2.1 Study Site and Context

In Chapter 2 of this thesis the wider study site is already outlined in terms of geographic and climatic setting. All watersheds within Greenland's ice sheet-free peripheral zone are delineated to defined coastal outlets. This chapter is concerned with connectivity in all areas not presently glacierised in Greenland, an area summing to ~350,000 km^2 in total. Though not directly concerned with the glaciers, this chapter is particularly

interested in sediment connectivity in proglacial catchments. The subsequent section details the methodological workflow in detail. The concern with glacier-fed catchments is twofold: i) the importance and passage of sediment and nutrients sourced from glaciers, and ii) the influence of late-Holocene debuttressing and fine sediment availability.

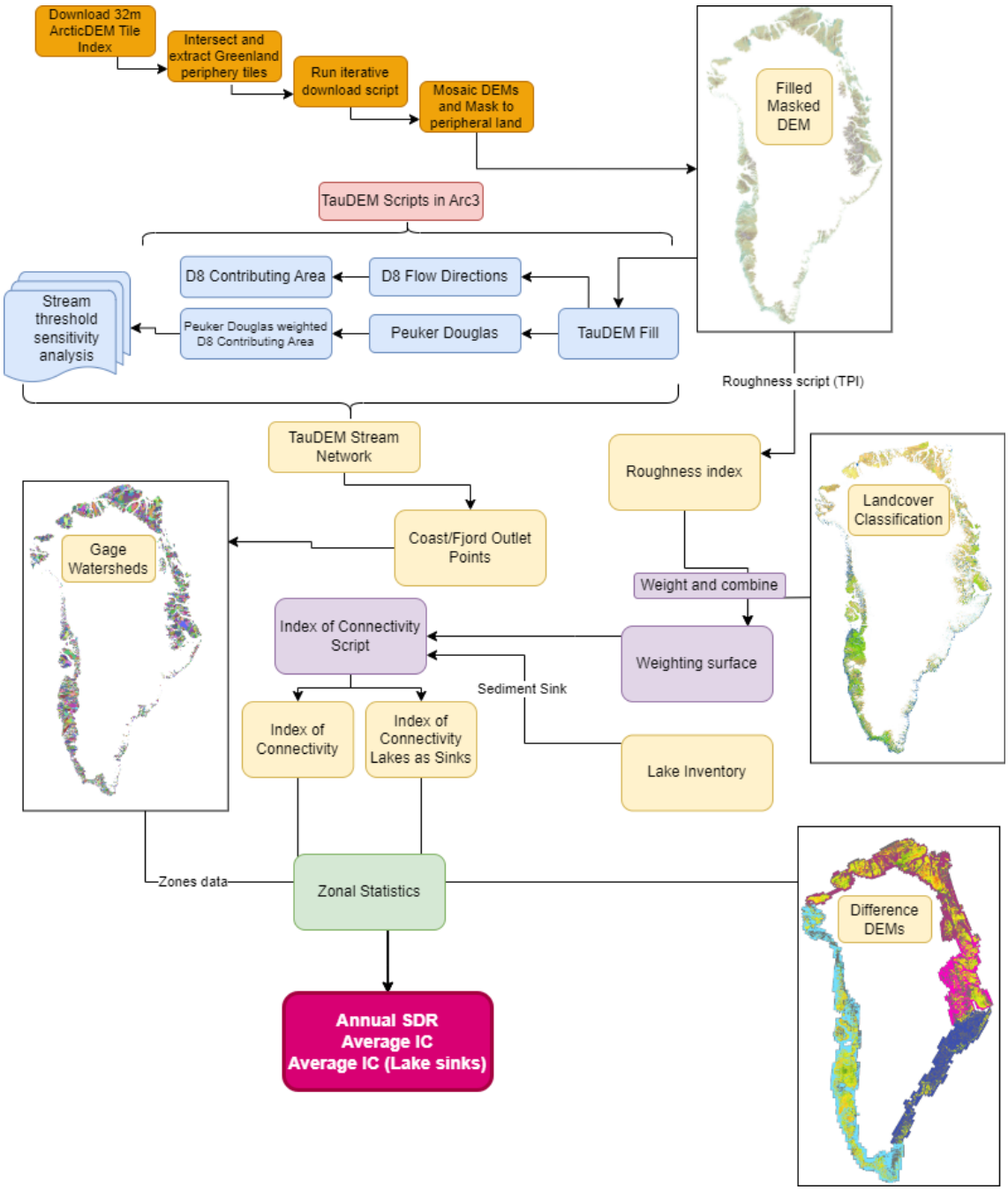

Figure 5.1 High-level data processing procedure for this chapter. The steps are described in detail in the subsequent sections. Yellow boxes and images represent data input and products, orange boxes represent DEM pre-processing steps, blue boxes represent hydrological processing using TauDEM scripts/algorithms, purple boxes represent specific connectivity analysis/processes, the green box is the final zonal statistic to common zones (watersheds), and the final pink box represents the calculated metrics per watershed from the zonal statistics.

5.2.2 Methodological Approach

Figure 5.1 presents the procedural workflow for calculating a national index of connectivity (IC). The process can be broken down into three main steps, pre-processing, hydrological analysis, and finally connectivity analysis. The methods applied are outlined in detail and some initial results and data outputs are presented in the relevant sections.

5.2.2.1 Data Pre-processing

Due to the vast spatial scale and computational complexity of the analysis, the ArcticDEM 32-metre resolution mosaic (Porter et al., 2023) was utilised as the dataset from which topographic, hydrological, and structural connectivity products are computed. This data allows the production of, to date, the highest resolution Greenland-wide hydrological products, surpassing the recently published datasets of Mankoff et al. (2020). Recent studies have found that elevation data down-sampled to lower resolution (i.e. 2m to 32m here) has higher accuracy than those generated at the already lower resolution, particularly in mountain regions (Chymyrov, 2021). Pre-processing and analysis were conducted between ArcGIS Pro and using numerous Python scripts executed on ARC3, a Linux environment and part of the High Performance Computing facilities at the University of Leeds, UK. The ArcticDEM 32m DEM Tile index shapefile was downloaded from the Polar Geospatial Centre website. Within ArcGIS Pro, tiles were extracted which intersected the Greenland periphery land mask layer. The process to produce this land mask is outlined in Chapter 3, whereby an improved version of the GIMP land mask (Howat et al., 2014) has the Ice sheet masked using the 2020 IMBIE ice sheet outline dataset (Shepherd et al., 2020). The intersecting tiles shapefile was converted to a csv, and uploaded to ARC3 where a Python script was used to iteratively download all tile DEMs. The DEMs were mosaicked using GDAL merge utility in Python in ARC3, before the mosaicked 32m DEM was downloaded to a desktop environment and peripheral land surfaces were extracted using the 'Extract by Mask' tool in ArcGIS Pro and the land mask. The masked ArcticDEM was then re-ingested into ARC3 for hydrological analysis.

5.2.2.2 Hydrological Analysis

Here, the first 32m hydrological analysis of Greenland's entire ice sheet free periphery is conducted, considering all peripheral landscapes uniformly in a single-pass, without dissecting the landscape and mosaicking smaller analysis areas for a most congruent

hydrologically accurate output data. TauDEM (Terrain Analysis Using Digital Elevation Models) comprises a collection of tools and scripts to conduct high-quality hydrological analysis on DEMs and was developed by David Tarboton at the Hydrology Research Group of Utah State University (US). TauDEM tools are made freely available at http://hydrology.usu.edu/dtarb/. Leveraging the parallel computing potential of the ARC3 system, and the inherent parallelism in TauDEMs tools, specifically message passing interface (MPI) parallelism, this study is able to conduct national scale hydrological analysis at less than half the resolution of the preceding best alternative of Mankoff et al. (2020). Mankoff et al. (2020) utilised the 100m ArcticDEM mosaic product and found no errors of land surfaces draining into incorrect fjords, even at over 3 times the resolution of this research. Other preceding studies also estimated similar hydrological outputs as those produced here, such as Lewis and Smith (2009) who utilised relatively coarse 5km input DEMs. The HydroSHEDS v1 dataset provides river basin outlines globally, citing ~90m resolution input data around the equator. However, in northern regions such as Greenland basins were created from the coarser and lower-quality HYDRO1k elevation model with a 1km resolution. Within ARC3, the computational processing load is spread across 24 nodes, each with 32gb of random access memory (RAM), summing to 768 total available RAM for processing. Figure 5.1 above broadly shows the final TauDEM workflow.

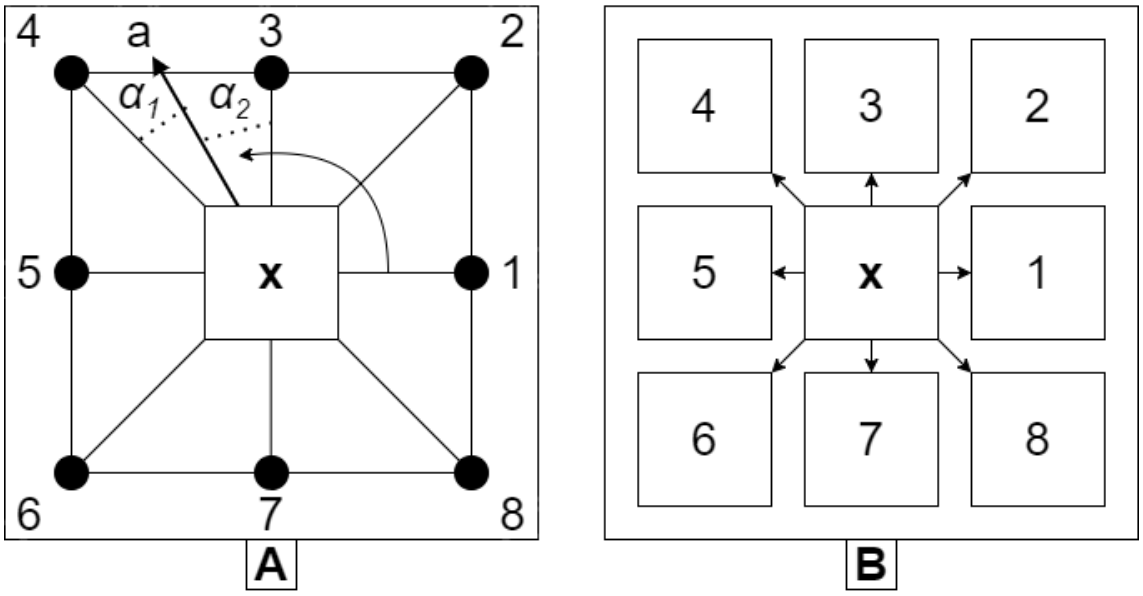

Figure 5.2 Flow directions as defined by the **(A)** D-Infinity algorithm, and **(B)** D8 algorithm. In panel **A** the diagonal arrow (a) between 3 and 4 represents the steepest downslope direction. The proportion flowing into the neighbouring cell at point 4 is $\alpha_2/(\alpha_2+\alpha_1)$, and into the cell at point 3 is $\alpha_1/(\alpha_2+\alpha_1)$. Flow direction is measured anti-clockwise from point 1. Panel B, D8 flow is to only one of the 8 connected cells based on the steepest downslope angle, calculated as the greatest drop in elevation. Panel A is reproduced from Tarboton (1997).

The first stage of analysis was to use the Pit Remove script to produce a depressionless version of the mosaicked 32m ArcticDEM. The script finds points surrounded by higher elevation pixels and raises their elevation so these artefact basins are able to 'drain' to lower elevations.

The definition of an accurate stream network is necessary to delineate watersheds draining to coastal outlets. Flow directions are determined using both the D8 and D-infinity algorithms, diagrammatically represented in Figure 5.2 above. The D8 Flow directions algorithm is non-dispersive and considers flow from a pixel into one of the neighbouring eight (O'Callaghan and Mark, 1984). The D8 script forces flow on flat and very low slope angle surfaces to be routed towards lower elevations using the method outlined in Garbrecht and Martz (1997). The D8 flow direction is output as an integer grid of values from 1 to 8 moving anti-clockwise from the east, with increasing values representing flow direction to neighbouring pixels, with a value of 1 representing flow into the pixel directly east, 2 flowing into the north east moving anti-clockwise through to south east with a value of 8. Conversely, the D-infinity algorithm represents flow direction from a pixel as the steepest downslope angle into one of eight triangular facets, however then partitions flow into two directions depending on how close the flow direction is to the given angle, making it semi-dispersive (Tarboton, 1997). D-infinity flow direction is output as a floating-point grid of flow angles in radians circling anti-clockwise from east and is represented by continuous values ranging between 0 and 2 π. Both flow direction algorithms iteratively calculate direction from each pixel to neighbouring pixels, a particularly computationally costly process. Contributing area, also known as the upslope area or flow accumulation, is also calculated using both the D8 and D-infinity algorithms here.

The Peuker Douglas algorithm is run on the filled 32m ArcticDEM to produce a weighting surface as input for second runs of contributing area (Peuker and Douglas, 1975). The Peuker Douglas script attempts to define likely channels within the topography by first smoothing the input DEM by a kernel with weights applied to the centre (0.4), side (0.1), and diagonal (0.05) (see (Band, 1986). The Peuker Douglas algorithm (outlined in more detail in O'Callaghan and Mark, 1984) is applied to output upwardly curving pixels by 'marking' the entire grid and subsequently iterating over each quadrant of 4 grid cells and 'unmarking' the highest value pixels within the quadrant. These remaining 'flagged' cells are considered upwardly curved and represent a proto-network, lacking connectivity but providing a weighting surface to improve the

accuracy of the D8 and D-infinity contributing area algorithms (Band, 1986; Cavalli, Trevisani, Goldin, et al., 2013).

The D8 algorithm contributing area is taken as each cell's own contribution plus the contribution from the upslope neighbouring pixel that drains into it based on the input D8 flow direction grid. The contribution of a pixel is counted as 1, though a second run of the algorithm took the Peuker Douglas upward curvature layer as a weighting surface and in this case, the contribution for each pixel is taken as the Peuker Douglas value, whereby pixels defined as upward sloping are more highly weighted. In the D-infinity contributing area algorithm, the contribution at each grid cell is taken as the grid cell length (Gruber and Peckham, 2009). The contributing area of each pixel is the cumulative of its own contribution plus the contribution from all upslope neighbours that have some fraction draining to it according to the D-infinity flow direction input (Tarboton et al., 2009). The flow from each cell either all drains to one neighbour, if the angle falls along a cardinal (0, π /2, π, 3 π /2) or ordinal (π /4, 3 π /4, 5 π /4, 7 π /4) direction (Tarboton, 1997). Should the angle fall between the direct angle to two adjacent neighbours then the flow is proportioned between these two neighbouring pixels according to how close the flow direction angle is to the direct angle to those cells (Tarboton, 1997). The algorithm was re-run with the Peuker Douglas surface as a weighting layer whereby the contribution at each pixel is taken as the Peuker Douglas value rather than the pixel length.

Stream networks are then extracted from both the Peuker Douglas weighted D8 and D-infinity contributing area grids by setting a value threshold and sensitivity testing these values through comparison with aerial imagery, the previous accuracy-assessed stream delineation data of Mankoff et al. (2020), and for the complexity necessary for this study. Too low a threshold and very small streams are extracted which are not of concern for this national scale research, however, too large a threshold and potentially important streams and basins are excluded. Sensitivity testing found a threshold of 120 to be most suitable for the D8 Peuker Douglas weighted flow accumulation grid, and 105 for the Peuker Douglas weighted D-infinity flow accumulation. Finally, the Strahler stream network and watersheds are defined.

A polyline stream file is produced from the input threshold stream rasters, utilising the associated (D8 or D-infinity) flow direction grid to trace flow paths to determine the Strahler order for each stream segment with the stream network organised based on the Strahler system (Horton, 1945; Strahler, 1957). Subwatersheds are also delineated for

each segment. Streams without tributaries are classed as order 1, when streams of different orders converge the downstream stream assumes the higher order and if streams of the same order meet, the downstream stream's order increases by one. The input threshold stream raster grid establishes the network, and the flow direction grid identifies interconnections. The filled DEM and contributing area grids are also factored into the production of the output Strahler network file. Using ArcGIS Pro, the lowest (nearest to coast) segment of the Strahler order streams polylines is extracted for all streams, and the outlet vertex of these extracted to produce the final outlet points for subsequent analysis. The total upstream area draining each point is then extracted to delineate the gage watersheds upon which subsequent connectivity analysis is aggregated.

An issue with the D-infinity layers is the allowance for multiple flow directions severely degrading the quality of the Strahler order, and multiple outlet points can be produced for single watersheds. Though the D-infinity streams are more accurate in low gradient

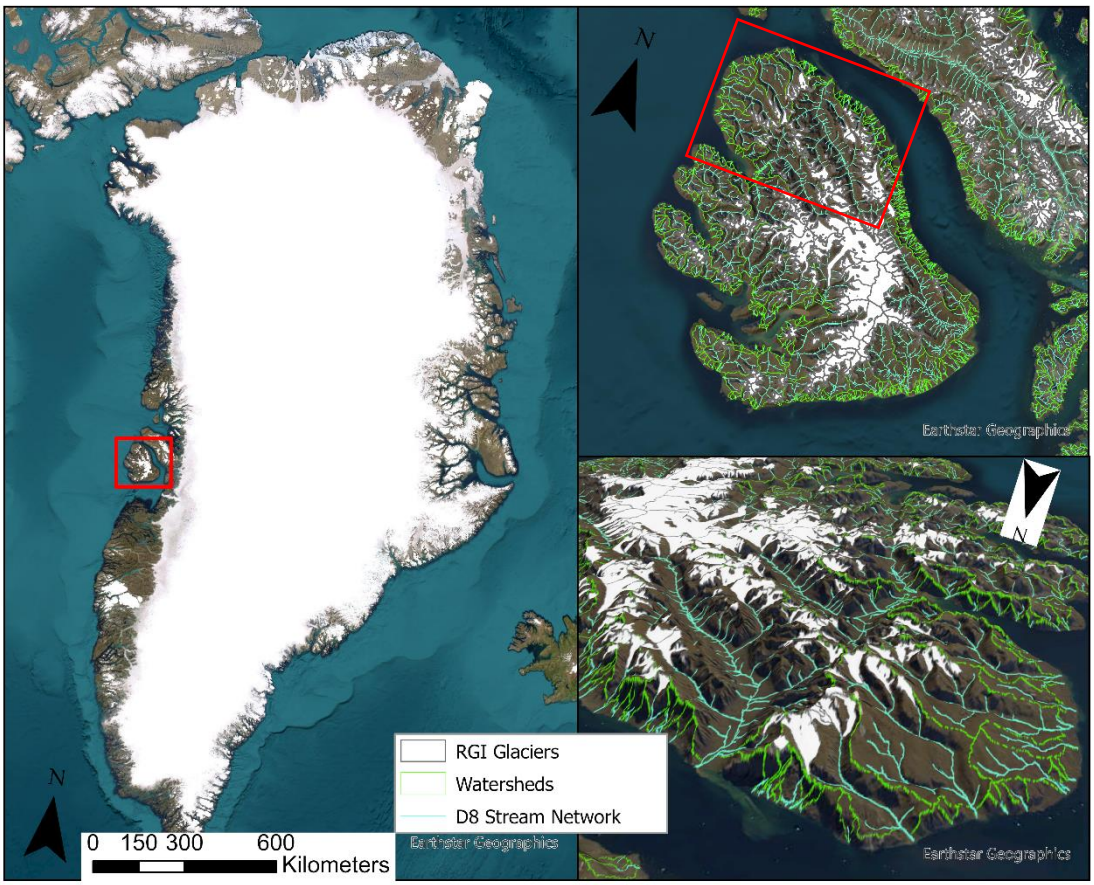

Figure 5.3 Left: Map of Greenland (Eurostar Geographics world imagery) with RHI Glaciers and Red extent box for Disko Island. Top Right: Disko Island D8 Stream Network, Watershed boundaries from D8 outlets, RGI glaciers, and red extend box of bottom right. Bottom Right: 3D ArcScene depiction (facing south east) of North Disko Island.

valley floors, the watershed delineation from multiple outlets is undesirable for defining the zones of analysis. For example, deltas and wide sandur valley floors draining into fjords can have multiple outlets, though the upslope contributing area for these points is largely the same. The D8 outlet points were therefore deemed most suitable for, and best facilitated the subsequent watershed connectivity analysis. These outlets are buffered by the data resolution (32m) and used as targets for connectivity analysis. Figure 5.3 shows an example of the final output D8 stream network and watersheds, specifically on Disko Island, West Greenland.

5.2.2.3 Index of Connectivity (Structural Connectivity)

Defined in the literature review of this thesis, the structural Index of Connectivity (IC) as first defined by Borselli et al. (2008) and later honed for mountain catchments by Cavalli et al. (2013) was adjusted and applied here to best suit the scale and resolution of the analysis. The filled ArcticDEM was used as the primary input; however, the weighting surface, reflecting the impedance of sediment movement, was not solely topography-derived and was represented as a novel combination roughness-landcover metric. Contemporary landcover data, produced during the first research chapter in this thesis, and similar to that used by Borselli et al. (2008) (who applied 100m CORINE data) was reclassified following the C-factor weighting scheme of USLE-RUSLE models (Wischmeier and Smith, 1978; Renard et al., 1997; Borselli et al., 2008). Table 5.1 below shows the landcover weight reclassification scheme for the C-factor component of the weight surface.

Table 5.1 Chapter 3 contemporary landcover classification C-factor weight scheme

Landcover Class	**C-factor weight**
Snow/Ice	n.c.
Meltwater	1
Freshwater (Fjords/Lakes)	0.2
Coarse Sediment	0.5
Fine Sediment	0.65
Bedrock	0.8
Tundra/Dry Vegetation	0.05
Dense/Wetland Vegetation	0.1

In the context of developing an index to understand sediment connectivity on slopes, a specific methodology focusing on the simple case of a homogenous slope was first considered. This approach initially assumes constant roughness, gradient, and vegetation across the slope. The model centres around a point 'A', which serves as a divide for flow lines, differentiating between sediment contributed to point 'A' itself (upslope oncoming sediment) and sediment transported downslope towards a designated sink, the coast/fjord in this case. The probability that sediment from 'A' reaches the downslope sink/target 'B' is inversely related to the distance along the flow line. It is noted that an increased amount of upslope oncoming sediment reduces the likelihood of all sediment reaching the downslope sink (Crema and Cavalli, 2018). This model proposes that the mass of sediment ready to flow to point 'A' (mA) is a factor of the probability that sediment from upslope actually reaches 'A', and this probability is also influenced by the connectivity of 'A's upslope source zone (Cavalli et al., 2013). To quantify these probabilities, the method turns to a conceptual model (see Cavalli et al., 2013). It is then the downslope component, referred to as D_{dn}, that considers factors beyond mere distance, in this case landcover and roughness, and slope gradient, all of which influence sediment transport to the downflow target (coast/fjord) (Coulthard and Van De Wiel, 2017). It is in the D_{dn} phase of the calculation that the computed landcover-roughness weighting factor (W) and a gradient factor (S) were introduced to account for local downflow conditions, with the distance being adjusted by these factors to estimate D_{dn}. On the other hand, the upslope component (D_{up}) addresses the potential for sediment routing from areas draining into point 'A'. This component is influenced by similar factors as D_{dn}, but extends the analysis to an up-flow contributing area as calculated using the D-infinity algorithm, using average values of the weighting factors over the contributing upslope area. The connectivity index (IC) was then calculated by combining these components. However, the IC is not a straightforward probability due to its non-normalised nature and variance across magnitudes. Instead, it is defined as the logarithm of a derived equation, providing a range for connectivity assessment (Cavalli et al., 2020). Finally, the method defines the weighting factors S and W, considering both the reclassified landcover C-factor variables and the surface roughness (as calculated following Cavalli and Marchi, 2008 and Trevisani and Cavalli, 2016). These factors are crucial in assessing the impedance to runoff and sediment fluxes. The IC model adapts existing parameters from other models, recognising the complexity and variability in defining a universal parameter for connectivity studies (Borselli et al., 2008; Cavalli et al., 2013; Crema and Cavalli, 2018; Heckmann et al., 2018). For

instance, as applied here the algorithm employs the reclassified landcover C-factor, adapted from USLE–RUSLE models designed to reflect the relative effectiveness of crop management systems in soil loss, as a proxy for ease of conveyance in the weighting factor W. By applying a combined landcover-geomorphology (roughness) weighting surface here, the IC calculated here consider the physical landscapes combined morphometry and surficial landcover composition in assessing sediment connectivity to coasts. Figure 5.4 below shows a diagrammatic representation of the calculation for the Index of Connectivity (IC), reproduced from Cavalli et al. (2013).

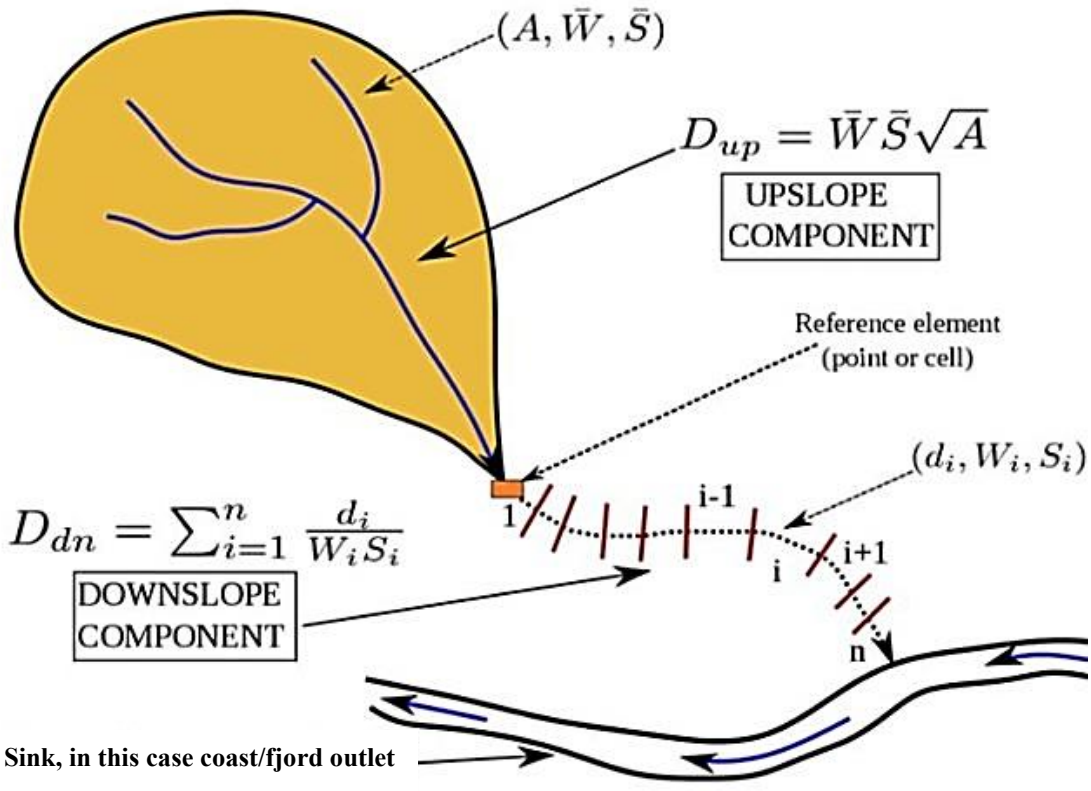

Figure 5.4 The definition of the upslope and downlope components of the IC, from Cavalli et al. (2013). D_{up} is the upslope component of IC, $\bar{W}$ is average weighting factor in upslope area, $\bar{S}$ is average slope in upslope area, and A is upslope contributing area (m^2). D_{dn} the downslope component, d_i is the length of the *i*th cell downslope (m), W_i is the weight of the *i*th cell, and S_i is the slope gradient of the *i*th cell (m/m).

IC was then calculated as shown in equation 5.1 below, with D_{up} and D_{dn} being the up and downslope components of connectivity as shown in Figure 5.4.

$$IC = \log_{10}\left(\frac{D_{dn}}{D_{up}}\right) \quad (5.1)$$

Equation 5.2 below shows the calculation of the roughness index, given a moving window of 5 x 5 cells used in the smoothing to produce residual topography. The roughness index is essentially the topographic position index, whereby a kernel smoothed version of the DEM was differenced from the original DEM. Areas notably higher and lower than the average of surrounding areas are marked as rough. At the scale considered here (32m x 32m) the roughness index reflects geomorphological units as impedance rather than smaller scale surface morphometry.

$$RI = \frac{\sum_{i=1}^{25}(x_i - x_m)^2}{25} \qquad (5.2)$$

Where 25 is the total number of cells considered (5 x 5), x_i is the value of the kernel cell within the window and x_m is the average within the 5 x 5 cell moving window. This RI was converted to a normalised 0 – 1 weighing component by dividing the RI surface by the maximum value and subtracting from 1.

Two indices of connectivity were computed for this study. The common 'targets' to which connectivity was assessed are the D8 watershed outlets as defined above. However, lakes are notable sinks of sediment within the landscape within which the majority of inflowing suspended sediment is lost (Carrivick and Tweed, 2013). Lakes are already partially considered by the landcover weighting C-factor (see Table 5.1); however, their low roughness may give an unrealistic weighting when using the combined roughness-C-factor method. Therefore lakes as classified in Chapter 3 are combined with the lake inventory produced by Carrivick et al. (2022). Lakes are considered in two ways: i) indirectly only using the combined weighting layer and using outlets as targets, and ii) directly as sinks with essentially zero connectivity to outlet targets for areas flowing into lakes. This was achieved by re-running the IC calculation with a weighting surface where areas covered by lakes as delineated by Carrivick et al. (2022) were reclassified to 0.001. This value essentially negates all up-flow connectivity, as zero values are not permissible due to 'divide-by-zero' failures in the computation.

5.2.2.4 Watershed Sediment Delivery Ratios (Functional Connectivity)

To assess the effectiveness of a national IC in predicting/estimating nationally distributed watershed's measured structural connectivity, Sediment Delivery Ratios (SDR) are calculated per watershed from DEMs of Difference. Here proglacial

ArcticDEM-AeroDEM DoD's are utilised and processed following the workflow outlined for the glacier surface elevations processed in the preceding chapter. Following uncertainty assessment, the level of detection per DoD was computed and changes within the level of detection around the mean were masked from analysis. Areas within 500m of current RGI glacier margins and 1km of the GrIS margin are also masked from analysis to reduce the influence of glacier melt from the assessment. Sediment delivery ratios are calculated as the sum of elevation changes upslope of a point divided by the total erosion, as defined in Heckmann and Vericat (2018) and shown below in equation 5.3.

$$SDR = SY/E \tag{5.3}$$

Where SDR is the watershed sediment delivery ratio, SY is the sediment yield calculated as the sum of elevation changes (erosion and deposition) within the watershed, and E is the watershed's total erosion calculated as the sum of negative elevation changes. Heckmann and Vericat (2018) calculate spatially distributed SDR and, as each watershed produced here delineates all areas upslope of coastal outlet points, SDRs are calculated per watershed. As the DoDs are produced using AeroDEM with regionally variable starting years (between 1978 and 1987), elevation changes were calculated per-year, per-watershed and so too are sediment delivery ratios for fair comparison. Figure 5.5 below shows the 4 DoD regions and located histograms of elevation change distributions with the level of detection. Inset labelled boxes (A-C) are extent location indicators for sites shown in Figure 5.6.

5.2.2.5 Correlation between IC and SDR

To test for the correlation between the Index of Connectivity (IC) and Sediment Delivery Ratio (SDR), both metrics were standardised and normalised. Although normalisation is not required for Ordinary Least Squares (OLS) regression, it is beneficial when variables have vastly different scales, as it can improve numerical stability and the performance of optimisation algorithms used to find the regression coefficients. Simple linear regression (OLS) was conducted, with the Sediment Delivery Ratio (normalised from -1 to 1) as the dependent variable and the Index of Connectivity (with and without lakes as sinks) as the independent predictor. This approach aims to elucidate the linear relationship between these variables and determine the extent to which catchment-scale average IC can be used to predict SDR.

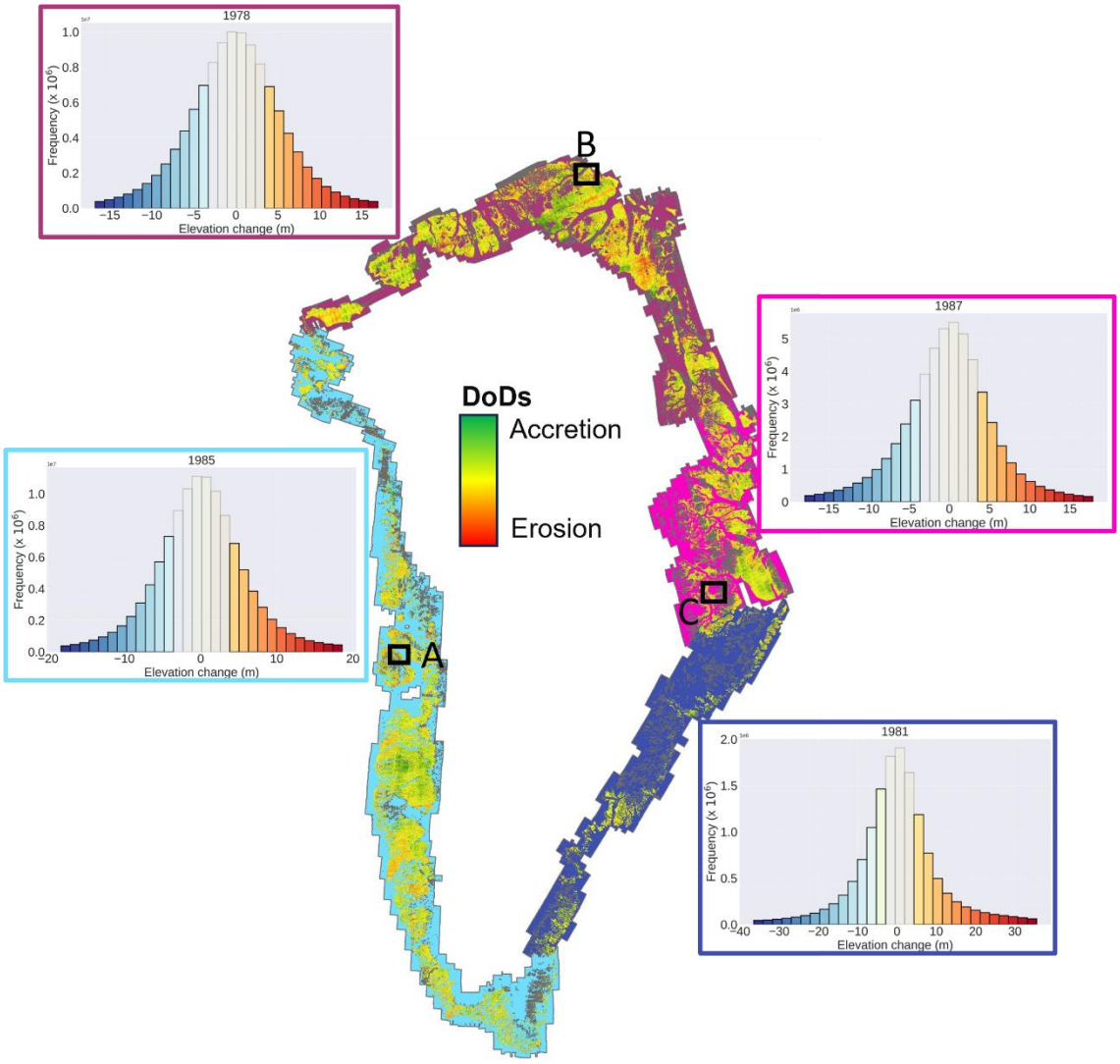

Figure 5.5 DEMs of difference for proglacial peripheral areas of AeroDEM differenced from ArcticDEM with negative values reflecting surface lowering. Located histograms show elevation change distributions, transparent bars reflect level of detection masked from analysis, and chart border colours correspond to DoD region colours. Inset extent indicators A, B and C relate to example sites in Figure 5.6.

The analysis of spatial autocorrelation in the residuals of an Ordinary Least Squares (OLS) regression was conducted using Moran's Global I. This measure provides an indication of whether the residuals are clustered, dispersed, or random (Chen, 2016). Moran's Global I is critical in understanding the spatial structure and distribution of the model's residuals, and it is particularly significant for assessing the adequacy and robustness of regression models in spatial analyses (Zhang et al., 2005). The Moran's Index was calculated and compared against the Expected Index to evaluate the presence of spatial autocorrelation.

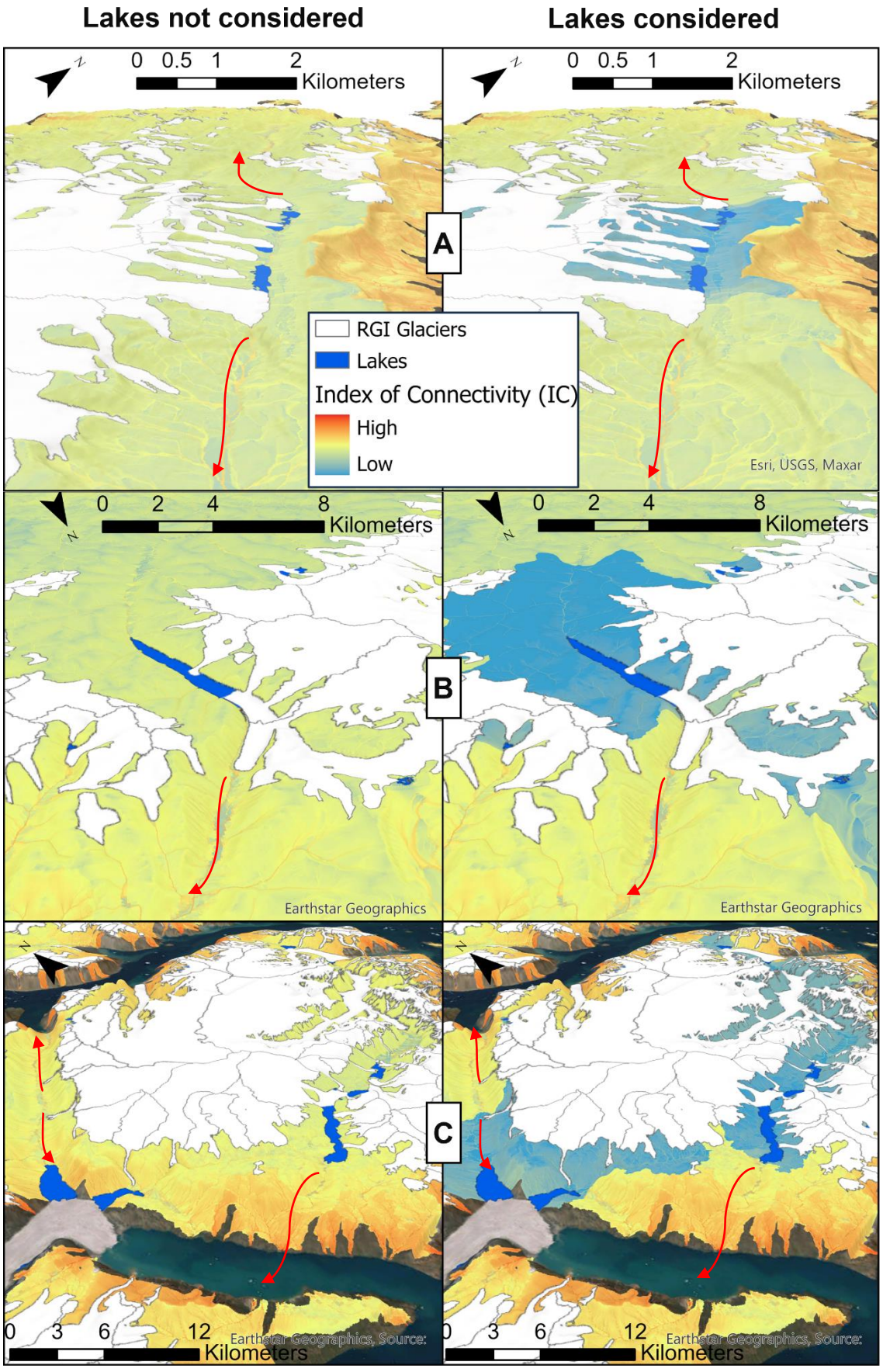

Figure 5.6 3D ArcScene visualisations comparing the spatially distributed Index of Connectivity without lakes modelled as sinks (left) and with lakes modelled as sinks (right). Panels rows A (Disko Island, West Greenland), B (Wyckoff Land, North East Greenland) and C (Renland, East Greenland) correspond to extend boxes in Figure 5.5. IC colour gradients are applied nationally and comparable across rows. Red arrows show flow direction.

5.3 Results

5.3.1 Spatial distribution of IC and SDR

Figure 5.6 below shows example locations (the extent of these panels is shown in Figure 5.5 above) comparing sediment connectivity with and without lakes considered as sinks for three locations around Greenland. The influence of lakes on contributing area connectivity is clearly evident in all three panels.

Panels in row A of Figure 5.6, in northern Disko Island, show small lakes formed in the relatively flat valley floor. The valley drains both towards the reader and away, however lakes on either side of the divide cause essentially all sediment sourced from these northern outlet lobes to be trapped. The nearest of the three lakes is ice-dammed by the largest piedmont lobe so there is potential for this lake to drain in future, should moraine formation be insufficient to continue to dam the lake. Some of the stored sediment may then be redistributed down the valley, altering both the down-valley connectivity and potentially a sudden spike in sediment output to the coast as a fairly large river flows along the valley and is apparently well connected to the outlet at the fjord mouth. A similar but exaggerated situation is seen in row B of Figure 5.6 in far north east Greenland. A large ice-dammed lake has formed, effectively nullifying connectivity from the large contributing area and glaciers flowing into the valley. A river has formed flowing along the eastern edge of the glacier terminus damming this lake. Moraine formation in this region is fairly subdued due to the cold based, ice cap style nature of glaciers in the region, and so there is considerable potential for a catastrophic outburst of lake water and trapped sediment, analogous to other outbursts as have been documented across Greenland (Carrivick et al., 2017; Grinsted et al., 2017; Carrivick and Tweed, 2019; Tomczyk et al., 2020). The final row C then shows how lakes, even when in close proximity to the coast, negate most contributing area connectivity assuming most particulate matter is trapped. Again, a number of these lakes are ice-dammed and so the ramifications for outbursts are present. Should lakes drain gradually the sediment trapped within may be less rapidly redistributed, though the contributing areas and glacigenic sediment will be more structurally connected to coasts and Fjords following drainage.

5.3.2 Watershed Characteristics and IC

Average IC was calculated per watershed both considering lakes as sinks and without lakes. The average watershed mean IC without lakes considered as sinks was -3.7, yet

with lakes as sinks the average was -4.1 across all watersheds. When only considering watersheds with lakes, the difference is even more apparent, with an average of -4.1 when lakes are not explicitly cast as sinks, compared to -6.6 when lakes are, a more than 50% decrease in average IC for watersheds with lakes. To further explore lakes' impact on IC at a watershed scale, analysis was conducted regionally of watershed average IC with and without lakes considered as sinks (using the same regions used for Glacier mass balance in the previous chapter and shown again in Figure 5.11). Analysis of Variance (ANOVA) was conducted to compare these metrics across different regions. However, subsequent tests on the ANOVA model residuals, specifically the Shapiro-Wilk test for normality and Levene's test for homogeneity of variances, indicated significant deviations from the assumptions required for ANOVA. Specifically, the residuals exhibited non-normal distribution and variances were not homogeneous across the groups. This deviation from the assumptions rendered the application of ANOVA and subsequent Tukey's Honest Significant Difference (HSD) test inappropriate for this analysis. Table 5.2 below shows the results of this exploratory analysis.

Table 5.2 Shapiro-Wilk and Levene's test results of IC distributions per watershed (averaged across all regions) with and without lakes considered, testing normality and homogeneity.

Metric	Shapiro-Wilk p-value (Normality)	Levene's test p-value (homogeneity)
IC (lakes not considered sinks)	0.113	0.035
IC (lakes considered sinks)	0.067	0.005

For both metrics, at least one region violates the normality assumption, and the homogeneity of variances assumption is also violated (p-values for Levene's test are below 0.05). Consequently, non-parametric statistical methods were employed. The Kruskal-Wallis test, a robust non-parametric alternative to ANOVA, was chosen to determine if there were overall differences among the groups for each metric (Vargha and Delaney, 1998). This test is particularly suited to analysing ordinal data or non-parametric variables and is less sensitive to non-normal distributions. The Kruskal-Wallis test indicated significant differences across regions for both metrics, necessitating further pairwise comparisons to identify specific groups with distinct median values. Accordingly, Dunn's post hoc test was applied, incorporating a Bonferroni correction to adjust for the multiple comparisons being conducted (Dinno, 2015). This test enabled a detailed and statistically sound comparison between pairs of

regions. The results of these pairwise comparisons are communicated through the assignment of post hoc letter codes for each region, shown in Figure 5.7 above each box plot. These codes provide a straightforward, visually intuitive method to interpret results. Plots sharing the same letter code indicate indistinct medians, with multiple letters (e.g., bd) showing indistinctness from multiple regions, in this case, one other. Figure 5.7 below shows box plots of IC by region, with lakes considered as sinks in the right plot and not considered in the left.

Given the significant deviations from ANOVA, the chosen method of using non-parametric statistical tests such as the Kruskal-Wallis test and Dunn's post hoc test was justified. These tests provided a robust and reliable framework for analysing the data without relying on assumptions of normality and homogeneity of variances. The detailed and statistically sound comparisons facilitated by these non-parametric methods ensured the integrity and interpretability of the results, validating the analytical approach applied in this research.

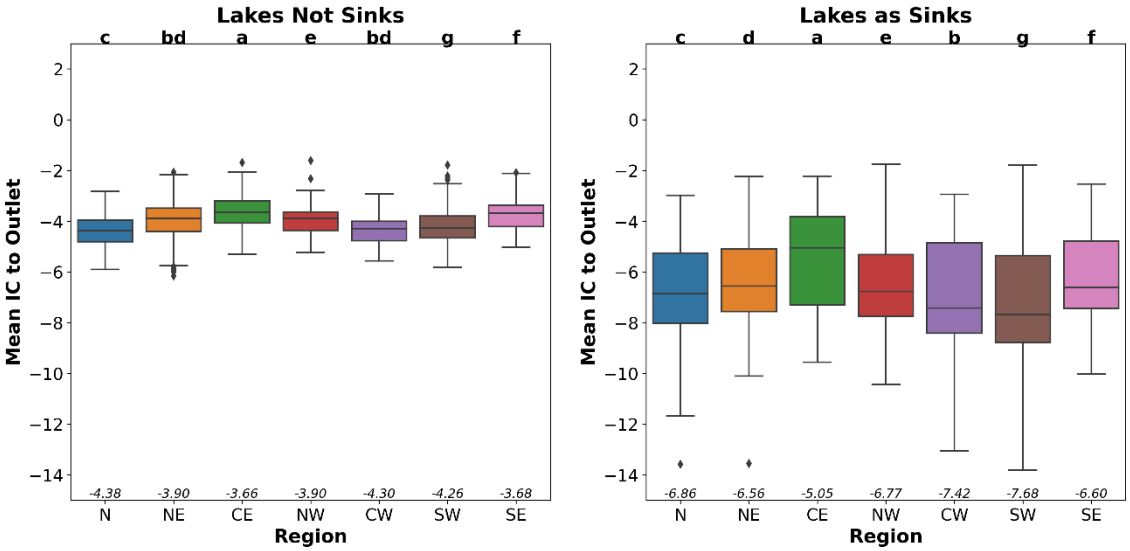

Figure 5.7 Box plots showing average IC per region, without lakes as sinks (left) and considering lakes as sinks (right). Letter codes above plots reflect Dunn's post-hoc significance.

The plots in Figure 5.7 provided a clear visual representation of the distribution of both metrics across the different regions. The post-hoc letter codes above each region in the plots reflect which regions' metrics were statistically similar or distinct. Those plots sharing a letter are not significantly different. Medians are shown in italics above the x-axis. Only the north east (NE) and central west (CW) have statistically indistinct

distributions. By considering lakes as sinks all regions see a reduction in average connectivity to coasts. When not considering lakes as sinks, the north has the lowest median average IC to coastlines (-4.38). Conversely, the north is the third lowest when considering lakes as sinks (-6.86), with the south west (-7.68) and central west (-7.42) having the lowest and second lowest IC yet the highest and second highest range respectively. Both when considering lakes as sinks(-5.05) and not (-3.9), the central east of Greenland has the highest relative connectivity to coastlines.

As studies have shown important nutrients are transported in proglacial rivers and streams to coastal waters, a second line of inquiry was to observe regional variability in the two IC metrics for watersheds containing direct PGIC or GrIS input. Figure 5.8 below presents boxplots as above but only for watersheds with direct glacier input. The same preliminary statistical tests were performed and Dunn's post-hoc pairwise letter codes are again displayed above plots.

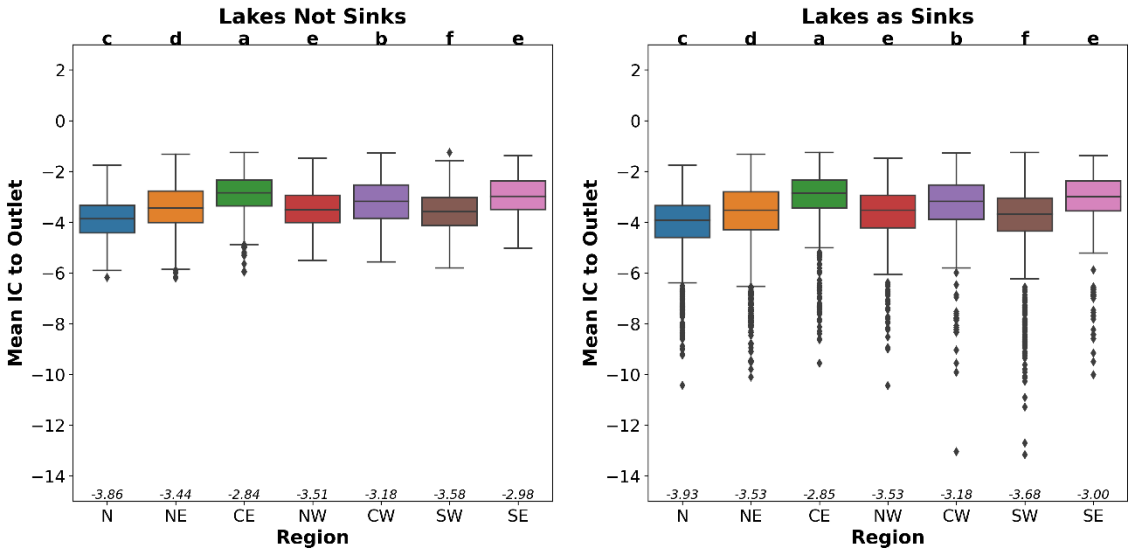

Figure 5.8 Box plots showing average IC per watershed per region but only for watersheds containing glaciers. IC with lakes as sinks (left) and IC calculated considering lakes as sinks (right). Letter codes above plots reflect Dunn's post-hoc statistical significance.

Again, the spread of IC is greater for all regions when lakes are considered sinks. However, the median average IC is higher for all regions when only considering glaciated watersheds. Potential causes of this are explored later in this chapter's discussion. A similar regional distribution is also seen for only glaciated watersheds, with the central east (CE) having the highest average IC (-2.84 and -2.85 without and with lakes as sinks respectively).

5.3.3 National Index of Connectivity as an Estimator of Watershed SDR

To further assess the spatial distribution of IC, and given the scale of this analysis it loans itself first to a visual comparison of the national distribution of the three metrics calculated per watershed: i) the average index of connectivity to coastal targets, ii) the average connectivity with lakes modelled as sinks, and iii) the sediment delivery ratio

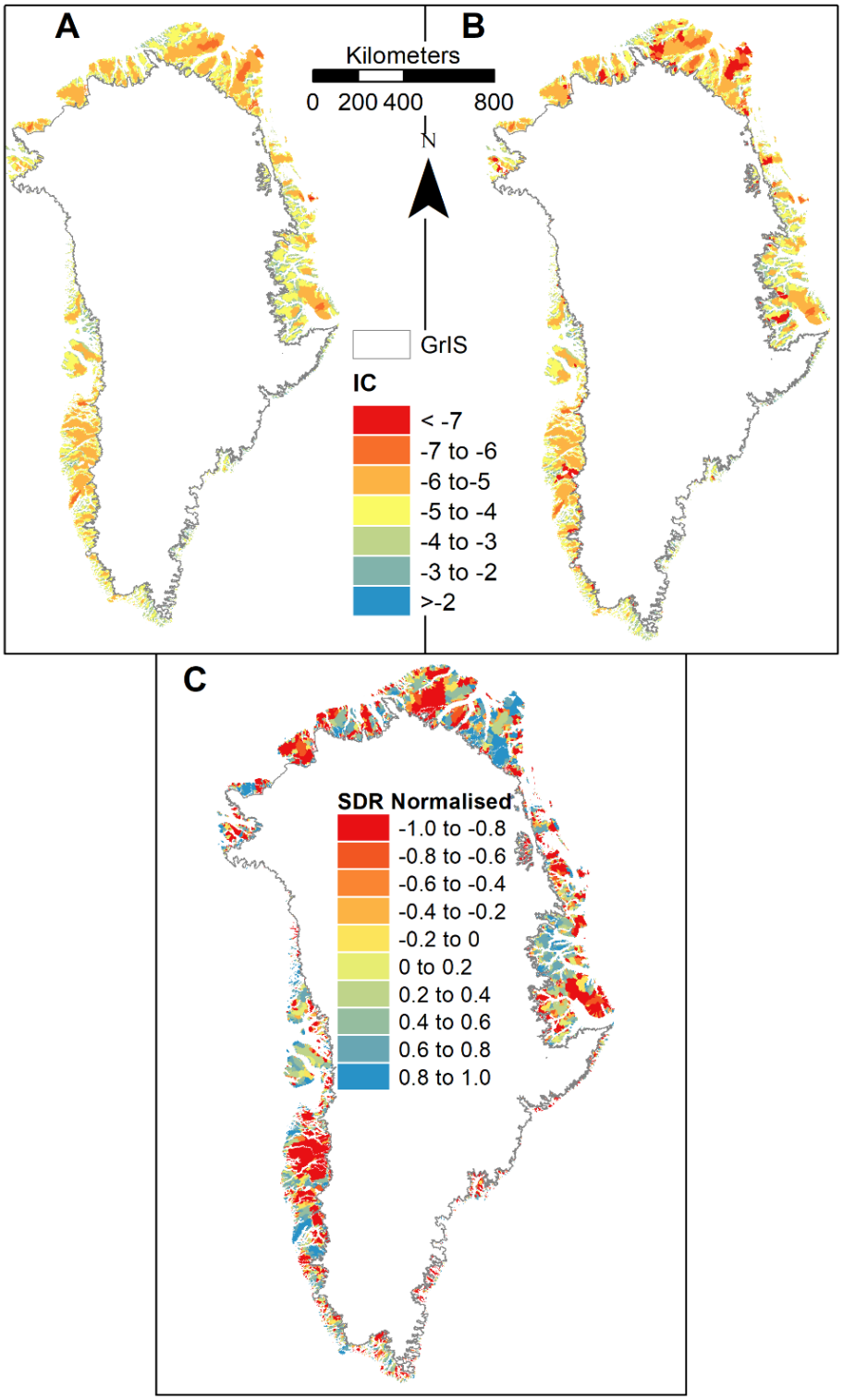

Figure 5.9 Maps of watersheds average (**A**) IC to outlets, (**B**) IC to outlets with lakes as sinks, and (**C**) Sediment Delivery Ratios. SDR is normalised to a -1 to 1 scale.

(SDR). The SDR is highly variable and correlated strongly with watershed size, and so the values are normalised by watershed area and to a range of -1 to 1. SDR is allowed minus values as some watersheds exhibit net accretion, the reasons behind which are explored in the following discussion. Figure 5.9 shows the national distributions of watershed's IC values with and without lakes considered. The figure also shows the normalised distribution of sediment delivery ratios per watershed for comparison.

The IC, though normally distributed, is skewed by the sizes of the watersheds, with more negative values appearing overrepresented due to the larger watersheds where pixels have further to travel to the coasts. To address this, IC and SDR were standardised and normalised before analysis. The OLS regression model revealed a linear relationship between the normalised Sediment Delivery Ratio and the Index of Connectivity, both with and without considering lakes as sinks. This analysis demonstrates that the catchment-scale average IC can be used to predict SDR, highlighting the impact of watershed size and the role of lakes in sediment transport.

Both IC variables show a positive correlation with SDR, indicating that increased structural/potential connectivity as modelled here correlates with increased sediment delivery ratios. Interestingly, for the IC without lakes as sinks, an R^2 (coefficient of determination) of 0.62 is reported, with a sigma (standard error) of 0.25 and an Akaike Information Criterion (AIC) of 1741.3. Conversely, when lakes are considered as sinks, the correlation is lower, with an R^2 of 0.32, a sigma of 0.28, and an AIC of 11437. The

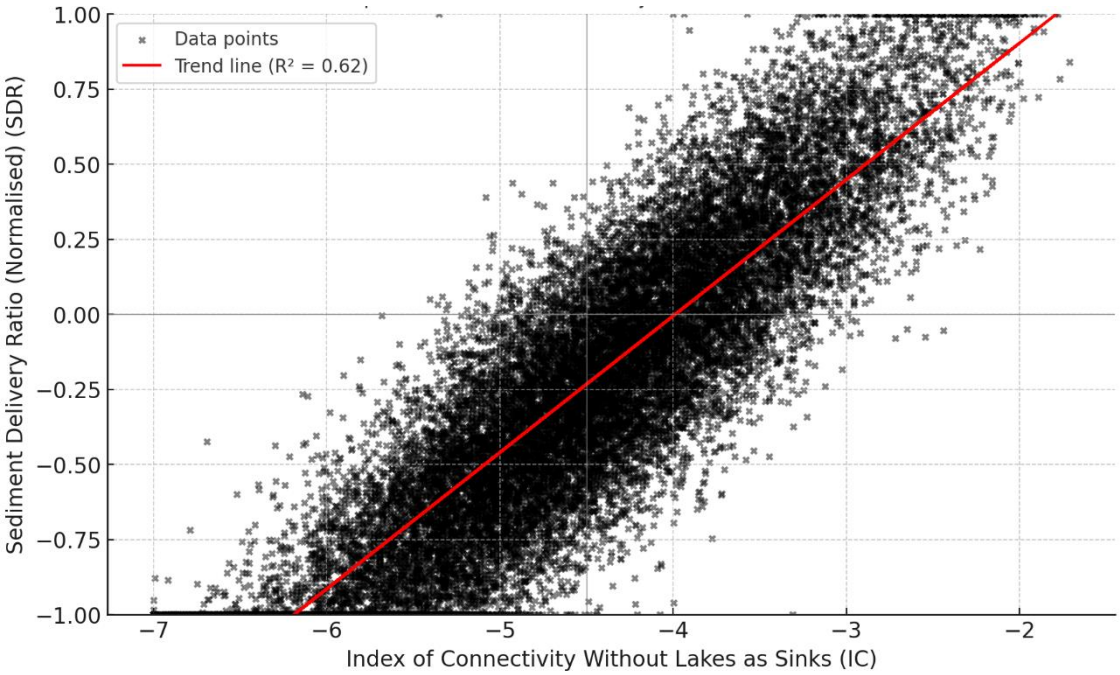

Figure 5.10 Scatter plot of watershed's IC (without lakes and sinks) and Sediment Delivery Ratios (SDR) (Normalised)

R^2 of 0.62 and a sigma of 0.25 suggest that the OLS IC to outlets model explains a significant portion of the variance in the watershed's SDR and that the predictions are reasonably precise. However, these values alone do not provide the complete picture.

Figure 5.10 above shows a scatter plot of normalised SDR against IC.

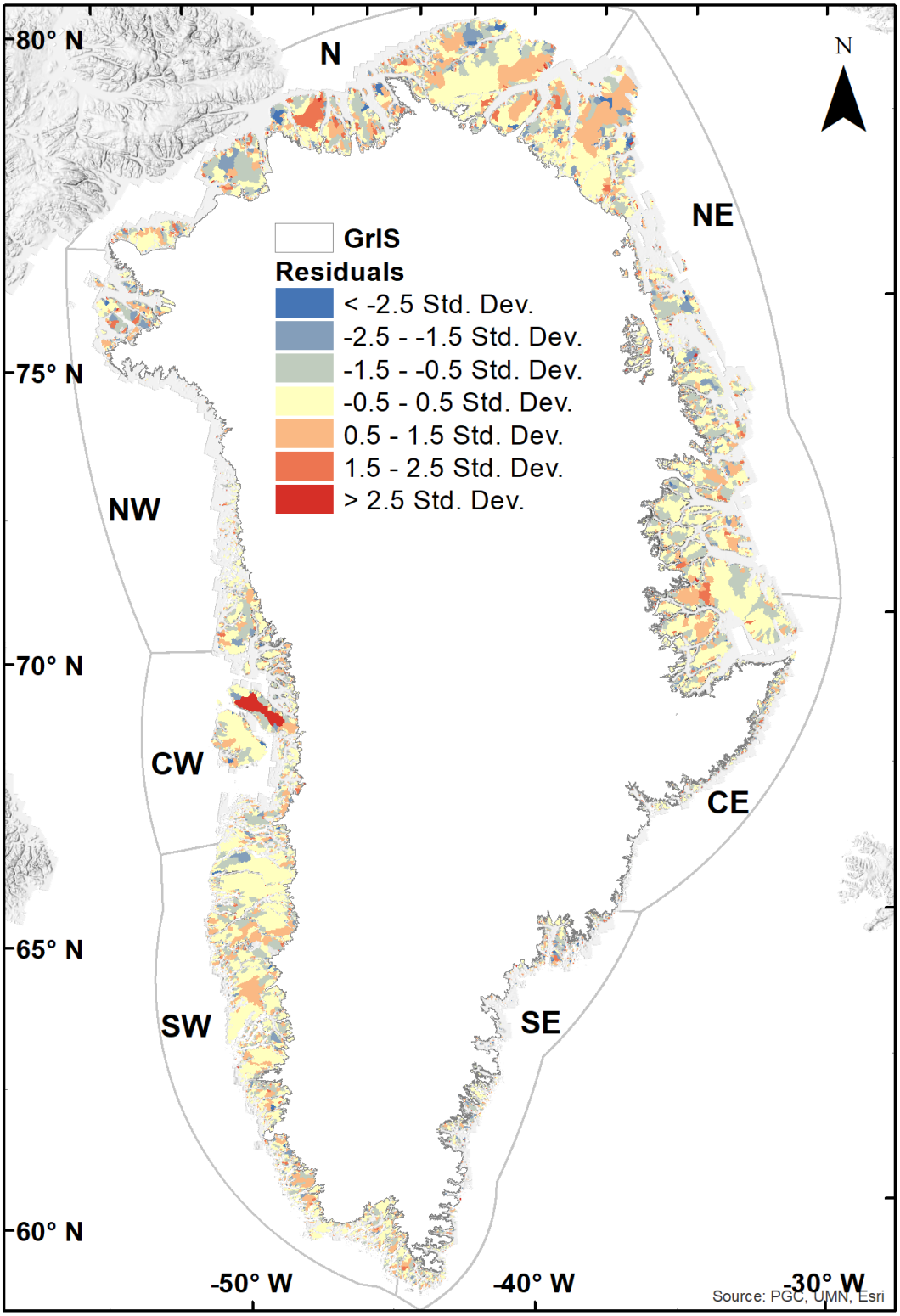

Figure 5.11 Map of OLS watersheds residuals of IC without lakes as sinks.

The residuals, representing the differences between observed and predicted values, are mapped across all watersheds to serve as a diagnostic tool for assessing the spatial adequacy and predictive accuracy of the OLS model. The potential causes of lower correlations for the IC when considering lakes as sinks are explored in the following discussion. This spatial visualisation of residuals allows for the identification of patterns or clusters of under- or over-estimation, which may indicate systematic biases or missing variables that exhibit spatial dependence. Such patterns are paramount in understanding locational discrepancies in model performance, guiding further refinement and indicating areas where additional explanatory variables may be required. For instance, regions with consistently high positive residuals might suggest areas where the Sediment Delivery Ratio is systematically underestimated by the model, possibly due to unique topographical or hydrological conditions not captured by the Index of Connectivity alone. Figure 5.11 below shows the spatial distribution of residuals from the OLS of IC (without lakes as sinks) predicting SDR.

Positive residuals indicate where the observed SDR is higher than the predicted, and negative the contrary. Visual interpretation of the distribution of residuals in Figure 5.11 shows generally predicted SDR falls within -0.5 and 0.5 standard deviations (STD) of the actual values, as shown by the yellow watersheds. Some notable hotspots of over and under-estimation are seen. A particular area where the SDR values predicted by the OLS model are significantly lower than the measured values is in the central west, with sporadic GrIS proximal hotspots in the central west. Some ice sheet distal watersheds of underestimation are also seen in the north. Interestingly, the north and central east (though more ice sheet distally) show watersheds of over-estimation. Though not particularly visible due to the small size of watersheds in the region, the south east shows notable clustering of watersheds where the model underestimates SDR, showing observed values here are generally higher than expected.

The calculated Moran's Index of 0.0027, although seemingly small in magnitude, is slightly higher than the Expected Index of -0.00052. This suggests a minor degree of spatial autocorrelation in the residuals, indicating that there are some spatial patterns present in the differences between observed and predicted SDR values. This deviation suggests a slight positive spatial autocorrelation, implying that nearby areas have similar residual values, more than would be expected if the residuals were randomly distributed (with a max search distance of ~32km reported). Essentially, the model's residuals are not independent of one another but instead exhibit a systematic spatial

pattern. The P-value of the Moran's I is 0.02 (less than 0.05) and corresponds to a z-score of 9.7, which is fairly high. This spatial autocorrelation of residuals provides compelling evidence that the observed spatial pattern is highly unlikely to be a result of random chance. This indicates that the model may be missing key explanatory variables with a spatial structure or that the relationships modelled exhibit spatial variability (non-stationarity).

Analysis of the residuals also indicated deviations from normality and heterogeneity of variances, as the Shapiro-Wilk test for normality and Levene's test for homogeneity of variances both indicated significant deviations. These findings imply that the residuals are not normally distributed and that the variances are not homogeneous across the groups. The R^2 value of 0.62 suggests that the Index of Connectivity (IC) partially explains the distribution of sediment delivery ratios (SDR). However, the spatial autocorrelation of residuals indicates that additional external variables also influence this distribution. These variables and their potential impact will be explored further in the following section, providing avenues for future research.

5.4 Discussion

This discussion delves into the multifaceted nature of Greenland's proglacial landscape connectivity and sediment dynamics, exploring the implications of the Index of Connectivity (IC) and Sediment Delivery Ratio (SDR) across various watersheds as observed here. The analysis, grounded in comprehensive regional and watershed level assessments as well as spatially distributed modelling, sheds light on the intricate interplay between hydrological processes, sediment transport, and structural connectivity assessments as a predictor of functional measures, particularly in the context of glacial influence and lake interactions. This work is the first national scale assessment of IC and, by computing SDR at the catchment scale, the first to compare the predictive capabilities of IC at this scale, grounded in the highest resolution hydrological analysis of Greenland's proglacial catchments to date.

5.4.1 Hydrological Analysis: relevance and implications

The hydrological processing outlined in section 5.2.2 of this chapter was conducted out of necessity for the following analysis. As the IC algorithms utilise the same input elevation data, the stream networks, coastal outlets, and watersheds must also be resolved using the same data for the highest IC accuracy. It was therefore not feasible to leverage the lower-resolution existing datasets, such as those of Mankoff et al. (2020).

The spatial distribution and mobilisation of sediment is most accurately resolved with the highest resolution data possible. The computational cost and national scale of the analysis allowed relatively accurate extraction of structural connectivity at the given 32m resolution, as evidenced through examination of the spatially distributed index at the watershed scale and its ability to predict measured functional connectivity at the national scale. IC values have been found to show a systematic decrease when considering higher-resolution data and extracted hydrological variables (Brardinoni et al., 2015; Cantreul et al., 2018; Cavalli et al., 2020). This is likely due to finer-scale landforms and features which impede connectivity but are systematically lost with upscaling resolution. The datasets produced here may serve as a crucial resource for a range of disciplines, including hydrology, geomorphology, ecology, and climatology. A significant advantage of these datasets is their adaptability. The flow direction and accumulation datasets can be leveraged to meet specific user-end requirements, extracting more or less detailed stream networks from the data to meet requirements. This makes the hydrological analysis and data, produced as requisite for the further IC analysis within, a versatile tool for various research and practical applications. Whether for detailed local studies or broader regional assessments, the data can be tailored to suit diverse needs.

5.4.2 Spatial distributions of IC and SDR

The spatially distributed IC, when calculated at the national scale using relatively coarse resolution data compared to traditional catchment level studies, emerges as a potent indicator of landscape units' connectedness to specific targets, such as coastal waters. The maximum IC value reported across Greenland is 4.12 (both with and without lakes as sinks). The minimum value without lakes as sinks is -8.0, and with lakes as sinks -15.5. This measure of connectedness is not merely a measure of physical proximity but an embodiment of the dynamic interplay between various landscape and climatological elements and the resultant pathways for sediment and nutrient flow (Lane et al., 2017; Overeem et al., 2017). The regional variability in IC, as elucidated through boxplots in Figures 5.7 and 5.8, reveals a compelling narrative, particularly concerning the effect of lakes. The median IC by watershed regionally is notably lowest in general in the north, however when lakes are considered as sinks this is superseded by both the south west and central west. The occurrence of lakes is far greater in these regions, and when coupled with the larger proglacial areas in these regions it is not surprising that landscapes are on average relatively poorly connected to coastlines. Table 5.3 below

shows the percentage of watersheds containing lakes per region as well as each regions average watershed area in km^2.

Interestingly, the north east has the highest percentage of watersheds with lakes and the second largest average area; however, when lakes are considered as sinks, it has the second highest median IC (Figure 5.7). Conversely, the south west has the second highest percentage of watersheds with lakes and the most negative IC when these lakes are considered as sinks, made more significant considering the average area of watersheds here is the third highest (Table 5.3). Smaller watersheds imply shorter travel distances for sediments to coastal outlets and thus higher IC given the Ddn component of the algorithm, suggesting that lakes do not uniformly impact connectivity.

Table 5.3 Percentage of watersheds which contain lakes and average watershed area in km^2 per region overall.

Region	Watersheds with lakes (%)	Average area km^2
North East	8.4	20.8
South West	7.6	13.9
North	7.5	23.7
Central East	7.4	15.7
North West	7.2	12.2
Central West	6.1	14.3
South East	4.4	5.9

Instead, their effect is modulated by regional characteristics, such as the constituents of proglacial landscapes, the relative location of lakes within the system, and other climatic variables not considered here. This includes precipitation, which, when falling as rainfall in summer, can facilitate greater erosion on hillslopes in regions experiencing higher average precipitation (e.g., Masselink et al., 2016; Zanandrea et al., 2021). Coincidentally, rainfall in Greenland is most pronounced in the south west, as observed throughout the late 20th and early 21st century (Huai et al., 2021; Huai et al., 2022). There are numerous watersheds in the west and south west, as shown in Figure 5.11, where, based on the OLS model, IC in isolation underestimates SDR.

It may be that increased rainfall in this region is driving local hillslope erosion rates to be expedited and, when coupled with coincident rainfall and meltwater-driven river discharges, sediment is more efficiently evacuated than the geomorphological IC

predicts in isolation (Shen et al., 2016). Moreover, increased rainfall, compared to snowmelt, has a more direct influence on sediment availability and peak flow. While snowmelt corresponds to higher river discharges, its action has a lower potential for sediment mobilisation than rainfall (Lamhonwah et al., 2017). Furthermore, permafrost thaw has been shown to influence erosion dynamics via slope disturbances, with the most disturbed watersheds contributing to greater heterogeneity of erosion on the landscape (Lamoureux et al., 2014). Changing permafrost conditions and thaw manifest as various thermokarst forms (French and Thorn, 2006; French, 2017) or physical events like mass movement and enhanced erosion (Rudy et al., 2017). These disturbances often take the form of thermo-erosional gullies and, particularly on steeper slopes, active layer detachments (Lafrenière and Lamoureux, 2019). Daanen et al. (2011) indicate that the southern tip of Greenland is largely devoid of permafrost, but high thaw potential regions exist in the south and central west, and central to the north east. This corresponds to clusters of watersheds where the OLS model overestimates SDR, suggesting that permafrost-related erosion in these catchments is not coinciding with effective removal from these systems.

There are no existing prior studies of connectivity in Greenland with which to compare these results. However, Overeem et al. (2017) utilised satellite imagery to produce estimates of suspended sediment concentration in 160 proglacial rivers across Greenland. By combining these estimated suspended sediment concentrations with numerical calculations of meltwater expulsion, Overeem et al. (2017) spatially mapped patterns of export for a distributed array of sites around Greenland, with the majority of results in the south and central west and central and north east. Covering the period 1999 to 2003, they identified notable hotspots of suspended sediment concentrations greater than 3,000 mg l-1 in and around Kangerlussuaq, for watersheds where this research reports average and low relative IC (-4 to -6). Similarly, SDRs in this region are relatively low (-0.6 to -1), specifically from proglacial catchments. However, for more GrIS distal hotspots identified by Overeem in the south west, this research reports higher SDR (0.4 to 0.8). This is interpreted to be a dominant input from ice sheet meltwater with relatively short flow routes to fjord outlets.

Where the IC and SDR measured in this research are relatively low, the suspended sediment measured by Overeem is nearly completely sourced from subglacial sources not reflected in either metric measured here. This aligns with the conclusion of Overeem, citing accelerated meltwater activity and larger proglacial river area during

the study period in these rivers. Hasholt et al. (2018) report notably high sediment and solute concentrations in the Watson and Umivit rivers, large rivers that drain from the Russel glacier area of the GrIS and have relatively short flow paths between the ice sheet and Kangerlussuaq Fjord. Hasholt et al. (2018) attribute most sediment in the rivers to direct glacier input. While the IC and SDR are generally good measures of catchment sediment sourcing and removal on hillslopes, for small watersheds with single well-connected flow paths from the glaciers to targets (as previously reported for glaciated catchments (Micheletti and Lane, 2016)), these metrics do not adequately correspond to measured sediment concentrations in rivers and at outlets.

Hasholt (1996) found, in a review synthesising measurements of sediment concentrations in Greenlandic rivers, that for locations with glaciers near to coasts and with water courses with a 'significant' glacierised area contribution, sediment concentrations ranged from 50 to 20,000 mg l-1. Yet, for catchments with minimal or no glacier contribution, concentrations are mostly less than 100 mg l-1 and regularly less than 20 mg l-1. This would indicate why IC and SDR findings measured from small proglacial areas fed by large ice sheet outlets do not correspond with Overeem et al.'s (2017) measured hotspots of sediment export. Overeem et al. (2017) identify less pronounced suspended sediment concentration hotspots of 2,000 to 3,000 mg l-1, which are more spatially distributed around Greenland's periphery, with a number in central and north east Greenland. These findings closely correspond with watersheds where this research finds relatively high SDR (0.4 to 0.8) and average to high IC (-5 to -2), particularly where lakes are not modelled as sinks.

Bendixen et al. (2017) report substantial and extensive delta progradation in south west Greenland between the 1980s and the 2010s, roughly the same period over which SDRs are calculated here. These regions of delta progradation correspond to some of the most negative SDR (-0.8 to -1) catchments reported here. One cause of this apparent discrepancy between observed widespread delta deposition in the vicinity of catchments with highly negative delivery ratios where apparently more material is deposited in the catchment than removed is related to phenomena outlined above, whereby the catchments measured here are not closed systems to input sediment due to glacier influence. Subglacially sourced sediment is introduced to the proglacial catchments, effectively transported to the coasts and fjords then deposited within the fans. Delta progradation is also reported in Sondre Mellemland, NE Greenland by (Carrivick and Tweed, 2021), another catchment with a relatively low SDR measured here. Hasholt et

al. (2018) find that the increase in meltwater-transported sediments from glaciers explains the delta progradation around Greenland, a phenomena contradictory to delta erosion found elsewhere in the Arctic (Bendixen et al., 2017). An intriguing feature of glacier-fed watersheds is their being open systems, receiving sediment input from glaciers as well as export to fjords. In scenarios where negative sediment delivery ratios are observed, these catchments exhibit signs of poor functional connectivity, with more sediment being discharged into and deposited within proglacial systems than is removed. Another source contributing to negative SDR values may not be linked to accretion but vegetation growth during the study period, as the input elevation data are digital elevation models rather than surface models which attempt to remove vegetation from the signal. This is explored further in the main thesis discussion (Chapter 6).

There are regions and locations shown in Figure 5.11 where IC notably over and under estimates SDR based on the reported OLS model. The R^2 of 0.62 and moderate spatial autocorrelation of residuals indicates that, though at a watershed scale IC can explain most of the variation in normalised SDR, other variables not measured here contribute to the regional distributions observed. This is particularly the case where residual values are high and low, reflecting under and over-estimation by the model respectively. Some potential explanations for this have been explored in this section, however, the results from the earlier chapters in this thesis may also indicate future avenues of exploration to explain the model's performance in some watersheds. These are explored in the overall thesis discussion (Chapter 6).

5.4.3 Lakes implications for connectivity now and in future

This study finds that for catchments containing lakes, assuming they are a net sink for suspended sediment leads to a marked reduction in average connectivity for these watersheds. A substantial proportion of the lakes in this study, however, are ice-contact, a factor not fully captured in these connectivity estimates, which may affect the overall connectivity results.. The formation and growth of proglacial ice-contact lakes is expected to increase with ongoing climate change (Carrivick and Tweed, 2013; Carrivick and Tweed, 2016; Carrivick and Tweed, 2021; Carrivick et al., 2022). It is likely that, within catchments, the IC as calculated with lakes as sinks more closely represents the connectedness of hillslopes and glaciers in the lake's contributing areas (Carrivick and Tweed, 2013; Bogen et al., 2015; Lane et al., 2017). Carrivick and Tweed (2021) suggest that lakes and increasing lake formation in proglacial catchments may reduce connectivity to the extent that they offset the potential increases in connectivity

of hillslopes and smaller tributary streams caused by increased channel formation, sediment mobility, and freshwater availability in these areas. Carrivick et al. (2022) identify that presently ice-marginal lakes occupy 10% of the GrIS margin and 5% of PGIC, with a predicted increase of ~ 7,404 km^2, stressing the importance of these features in future models of ice retreat. The work produced here provides further evidence for the consideration of these growing proglacial lakes, as underrepresented in this study yet proven to have a large effect on downstream connectivity and by extension nutrient delivery (Hopwood et al., 2020). Future research may seek to unravel the impact of these ice-contact lakes, particularly in terms of how they might starve downflow catchments and coastal waters of sediment. This consideration is crucial in understanding the broader ecological and geomorphological impacts of such systems.

While the IC with lakes considered as sinks offers useful insights when represented spatially as in Figure 5.5, and likely does reflect actual hillslope connectivity to outlets more effectively, this research shows it to be less useful for predicting functional connectivity (SDR) within the linear regression tests performed here. One reason for this is the structure of the analysis, considering connectivity to coasts only. Sediment eroded within the contributing area of a lake and deposited within said lake has not reached catchment outlets but will be measured as such within the SDR. The sediments sourced from lake contributing areas are eroded and deposited within the watershed, but within the lake and so are not represented by positive values in the DoD and accordingly SDR is over-estimated. The IC not considering lakes as sinks will therefore represent areas in lake contributing areas as connected to the coasts, and thus performs better at predicting watershed SDR. Future work may seek to extract watersheds identified here where lakes as sinks significantly reduce average IC and to produce spatially distributed SDR, delineating watersheds first to lakes and then from lakes onwards to coasts.

Some of the lakes identified in this study which are currently dramatically reducing catchments connectivity are ice-dammed. This phenomenon is particularly evident in Figure 5.6, where the middle panels (B) for the north of Greenland illustrate ice-dammed lakes capturing sediment from extensive contributing areas. The potential for catastrophic outbursts, analogous to events documented in other regions, raises concerns about the extensive sediment washing into the northern ocean, with long-lasting implications for local marine flora, fauna, and productivity (Grinsted et al., 2017; Carrivick and Tweed, 2019; Tomczyk et al., 2020). Essentially, these lakes may

catastrophically drain and wash much of this previously stored sediment into Fjords and coastal oceans rapidly. Forward modelling of glacier retreat for these regions may be able to predict timings for these events, and so post-event IC and SDR assessments may be compared with this research to define the proportion of deposited sediment within the watershed downstream of the lake.

The connotations of this research for nutrient delivery sourced from glaciers and catchments containing glaciers coincident with lakes are significant, particularly as paraglacially sourced sediment might dominate plumes now and in future where lakes occur and are predicted to form and expand in proglacial catchments (Micheletti and Lane, 2016; Lane et al., 2017; Carrivick and Tweed, 2021). This may then influence not just the physical landscape but also the biological systems reliant on these nutrient flows, a potential avenue of future research examining the measurement of sediment plume constituents for these catchments identified as having glacial and fluence and reduced IC by lake presence (Rysgaard et al., 1999; Hawkings et al., 2015; Mark J Hopwood et al., 2020).

5.5 Conclusions

This chapter conducts the first nationally consistent assessment of the Index of Connectivity (IC) and Sediment Delivery Ratio (SDR) in Greenland, whilst also assessing the performance of the structural connectivity measure (IC) as a predictor of SDR, a measure of functional connectivity. The comprehensive regional and watershed-level analysis, grounded in high-resolution hydrological data, has illuminated the complex interplay between hydrological processes, sediment transport, and connectivity assessments in Greenland's proglacial landscape. Notably, the data employed significantly proved that national assessments of structural connectivity with relatively coarse topographic data have predictive capabilities of measured sediment redistribution.

On aggregate, watersheds in the central and north east of Greenland have the highest average watershed structural connectivity, whilst watersheds in the central and south west have the lowest. When only those watersheds containing glaciers are considered, watersheds in the north are found to have the lowest average IC, whereas the central east consistently has higher average IC values, both considering lakes as sinks and not. Greenland's diverse watersheds indicate that landscape connectedness to coastal waters varies significantly, influenced by regional characteristics and the presence of lakes.

This is assessed by computing the index of connectivity both explicitly casting lakes as sinks in the model, and not. Particularly, the lakes' role as sediment sinks markedly affect connectivity, with their impact modulated by regional landscape constituents including the location of lakes, catchment size, and most likely unmeasured climatic variables like precipitation. Interestingly, in areas with high glacier influence, IC and SDR measurements diverge from observed relative sediment concentrations reported for proglacial rivers (Hasholt, 1996; Overeem et al., 2017; Hasholt et al., 2018), suggesting the need for further investigation into glacier-fed proglacial watersheds as open systems, receiving subglacial sediment and evacuating both glacigenic and hillslope derived sediments.

The study's findings underscore the profound implications of proglacial lakes on sediment connectivity. The growth of proglacial lakes, anticipated to increase with ongoing climate change (Carrivick et al., 2022), necessitates future research to understand their impact on sediment and nutrient delivery. The spatially distributed SDRs, particularly in catchments significantly affected by lakes, highlight the dynamic nature of sediment transport in these evolving landscapes.

In summary, this research provides crucial insights into Greenland's sediment connectivity, offering a foundation for future studies and practical applications across various disciplines. As Greenland continues to experience climatic and geomorphological changes, understanding the nuanced interplay of forces shaping sediment connectivity in the transient proglacial landscapes is paramount for predicting and managing the ecological and geomorphological impacts of these changes.

5.6 Chapter 5 References

Bach, E., RadiĆ, V. and Schoof, C. 2018. How sensitive are mountain glaciers to climate change? Insights from a block model. *Journal of Glaciology*. **64**(244), pp.247–258.

Ballantyne, C.K. 2002a. A general model of paraglacial landscape response. *Holocene*. **12**(3), pp.371–376.

Ballantyne, C.K. 2002b. Paraglacial geomorphology. *Quaternary Science Reviews*. **21**(18–19), pp.1935–2017.

Band, L.E., 1986. Topographic partition of watersheds with digital elevation models. Water resources research, 22(1), pp.15-24.

Bendixen, M., Lonsmann Iversen, L., Anker Bjork, A., Elberling, B., Westergaard-Nielsen, A., Overeem, I., Barnhart, K.R., Abbas Khan, S., Box, J.E., Abermann, J., Langley, K. and Kroon, A. 2017. Delta progradation in Greenland driven by increasing glacial mass loss. *Nature*. **550**(7674), pp.101–104.

Bogen, J., Xu, M. and Kennie, P. 2015. The impact of pro-glacial lakes on downstream sediment delivery in Norway. *Earth Surface Processes and Landforms*. **40**(7).

Borselli, L., Cassi, P. and Torri, D. 2008. Prolegomena to sediment and flow connectivity in the landscape: A GIS and field numerical assessment. *Catena*. **75**(3), pp.268–277.

Box, J.E., Colgan, W.T., Christensen, T.R., Schmidt, N.M., Lund, M., Parmentier, F.J.W., Brown, R., Bhatt, U.S., Euskirchen, E.S., Romanovsky, V.E., Walsh, J.E., Overland, J.E., Wang, M., Corell, R.W., Meier, W.N., Wouters, B., Mernild, S., Mård, J., Pawlak, J. and Olsen, M.S. 2019. Key indicators of Arctic climate change: 1971-2017. *Environmental Research Letters*. **14**(4).

Bracken, L.J., Turnbull, L., Wainwright, J. and Bogaart, P. 2015. Sediment connectivity: a framework for understanding sediment transfer at multiple scales. *Earth Surface Processes and Landforms*. **40**(2), pp.177–188.

Brardinoni, F., Cavalli, M., Heckmann, T., Liébault, F. and Rimböck, A. 2015. Guidelines for assessing sediment dynamics in alpine basins and channel reaches-WP4 Basin-scale Sediment Dynamics.

Cantreul, V., Bielders, C., Calsamiglia, A. and Degré, A., 2018. How pixel size affects a sediment connectivity index in central Belgium. Earth Surface Processes and Landforms, 43(4), pp.884-893.

Carrivick, J.L. and Heckmann, T. 2017. Short-term geomorphological evolution of proglacial systems. *Geomorphology*. **287**, pp.3–28.

Carrivick, J.L., How, P., Lea, J.M., Sutherland, J.L., Grimes, M., Tweed, F.S., Cornford, S., Quincey, D.J. and Mallalieu, J. 2022. Ice-marginal proglacial lakes across Greenland: Present status and a possible future. *Geophysical Research Letters*. **49**(12), e2022GL099276.

Carrivick, J.L. and Tweed, F.S. 2016. A global assessment of the societal impacts of glacier outburst floods. *Global and Planetary Change*. **144**.

Carrivick, J.L. and Tweed, F.S. 2019. A review of glacier outburst floods in Iceland and Greenland with a megafloods perspective. *Earth-Science Reviews*. **196**.

Carrivick, J.L. and Tweed, F.S. 2021. Deglaciation controls on sediment yield: Towards capturing spatio-temporal variability. *Earth-Science Reviews*. **221**.

Carrivick, J.L. and Tweed, F.S. 2013. Proglacial lakes: character, behaviour and geological importance. *Quaternary Science Reviews*. **78**, pp.34–52.

Carrivick, J.L., Tweed, F.S., Ng, F., Quincey, D.J., Mallalieu, J., Ingeman-Nielsen, T., Mikkelsen, A.B., Palmer, S.J., Yde, J.C., Homer, R., Russell, A.J. and Hubbard, A. 2017. Ice-dammed lake drainage evolution at russell glacier, west greenland. *Frontiers in Earth Science*. **5**.

Cavalli, M., Crema, S. and Marchi, L. 2020. Structural sediment connectivity assessment through a geomorphometric approach : review of recent applications. *Proceedings of the Geomorphometry 2020 Conference*. (July).

Cavalli, M. and Marchi, L. 2008. Characterisation of the surface morphology of an alpine alluvial fan using airborne LiDAR. *Natural Hazards and Earth System Sciences*. **8**(2), pp.323–333.

Cavalli, M., Trevisani, S., Comiti, F. and Marchi, L. 2013. Geomorphometric assessment of spatial sediment connectivity in small Alpine catchments. *Geomorphology*. **188**, pp.31–41.

Cavalli, M., Trevisani, S., Goldin, B., Mion, E., Crema, S. and Valentinotti, R. 2013. Semi-automatic derivation of channel network from a high-resolution DTM: The example of an italian alpine region. *European Journal of Remote Sensing*. **46**(1).

Chen, Y. 2016. Spatial autocorrelation approaches to testing residuals from least squares regression. *PLoS ONE*. **11**(1).

Christiansen, H.H. and Humlum, O. 2013. Glacial History and Periglacial Landforms of the Zackenberg area, Northeast Greenland: Preliminary results. *Geografisk Tidsskrift-Danish Journal of Geography*. **93**(1), pp.19–29.

Chymyrov, A. 2021. Comparison of different DEMs for hydrological studies in the mountainous areas. *Egyptian Journal of Remote Sensing and Space Science*. **24**(3).

Coulthard, T.J. and Van De Wiel, M.J. 2017. Modelling long term basin scale sediment connectivity, driven by spatial land use changes. *Geomorphology*. **277**, pp.265–281.

Crema, S. and Cavalli, M. 2018. SedInConnect: a stand-alone, free and open source tool for the assessment of sediment connectivity. *Computers & Geosciences*. **111**, pp.39–45.

Daanen, R.P., Ingeman-Nielsen, T., Marchenko, S.S., Romanovsky, V.E., Foged, N., Stendel, M., Christensen, J.H. and Hornbech Svendsen, K. 2011. Permafrost degradation risk zone assessment using simulation models. *Cryosphere*. **5**(4).

Dinno, A. 2015. Nonparametric pairwise multiple comparisons in independent groups using Dunn's test. *Stata Journal*. **15**(1).

Fowler, R.A., Osburn, C.L. and Saros, J.E. 2020. Climate-Driven Changes in Dissolved Organic Carbon and Water Clarity in Arctic Lakes of West Greenland. *Journal of Geophysical Research: Biogeosciences*. **125**(2).

French, H. and Thorn, C.E. 2006. The changing nature of periglacial geomorphology. *Geomorphologie-Relief Processus Environnement*. (3), pp.165–173.

French, H.M. 2017. Periglacial Climates *In*: *The Periglacial Environment 4e*.

Garbrecht, J. and Martz, L.W. 1997. The assignment of drainage direction over flat surfaces in raster digital elevation models. *Journal of Hydrology*. **193**(1–4).

Grinsted, A., Hvidberg, C.S., Campos, N. and Dahl-Jensen, D. 2017. Periodic outburst floods from an ice-dammed lake in East Greenland. *Scientific Reports*. **7**(1).

Gruber, S. and Peckham, S. 2009. *Land-surface parameters and objects in hydrology*.

Haeberli, W., Frauenfelder, R., Hoelzle, M. and Maisch, M. 1999. On rates and acceleration trends of global glacier mass changes. *Geografiska Annaler Series a-Physical Geography*. **81a**(4), pp.585–591.

Hamilton, L., Lyster, P. and Otterstad, O. 2000. Social change, ecology and climate in 20th-century Greenland. *Climatic Change*. **47**(1–2).

Hasholt, B. 1996. Sediment transport in Greenland. *IAHS-AISH Publication*. **236**.

Hasholt, B., van As, D., Mikkelsen, A.B., Mernild, S.H. and Yde, J.C. 2018. Observed sediment and solute transport from the Kangerlussuaq sector of the Greenland Ice Sheet (2006–2016). *Arctic, Antarctic, and Alpine Research*. **50**(1).

Hawkings, J.R., Wadham, J.L., Tranter, M., Lawson, E., Sole, A., Cowton, T., Tedstone, A.J., Bartholomew, I., Nienow, P., Chandler, D. and Telling, J. 2015. The effect of warming climate on nutrient and solute export from the Greenland Ice Sheet. *Geochemical Perspectives Letters*. **1**(1), pp.94–104.

Heckmann, T., Cavalli, M., Cerdan, O., Foerster, S., Javaux, M., Lode, E., Smetanová, A., Vericat, D. and Brardinoni, F. 2018. Indices of sediment connectivity: opportunities, challenges and limitations. *Earth-Science Reviews*. **187**, pp.77–108.

Heckmann, T. and Vericat, D. 2018. Computing spatially distributed sediment delivery ratios: inferring functional sediment connectivity from repeat high-resolution digital elevation models. *Earth Surface Processes and Landforms*. **43**(7), pp.1547–1554.

Hopwood, Mark J, Carroll, D., Dunse, T., Hodson, A., Holding, J.M., Iriarte, J.L., Ribeiro, S., Achterberg, E.P., Cantoni, C. and Carlson, D.F. 2020. How does glacier discharge affect marine biogeochemistry and primary production in the Arctic? *The Cryosphere*. **14**(4), pp.1347–1383.

Hopwood, Mark J., Carroll, D., Dunse, T., Hodson, A., Holding, J.M., Iriarte, J.L., Ribeiro, S., Achterberg, E.P., Cantoni, C., Carlson, D.F., Chierici, M., Clarke, J.S., Cozzi, S., Fransson, A., Juul-Pedersen, T., Winding, M.H.S. and Meire, L. 2020. Review article: How does glacier discharge affect marine biogeochemistry and primary production in the Arctic? *Cryosphere*. **14**(4).

Horton, R.E. 1945. Erosional development of streams and their drainage basins; Hydrophysical approach to quantitative morphology. *Bulletin of the Geological Society of America*. **56**(3).

Howat, I.M., Negrete, A. and Smith, B.E. 2014. The Greenland Ice Mapping Project (GIMP) land classification and surface elevation data sets. *Cryosphere*. **8**(4), pp.1509–1518.

Huai, B., Van Den Broeke, M.R., Reijmer, C.H. and Cappellen, J. 2021. Quantifying rainfall in greenland: A combined observational and modeling approach. *Journal of Applied Meteorology and Climatology*. **60**(8).

Huai, B., van den Broeke, M.R., Reijmer, C.H. and Noël, B. 2022. A Daily 1-km Resolution Greenland Rainfall Climatology (1958–2020) From Statistical Downscaling of a Regional Atmospheric Climate Model. *Journal of Geophysical Research: Atmospheres*. **127**(17).

Johansson, E., Berglund, S., Lindborg, T., Petrone, J., Van As, D., Gustafsson, L.G., Näslund, J.O. and Laudon, H. 2015. Hydrological and meteorological investigations in a periglacial lake catchment near Kangerlussuaq, west Greenland - Presentation of a new multi-parameter data set. *Earth System Science Data*. **7**(1).

Knight, J. and Harrison, S. 2014. Mountain Glacial and Paraglacial Environments under Global Climate Change: Lessons from the Past, Future Directions and Policy Implications. *Geografiska Annaler Series a-Physical Geography*. **96**(3), pp.245–264.

Knight, J. and Harrison, S. 2009. Periglacial and paraglacial environments: a view from the past into the future. *Periglacial and Paraglacial Processes and Environments*. **320**, pp.1–4.

Lafrenière, M.J. and Lamoureux, S.F. 2019. Effects of changing permafrost conditions on hydrological processes and fluvial fluxes. *Earth-Science Reviews*. **191**.

Lamhonwah, D., Lafrenière, M.J., Lamoureux, S.F. and Wolfe, B.B. 2017. Evaluating the hydrological and hydrochemical responses of a High Arctic catchment during an exceptionally warm summer. *Hydrological Processes*. **31**(12).

Lamoureux, S.F., Lafrenière, M.J. and Favaro, E.A. 2014. Erosion dynamics following localized permafrost slope disturbances. *Geophysical Research Letters*. **41**(15).

Lane, S.N., Bakker, M., Gabbud, C., Micheletti, N. and Saugy, J.N. 2017. Sediment export, transient landscape response and catchment-scale connectivity following rapid climate warming and Alpine glacier recession. *Geomorphology*. **277**, pp.210–227.

Lewis, S.M. and Smith, L.C. 2009. Hydrologic drainage of the Greenland Ice Sheet. *Hydrological Processes*. **23**(14).

Mancini, D. and Lane, S.N. 2020. Changes in sediment connectivity following glacial debuttressing in an Alpine valley system. *Geomorphology*. **352**.

Mankoff, K.D., Noël, B., Fettweis, X., Ahlstrøm, A.P., Colgan, W., Kondo, K., Langley, K., Sugiyama, S., Van As, D. and Fausto, R.S. 2020. Greenland liquid water discharge from 1958 through 2019. *Earth System Science Data*. **12**(4).

Masselink, R.J.H., Keesstra, S.D., Temme, A.J.A.M., Seeger, M., Giménez, R. and Casalí, J. 2016. Modelling Discharge and Sediment Yield at Catchment Scale Using Connectivity Components. *Land Degradation and Development*. **27**(4).

Masson-Delmotte, V., Swingedouw, D., Landais, A., Seidenkrantz, M.S., Gauthier, E., Bichet, V., Massa, C., Perren, B., Jomelli, V., Adalgeirsdottir, G., Hesselbjerg Christensen, J., Arneborg, J., Bhatt, U., Walker, D.A., Elberling, B., Gillet-Chaulet, F., Ritz, C., Gallée, H., van den Broeke, M., Fettweis, X., de Vernal, A. and Vinther, B. 2012. Greenland climate change: From the past to the future. *Wiley Interdisciplinary Reviews: Climate Change*. **3**(5), pp.427–449.

Matsuoka, N. 2010. Solifluction and Mudflow on a Limestone Periglacial Slope in the Swiss Alps: 14 Years of Monitoring. *Permafrost and Periglacial Processes*. **21**(3), pp.219–240.

Mercier, D. 2008. Paraglacial and paraperiglacial landsystems: concepts, temporal scales and spatial distribution. *Geomorphologie-Relief Processus Environnement*. (4), pp.223–233.

Mercier, D. and Etienne, S. 2008. Paraglacial geomorphology: Processes and paraglacial context. *Geomorphology*. **95**(1–2), pp.1–2.

Micheletti, N. and Lane, S.N. 2016. Water yield and sediment export in small, partially glaciated Alpine watersheds in a warming climate. *Water Resources Research*. **52**(6).

Najafi, S., Dragovich, D., Heckmann, T. and Sadeghi, S.H. 2021. Sediment connectivity concepts and approaches. *Catena*. **196**.

O'Callaghan, J.F. and Mark, D.M. 1984. The extraction of drainage networks from digital elevation data. *Computer Vision, Graphics, & Image Processing*. **28**(3).

Oksman, M., Kvorning, A.B., Larsen, S.H., Kjeldsen, K.K., Mankoff, K.D., Colgan, W., Andersen, T.J., Nørgaard-Pedersen, N., Seidenkrantz, M.S., Mikkelsen, N. and Ribeiro, S. 2022. Impact of freshwater runoff from the southwest Greenland Ice Sheet on fjord productivity since the late 19th century. *Cryosphere*. **16**(6).

Overeem, I., Hudson, B.D., Syvitski, J.P.M., Mikkelsen, A.B., Hasholt, B., van den Broeke, M.R., Noël, B.P.Y. and Morlighem, M. 2017. Substantial export of suspended sediment to the global oceans from glacial erosion in Greenland. *Nature Geoscience*. **10**(11), pp.859–863.

Peucker, T.K. and Douglas, D.H. 1975. Detection of Surface-Specific Points by Local Parallel Processing of Discrete Terrain Elevation Data. *Computer Graphics and Image Processing*. **4**(4).

Porter, C., Morin, P., Howat, I., Noh, M.-J., Bates, B., Peterman, K., Keesey, S., Schlenk, M., Gardiner, J., Tomko, K., Willis, M., Kelleher, C., Cloutier, M., Husby, E., Foga, S., Nakamura, H., Platson, M., Wethington, Michael, Jr., Williamson, C., Bauer, G., Enos, J., Arnold, G., Kramer, W., Becker, P., Doshi, A., D'Souza, C., Cummens, P., Laurier, F. and Bojesen, M. 2023. ArcticDEM - Mosaic, Version 4.1. *Harvard Dataverse, V1*. [Online]. [Accessed 21 November 2023]. Available from: https://doi.org/10.7910/DVN/3VDC4W.

Renard, K., Foster, G., Weesies, G., McCool, D. and Yoder, D. 1997. Predicting soil erosion by water: a guide to conservation planning with the Revised Universal Soil Loss Equation (RUSLE). *Agricultural Handbook No. 703*.

Rudy, A.C.A., Lamoureux, S.F., Kokelj, S. V., Smith, I.R. and England, J.H. 2017. Accelerating Thermokarst Transforms Ice-Cored Terrain Triggering a Downstream Cascade to the Ocean. *Geophysical Research Letters*. **44**(21).

Rysgaard, S., Nielsen, T.G. and Hansen, B.W. 1999. Seasonal variation in nutrients, pelagic primary production and grazing in a high-Arctic coastal marine ecosystem, Young Sound, Northeast Greenland. *Marine Ecology Progress Series*. **179**, pp.13–25.

Rysgaard, S., Thamdrup, B., Risgaard-Petersen, N., Fossing, H., Berg, P., Christensen, P.B. and Dalsgaard, T. 1998. Seasonal carbon and nutrient mineralization in a high-Arctic coastal marine sediment, Young Sound, Northeast Greenland. *Marine Ecology Progress Series*. **175**.

Shen, H., Zheng, F., Wen, L., Han, Y. and Hu, W. 2016. Impacts of rainfall intensity and slope gradient on rill erosion processes at loessial hillslope. *Soil and Tillage Research*. **155**.

Shepherd, A., Ivins, E., Rignot, E., Smith, B., van den Broeke, M., Velicogna, I., Whitehouse, P., Briggs, K., Joughin, I., Krinner, G., Nowicki, S., Payne, T., Scambos, T., Schlegel, N., A, G., Agosta, C., Ahlstrøm, A., Babonis, G., Barletta, V.R., Bjørk, A.A., Blazquez, A., Bonin, J., Colgan, W., Csatho, B., Cullather, R., Engdahl, M.E., Felikson, D., Fettweis, X., Forsberg, R., Hogg, A.E., Gallee, H., Gardner, A., Gilbert, L., Gourmelen, N., Groh, A., Gunter, B., Hanna, E., Harig, C., Helm, V., Horvath, A., Horwath, M., Khan, S., Kjeldsen, K.K., Konrad, H., Langen, P.L., Lecavalier, B., Loomis, B., Luthcke, S., McMillan, M., Melini, D., Mernild, S., Mohajerani, Y., Moore, P., Mottram, R., Mouginot, J., Moyano, G., Muir, A., Nagler, T., Nield, G., Nilsson, J., Noël, B., Otosaka, I., Pattle, M.E., Peltier, W.R., Pie, N., Rietbroek, R., Rott, H., Sandberg Sørensen, L., Sasgen, I., Save, H., Scheuchl, B., Schrama, E., Schröder, L., Seo, K.W., Simonsen, S.B., Slater, T., Spada, G., Sutterley, T., Talpe, M., Tarasov, L., van de Berg, W.J., van der Wal, W., van Wessem, M., Vishwakarma, B.D., Wiese, D., Wilton, D., Wagner, T., Wouters, B. and Wuite, J. 2020. Mass balance of the Greenland Ice Sheet from 1992 to 2018. *Nature*. **579**(7798).

Slaymaker, O. 2011. Criteria to Distinguish Between Periglacial, Proglacial and Paraglacial Environments. *Quaestiones Geographicae*. **30**(1), pp.85–94.

Slaymaker, O. 2009. Proglacial, periglacial or paraglacial? *Periglacial and Paraglacial Processes and Environments*. **320**, pp.71–84.

Strahler, A.N. 1957. Quantitative analysis of watershed geomorphology. *Eos, Transactions American Geophysical Union*. **38**(6).

Tarboton, D.G. 1997. A new method for the determination of flow directions and upslope areas in grid digital elevation models. *Water Resources Research*. **33**(2), pp.309–319.

Tarboton, D.G., Schreuders, K.A.T., Watson, D.W. and Baker, M.E. 2009. Generalized terrain-based flow analysis of digital elevation models *In*: *18th World IMACS Congress and MODSIM 2009 - International Congress on Modelling and Simulation: Interfacing Modelling and Simulation with Mathematical and Computational Sciences, Proceedings*.

Tomczyk, A.M., Ewertowski, M.W. and Carrivick, J.L. 2020. Geomorphological impacts of a glacier lake outburst flood in the high arctic Zackenberg River, NE Greenland. *Journal of Hydrology*. **591**.

Trevisani, S. and Cavalli, M. 2016. Topography-based flow-directional roughness: Potential and challenges. *Earth Surface Dynamics*. **4**(2).

Vargha, A. and Delaney, H.D. 1998. The Kruskal-Wallis Test and Stochastic Homogeneity. *Journal of Educational and Behavioral Statistics*. **23**(2).

Wischmeier, W. and Smith, D. 1978. *Predicting rainfall erosion losses: a guide to conservation planning*.

Zanandrea, F., Michel, G.P., Kobiyama, M., Censi, G. and Abatti, B.H. 2021. Spatial-temporal assessment of water and sediment connectivity through a modified connectivity index in a subtropical mountainous catchment. *Catena*. **204**.

Zhang, L., Gove, J.H. and Heath, L.S. 2005. Spatial residual analysis of six modeling techniques. *Ecological Modelling*. **186**(2).

Chapter 6: Discussion

This thesis provides an in-depth analysis of the environmental changes occurring around Greenland's ice sheet peripheral proglacial landscapes over the past four decades. The first subsection of this discussion begins by summarising the main findings of each research chapter. The overarching aim of this thesis was to comprehensively analyse proglacial landscape evolution across Greenland over the past four decades, with specific emphasis on land cover alterations, glacier mass balance, and sediment connectivity. Accordingly, several research objectives were defined:

1) The first objective of this thesis was to conduct a quantitative analysis of landcover evolution, specifically to classify for two time periods, predominant geophysical landcover classes in Greenland and quantify change in landscape composition in response to climate change.
2) The second objective was an assessment of glacier mass balance, specifically to determine PGIC mass changes over a multi-decadal timescale.
3) The third research objective was to conduct a national-scale analysis of sediment connectivity, more specifically to produce the first nationally consistent index of connectivity for Greenland and to assess its utility in estimating catchment sediment delivery ratios.

The fourth overall aim was to synthesise the findings of the above objectives, and so in the second subsection of this discussion, the relationships between the reported landcover changes, glacier dynamics, and sediment connectivity are then dissected. This section aims to clarify how these factors apparently influence one another and contribute to the overall landscape alterations observed. By examining these interactions, the research sheds light on the complex mechanisms driving environmental change in Arctic regions such as Greenland.

Subsequently, this discussion positions the research conducted here within the existing body of literature by filling gaps in our understanding of Greenland's proglacial functioning. Each research chapter has already discussed and compared individual findings with wider literature. Therefore, this section offers comparisons with previous studies by highlighting specific influential themes and contributions across the three empirical chapters' findings, highlighting where the findings of this

thesis confirm, challenge, or add to current knowledge. Both the findings and datasets produced within this thesis may find utility within future academic research and wider policy and decision-making strategies. The research's methodology and findings provide a robust framework for future studies, offering a comprehensive baseline for ongoing monitoring efforts. These potential avenues of utility for this work are then discussed following the assessment of the work's position in existing literature.

The thesis findings have significant implications for future scientific research, but also for environmental management and policy in Greenland, particularly in understanding the effects of climate change. Accordingly, the discussion then explores the implications for future research. Areas are identified where further study is recommended, suggesting potential methods and approaches for upcoming work. The importance of continuous monitoring and analysis in this rapidly changing environment is emphasised, highlighting the need for adaptive and forward-thinking research strategies to keep pace with the evolving landscape. Finally, concluding marks are made by providing an overall summary of the thesis.

6.1 Overview of Findings

To provide context for the subsequent synthesis of results, this section endeavours to give an overview of the findings garnered from each of the preceding research chapters undertaken within this thesis. The overarching theme of which was to methodically examine the multifaceted dynamics, composition and functioning of Greenland's proglacial systems over the past four decades at a consistent spatial scale and resolution.

6.1.1 Landcover Change in Greenland since the 1980s

The first research chapter quantified and analysed patterns of landcover change within Greenland, a narrative intrinsically linked to the overarching theme of climate change. This analysis not only sheds light on the dominant spatial and temporal variability of vegetative and non-vegetative cover, but also underscores the profound impact of climatic alterations across various terrestrial systems and geophysical processes.

In summary, the work conducted here elucidates the complex dynamics of landcover changes in Greenland since the late 1980s, revealing a substantial -28,707 km² (± 9,767 km²) reduction in the ice sheet margin and PGIC. This loss, primarily converted into barren ground like bedrock and coarse sediment, has profound implications, contributing to global sea level rise and affecting regional hydrological and ecological systems. Notably, ice loss has been particularly pronounced in the north and south west of Greenland, with the greatest local losses reaching up to -22% of change vector polygons in certain areas. Meltwater and freshwater areas have shown spatially heterogeneous changes with a 15% (± 15%) increase in meltwater occurrence, particularly in the south west and north east, indicating enhanced river discharge and associated coastal sediment plumes. Conversely, a -11% (± 22%) decrease in freshwater areas is observed, largely attributed to permafrost degradation and episodic fluxes from glacial lake drainages. These alterations in water bodies significantly affect the local and regional ecosystems, influencing sea surface temperature, salinity, and nutrient dynamics. Barren ground classes, notably bedrock and coarse sediment, have undergone spatially varied changes. While the net change in coarse sediment is relatively small, there has been a significant -16% (± 4%) decrease in exposed bedrock, attributed to the encroachment and growth of vegetation due to warming temperatures. This shift has led to increased vegetation cover across Greenland by 111% (± 12%), with significant increases particularly in the south west, east, and north east regions. The expansion of wet/dense vegetation, including in areas like Shannon Island, indicates wetland development and a potential increase in greenhouse gas emissions due to permafrost thaw. Intriguingly, fine sediment coverage across Greenland has seen a marginal overall increase of 4% (± 13%), with localised losses in the south west near Kangerlussuaq. These changes in sediment are closely linked to land degradation, glacial meltwater action, and increased sediment mobility, reflecting broader geomorphological processes at play.

To relate these landcover changes to climate warming, regression analyses were conducted. However, traditional methods like Ordinary Least Squared (OLS) correlations indicated a non-parametric relationship, suggesting that average temperature increase is not a straightforward indicator of landcover change. This is particularly true when temperatures fluctuate around crucial thresholds like 0 °C, where a few degrees' difference could mean the transition between frozen and

thawed states. Consequently, this research devised a set of climate warming variables known as the Difference in Degree Days Above Temperature (DDDAT) to capture these crucial threshold effects more accurately. Geographically Weighted Regression (GWR) was employed to accommodate the spatial non-stationarity of climate data and the inherent spatial autocorrelation. The regression results show the closest associations between climate change and landcover changes, particularly for vegetation, bedrock, and ice classes. Notably, the highest R^2 and Akaike information criterion values across all landcover classes are found for the difference in the number of days above the 6°C threshold, indicating that regions experiencing a rapid increase in the number of warm days per year are likely to undergo marked and accelerated landcover changes.

The final output of this chapter was to integrate the regional patterns of class change, specific inter-class transitions, and associated processes, all in the context of the increasing number of days over 6°C, into a comprehensive conceptual transition model for Greenland's landcover phase changes. A notable finding from this model is the distinct latitudinal pattern of predominant landcover inter-class changes between the east and west coasts of Greenland. This difference is likely attributable to the size of proglacial areas, which are larger on the west coast in the south, and on the east coast in the north. Also, the topographic relief differences are considerable, which is more subdued in the west, facilitating regolith and tundra vegetation establishment. Furthermore, climatic changes experienced by the two coasts have differed, influenced by factors such as the North Atlantic Oscillation and the Atlantic Meridional Overturning Circulation, particularly affecting the east coast. In essence, this comprehensive model not only delineates the regional and latitudinal variations in landcover transitions across Greenland but also contextualises these changes within the broader framework of climatic influences, particularly the increasing warmth signified by more days over 6°C.

6.1.2 Peripheral Glacier and Ice Cap Mass Balance Change Since the late 1970s

Following on from the landcover change assessment summarised above, the focus shifts to the peripheral glaciers and ice caps (PGIC), where the second research chapter provides an in-depth examination of their mass balance changes and the first Greenland-wide 30m resolution quantification of up to ~40 years of glacier elevation

change. This was made possible by leveraging the AeroDEM dataset of Korsgaard et al. (2016), and overcoming widespread glacier accumulation area data errors by restricting analysis to glacier's calculated ablation areas. PGIC were considered regionally, as well as being further dissected by their terminus type (lake, marine, terrestrial), behaviour (surge or non-surge), and surface characteristics (debris cover), offering insights into their current state and future trajectories. This work is placed in context and compared with other existing studies of PGIC mass change in Greenland over varying timescales.

In summary, this research reports a substantial ice loss of at least 276 Gt, equivalent to a 0.76 mm rise in global sea level from Greenland's PGIC since 1978. During this period, all regions around Greenland experienced negative mass balance rates, with a median rate across the PGICs of -0.1 ± 0.02 m w.e. yr^{-1}. The research revealed that PGICs on the west of Greenland have suffered more negative mass balances compared to those on the east. There's a clear latitudinal trend, with the mean mass balance becoming less negative towards the north. North Greenland exhibits the least negative median mass balance of -0.05 ± 0.02 m w.e. yr^{-1}. Spatial distribution maps of mass balance rates for three distinct periods (*T0, T1*, and *T2*) were created, showing variations and highlighting areas of accelerating mass loss. Hotspots of increased negative glacier mass balance were identified in the west and south, with the south west and central west regions of Greenland experiencing the most substantial increases in mass loss rates. In contrast, the south east region showed a notable decrease in mass loss rates.

Moreover, this research explores the mass balance trends of Greenland's PGICs based on their characteristics such as terminus type, behaviour, and debris cover. The study reveals that mass balance during the total study period (*T0*) varies significantly depending on these glacier attributes, with distinct patterns emerging nationally and across regions. Box plots for each of the six terminus-surface character combinations show that glaciers terminating in lakes with debris-covered surfaces exhibit the most negative mass balance (-0.15 ± 0.02 m w.e. yr^{-1}), followed by marine-debris, lake-clean, land-debris, land-clean, and marine-clean glaciers. Overall, debris-covered PGICs across all regions tend to have more negative mass balances compared to clean surface glaciers. Water-terminating glaciers (both in lakes and oceans) also generally exhibit more negative mass balances than land-terminating glaciers, with

lake-terminating glaciers showing the most negative balances. Additionally, water-terminating glaciers display greater variation in their mass balances than land-terminating glaciers. Surge-type glaciers are found to have a more negative mass balance than their non-surging counterparts, except in the south west region.

6.1.3 Structural and Functional Sediment Connectivity in Greenland

The final research chapter extends the scope of the investigation to encompass structural sediment connectivity and sediment delivery ratios around Greenland's proglacial periphery. The research presents the first 32m national spatially distributed calculation of the index of connectivity (IC) and applies a novel assessment of lake's impact on connectivity by considering them as sediment sinks within watersheds. Index of connectivity results are aggregated based on watersheds produced as part of the highest resolution hydrological analysis of this kind at a Greenland-wide scale to date. IC is then compared to a metric of functional connectivity per watershed, computed as each watershed's sediment delivery ratio (SDR), using DEMs of Difference calculated between the AeroDEM (1978-1985) and ArcticDEM (2016) datasets. The degree to which IC can be used as an estimator of watershed SDR, and therefore functional connectivity is assessed.

This research delves into the spatial distribution of IC and SDR around Greenland, revealing the substantial impact of lakes on sediment connectivity. SDR is calculated as an annual rate using DEM's of difference covering nearly 40 years from 1978 to 2016. The spatial distribution of IC and SDR in Greenland reveals a complex landscape where lakes, with notable ice-dammed examples shown, significantly disrupt sediment connectivity by acting as sinks, thus drastically altering connectivity from source areas to coastal zones. This impact is quantitatively evident as average IC notably decrease when lakes are included as sinks in the modelling. Correspondingly, SDR, which varies with watershed size and is positively correlated with IC, shows that areas with higher connectivity generally have higher sediment delivery ratios, though this relationship weakens when lakes are explicitly modelled as sinks. The analysis of residuals from the Ordinary Least Squares (OLS) regression model further highlights the spatial complexity, revealing systematic patterns of over or underestimation in sediment delivery across regions when using IC as the independent variable. The presence of spatial autocorrelation in these residuals

suggests the influence of additional spatially structured variables not captured by the model, indicating avenues for future research and model refinement to better understand and predict sediment transport dynamics in Greenland's proglacial landscapes.

Together, these chapters contribute a mosaic of findings that not only stand individually in their respective fields but also interlink to form a cohesive narrative, setting the stage for a comparative and synthesised discussion of how these interconnected elements collectively narrate the story of Greenland's late 20th and early 21st-century environmental transformation.

6.2 Interplay of Landcover Change, Glacier Mass Dynamics, and Sediment Connectivity

The methodological coherence and structured format of the research chapters presented in this thesis provide an ideal framework for comparing findings. The analysis consistently spans the entirety of Greenland's proglacial area, employing a closely matched spatial resolution between 30m and 32m. Moreover, where the analysis is multitemporal, the periods largely overlap, encompassing the late 1970s and 1980s through to the late 2010s. This allows for a nuanced synthesis of the results from each chapter under three broad thematic areas as revealed in this research: the influence of landcover change on glaciers and connectivity, the impact of glacier mass balance change evident in landcover change and sediment connectivity, and the manifestation of sediment connectivity within the landcover changes and its inferred interactions with PGIC dynamics. Moreover, anomalous results between chapters are considered, and causes of the apparent misalignments are postulated. The following discussion will critically assess these interlinked themes, shedding light on the complex interplay between landcover change, glacier activity, and sediment connectivity in Greenland's evolving proglacial landscape. A consistent theme between the three research chapters is lakes and how they are manifest in the observations. This section concludes by synthesising the connotations of lakes in Greenland’s proglacial systems in light of the research conducted here.

6.2.1 Landcover Change Influence on Glacier Mass Balance and Sediment Connectivity

The landcover alterations in Greenland in response to climatic warming, as detailed in this thesis, are anticipated to be tightly linked with variations in glacier mass balance over the same timeframe. Consequently, areas with significant decreases in the areal coverage of the snow and ice class, as identified in Chapter 3, correspond closely to regions exhibiting the most negative mass balance (*T0*) as presented in Chapter 4. The north west of Greenland is reported to have the second lowest mass balance of all regions (-0.14 m w.e. yr^{-1}), as shown in Figures 4.3 and 4.4. In Chapter 3, Figure 3.14A shows the distribution of snow and ice loss around Greenland, with a notable hotspot in the north west. The south west is also highlighted as a region of particularly high decreases in snow and ice areal coverage, particularly around the Maniitsoq ice cap. The Maniitsoq ice cap is shown in Chapter 4, Figure 4.2A, as an exemplar location of marked glacier surface lowering, especially demonstrating acceleration in lowering over the study period. The south west has the lowest *T0* mass balance, and shows the greatest acceleration in mass loss over the study period. Conversely, the north and north east of Greenland show comparatively the least negative mass balance (-0.05 w.e. yr^{-1} and -0.08 w.e. yr^{-1} respectively). In Chapter 3 these regions are marked by decreases in all three barren ground classes, however a notable hotspot of increasing meltwater and vegetation expansion, particularly around Scoresby Sund in the central east (Figure 3.14). Interestingly, in the specific location where the barren ground (sediment and bedrock) classes are seen to decrease, both vegetation classes increase substantially, and Chapter 5 reports notable watersheds with particularly low IC (<-6) and SDR (<-0.6) (Figure 5.9). Similarly, watersheds with low measured SDR and IC in the south west and north east correspond closely with areas of vegetation expansion (Figure 3.14 and 5.9). Both considering lakes as sinks and not, the south west has the second lowest average IC (Figure 5.8), while the latitudinal plots of percentage change in Figure 3.14 (G and H) show the south west to have the highest percentage increases of both vegetation classes. It can be inferred then that vegetation expansion is consolidating hillslopes and reducing connectivity, even where meltwater is increasing. It may be that meltwater rivers are effectively mobilising and redistributing sediment in and around channels, but hillslopes, in part due to vegetation expansion, are poorly

connected. However, it should be noted that the SDRs utilise digital elevation change data and not digital surface data, so some vegetation growth may be considered as deposition in these regions, reducing the locally calculated SDR. Moreover, as the contemporary landcover data produced here is considered in the calculation of the IC within the weighting surface, it is to be expected that the IC will be to some degree correlated with the landcover changes reported here.

6.2.2 Glacier Mass Balance Changes Coincident with Landcover Changes and Sediment Connectivity

Glaciers exhibiting a more negative mass balance are indicative of accelerated melting processes and surface lowering. Therefore, it would be reasonable to postulate that regions manifesting lower mass balances will concomitantly be experiencing heightened increments in meltwater activity over the same timeframe. Accordingly, notable hotspots of meltwater increase in Figure 3.14B correspond closely with locations of the most negative (<-0.2 m w.e. yr^{-1}) mass balance over *T0*. Specifically, south of Kangerlussuaq in the vicinity of the Maniitsoq ice cap is marked as a location where meltwater increase on the west coast is highest (which for all latitudes exceeds the east in terms of percentage area increase of meltwater, Figure 3.12C), with increases of >6% total area for vector cells (Figure 3.14 B). As previously explored, this is the location of some of the lowest mass balance over *T0*. The central and south west also show the greatest accelerations in mass loss (Figure 4.4D and E), inferring melt over the period is concentrated in the past 10 years, and so heightened meltwater activity related to this melt would be present in the contemporary landcover classification, thus the inferred links between negative mass balance and increased meltwater activity are likely justified. Notable examples of high connectivity, both functional (SDR) and structural (IC), are found in the central west, central east, and north east as shown in Figure 5.9. These watershed clusters largely correspond to areas of highly negative mass balance in Figure 4.4C and accelerated mass balance reduction in Figure 4.4D. It may then be inferred that glacier loss and increased connectivity are both a function of increasing temperatures, as explored in Chapter 3. Permafrost degradation coupled with increased meltwater discharge to effectively remove hillslope-sourced sediment is inferred as a cause of this spatial correspondence between mass balance and connectivity. These regions also experience heightened vegetation expansion, another

indicator of potential permafrost degradation. However, this expansion is also associated with hillslope sediment consolidation. The relationship between vegetation growth and permafrost degradation is complex, and it inferred that periglacial mass movements and thermokarst forms may be excavating and eroding sediment, facilitated by vegetation growth in the early stages of development before root structures are sufficient to completely consolidate sediments (Heijmans et al., 2022; Kropp et al., 2021). Chapter 5 found that SDR and IC are most aligned and match previous findings on sediment concentrations in proglacial rivers (Bendixen et al., 2017; Hasholt, 1996; Overeem et al., 2017) where watersheds are more ice-distal and larger in area, and this corresponds to locations where melt and mass balance are generally lower in Chapter 4. It can be interpreted then that these metrics of sediment connectivity (SDR and IC) perform best and reflect actual sediment export where glacier water storage in the landscape exists, as the index with lakes modelled as sinks also more closely matches sediment export rates in these regions too (Figures 3.6, 5.8 and 5.9).

6.2.3 Sediment Connectivity and its Influences on Proglacial Landcover Changes

In Greenland's proglacial regions, sediment connectivity is not anticipated to be a primary driver behind the changes in glacier mass balance and surface lowering observed in this study. However, regarding changes in landcover classes, it is expected that enhanced sediment connectivity would catalyse extensive sediment redistribution in watersheds characterised by a higher Index of Connectivity (IC). Furthermore, the Sediment Delivery Ratio (SDR), which reflects the export of sediment, might also substantiate alterations in barren ground classes and sediment composition where a negative SDR would signify sediment deposition within a watershed, potentially leading to an increase in sediment classes. Whether these increases outpace the loss of sediment class coverage to vegetation and meltwater expansion is unknown and likely spatially heterogeneous. Accordingly, many regions of relatively higher structural connectivity do correspond with notable regions of coarse and fine sediment increase. For example, the central west is the location of coarse sediment increases >8% (Figure 3.14D), and this region possesses watersheds with average to relatively high IC values, particularly considering the size of the watersheds (Figure 5.9). SDR however is also fairly high here (>0.8), indicating most eroded sediment is being removed from the catchments. However, in the central east,

a notable hotspot of negative SDR indicating deposition within the landscape (Figure 5.9) corresponds with a hotspot of fine sediment increases, potentially glacially sourced and deposited within the terrestrial landscape (Figure 3.14E).

6.2.4 The Implications of Lakes in Greenland's Proglacial Systems

A pervasive theme throughout the research chapters is the role and impact of lakes within Greenland's proglacial systems. While Chapter 3 reports a decline in freshwater occurrence across Greenland, the underlying causes become somewhat elucidated through subsequent analysis. A considerable number of proglacial lakes are classified as meltwater bodies due to their high suspended sediment content. Concurrently, some of the observed freshwater reduction is offset by the progradation of deltas and the expansion of wetland vegetation around lake margins and at fjords and coasts, which are also designated as freshwater in this context. Chapter 4 reveals that of all PGIC terminus types, lakes exert the most substantial negative impact on glacier mass balance. Furthermore, Chapter 5 illustrates that lakes, despite being relatively scarce in watersheds (as noted in Table 5.3), significantly influence the IC and so structural sediment connectivity (Figures 5.6 and 5.7), both at the watershed level and in a broader regional context. Notable watersheds of particularly low IC are found in north east Greenland, particularly reduced when lakes are considered as sinks (Figure 5.9). Figure 4.1 shows that this region has the lowest percentage of glaciers with proglacial lakes, with only 47 glaciers (as shown in Figure 4.5) having a lake terminus. Contrastingly, in Table 5.3, the north east is found to have the highest percentage of watersheds with lakes (8.4%), as well as the second-highest average watershed area (20.8km^2). However, in the south east 5% of glaciers terminate in lakes (Figure 4.1), fairly average across regions, yet the lowest percentage of watersheds with lakes (4.4%), and the smallest average area (5.9 km2) (Table 5.3). The consideration of lakes as sinks in the south east is seen to have a similarly detrimental impact on regional average IC to watersheds in the north east (Figure 5.7). Both the north east (decreasing from -3.9 to -6.56) and south east (decreasing from -3.68 to -6.60) experience similar regional changes in average watershed IC with lakes considered as sinks. This highlights the importance of lakes' location within the proglacial system and their effect on IC, as the south east has a much smaller average watershed size yet similar IC, whereas the north east demonstrates similar patterns of IC change with lakes as sinks but for a region with

much larger (~3.5 times) average watershed size. As a greater percent of the lakes in north east Greenland are not ice-marginal, they therefore appear to be having a relatively higher negative influence on proglacial structural connectivity.

As explored earlier, the south west, and in particular around the Maniitsoq ice cap, is marked by some of the lowest measured connectivity (both IC and SDR) yet experiences increasing meltwater activity and decreasing mass balance. The freshwater class however is also found to increase in this area (Figure 3.14C), and an associated growth in lakes may be inferred. It is interpreted that proglacial lake expansion here, alongside vegetation growth, is largely hindering the potential increases in connectivity which might otherwise be expected. This is particularly evident comparing Figure 5.9A and B, where the change between the maps considering lakes as sinks and not is considerable. Interestingly, the south west where the greatest increases in the freshwater class are seen (Figure 3.14C) is also where Chapter 4 finds the most negative PGIC mass balance and acceleration in decreasing mass balance between *T1* and *T2* (Figures 4.3 and 4.4). The south west also has the second highest percentage of PGIC terminating in lakes, where the second lowest lake terminating glaciers' average mass balance (-0.21 w.e. yr^{-1}) is also reported. It is therefore likely that lake expansion as seen in the landcover change of Chapter 3 is somewhat correlated with the highly negative mass balances reported in the south west of Greenland in Chapter 4.

6.3 Position within Existing Literature

This section endeavours to contextualise the outcomes of this thesis against the backdrop of broader scholarly discourse, particularly focusing on overarching insights gleaned across the chapters. While individual research chapters have already juxtaposed their findings with broader existing studies within their respective discussion sections, this segment will deliberate on the wider implications and findings deemed most prescient from each chapter under three distinct categories: i) Observations pertaining to research in Arctic vegetation expansion, ii) The implications of sediment connectivity and Arctic landscape functioning, and iii) The impact of PGIC mass balance on global sea level rise.

6.3.1 Observations Pertaining to Research in Arctic Vegetation Expansion

Situated within the broader context of Arctic studies, the trends identified in this research are significant. They align well with ongoing discussions within both Greenlandic and wider Arctic scholarly discourse, thereby reinforcing and expanding the current understanding of Arctic landscape evolution. A dominant finding of this research is the doubling in vegetation cover classes since the late 80s revealed in Chapter 1. Arctic greening, as identified here, is a widely reported phenomenon. Long-term patterns of greening have been reported in Arctic Alaska and Canada (Arndt et al., 2019; Edwards & Treitz, 2017; Jia et al., 2003; Ju & Masek, 2016; May et al., 2017), where prolonged and extending growing seasons, increases in the number of warm days in the summer as shown in this research, are unanimously cited for shrub expansion and diversification. Though most of these studies cover multiple decades from the 1980s (e.g. Edwards & Treitz, 2017; Jia et al., 2003; Ju & Masek, 2016), shorter, more contemporary studies also identify greening during the study period, for example, Arndt et al. (2019) who observed increased greening, particularly for wetland species over a 14-year period from 2001 in Utqiaġvik (formerly known as Barrow), and May et al. (2017) who observed greening in the north slope of Alaska between 2012 and 2016, noting heterogeneous shrub responses to the timing of warming.

Overall, increased growing season length and temperatures were consistently contributing to the greening. Similarly, in Arctic Europe and Russia, widespread shrubification and greening have been identified (e.g. Forbes et al., 2010; Karlsen et al., 2014, 2021; Liu et al., 2021; MacIas-Fauria et al., 2012; Vickers et al., 2016; Voronina, 2021; Walker et al., 2009). Unanimously, increased temperatures and the length of the growing season are again cited as the drivers of vegetation expansion. Liu et al. (2021) tracked greenness trends across Arctic Russia between 1984 and 2018 using Landsat at 30m, synonymous with the duration and resolution applied here. They found substantial greening and an acceleration since 2000. Similarly, MacIas-Fauria et al. (2012) reveal over a 50-year period the growth response of Arctic shrubs across the Eurasian Arctic is driven by increasing summer temperatures. Arctic greening has been linked to causing earlier seasonality of the Arctic amplification, as species diversify and shift to boreal species, which have a

pronounced effect on surface albedo and potentially doubling CO2 release in these regions (Chae et al., 2015).

In 2013 Normand et al. (2013) reported localised boreal woody flora species in Greenland, and predicted a proliferation of rich woody flora in Greenland throughout the 21st century, a claim to which this thesis loans credence. If the observed trend of greening in Greenland observed here and across the Arctic continues, then the knock-on effects for mass balance, and potentially permafrost degradation and related sediment availability may contribute to the other trends observed in this work, as increased vegetation drives an increase in Arctic amplified climate warming (Chae et al., 2015). The regions of most pronounced greening observed in this research are found to correspond quite closely with reduced functional sediment connectivity since the late 1970s and 80s revealed in Chapter 5. This is largely attributed to two processes, one of which is the increase in vegetation being measured as deposition; however, much of the vegetation growth measured will be less than the level of detection and so masked, as shown in Figure 5.5. It is likely then that a large portion of this corroboration between vegetation growth and reduced sediment export is linked to the consolidating action of tundra vegetation species on hillslope sediments (Haselberger et al., 2021; Ohler et al., 2023).

Though it is speculated that vegetation will continue its trajectory of increase, the species and form of vegetation may change significantly. For example, Gamm et al. (2018) identified a decline in deciduous shrub species growth, specifically Betula and Salix species, with summer warming in Kangerlussuaq, west Greenland. The authors identify that these findings contrast with the widespread reporting of vegetation and shrub expansion in the Arctic, as reported here. However, they note drought-induced stomatal closure as a possible cause, due to the strong decline in α-cellulose (Δ13C) observed during reduced growth periods. The decline in α-cellulose (Δ13C) serves as an indicator of photosynthetic activity and water use efficiency in plants. During periods of reduced growth, a strong decline in Δ13C suggests limited carbon assimilation due to stomatal closure, which is often a response to drought conditions (Gamm et al., 2018). Interestingly, May–August mean air temperatures at and exceeding 7°C are cited as an important threshold, where here the number of positive degree days over 6°C is identified as the highest correlate with increased vegetation expansion. Arctic drought has been associated with certain shrub die-

back, coincident with the recently identified process of arctic browning (Phoenix & Bjerke, 2016).

Most records identify long-term greening, however, the NOAA in 2016 reported a browning in the Arctic between 2011 and 2014. Multiple studies have reported apparent browning across the Arctic (Bhatt et al., 2013; de Jong et al., 2011; Lara et al., 2018; Miles & Esau, 2016; Phoenix & Bjerke, 2016; Zhang et al., 2017). Research cites multiple factors driving Arctic browning, such as drought (Seo et al., 2015), widespread permafrost degradation and mass failure (Grosse et al., 2016), pest outbreaks (Bjerke et al., 2014), nutrient availability (Martin et al., 2017), and decreased snow cover reducing soil insulation and leading to colder winter soil conditions killing vegetation (Gamon et al., 2013). The response is heterogeneous and largely dependent on the scale and style of analysis (Frost et al., 2014). Widespread browning in Greenland has not been reported, however, most of the proglacial regions in Greenland are relatively freshly exposed (see Literature Review, Chapter 2) compared to many others in North America, Russia, and Europe owing to the location and activity of the GrIS. Gamm et al., (2018) report vegetation decreasing around Kangerlussuaq (south west Greenland), and (Lund et al., 2017) report larval (noctuid moth - Eurois occulta) outbreaks in the same region, reducing vegetation productivity. They did, however, cite that in the seasons following their observation, there was increased primary productivity, potentially driven by increasing nutrient turnover rates facilitated by the larval outbreak.

Interestingly, a quiescence of glacier mass loss in east Greenland is juxtaposed by an acceleration in loss in the west. A similar asynchrony is identified by Bjork et al. (2018), citing positive NAO as reducing precipitation delivery to west Greenland (Mosley-Thompson et al., 2005). The NAO is projected to trend positive in the future (Gillett & Fyfe, 2013). As identified by Gamm et al. (2018), drought in west Greenland has already been shown to reduce productivity. This phenomenon may become more common when reduced precipitation in the region is coupled with an increasing number of positive degree days, as observed in this study. Such conditions could have a highly detrimental impact on the previously flourishing vegetation. It is possible that the regions highlighted in this study as experiencing the most significant increase in vegetation are approaching, or may have already reached, an ecological tipping point, thereby anticipating a contemporary deceleration or reversal

of this trend requiring further research. The studies and their findings regarding Arctic greening and browning are summarised in Table 6.1 below. Although Arctic greening continues to be the predominant process observed, more recent studies, particularly those focusing on short-term changes and broader Arctic-wide scales, increasingly report instances of Arctic browning.

Table 6.1 Summary table of studies pertaining to research in Arctic vegetation change

Paper	Region	Period	Findings	Greening or Browning
Greenland				
Gamm et al., 2018	Kangerlussuaq, Greenland	Various (1980s-2010s)	Decline in deciduous shrub species growth due to summer warming and drought-induced stomatal closure.	Browning
Normand et al., 2013	Greenland	21st century	Predicted proliferation of rich woody flora.	Greening
Lund et al., 2017	Kangerlussuaq, Greenland	2014-2015	Larval outbreaks reducing vegetation productivity, with increased primary productivity in following seasons.	Browning
Riis et al., 2023	Northeast Greenland	2021	NO_3 (Nitrate) was negatively and DON (Dissolved Organic Nitrate) positively linked to median spectral NDVI in the catchment of 14 streams. Changes in vegetation cover may alter stream water chemistry.	Greening
Speir et al., 2024	Northeast Greenland	18 years (up to 2024)	Decreasing inorganic and organic (N) Nitrogen loads linked to decreasing snow stores, warming soils, and enhanced plant uptake. Higher variability in N export across years.	Greening
Arctic Wide				
Chae et al., 2015	Arctic	Various (2000s-2010s)	Greening linked to earlier seasonality and doubling CO_2 release.	Greening
Phoenix & Bjerke, 2016	Arctic	Various (2010s)	Arctic drought associated with shrub die-back and arctic browning.	Browning
Bhatt et al., 2013	Arctic	1982-2010	Browning across the Arctic due to various factors such as drought, permafrost degradation, pest outbreaks,	Browning

			nutrient availability, and decreased snow cover.	
de Jong et al., 2011	Arctic	1982-2008	Browning across the Arctic due to various factors such as drought, permafrost degradation, pest outbreaks, nutrient availability, and decreased snow cover.	Browning
Lara et al., 2018	Arctic	2000-2016	Browning across the Arctic due to various factors such as drought, permafrost degradation, pest outbreaks, nutrient availability, and decreased snow cover.	Browning
Miles & Esau, 2016	Arctic	2000-2014	Browning across the Arctic due to various factors such as drought, permafrost degradation, pest outbreaks, nutrient availability, and decreased snow cover.	Browning
Zhang et al., 2017	Arctic	2000-2014	Browning across the Arctic due to various factors such as drought, permafrost degradation, pest outbreaks, nutrient availability, and decreased snow cover.	Browning
Frost et al., 2014	Arctic	Various (2000s-2010s)	Heterogeneous response to browning depending on scale and style of analysis.	Browning
Arctic Alaska and Canada				
Arndt et al., 2019	Utqiaġvik (Barrow), Alaska	2001-2015	Increased greening, particularly for wetland species.	Greening
Edwards & Treitz, 2017	Arctic Alaska and Canada	1980s-2015	Long-term greening patterns due to prolonged growing seasons and warm days.	Greening
Jia et al., 2003	Arctic Alaska and Canada	1980s-2000s	Shrub expansion and diversification driven by longer growing seasons and increased warm days.	Greening
Ju & Masek, 2016	Arctic Alaska and Canada	1984-2014	Greening due to longer growing seasons and increased temperatures.	Greening
May et al., 2017	North Slope, Alaska	2012-2016	Greening with heterogeneous shrub responses to timing of warming.	Greening
Arctic Europe and Russia				
Forbes et al., 2010	Arctic Europe and Russia	2000-2010	Widespread shrubification and greening due to increased temperatures and longer growing seasons.	Greening

Karlsen et al., 2014	Arctic Europe and Russia	1982-2012	Greening driven by increased temperatures and longer growing seasons.	Greening
Karlsen et al., 2021	Arctic Europe and Russia	2000-2016	Greening driven by increased temperatures and longer growing seasons.	Greening
Liu et al., 2021	Arctic Russia	1984-2018	Substantial greening with an acceleration since 2000.	Greening
MacIas-Fauria et al., 2012	Eurasian Arctic	1960-2010	Growth response of Arctic shrubs driven by increasing summer temperatures.	Greening
Vickers et al., 2016	Arctic Europe and Russia	Various (2000s-2010s)	Greening due to increased temperatures and longer growing seasons.	Greening
Voronina, 2021	Arctic Europe and Russia	Various (2000s-2010s)	Greening due to increased temperatures and longer growing seasons.	Greening
Walker et al., 2009	Arctic Europe and Russia	Various (1980s-2000s)	Increased shrubification and greening linked to higher temperatures.	Greening

6.3.2 The implications of sediment connectivity Arctic landscape functioning

A review of existing sediment connectivity literature reveals that no work explicitly researching sediment connectivity in Arctic landscapes existed before this. The extensive review by Najafi et al. (2021) of 117 academic papers citing and analysing sediment connectivity reveals no studies in the Arctic. Therefore, the findings presented here stand out as not only the first in Greenland but potentially the first within the Arctic as a whole. In the context of Arctic landscape functioning, sediment connectivity as reported here plays a critical role in shaping ecological and geomorphological processes. The signature of increased hillslope sediment flux in proglacial and post-glacial settings, as observed in the heightened sedimentation of floodplains and offshore basins during past warming events in the Arctic (Kaufman et al., 2016; Mann et al., 2010; Tesi et al., 2016), provides a historical backdrop against which contemporary changes as measured here can be understood.

Modern observations indicate that both anomalously warm and wet conditions driven by Arctic amplified temperatures act as catalysts for slope failures and permafrost degradation, with an increasing frequency in line with recent warming trends (Balser et al., 2014; Lewkowicz & Way, 2019). This suggests a landscape increasingly susceptible to disruption and reconfiguration, and so with more sediment available and increased meltwater discharge, relative hillslope connectivity is crucial for

understanding hillslope coupling to rivers and coastal outlets. Changing hydroclimatic conditions in the high latitudes may also alter the timing and extent of tundra soil saturation. Earlier infiltration can saturate low-conductivity soil layers that were historically frozen in early spring, leading to increased sediment mobilisation (Walvoord & Kurylyk, 2016). Additionally, the shift in discharge timing from spring snowmelt to summer rainfall (Bintanja & Andry, 2017) can further modify sediment transport patterns and connectivity across the Arctic landscape.

These changes have profound implications for sediment delivery systems and can drastically alter landscape morphology over time, highlighting the necessity of this and future work to link regions of permafrost degradation and increased rainfall to hillslope connectivity to outlets. Furthermore, the phenomena of Arctic browning, driven partially by failures on hillslopes supporting vegetation, particularly in permafrost regions, is another facet of this complex system (Myers-Smith et al., 2020). The destabilisation of these slopes not only contributes to increased sediment flux but also impacts the vegetative cover, further altering the landscape's ecological balance and feedback mechanisms. In this research, lakes are seen to dramatically reduce watersheds' overall connectivity to coasts where they are present, and this discussion has already indicated lake's location within catchments largely determines the measured impact on average IC.

Proglacial lake expansion has been cited throughout this thesis (Carrivick et al., 2022), however, proglacial lakes in this context are ice-contact and are set to grow as glaciers retreat into, occasionally moraine-dammed, overdeepenings. The Arctic trend for ice distal lakes is to the contrary, largely driven by thermal and hydrological change (Andresen & Lougheed, 2015; Barnett et al., 2005; Bring et al., 2016; Carroll et al., 2011). The phenomenon of Arctic lake decrease has been identified in the Sisimiut - Kangerlussuaq area of Greenland, where Law et al. (2018) identified a decrease in total lake surface area between 1995 and 2017 of 855,449 m2. Moreover, Finger Higgens et al. (2019) found over the past 50 years in a 1,250-km2 area around Kangerlussuaq a decrease in total lake count (21%) and surface area (2%), with smaller ponds (<10,000 m2) particularly prone with a 28% and 15% decrease in count and area respectively. This thesis' research identifies widespread reductions in freshwater coverage across Greenland in Chapter 3, often changing from freshwater to vegetation classes, a phenomenon identified around Kangerlussuaq by Finger

Higgens et al. (2019). Therefore, as proglacial ice-contact lakes are growing, acting as sinks for a large portion of glacially derived sediment where they exist, the widespread reduction in ice distal lakes, coupled with permafrost degradation, may bolster hillslope connectivity, and therefore the importance of hillslope-derived sediments in coastal sediment plumes.

Hillslope-derived sediments in regions of permafrost degradation contain higher concentrations of dissolved and particulate organic carbon (DOC & POC). Permafrost thaw in the Arctic is enhancing soil drainage and the flow of water, carbon, nutrients, and sediment across Arctic landscapes, which in turn increases the export of DOC and POC to coastal waters and oceans (Lynch et al., 2019; Rowland et al., 2010). This process of permafrost degradation is crucial because it affects atmospheric CO2 levels and the hydrology and sediment connectivity of Arctic areas (Walvoord & Kurylyk, 2016). As permafrost degrades, it alters subsurface storage and water routing, leading to more connected surface and subsurface flow paths (Chiasson-Poirier et al., 2020). This change has significant implications for catchment biogeochemistry and the fate of natural particulate organic matter (POM), which is the dominant form of organic carbon in Arctic tundra waters. The chemical diversity of POM impacts microbial metabolism and, when considered alongside sediment connectivity, links terrestrial and aquatic ecosystems, influencing the carbon balance of Arctic landscapes (Lynch et al., 2018). As lakes act as effective sinks of particulate matter (Rantala et al., 2016; Vonk et al., 2016), in this research being seen to reduce net watershed connectivity, however, they are reducing ice-distally in regions of permafrost degradation such as southwest Greenland (Finger Higgens et al., 2019; Law et al., 2018). This thesis sets a baseline for future work to understand how POM is mobilised and transformed in Greenland under continued warming and connectivity. It is vital to predict whether Arctic catchments will continue to act as significant carbon sinks or become net sources of carbon, and to what extent this organic material, once mobilised, is connected to coastal marine ecosystems.

In this work it is assumed that all material eroded and marked as removed from watersheds within the SDR is a function of downslope movement, and there is no cross-catchment removal and deposition of eroded material. However, wind-blown sediment redistribution has been identified in Greenland, particularly aeolian soil

erosion in the south west (Heindel et al., 2015; Willemse et al., 2003). Concerning proglacial catchment sediment yields estimated from hydrological assessments such as suspended sediment measurements and in-stream gauging, Carrivick & Tweed (2021) note it is unlikely aeolian sediment transport is included in these estimates, with aeolian contributions representing an insignificant proportion of glaciated catchments sediment yield. One benefit of the method as applied here is that the SDR measures all sediment erosion and removal within a contributing area in a watershed, and not specific measurements of sediment output at a portal or gauge.

6.3.3 The Impact of PGIC Mass Balance on Global Sea Level Rise

Glacier mass balance changes, as reported here, are largely considered in line with existing literature in the Chapter 4 discussion, where the rates reported here are compared with other reported rates for PGIC in Greenland. For instance, the long-term mass loss findings from this research corroborate the east-west trend of asynchronous mass loss and stability reported by Bjørk et al. (2018), however this work adds a dimension by concerning lake occurrence and their relative prevalence between the east and west on top of NAO influences. Greenland's PGICs present a unique geomorphological setting that distinguishes them from other Arctic glaciers. Their proximity to the GrIS means they are influenced by a distinct set of climatic and environmental conditions, such as the katabatic winds from the ice sheet and the microclimates created by its vast expanse (Ballinger et al., 2019; Heinemann, 2020). Also, the aforementioned NAO influence as experienced in Greenland is unique, exacerbated by the relatively close maritime proximity of Greenlandic glaciers compared to those elsewhere in the Arctic (Bevis et al., 2019; Straneo & Heimbach, 2013). These factors contribute to a specific glacial dynamic and melting pattern that is less comparable to other Arctic glaciers.

The specific rates of retreat over extended periods for Greenland's PGICs, as delineated in this research, are essential for a refined understanding of global sea-level rise and the broader cryospheric responses to climate change (Bamber et al., 2018a). While some studies have considered the mass balance of ice sheets and PGICs separately, there has often been a lack of clarity and consistency in their treatment. This ambiguity, as highlighted in the works of (Bolch et al., 2013) and others, can lead to an underappreciation of the PGICs' role and significance. As

PGICs account for a considerable and disproportionate portion of Greenland's total freshwater discharge (around 15%–20%), their specific behaviour and changes are crucial to understanding the entire cryosphere's dynamics (Bjørk et al., 2018; Bolch et al., 2013; Rastner et al., 2012). This research's focused and detailed analysis of the retreat rates of PGICs, as well as the consideration of terminus and debris cover condition, provides insights that are often overlooked or generalised in larger-scale sea level rise studies (Bamber et al., 2012; Bamber et al., 2018a; Bamber et al., 2018b). The general inclusion of all land ice within the coarse spatial resolution of satellite data, such as that from GRACE, often amalgamates the distinct behaviours of ice sheets and PGICs (Forsberg et al., 2017; Van Den Broeke et al., 2016). Such an approach, while broad-reaching, can mask the unique dynamics and contributions of PGICs to the total ice mass trends. By offering a dedicated study of these specific entities, this work contributes to a more nuanced and complete picture. The aggregate 500km^2 hexagonal or broader regional long-term trends may be incorporated into global SLR estimates. Understanding the long-term retreat rates of PGICs is critical for enhancing the accuracy of global sea-level rise models and climate simulations. This specificity ensures that the contributions of PGICs to sea-level rise are accurately represented, avoiding underestimation (Yi et al., 2015). Moreover, this work illuminates the regional variability in the response of PGICs to climate change, as well as the responses relating to terminus conditions and surface debris, identifying patterns and trends that might not be evident in broader, less-detailed studies and are largely overlooked in existing PGIC studies in Greenland (Bjørk et al., 2018; Leclercq et al., 2012; Machguth et al., 2013). Accurate data on PGIC retreat rates are also essential for informing policy decisions and climate mitigation strategies. With a clearer understanding of the specific contributions of PGICs to sea-level rise, efforts can be targeted more effectively. In sum, this focused investigation into the long-term retreat rates of Greenland's PGICs is not merely an addition to the existing literature; it may find utility as a critical input for understanding the intricacies of global ice mass trends and their implications.

6.4 Utility of the Findings

As alluded to in the previous section, the outputs of this work may find wider utility, both within academic discourse and literature and with a broader audience. This

section delineates various contexts and scenarios where the findings and data generated from this research could be significantly applied.

The data and insights gained from long-term landcover changes, glacier mass balance rates, and hydrological analyses in Greenland can significantly enhance Earth System Models (ESMs) (Flato, 2011). ESMs are sophisticated tools used to understand and predict changes in the Earth's climate and ecosystems by simulating the interactions between the atmosphere, oceans, land surface, ice, and living organisms (Bonan & Doney, 2018). Detailed landcover, glacier, and hydrological/sediment connectivity data can help refine the parameters used in ESMs, leading to more accurate simulations of physical processes in Arctic regions, like snow and ice melt, vegetation dynamics, and water flow (Le Page et al., 2016; Séférian et al., 2019). Long-term observational data provide a critical baseline for validating and calibrating model outputs, ensuring that the models accurately reflect observed reality. Understanding how days over a certain temperature threshold affect landcover, as produced here, can improve predictions about future climate conditions, particularly in Arctic regions sensitive to warming. Accurate data on glacier mass balance rates are also crucial for predicting future sea-level rise, a significant component of climate models affecting global and regional climate patterns (Meier et al., 2007). Moreover, ESMs which incorporate detailed landcover and hydrological data designed specifically for certain underrepresented regions, such as those produced in this thesis, can better predict how ecosystems will respond to various climate scenarios and may help in local Greenlandic biodiversity conservation and natural resource management (Tommasini, 2015). The Northeast Greenland National Park, established in 1974, is the world's largest national park and 10th largest protected area at nearly 1 million km^2 (~972,000 km^2). The detailed landcover, glacier, and sediment connectivity findings presented here may applied for improved future planning and management, identifying high-risk habitat and culturally relevant areas to aid in the development of unique planning tools.

Incorporating new indices like the Index of Connectivity into ESMs and planning tools can lead to innovative approaches to model land-water interactions and sediment transport, which has influences beyond the terrestrial landscapes, impacting nutrient delivery to coastal marine environments which in turn impacts fishing and hunting and so human community sustainability (Nuttall, 2016). While ESMs often

operate on a global scale, incorporating detailed local data like that from Greenland allows for more accurate regional predictions and can inform local adaptation strategies, and information about sediment and nutrient flows can offer insights into how climate change impacts and is influenced by coupled human-environment systems (Burpee et al., 2018; Ford & Goldhar, 2012; Hawkings et al., 2015; Rysgaard et al., 1999). In summary, incorporating detailed, long-term data from specific regions like Greenland into Earth System Models can significantly enhance their accuracy, relevance, and utility. This, in turn, benefits scientific understanding, policy-making, and societal preparedness in the face of climate change and its many impacts.

Within wider academic and scientific research, the utility of the findings and data are manifold. The long-term (>30 years) of data on land cover change, including vegetation, sediment, and meltwater, can provide critical insights into the impacts of rising temperatures. Researchers can use this data to model and predict future changes, understand ecological shifts, and study the relationship between temperature increases and physical changes in the environment. The data on peripheral glacier and ice cap mass balance rates, produced here at the raw individual glacier scale as well as 500 km^2 and regional aggregations, might contribute to understanding the dynamics of ice mass loss and its implications for sea-level rise. The detailed hydrological analysis and sediment connectivity assessment offers valuable information for geomorphologists and hydrologists studying natural processes and cycles. This research might also be used for local community education, as the changes measured here over nearly 40 years are relatable and visible to many living within these communities, as opposed to longer-term multi-generational data. Disseminating this information can raise awareness about the impacts of climate change on local and global scales. It can also educate communities living in and around these areas, helping them to understand the changes occurring in their environment and how they can adapt. Understanding environmental changes is crucial for protecting sites of cultural significance that might be threatened by shifting landscapes, melting glaciers, or changing waterways. The utility of such detailed and long-term environmental data is vast, offering valuable insights for a wide range of stakeholders.

6.5 Implications for Future Research

Building upon the academic use cases outlined in earlier sections, the work encompassing this thesis opens up intriguing possibilities for future scientific investigation. This section will delineate a range of prospective and potentially lucrative research avenues that could be pursued based on the work and datasets produced here. The automation of the workflow presented in this long-term assessment of land cover, glacier mass balance, and sediment connectivity offers a robust framework for the continuous monitoring of Greenland's environmental changes. By automating the process, it allows for consistent, efficient, and scalable observations, critical for understanding the rapid changes occurring in this sensitive region. If computational resources permit, this methodology has the potential to be expanded beyond Greenland, offering a comprehensive tool for a wider Arctic assessment or for ongoing monitoring of Arctic landscapes. However, while the prospect of extending this methodology to a broader Arctic context is enticing, it is crucial to acknowledge that its effectiveness is partly due to its customisation to Greenland's unique environmental conditions. Adapting the workflow for a broader Arctic application may result in a dilution of the specificity and relevance of the results, necessitating a careful balance between generalisation for wider geographic coverage and the maintenance of detailed, localised insights.

The research presented in Chapter 3 identified spatially heterogeneous freshwater class reduction, and this is in part associated with the wider trend of reducing lakes in the Arctic. The analysis of lake decrease, particularly around Kangerlussuaq in south west Greenland, has provided valuable insights, yet it remains spatially restricted (Finger Higgens et al., 2019; Law et al., 2018). Expanding this analysis to a Greenland-wide assessment would offer a more comprehensive understanding of the trajectories of lake decrease across diverse landscapes and climates. Future studies should aim to correlate these trajectories with climatic changes and permafrost degradation to pinpoint regions at heightened risk of lake decrease. Understanding the regional specifics of lake decrease is crucial, as these bodies of water play a significant role in local ecosystems, hydrological cycles, and, as this research has shown, sediment connectivity. The potential ramifications of continued lake decrease are profound, affecting not just the hydrology but also the ecological and atmospheric dynamics of the Arctic. Lakes are key reservoirs of biodiversity and are

critical for maintaining the balance of greenhouse gases. However, studies have shown that Arctic lakes can be significant sources of methane and other greenhouse gases (Wik et al., 2016; Cole et al., 2007), and their role can vary depending on climatic and environmental conditions (Tranvik et al., 2009; Bastviken et al., 2004). The complex interplay between lakes acting as both carbon sinks and sources (Walter Anthony et al., 2014) underscores the need for detailed regional studies to understand their net impact on greenhouse gas balances. Their loss could lead to changes in the region's albedo effect, further accelerating warming trends. Additionally, as lakes shrink, the connectivity between proglacial catchments and the ocean will alter, affecting the sediment transport and nutrient cycling essential for aquatic life. Therefore, it's vital for future work to not only broaden the spatial scope of lake decrease analysis but also to integrate multidisciplinary studies that consider the ecological, hydrological, connectivity and climatic implications of such changes.

The phenomenon of Arctic browning, a process marked by vegetation decline and ecosystem stress, contrasts with the widespread increase in vegetation, both tundra and wetland, observed here over the long multi-decadal study period. This research has illuminated the complex dynamics of Arctic vegetation growth, but the potential shift towards browning under changing environmental conditions warrants further exploration. Future studies should aim to investigate the theories of drought and its persistence, which are critical factors in Arctic browning. By integrating the 6-degree day data utilised in this research with detailed precipitation records and NAO trends, researchers can begin to unravel the multifaceted interactions between climate variables and vegetation health. Understanding the triggers and trajectories of Arctic browning is crucial for several reasons. First, it has direct implications for the carbon cycle. Vegetation acts as a significant carbon sink, and its decline could accelerate the release of stored carbon into the atmosphere, further exacerbating climate change (Gagnon et al., 2019; Mekonnen et al., 2021). Second, the process affects local and indigenous communities who depend on the stability and resources of these ecosystems for their livelihoods and cultural practices, less from directly utilising the native vegetation but hunting the fauna which feeds on it (Cuyler et al., 2020; Tveraa et al., 2013). Third, changes in vegetation cover can alter the albedo effect, potentially leading to further regional warming (Blok et al., 2011; Loranty et al., 2011). Future work should also focus on the spatial and temporal variations of Arctic

browning, identifying regions most at risk and the timescales over which changes are occurring. This research could help in predicting the future states of Arctic ecosystems under various climate scenarios. Moreover, understanding the interplay between drought, temperature, and large-scale atmospheric patterns like the NAO is vital for creating more accurate models of future Arctic conditions.

This study demonstrated a reasonably good correlation between the index of connectivity and actual long-term watershed sediment delivery ratios, suggesting its potential applicability in other Arctic settings. It particularly noted the impact of glaciers' proximity to coasts on the over and underestimation of certain watershed residuals. Future research might extend these principles to similar Arctic environments, paying special attention to regions where glaciers are close to coastlines. Additionally, it's crucial to explore the regional autocorrelation observed in residuals and delve deeper into how factors like precipitation and permafrost conditions affect areas where the model was less accurate. Employing multivariate analyses that incorporate various relevant variables could significantly enhance our understanding of widespread connectivity. Future work may identify a spatial distribution of watersheds around Greenland with notable IC and SDR results for more intricate analysis and calculation of spatially distributed SDR following Heckmann & Vericat (2018). The intricate spatial patterns of IC and SDR may then be investigated at these sites. These targeted studies might utilise shorter-interval modern, higher-resolution elevation data to refine the long-term trends identified in this research. The quality of elevation change data, especially when derived as a Digital Surface Model (DSM), adds complexity, particularly as much of the sediment redistribution may fall within the level of detection. These future studies should seek to enhance the methodologies and data quality, possibly by incorporating changes in vegetation identified here to improve elevation change data. This would provide a more nuanced understanding of sediment redistribution and contribute to more precise and effective environmental monitoring and prediction models in Greenland and potentially the wider Arctic. As mentioned earlier, Carrivick and Tweed (2021) cite aeolian sediment removal as being overlooked in sediment yield studies. As aeolian removal might be measured in the SDR reported here, future work might seek to further assess the contribution of aeolian sediment redistribution in

Greenland, with implications for erosion and deposition across watershed boundaries.

Future work may also seek to explore glaciers' influence in catchments as sediment sources and the interplay where glacier termini occur within lakes' contributing areas. This work, while largely concerned with lakes and their influence, found no remarkable findings in the examination of glacier-fed watersheds (Figure 5.7), suggesting a potential avenue for more targeted research. The contributions of Carrivick et al. (2018) on proglacial glacier influence and geomorphological units in proglacial areas could be particularly instructive. Identifying catchments with both lake and glacier differences in IC and conducting higher resolution studies of sediment redistribution and connectivity could provide deeper insights. Specifically, investigating IC within areas explicitly influenced by glacier meltwater at a higher resolution might elucidate more directly relevant glacigenic sediment connectivity, as well as pinpoint specific in-channel points of net erosion and deposition. The probability density function (PDF) based landscape segmentation as applied in Carrivick et al. (2018) may allow the identification and classification of sediment source hillslope geomorphological units when combined with the IC. Slope angles are considered within the IC algorithm for both the upslope and downslope components, but slopes are not explicitly cast to geomorphological units which have considerable connotation for sediment delivery and storage. Cavalli et al. (2020) identify that combining spatially distributed calculations of IC with sediment source data can optimise sediment management and focus on the most critical hotspots (Persichillo et al., 2018; Tiranti et al., 2016).

In Chapter 4 it is seen that debris cover appears to expedite mass loss and melt. It is acknowledged though that the debris cover on some glaciers could have changed during the study period, and that the properties of supraglacial debris on Greenland PGICs are almost unknown. Future work bolstered by these findings may seek to explore the thickness and distribution of sediment of Greenland's PGIC. An important input for modelling future ice loss. Trajectories of change over time are also crucial. Regions showing increasing debris cover may indicate debris cover is a factor of melt and exposure and accumulation of melt-out material. Debris cover may then increase to a threshold, above which it decreases. However, the accumulation rate needed to reach said threshold is currently completely unknown, providing an

interesting avenue for future research, and regions identified in this study may be used to direct targeted sites for said research. This research has also identified that lakes have the most significant negative impact on mass balance compared to marine and terrestrial termini, indicating a critical area for further investigation. For proglacial lakes, future studies could focus on understanding the mechanisms by which these lakes accelerate ice loss specifically around Greenland. This may include examining the thermal and dynamic interactions between lake water and ice, the role of calving into lakes, and the impact of lake drainage events on glacier stability. Additionally, tracking the formation and evolution of these lakes over time would provide valuable data on their contribution to glacier retreat and mass balance changes. The observed regional disparities, particularly the lower overall mass balance and accelerated decrease in the west compared to the east, have been partially addressed by Bjørk et al. (2018) and attributed to oscillation in the NAO. Future work however may build upon this identified historic trend for specific glaciers identified as showing asymmetry between the coasts in this research and conduct high-resolution monitoring of surface elevation changes alongside climate data to understand the precise climate drivers going forward. Finally, the somewhat unusual link between surge-type glaciers having lower mass balance in their accumulation areas than non-surge glaciers identified here during the study period presents a fascinating avenue for further research. Future studies might focus on identifying and timing glacier surges and examining the conditions leading up to and following these events, to better understand their overall impact on regional glacier dynamics.

6.6 Concluding Remarks

The thesis presented here and the research conducted within offer a comprehensive examination of the complex dynamics, composition, and functioning of Greenland's proglacial systems over the past four decades, providing a detailed narrative of the land's transformation under the influences of climate change and other geophysical processes. The research has made significant contributions to the wider literature on landcover change, glacial dynamics, and sediment connectivity in the Arctic, offering valuable insights into the profound and varied impacts of environmental alterations.

The third chapter's exploration of landcover change in Greenland since the 1980s highlights the significant proliferation of vegetation, a key aspect of Arctic Greening. Utilising Difference in Degree Days Above Temperature (DDDAT) and Geographically Weighted Regression (GWR), the study provides nuanced insights into how warming trends are driving this vegetative expansion, with implications for carbon sequestration and ecosystem dynamics. Additionally, the fine-scale analysis of barren ground and water body changes offers a deeper understanding of the underlying processes of landcover transition, contributing to a more comprehensive picture of Arctic environmental transformations. The datasets produced enhance the understanding of how warming influences landcover changes, providing a nuanced approach that can be applied in future studies. In assessing the mass balance changes of peripheral glaciers and ice caps in Chapter 4, the thesis has documented a substantial ice loss and identified regional variations and characteristics influencing these changes. The exploration of mass balance trends based on terminus type, behaviour, and debris cover has provided a detailed understanding of the factors driving glacial dynamics and has offered a comparative context with other studies, contributing to a more comprehensive picture of Greenland's glacial system. The fifth chapter on structural and functional sediment connectivity has presented novel findings on the impact of lakes as sediment sinks and the spatial distribution of the Index of Connectivity (IC) and Sediment Delivery Ratios (SDR) around Greenland's proglacial periphery. This is the first study of its kind in Greenland and the Arctic and proves the utility of this approach in assessing national connectivity for inter-catchment comparisons. This chapter has provided a new perspective on how sediment is transported and deposited in Arctic landscapes when compared with the findings of the preceding chapters, offering a model that can be refined and expanded in future research.

The contributions of this thesis extend beyond its specific findings, offering a proof of concept for the methods applied. The integration of relatively high-resolution datasets for national scale analysis, innovative analytical approaches, and a multi-faceted perspective on environmental change demonstrates the potential for similar methodologies to be applied in other Arctic regions and beyond. This research serves as a foundation upon which future studies can build, refining the understanding of landcover, glacial, and sediment dynamics under changing climatic conditions.

In conclusion, this thesis has not only advanced the understanding of Greenland's environmental changes over the past four decades but has also provided a robust methodological framework for future research and data sets which might find utility across a broad spectrum of academic and scientific applications. It has highlighted the importance of considering a multitude of factors and their interrelations to fully comprehend the complex dynamics of Greenland's proglacial landscapes. As the global community continues to grapple with the implications of climate change, the insights and approaches offered by this research will undoubtedly contribute to more informed and effective responses.

6.7 Chapter 6 References

Andresen, C. G., & Lougheed, V. L. (2015). Disappearing Arctic tundra ponds: Fine-scale analysis of surface hydrology in drained thaw lake basins over a 65 year period (1948-2013). *Journal of Geophysical Research: Biogeosciences*, *120*(3). https://doi.org/10.1002/2014JG002778

Anthony, K.W., Zimov, S.A., Grosse, G., Jones, M.C., Anthony, P.M., Iii, F.C., Finlay, J.C., Mack, M.C., Davydov, S., Frenzel, P. and Frolking, S. (2014). A shift of thermokarst lakes from carbon sources to sinks during the Holocene epoch. Nature, 511(7510), pp.452-456.

Arndt, K. A., Santos, M. J., Ustin, S., Davidson, S. J., Stow, D., Oechel, W. C., Tran, T. T. P., Graybill, B., & Zona, D. (2019). Arctic greening associated with lengthening growing seasons in Northern Alaska. *Environmental Research Letters*, *14*(12). https://doi.org/10.1088/1748-9326/ab5e26

Ballinger, T. J., Mote, T. L., Mattingly, K., Bliss, A. C., Hanna, E., Van As, D., Prieto, M., Gharehchahi, S., Fettweis, X., Noël, B., Smeets, P. C. J. P., Reijmer, C. H., Ribergaard, M. H., & Cappelen, J. (2019). Greenland Ice Sheet late-season melt: Investigating multiscale drivers of K-transect events. *Cryosphere*, *13*(8). https://doi.org/10.5194/tc-13-2241-2019

Balser, A. W., Jones, J. B., & Gens, R. (2014). Timing of retrogressive thaw slump initiation in the Noatak Basin, northwest Alaska, USA. *Journal of Geophysical Research: Earth Surface*, *119*(5). https://doi.org/10.1002/2013JF002889

Bamber, J. L., Tedstone, A. J., King, M. D., Howat, I. M., Enderlin, E. M., van den Broeke, M. R., & Noel, B. (2018a). Land Ice Freshwater Budget of the Arctic and North Atlantic Oceans: 1. Data, Methods, and Results. *Journal of Geophysical Research: Oceans*, *123*(3). https://doi.org/10.1002/2017JC013605

Bamber, J. L., Westaway, R. M., Marzeion, B., & Wouters, B. (2018b). The land ice contribution to sea level during the satellite era. *Environmental Research Letters*, *13*(6). https://doi.org/10.1088/1748-9326/aac2f0

Bamber, J., Van Den Broeke, M., Ettema, J., Lenaerts, J. and Rignot, E., 2012. Recent large increases in freshwater fluxes from Greenland into the North Atlantic. Geophysical Research Letters, 39(19).

Barnett, T.P., Adam, J.C. and Lettenmaier, D.P., 2005. Potential impacts of a warming climate on water availability in snow-dominated regions. Nature, 438(7066), pp.303-309.

Bastviken, D., Cole, J., Pace, M., & Tranvik, L. (2004). Methane emissions from lakes: Dependence of lake characteristics, two regional assessments, and a global estimate. Global Biogeochemical Cycles, 18(4).

Bendixen, M., Lonsmann Iversen, L., Anker Bjork, A., Elberling, B., Westergaard-Nielsen, A., Overeem, I., Barnhart, K. R., Abbas Khan, S., Box, J. E., Abermann, J., Langley, K., & Kroon, A. (2017). Delta progradation in Greenland driven by increasing glacial mass loss. *Nature*, *550*(7674), 101–104. https://doi.org/10.1038/nature23873

Bevis, M., Harig, C., Khan, S. A., Brown, A., Simons, F. J., Willis, M., Fettweis, X., Van Den Broeke, M. R., Madsen, F. B., Kendrick, E., Caccamise, D. J., Van Dam, T., Knudsen, P., & Nylen, T. (2019). Accelerating changes in ice mass within Greenland, and the ice sheet's sensitivity to atmospheric forcing. *Proceedings of the National Academy of Sciences of the United States of America*, *116*(6). https://doi.org/10.1073/pnas.1806562116

Bhatt, U. S., Walker, D. A., Raynolds, M. K., Bieniek, P. A., Epstein, H. E., Comiso, J. C., Pinzon, J. E., Tucker, C. J., & Polyakov, I. V. (2013). Recent declines in warming and vegetation greening trends over pan-arctic tundra. *Remote Sensing*, *5*(9). https://doi.org/10.3390/rs5094229

Bintanja, R., & Andry, O. (2017). Towards a rain-dominated Arctic. *Nature Climate Change*, *7*(4). https://doi.org/10.1038/nclimate3240

Bjerke, J. W., Rune Karlsen, S., Arild Hogda, K., Malnes, E., Jepsen, J. U., Lovibond, S., Vikhamar-Schuler, D., & Tommervik, H. (2014). Record-low primary productivity and high plant damage in the Nordic Arctic Region in 2012 caused by multiple weather events and pest outbreaks. *Environmental Research Letters*, *9*(8). https://doi.org/10.1088/1748-9326/9/8/084006

Bjørk, A. A., Aagaard, S., Lütt, A., Khan, S. A., Box, J. E., Kjeldsen, K. K., Larsen, N. K., Korsgaard, N. J., Cappelen, J., Colgan, W. T., Machguth, H., Andresen, C. S., Peings, Y., & Kjær, K. H. (2018a). Changes in Greenland's peripheral glaciers linked to the North Atlantic Oscillation. *Nature Climate Change*, *8*(1). https://doi.org/10.1038/s41558-017-0029-1

Blok, D., Schaepman-Strub, G., Bartholomeus, H., Heijmans, M. M. P. D., Maximov, T. C., & Berendse, F. (2011). The response of Arctic vegetation to the summer climate: Relation between shrub cover, NDVI, surface albedo and temperature. *Environmental Research Letters*, *6*(3). https://doi.org/10.1088/1748-9326/6/3/035502

Bolch, T., Sorensen, L. S., Simonsen, S. B., Molg, N., Machguth, H., Rastner, P., & Paul, F. (2013). Mass loss of Greenland's glaciers and ice caps 2003-2008 revealed from ICESat laser altimetry data. *Geophysical Research Letters*, *40*(5), 875–881. https://doi.org/10.1002/grl.50270

Bonan, G. B., & Doney, S. C. (2018). Climate, ecosystems, and planetary futures: The challenge to predict life in Earth system models. In *Science* (Vol. 359, Issue 6375). https://doi.org/10.1126/science.aam8328

Bring, A., Fedorova, I., Dibike, Y., Hinzman, L., Mård, J., Mernild, S. H., Prowse, T., Semenova, O., Stuefer, S. L., & Woo, M. K. (2016). Arctic terrestrial hydrology: A synthesis of processes, regional effects, and research challenges. In *Journal of Geophysical Research: Biogeosciences* (Vol. 121, Issue 3). https://doi.org/10.1002/2015JG003131

Burpee, B. T., Anderson, D., & Saros, J. E. (2018). Assessing ecological effects of glacial meltwater on lakes fed by the Greenland Ice Sheet: The role of nutrient subsidies and turbidity. *Arctic, Antarctic, and Alpine Research*, *50*(1). https://doi.org/10.1080/15230430.2017.1420953

Carrivick, J. L., Heckmann, T., Turner, A., & Fischer, M. (2018). An assessment of landform composition and functioning with the first proglacial systems dataset of the central European Alps. *Geomorphology*, *321*, 117–128. https://doi.org/10.1016/j.geomorph.2018.08.030

Carrivick, J. L., How, P., Lea, J. M., Sutherland, J. L., Grimes, M., Tweed, F. S., Cornford, S., Quincey, D. J., & Mallalieu, J. (2022). Ice-marginal proglacial lakes across Greenland: Present status and a possible future. *Geophysical Research Letters*, *49*(12), e2022GL099276.

Carrivick, J. L., & Tweed, F. S. (2021). Deglaciation controls on sediment yield: Towards capturing spatio-temporal variability. In *Earth-Science Reviews* (Vol. 221). https://doi.org/10.1016/j.earscirev.2021.103809

Carroll, M. L., Townshend, J. R. G., Dimiceli, C. M., Loboda, T., & Sohlberg, R. A. (2011). Shrinking lakes of the Arctic: Spatial relationships and trajectory of change. *Geophysical Research Letters*, *38*(20). https://doi.org/10.1029/2011GL049427

Cavalli, M., Crema, S., & Marchi, L. (2020). Structural sediment connectivity assessment through a geomorphometric approach : review of recent applications. *Proceedings of the Geomorphometry 2020 Conference*, *July*.

Chae, Y., Kang, S. M., Jeong, S. J., Kim, B., & Frierson, D. M. W. (2015). Arctic greening can cause earlier seasonality of Arctic amplification. *Geophysical Research Letters*, *42*(2). https://doi.org/10.1002/2014GL061841

Chiasson-Poirier, G., Franssen, J., Lafrenière, M. J., Fortier, D., & Lamoureux, S. F. (2020). Seasona evolution of active layer thaw depth and hillslope-stream connectivity in a permafrost watershed. *Water Resources Research*, *56*(1). https://doi.org/10.1029/2019WR025828

Cole, J.J., Prairie, Y.T., Caraco, N.F., McDowell, W.H., Tranvik, L.J., Striegl, R.G., Duarte, C.M., Kortelainen, P., Downing, J.A., Middelburg, J.J. and Melack, J. (2007). Plumbing the global carbon cycle: integrating inland waters into the terrestrial carbon budget. Ecosystems, 10, pp.172-185.

Cuyler, C., Daniel, C. J., Enghoff, M., Levermann, N., Møller-Lund, N., Hansen, P. N., Damhus, D., & Danielsen, F. (2020). Using local ecological knowledge as evidence to guide management: A community-led harvest calculator for

muskoxen in Greenland. *Conservation Science and Practice*, *2*(3). https://doi.org/10.1111/csp2.159

de Jong, R., de Bruin, S., de Wit, A., Schaepman, M. E., & Dent, D. L. (2011). Analysis of monotonic greening and browning trends from global NDVI time-series. *Remote Sensing of Environment*, *115*(2). https://doi.org/10.1016/j.rse.2010.10.011

Edwards, R., & Treitz, P. (2017). Vegetation greening trends at two sites in the Canadian Arctic: 1984-2015. *Arctic, Antarctic, and Alpine Research*, *49*(4). https://doi.org/10.1657/AAAR0016-075

Finger Higgens, R. A., Chipman, J. W., Lutz, D. A., Culler, L. E., Virginia, R. A., & Ogden, L. A. (2019). Changing Lake Dynamics Indicate a Drier Arctic in Western Greenland. *Journal of Geophysical Research: Biogeosciences*, *124*(4). https://doi.org/10.1029/2018JG004879

Flato, G. M. (2011). Earth system models: An overview. *Wiley Interdisciplinary Reviews: Climate Change*, *2*(6). https://doi.org/10.1002/wcc.148

Forbes, B. C., Fauria, M. M., & Zetterberg, P. (2010). Russian Arctic warming and "greening" are closely tracked by tundra shrub willows. *Global Change Biology*, *16*(5). https://doi.org/10.1111/j.1365-2486.2009.02047.x

Ford, J. D., & Goldhar, C. (2012). Climate change vulnerability and adaptation in resource dependent communities: A case study from West Greenland. *Climate Research*, *54*(2). https://doi.org/10.3354/cr01118

Forsberg, R., Sørensen, L., & Simonsen, S. (2017). Greenland and Antarctica Ice Sheet Mass Changes and Effects on Global Sea Level. In *Surveys in Geophysics* (Vol. 38, Issue 1). https://doi.org/10.1007/s10712-016-9398-7

Frost, G. V., Epstein, H. E., & Walker, D. A. (2014). Regional and landscape-scale variability of Landsat-observed vegetation dynamics in northwest Siberian tundra. *Environmental Research Letters*, *9*(2). https://doi.org/10.1088/1748-9326/9/2/025004

Gagnon, M., Domine, F., & Boudreau, S. (2019). The carbon sink due to shrub growth on Arctic tundra: a case study in a carbon-poor soil in eastern Canada. *Environmental Research Communications*, *1*(9). https://doi.org/10.1088/2515-7620/ab3cdd

Gamm, C. M., Sullivan, P. F., Buchwal, A., Dial, R. J., Young, A. B., Watts, D. A., Cahoon, S. M. P., Welker, J. M., & Post, E. (2018). Declining growth of deciduous shrubs in the warming climate of continental western Greenland. *Journal of Ecology*, *106*(2). https://doi.org/10.1111/1365-2745.12882

Gamon, J. A., Huemmrich, K. F., Stone, R. S., & Tweedie, C. E. (2013). Spatial and temporal variation in primary productivity (NDVI) of coastal Alaskan tundra: Decreased vegetation growth following earlier snowmelt. *Remote Sensing of Environment*, *129*. https://doi.org/10.1016/j.rse.2012.10.030

Gillett, N. P., & Fyfe, J. C. (2013). Annular mode changes in the CMIP5 simulations. *Geophysical Research Letters*, *40*(6). https://doi.org/10.1002/grl.50249

Grosse, G., Goetz, S., McGuire, A. D., Romanovsky, V. E., & Schuur, E. A. G. (2016). Changing permafrost in a warming world and feedbacks to the Earth

system. In *Environmental Research Letters* (Vol. 11, Issue 4). https://doi.org/10.1088/1748-9326/11/4/040201

Haselberger, S., Ohler, L. M., Junker, R. R., Otto, J. C., Glade, T., & Kraushaar, S. (2021). Quantification of biogeomorphic interactions between small-scale sediment transport and primary vegetation succession on proglacial slopes of the Gepatschferner, Austria. *Earth Surface Processes and Landforms*, *46*(10). https://doi.org/10.1002/esp.5136

Hasholt, B. (1996). Sediment transport in Greenland. *IAHS-AISH Publication*, *236*.

Hawkings, J. R., Wadham, J. L., Tranter, M., Lawson, E., Sole, A., Cowton, T., Tedstone, A. J., Bartholomew, I., Nienow, P., Chandler, D., & Telling, J. (2015). The effect of warming climate on nutrient and solute export from the Greenland Ice Sheet. *Geochemical Perspectives Letters*, *1*(1), 94–104. https://doi.org/10.7185/geochemlet.1510

Heckmann, T., & Vericat, D. (2018). Computing spatially distributed sediment delivery ratios: inferring functional sediment connectivity from repeat high-resolution digital elevation models. *Earth Surface Processes and Landforms*, *43*(7), 1547–1554. https://doi.org/10.1002/esp.4334

Heijmans, M. M. P. D., Magnússon, R., Lara, M. J., Frost, G. V., Myers-Smith, I. H., van Huissteden, J., Jorgenson, M. T., Fedorov, A. N., Epstein, H. E., Lawrence, D. M., & Limpens, J. (2022). Tundra vegetation change and impacts on permafrost. In *Nature Reviews Earth and Environment* (Vol. 3, Issue 1). https://doi.org/10.1038/s43017-021-00233-0

Heindel, R. C., Chipman, J. W., & Virginia, R. A. (2015). The Spatial Distribution and Ecological Impacts of Aeolian Soil Erosion in Kangerlussuaq, West Greenland. *Annals of the Association of American Geographers*, *105*(5). https://doi.org/10.1080/00045608.2015.1059176

Heinemann, G. (2020). Assessment of regional climate model simulations of the katabatic boundary layer structure over Greenland. *Atmosphere*, *11*(6). https://doi.org/10.3390/atmos11060571

Jia, G. J., Epstein, H. E., & Walker, D. A. (2003). Greening of arctic Alaska, 1981-2001. *Geophysical Research Letters*, *30*(20). https://doi.org/10.1029/2003GL018268

Ju, J., & Masek, J. G. (2016). The vegetation greenness trend in Canada and US Alaska from 1984-2012 Landsat data. *Remote Sensing of Environment*, *176*. https://doi.org/10.1016/j.rse.2016.01.001

Karlsen, S. R., Elvebakk, A., Høgda, K. A., & Grydeland, T. (2014). Spatial and temporal variability in the onset of the growing season on svalbard, arctic Norway - Measured by MODIS-NDVI satellite data. *Remote Sensing*, *6*(9). https://doi.org/10.3390/rs6098088

Karlsen, S. R., Stendardi, L., Tømmervik, H., Nilsen, L., Arntzen, I., & Cooper, E. J. (2021). Time-series of cloud-free sentinel-2 ndvi data used in mapping the onset of growth of central spitsbergen, svalbard. *Remote Sensing*, *13*(15). https://doi.org/10.3390/rs13153031

Kaufman, D. S., Axford, Y. L., Henderson, A. C. G., McKay, N. P., Oswald, W. W., Saenger, C., Anderson, R. S., Bailey, H. L., Clegg, B., Gajewski, K., Hu, F. S., Jones, M. C., Massa, C., Routson, C. C., Werner, A., Wooller, M. J., & Yu, Z. (2016). Holocene climate changes in eastern Beringia (NW North America) – A systematic review of multi-proxy evidence. *Quaternary Science Reviews*, *147*. https://doi.org/10.1016/j.quascirev.2015.10.021

Korsgaard, N. J., Nuth, C., Khan, S. A., Kjeldsen, K. K., Bjork, A. A., Schomacker, A., & Kjaer, K. H. (2016). Digital elevation model and orthophotographs of Greenland based on aerial photographs from 1978-1987. *Sci Data*, *3*, 160032. https://doi.org/10.1038/sdata.2016.32

Kropp, H., Loranty, M. M., Natali, S. M., Kholodov, A. L., Rocha, A. V., Myers-Smith, I., Abbot, B. W., Abermann, J., Blanc-Betes, E., Blok, D., Blume-Werry, G., Boike, J., Breen, A. L., Cahoon, S. M. P., Christiansen, C. T., Douglas, T. A., Epstein, H. E., Frost, G. V., Goeckede, M., … Lund, M. (2021). Shallow soils are warmer under trees and tall shrubs across Arctic and Boreal ecosystems. *Environmental Research Letters*, *16*(1). https://doi.org/10.1088/1748-9326/abc994

Lara, M. J., Nitze, I., Grosse, G., Martin, P., & David McGuire, A. (2018). Reduced arctic tundra productivity linked with landform and climate change interactions. *Scientific Reports*, *8*(1). https://doi.org/10.1038/s41598-018-20692-8

Law, A. C., Nobajas, A., & Sangonzalo, R. (2018). Heterogeneous changes in the surface area of lakes in the Kangerlussuaq area of southwestern Greenland between 1995 and 2017. *Arctic, Antarctic, and Alpine Research*, *50*(1). https://doi.org/10.1080/15230430.2018.1487744

Le Page, Y., West, T. O., Link, R., & Patel, P. (2016). Downscaling land use and land cover from the Global Change Assessment Model for coupling with Earth system models. *Geoscientific Model Development*, *9*(9). https://doi.org/10.5194/gmd-9-3055-2016

Leclercq, P. W., Weidick, A., Paul, F., Bolch, T., Citterio, M., & Oerlemans, J. (2012). Brief communication “Historical glacier length changes in West Greenland.” *Cryosphere*, *6*(6), 1339–1343. https://doi.org/10.5194/tc-6-1339-2012

Lewkowicz, A. G., & Way, R. G. (2019). Extremes of summer climate trigger thousands of thermokarst landslides in a High Arctic environment. *Nature Communications*, *10*(1). https://doi.org/10.1038/s41467-019-09314-7

Liu, C., Huang, H., & Sun, F. (2021). A pixel-based vegetation greenness trend analysis over the Russian tundra with all available landsat data from 1984 to 2018. *Remote Sensing*, *13*(23). https://doi.org/10.3390/rs13234933

Loranty, M. M., Goetz, S. J., & Beck, P. S. A. (2011). Tundra vegetation effects on pan-Arctic albedo. *Environmental Research Letters*, *6*(2). https://doi.org/10.1088/1748-9326/6/2/029601

Lund, M., Raundrup, K., Westergaard-Nielsen, A., López-Blanco, E., Nymand, J., & Aastrup, P. (2017). Larval outbreaks in West Greenland: Instant and subsequent

effects on tundra ecosystem productivity and CO2 exchange. *Ambio*, *46*. https://doi.org/10.1007/s13280-016-0863-9

Lynch, L. M., Machmuller, M. B., Boot, C. M., Covino, T. P., Rithner, C. D., Cotrufo, M. F., Hoyt, D. W., & Wallenstein, M. D. (2019). Dissolved Organic Matter Chemistry and Transport Along an Arctic Tundra Hillslope. *Global Biogeochemical Cycles*, *33*(1). https://doi.org/10.1029/2018GB006030

Lynch, L. M., Machmuller, M. B., Cotrufo, M. F., Paul, E. A., & Wallenstein, M. D. (2018). Tracking the fate of fresh carbon in the Arctic tundra: Will shrub expansion alter responses of soil organic matter to warming? *Soil Biology and Biochemistry*, *120*. https://doi.org/10.1016/j.soilbio.2018.02.002

Machguth, H., Rastner, P., Bolch, T., Mölg, N., Sørensen, L. S., Aðalgeirsdottir, G., van Angelen, J. H., van den Broeke, M. R., & Fettweis, X. (2013). The future sea-level rise contribution of Greenland's glaciers and ice caps. *Environmental Research Letters*, *8*(2). https://doi.org/10.1088/1748-9326/8/2/025005

MacIas-Fauria, M., Forbes, B. C., Zetterberg, P., & Kumpula, T. (2012). Eurasian Arctic greening reveals teleconnections and the potential for structurally novel ecosystems. *Nature Climate Change*, *2*(8). https://doi.org/10.1038/nclimate1558

Mann, D. H., Groves, P., Reanier, R. E., & Kunz, M. L. (2010). Floodplains, permafrost, cottonwood trees, and peat: What happened the last time climate warmed suddenly in arctic Alaska? *Quaternary Science Reviews*, *29*(27–28). https://doi.org/10.1016/j.quascirev.2010.09.002

Martin, A. C., Jeffers, E. S., Petrokofsky, G., Myers-Smith, I., & MacIas-Fauria, M. (2017). Shrub growth and expansion in the Arctic tundra: An assessment of controlling factors using an evidence-based approach. *Environmental Research Letters*, *12*(8). https://doi.org/10.1088/1748-9326/aa7989

May, J., Healey, N., Ahrends, H., Hollister, R., Tweedie, C., Welker, J., Gould, W., & Oberbauer, S. (2017). Short-Term Impacts of the Air Temperature on Greening and Senescence in Alaskan Arctic Plant Tundra Habitats. *Remote Sensing*, *9*(12). https://doi.org/10.3390/rs9121338

Meier, M. F., Dyurgerov, M. B., Rick, U. K., O'Neel, S., Pfeffer, W. T., Anderson, R. S., Anderson, S. P., & Glazovsky, A. F. (2007). Glaciers dominate Eustatic sea-level rise in the 21st century. *Science*, *317*(5841), 1064–1067. https://doi.org/10.1126/science.1143906

Mekonnen, Z. A., Riley, W. J., Berner, L. T., Bouskill, N. J., Torn, M. S., Iwahana, G., Breen, A. L., Myers-Smith, I. H., Criado, M. G., Liu, Y., Euskirchen, E. S., Goetz, S. J., Mack, M. C., & Grant, R. F. (2021). Arctic tundra shrubification: a review of mechanisms and impacts on ecosystem carbon balance. In *Environmental Research Letters* (Vol. 16, Issue 5). https://doi.org/10.1088/1748-9326/abf28b

Miles, V. V., & Esau, I. (2016). Spatial heterogeneity of greening and browning between and within bioclimatic zones in northern West Siberia. *Environmental Research Letters*, *11*(11). https://doi.org/10.1088/1748-9326/11/11/115002

Mosley-Thompson, E., Readinger, C. R., Craigmile, P., Thompson, L. G., & Calder, C. A. (2005). Regional sensitivity of Greenland precipitation to NAO

variability. *Geophysical Research Letters*, *32*(24). https://doi.org/10.1029/2005GL024776

Myers-Smith, I. H., Kerby, J. T., Phoenix, G. K., Bjerke, J. W., Epstein, H. E., Assmann, J. J., John, C., Andreu-Hayles, L., Angers-Blondin, S., Beck, P. S. A., Berner, L. T., Bhatt, U. S., Bjorkman, A. D., Blok, D., Bryn, A., Christiansen, C. T., Cornelissen, J. H. C., Cunliffe, A. M., Elmendorf, S. C., … Wipf, S. (2020). Complexity revealed in the greening of the Arctic. In *Nature Climate Change* (Vol. 10, Issue 2). https://doi.org/10.1038/s41558-019-0688-1

Najafi, S., Dragovich, D., Heckmann, T. and Sadeghi, S.H., 2021. Sediment connectivity concepts and approaches. Catena, 196, p.104880.

Normand, S., Randin, C., Ohlemüller, R., Bay, C., Høye, T. T., Kjær, E. D., Körner, C., Lischke, H., Maiorano, L., Paulsen, J., Pearman, P. B., Psomas, A., Treier, U. A., Zimmermann, N. E., & Svenning, J. C. (2013). A greener Greenland? Climatic potential and long-term constraints on future expansions of trees and shrubs. *Philosophical Transactions of the Royal Society B: Biological Sciences*, *368*(1624). https://doi.org/10.1098/rstb.2012.0479

Nuttall, M. (2016). Living in a world of movement: Human resilience to environmental instability in Greenland. In *Anthropology and Climate Change: From Encounters to Actions*. https://doi.org/10.4324/9781315434773-26

Ohler, L. M., Haselberger, S., Janssen, S., Otto, J. C., Kraushaar, S., & Junker, R. R. (2023). Proglacial slopes are protected against erosion by trait diverse and dense plant communities associated with specific microbial communities. *Basic and Applied Ecology*, *71*. https://doi.org/10.1016/j.baae.2023.05.008

Overeem, I., Hudson, B. D., Syvitski, J. P. M., Mikkelsen, A. B., Hasholt, B., van den Broeke, M. R., Noël, B. P. Y., & Morlighem, M. (2017). Substantial export of suspended sediment to the global oceans from glacial erosion in Greenland. *Nature Geoscience*, *10*(11), 859–863. https://doi.org/10.1038/ngeo3046

Persichillo, M. G., Bordoni, M., Cavalli, M., Crema, S., & Meisina, C. (2018). The role of human activities on sediment connectivity of shallow landslides. *Catena*, *160*. https://doi.org/10.1016/j.catena.2017.09.025

Phoenix, G. K., & Bjerke, J. W. (2016). Arctic browning: extreme events and trends reversing arctic greening. In *Global Change Biology* (Vol. 22, Issue 9). https://doi.org/10.1111/gcb.13261

Rantala, M. V., Luoto, T. P., & Nevalainen, L. (2016). Temperature controls organic carbon sequestration in a subarctic lake. *Scientific Reports*, *6*. https://doi.org/10.1038/srep34780

Rastner, P., Bolch, T., Molg, N., Machguth, H., Le Bris, R., & Paul, F. (2012). The first complete inventory of the local glaciers and ice caps on Greenland. *Cryosphere*, *6*(6), 1483–1495. https://doi.org/10.5194/tc-6-1483-2012

Riis, T., Tank, J.L., Holmboe, C.M., Giménez-Grau, P., Mastepanov, M., Catalán, N., Stott, D., Hansen, B., Kristiansen, S.M. and Pastor, A., 2023. Links between stream water nitrogen and terrestrial vegetation in Northeast Greenland. *Journal of Geophysical Research: Biogeosciences*, 128(12), p.e2023JG007688.

Rowland, J. C., Jones, C. E., Altmann, G., Bryan, R., Crosby, B. T., Geernaert, G. L., Hinzman, L. D., Kane, D. L., Lawrence, D. M., Mancino, A., Marsh, P., McNamara, J. P., Romanovsky, V. E., Toniolo, H., Travis, B. J., Trochim, E., & Wilson, C. J. (2010). Arctic landscapes in transition: Responses to thawing permafrost. *Eos*, *91*(26). https://doi.org/10.1029/2010EO260001

Rysgaard, S., Nielsen, T. G., & Hansen, B. W. (1999). Seasonal variation in nutrients, pelagic primary production and grazing in a high-Arctic coastal marine ecosystem, Young Sound, Northeast Greenland. *Marine Ecology Progress Series*, *179*, 13–25. https://doi.org/DOI 10.3354/meps179013

Séférian, R., Nabat, P., Michou, M., Saint-Martin, D., Voldoire, A., Colin, J., Decharme, B., Delire, C., Berthet, S., Chevallier, M., Sénési, S., Franchisteguy, L., Vial, J., Mallet, M., Joetzjer, E., Geoffroy, O., Guérémy, J. F., Moine, M. P., Msadek, R., … Madec, G. (2019). Evaluation of CNRM Earth System Model, CNRM-ESM2-1: Role of Earth System Processes in Present-Day and Future Climate. *Journal of Advances in Modeling Earth Systems*, *11*(12). https://doi.org/10.1029/2019MS001791

Seo, J., Jang, I., Jung, J. Y., Lee, Y. K., & Kang, H. (2015). Warming and increased precipitation enhance phenol oxidase activity in soil while warming induces drought stress in vegetation of an Arctic ecosystem. *Geoderma*, *259–260*. https://doi.org/10.1016/j.geoderma.2015.03.017

Speir, S.L., Tank, J.L., Pastor, A., Muller, M.F., Mastepanov, M. and Riis, T., 2024. Catchment-scale thawing and greening decreases long-term nitrogen export in NE Greenland. *Environmental Research Letters*, 19(5), p.054031.

Straneo, F., & Heimbach, P. (2013). North Atlantic warming and the retreat of Greenland's outlet glaciers. In *Nature* (Vol. 504, Issue 7478). https://doi.org/10.1038/nature12854

Tesi, T., Muschitiello, F., Smittenberg, R. H., Jakobsson, M., Vonk, J. E., Hill, P., Andersson, A., Kirchner, N., Noormets, R., Dudarev, O., Semiletov, I., & Gustafsson. (2016). Massive remobilization of permafrost carbon during post-glacial warming. *Nature Communications*, *7*. https://doi.org/10.1038/ncomms13653

Tiranti, D., Cavalli, M., Crema, S., Zerbato, M., Graziadei, M., Barbero, S., Cremonini, R., Silvestro, C., Bodrato, G., & Tresso, F. (2016). Semi-quantitative method for the assessment of debris supply from slopes to river in ungauged catchments. *Science of the Total Environment*, *554–555*. https://doi.org/10.1016/j.scitotenv.2016.02.150

Tommasini, D. (2015). The governance of protected areas in Greenland: The resource national park among conservation and exploitation. In *Indigenous Peoples' Governance of Land and Protected Territories in the Arctic*. https://doi.org/10.1007/978-3-319-25035-9_7

Tranvik, L.J., Downing, J.A., Cotner, J.B., Loiselle, S.A., Striegl, R.G., Ballatore, T.J., Dillon, P., Finlay, K., Fortino, K., Knoll, L.B. and Kortelainen, P.L. (2009). Lakes and reservoirs as regulators of carbon cycling and climate. Limnology and oceanography, 54(6part2), pp.2298-2314.

Tveraa, T., Stien, A., Bårdsen, B. J., & Fauchald, P. (2013). Population Densities, Vegetation Green-Up, and Plant Productivity: Impacts on Reproductive Success and Juvenile Body Mass in Reindeer. *PLoS ONE*, *8*(2). https://doi.org/10.1371/journal.pone.0056450

Van Den Broeke, M. R., Enderlin, E. M., Howat, I. M., Kuipers Munneke, P., Noël, B. P. Y., Jan Van De Berg, W., Van Meijgaard, E., & Wouters, B. (2016). On the recent contribution of the Greenland ice sheet to sea level change. *Cryosphere*, *10*(5). https://doi.org/10.5194/tc-10-1933-2016

Vickers, H., HØgda, K. A., SolbØ, S., Karlsen, S. R., TØmmervik, H., Aanes, R., & Hansen, B. B. (2016). Changes in greening in the high Arctic: Insights from a 30 year AVHRR max NDVI dataset for Svalbard. *Environmental Research Letters*, *11*(10). https://doi.org/10.1088/1748-9326/11/10/105004

Vonk, J. E., Dickens, A. F., Giosan, L., Hussain, Z. A., Kim, B., Zipper, S. C., Holmes, R. M., Montlucon, D. B., Galy, V., & Eglinton, T. I. (2016). Arctic deltaic lake sediments as recorders of fluvial organic matter deposition. *Frontiers in Earth Science*, *4*. https://doi.org/10.3389/feart.2016.00077

Voronina, E. (2021). Development of the Arctic regions of the Russian Federation: Drivers of greening. *E3S Web of Conferences*, *244*. https://doi.org/10.1051/e3sconf/202124410051

Walker, D. A., Leibman, M. O., Epstein, H. E., Forbes, B. C., Bhatt, U. S., Raynolds, M. K., Comiso, J. C., Gubarkov, A. A., Khomutov, A. V., Jia, G. J., Kaarlejärvi, E., Kaplan, J. O., Kumpula, T., Kuss, P., Matyshak, G., Moskalenko, N. G., Orekhov, P., Romanovsky, V. E., Ukraientseva, N. G., & Yu, Q. (2009). Spatial and temporal patterns of greenness on the Yamal Peninsula, Russia: Interactions of ecological and social factors affecting the Arctic normalized difference vegetation index. *Environmental Research Letters*, *4*(4). https://doi.org/10.1088/1748-9326/4/4/045004

Walvoord, M. A., & Kurylyk, B. L. (2016). Hydrologic Impacts of Thawing Permafrost—A Review. *Vadose Zone Journal*, *15*(6). https://doi.org/10.2136/vzj2016.01.0010

Wik, M., Varner, R.K., Anthony, K.W., MacIntyre, S. and Bastviken, D. (2016). Climate-sensitive northern lakes and ponds are critical components of methane release. Nature Geoscience, 9(2), pp.99-105.

Willemse, N. W., Koster, E. A., Hoogakker, B., & Van Tatenhove, F. G. M. (2003). A continuous record of Holocene eolian activity in West Greenland. *Quaternary Research*, *59*(3). https://doi.org/10.1016/S0033-5894(03)00037-1

Yi, S., Sun, W., Heki, K., & Qian, A. (2015). An increase in the rate of global mean sea level rise since 2010. *Geophysical Research Letters*, *42*(10). https://doi.org/10.1002/2015GL063902

Zhang, Y., Song, C., Band, L. E., Sun, G., & Li, J. (2017). Reanalysis of global terrestrial vegetation trends from MODIS products: Browning or greening? *Remote Sensing of Environment*, *191*. https://doi.org/10.1016/j.rse.2016.12.018

Appendix A: Latitudinal 64-class change matrices

80 - 82

From \ To	Snow/ Ice	Wetice/ Meltwater	Deep/ LowSSWater	Coarse Sediment	Fine Sediment	Bedrock	Tundra Vegetation	Wet/ DenseVeg	
Snow/ Ice	0.00	2.68	0.77	8.18	15.31	8.29	0.04	0.07	35.33
Wetice/ Meltwater	0.31	0.00	0.71	0.41	0.42	0.55	0.01	0.01	2.42
Deep/ LowSSWater	0.04	0.25	0.00	0.07	0.05	0.09	0.00	0.00	0.51
Coarse Sediment	0.10	0.41	0.14	0.00	8.23	7.57	0.68	0.14	17.26
Fine Sediment	0.07	0.25	0.04	16.57	0.00	15.07	0.12	0.05	32.17
Bedrock	0.15	0.88	0.26	5.42	4.13	0.00	1.22	0.15	12.21
Tundra Vegetation	0.00	0.00	0.01	0.00	0.00	0.02	0.00	0.05	0.08
Wet/ DenseVeg	0.00	0.00	0.00	0.00	0.00	0.00	0.00	0.00	0.01
	0.675	4.464	1.930	30.660	28.139	31.600	2.067	0.463	

From \ To	Snow/ Ice	Wetice/ Meltwater	Deep/ LowSSWater	Coarse Sediment	Fine Sediment	Bedrock	Tundra Vegetation	Wet/ DenseVeg	
Snow/ Ice	0.00	3.96	0.28	4.19	1.45	3.67	0.00	0.03	13.59
Wetice/ Meltwater	1.51	0.00	0.46	1.87	0.03	1.80	0.01	0.02	5.69
Deep/ LowSSWater	0.50	1.34	0.00	0.24	0.01	0.27	0.02	0.03	2.40
Coarse Sediment	0.83	1.80	0.17	0.00	6.23	23.20	2.09	0.98	35.28
Fine Sediment	0.11	0.14	0.00	8.45	0.00	2.26	0.28	0.19	11.43
Bedrock	0.92	1.80	0.26	18.51	2.63	0.00	5.99	0.91	31.03
Tundra Vegetation	0.00	0.01	0.05	0.04	0.03	0.06	0.00	0.37	0.56
Wet/ DenseVeg	0.00	0.00	0.00	0.00	0.00	0.00	0.00	0.00	0.01
	3.87	9.06	1.22	33.30	10.38	31.26	8.39	2.53	

78 - 80

From \ To	Snow/ Ice	Wetice/ Meltwater	Deep/ LowSSWater	Coarse Sediment	Fine Sediment	Bedrock	Tundra Vegetation	Wet/ DenseVeg	
Snow/ Ice	0.00	1.53	0.57	1.09	3.01	0.81	0.01	0.01	7.01
Wetice/ Meltwater	0.69	0.00	0.84	0.72	0.07	1.67	0.05	0.02	4.06
Deep/ LowSSWater	0.82	1.58	0.00	0.28	0.12	1.82	0.44	0.11	5.16
Coarse Sediment	0.19	0.59	0.68	0.00	5.13	33.38	2.33	0.30	42.60
Fine Sediment	0.14	0.04	0.05	4.76	0.00	7.51	0.23	0.02	12.74
Bedrock	0.33	0.66	0.69	9.97	3.68	0.00	5.77	0.39	21.48
Tundra Vegetation	0.00	0.02	0.23	0.02	0.07	5.94	0.00	0.42	6.70
Wet/ DenseVeg	0.00	0.01	0.02	0.00	0.00	0.07	0.14	0.00	0.24
	2.17	4.42	3.08	16.84	12.07	51.20	8.95	1.27	

From \ To	Snow/ Ice	Wetice/ Meltwater	Deep/ LowSSWater	Coarse Sediment	Fine Sediment	Bedrock	Tundra Vegetation	Wet/ DenseVeg	
Snow/ Ice	0.00	4.14	0.73	3.14	0.56	4.98	0.01	0.06	13.62
Wetice/ Meltwater	4.18	0.00	0.53	1.87	0.01	1.68	0.01	0.04	8.31
Deep/ LowSSWater	0.46	0.57	0.00	0.15	0.00	0.17	0.05	0.07	1.46
Coarse Sediment	2.36	1.78	0.22	0.00	4.11	15.17	2.25	1.33	27.23
Fine Sediment	0.09	0.06	0.00	4.30	0.00	0.82	0.09	0.09	5.45
Bedrock	3.98	2.57	0.35	29.07	1.65	0.00	3.18	2.38	43.20
Tundra Vegetation	0.01	0.01	0.05	0.03	0.05	0.08	0.00	0.48	0.72
Wet/ DenseVeg	0.00	0.00	0.00	0.00	0.00	0.00	0.01	0.00	0.02
	11.08	9.13	1.90	38.56	6.39	22.90	5.60	4.46	

76 - 78

From \ To	Snow/ Ice	Wetice/ Meltwater	Deep/ LowSSWater	Coarse Sediment	Fine Sediment	Bedrock	Tundra Vegetation	Wet/ DenseVeg	
Snow/ Ice	0.00	6.70	2.15	16.54	3.95	38.12	1.53	0.43	69.43
Wetice/ Meltwater	0.62	0.00	0.37	0.70	0.06	1.55	0.10	0.03	3.43
Deep/ LowSSWater	0.08	0.18	0.00	0.06	0.01	0.11	0.02	0.01	0.48
Coarse Sediment	0.17	0.33	0.08	0.00	0.29	11.24	0.53	0.13	12.76
Fine Sediment	0.00	0.00	0.00	0.64	0.00	1.50	0.07	0.02	2.24
Bedrock	0.56	0.66	0.12	7.61	0.22	0.00	1.82	0.24	11.24
Tundra Vegetation	0.00	0.00	0.02	0.01	0.00	0.20	0.00	0.17	0.40
Wet/ DenseVeg	0.00	0.00	0.00	0.00	0.00	0.01	0.01	0.00	0.02
	1.43	7.88	2.74	25.57	4.54	52.74	4.07	1.03	

From \ To	Snow/ Ice	Wetice/ Meltwater	Deep/ LowSSWater	Coarse Sediment	Fine Sediment	Bedrock	Tundra Vegetation	Wet/ DenseVeg	
Snow/ Ice	0.00	3.11	0.24	1.55	0.15	2.32	0.00	0.02	7.39
Wetice/ Meltwater	3.46	0.00	0.91	1.42	0.01	1.02	0.01	0.02	6.86
Deep/ LowSSWater	0.73	1.06	0.00	0.14	0.00	0.13	0.03	0.05	2.15
Coarse Sediment	3.41	2.12	0.29	0.00	2.07	18.26	2.76	0.86	29.77
Fine Sediment	0.14	0.06	0.00	2.96	0.00	0.80	0.29	0.07	4.32
Bedrock	5.56	3.11	0.56	25.25	1.41	0.00	9.87	1.31	47.06
Tundra Vegetation	0.01	0.04	0.21	0.08	0.09	1.28	0.00	0.66	2.38
Wet/ DenseVeg	0.00	0.01	0.03	0.00	0.00	0.03	0.02	0.00	0.08
	13.31	9.51	2.24	31.40	3.74	23.84	12.98	2.98	

74 - 76

From \ To	Snow/ Ice	Wetice/ Meltwater	Deep/ LowSSWater	Coarse Sediment	Fine Sediment	Bedrock	Tundra Vegetation	Wet/ DenseVeg	
Snow/ Ice	0.00	13.90	5.17	3.87	0.42	12.49	0.04	0.02	35.91
Wetice/ Meltwater	2.46	0.00	2.71	1.02	0.00	1.51	0.00	0.01	7.72
Deep/ LowSSWater	0.21	0.94	0.00	0.07	0.00	0.07	0.00	0.00	1.29
Coarse Sediment	0.51	0.92	0.53	0.00	0.18	17.45	1.26	0.14	21.00
Fine Sediment	0.01	0.00	0.00	0.43	0.00	0.85	0.04	0.01	1.35
Bedrock	1.24	1.55	0.56	22.61	0.15	0.00	5.57	0.26	31.95
Tundra Vegetation	0.00	0.00	0.07	0.01	0.00	0.54	0.00	0.15	0.78
Wet/ DenseVeg	0.00	0.00	0.00	0.00	0.00	0.00	0.00	0.00	0.00
	4.44	17.32	9.05	28.01	0.76	32.92	6.92	0.59	

From \ To	Snow/ Ice	Wetice/ Meltwater	Deep/ LowSSWater	Coarse Sediment	Fine Sediment	Bedrock	Tundra Vegetation	Wet/ DenseVeg	
Snow/ Ice	0.00	2.74	0.15	1.65	0.33	3.14	0.06	0.11	8.19
Wetice/ Meltwater	2.29	0.00	0.46	1.65	0.01	1.46	0.05	0.12	6.05
Deep/ LowSSWater	0.44	0.92	0.00	0.15	0.00	0.19	0.06	0.19	1.95
Coarse Sediment	3.66	2.27	0.36	0.00	3.29	16.62	4.05	1.08	31.33
Fine Sediment	0.42	0.06	0.00	2.79	0.00	1.16	0.37	0.14	4.95
Bedrock	4.89	2.82	0.54	17.83	2.24	0.00	12.96	1.70	42.98
Tundra Vegetation	0.05	0.09	0.38	0.11	0.10	1.23	0.00	2.44	4.40
Wet/ DenseVeg	0.01	0.02	0.03	0.00	0.00	0.02	0.06	0.00	0.14
	11.77	8.91	1.94	24.19	5.96	23.83	17.62	5.79	

72 - 74

From \ To	Snow/ Ice	Wetice/ Meltwater	Deep/ LowSSWater	Coarse Sediment	Fine Sediment	Bedrock	Tundra Vegetation	Wet/ DenseVeg	
Snow/ Ice	0.00	7.30	1.30	3.67	0.29	3.91	0.08	0.26	16.81
Wetice/ Meltwater	1.00	0.00	1.67	2.03	0.02	1.06	0.03	0.07	5.89
Deep/ LowSSWater	0.07	1.10	0.00	0.14	0.00	0.09	0.01	0.04	1.46
Coarse Sediment	0.28	1.12	0.64	0.00	0.54	13.05	9.64	1.29	26.57
Fine Sediment	0.00	0.00	0.00	0.38	0.00	0.59	0.07	0.02	1.06
Bedrock	0.18	0.73	0.81	14.08	0.52	0.00	24.49	1.57	42.38
Tundra Vegetation	0.00	0.02	0.75	0.24	0.06	1.60	0.00	3.08	5.76
Wet/ DenseVeg	0.00	0.01	0.04	0.00	0.00	0.00	0.01	0.00	0.06
	1.53	10.29	5.22	20.54	1.43	20.31	34.34	6.33	

From \ To	Snow/ Ice	Wetice/ Meltwater	Deep/ LowSSWater	Coarse Sediment	Fine Sediment	Bedrock	Tundra Vegetation	Wet/ DenseVeg	
Snow/ Ice	0.00	3.93	0.10	1.52	0.39	2.50	0.06	0.10	8.60
Wetice/ Meltwater	3.88	0.00	0.22	1.51	0.04	1.51	0.06	0.10	7.33
Deep/ LowSSWater	0.39	0.47	0.00	0.14	0.01	0.16	0.02	0.03	1.22
Coarse Sediment	5.13	3.48	0.18	0.00	4.69	13.52	5.15	1.38	33.53
Fine Sediment	0.62	0.13	0.05	1.84	0.00	0.88	0.29	0.13	3.95
Bedrock	5.26	2.97	0.32	14.26	4.40	0.00	12.23	1.73	41.17
Tundra Vegetation	0.14	0.17	0.17	0.26	0.31	1.19	0.00	1.74	3.97
Wet/ DenseVeg	0.04	0.03	0.01	0.03	0.01	0.06	0.05	0.00	0.22
	15.45	11.19	1.06	19.57	9.84	19.82	17.85	5.21	

70 - 72

From \ To	Snow/ Ice	Wetice/ Meltwater	Deep/ LowSSWater	Coarse Sediment	Fine Sediment	Bedrock	Tundra Vegetation	Wet/ DenseVeg	
Snow/ Ice	0.00	7.18	0.38	4.35	0.32	5.12	0.76	0.13	18.23
Wetice/ Meltwater	1.40	0.00	0.82	2.98	0.00	2.09	0.03	0.06	7.38
Deep/ LowSSWater	0.08	0.84	0.00	0.16	0.00	0.16	0.01	0.05	1.30
Coarse Sediment	0.72	1.51	0.25	0.00	0.45	11.19	7.53	2.24	23.89
Fine Sediment	0.00	0.00	0.00	0.20	0.00	0.21	0.17	0.05	0.65
Bedrock	0.19	1.05	0.34	16.61	0.72	0.00	22.38	2.45	43.73
Tundra Vegetation	0.00	0.04	0.28	0.27	0.08	0.89	0.00	3.23	4.80
Wet/ DenseVeg	0.00	0.01	0.01	0.00	0.00	0.00	0.01	0.00	0.02
	2.39	10.63	2.07	24.57	1.57	19.67	30.89	8.21	

From \ To	Snow/ Ice	Wetice/ Meltwater	Deep/ LowSSWater	Coarse Sediment	Fine Sediment	Bedrock	Tundra Vegetation	Wet/ DenseVeg	
Snow/ Ice	0.00	4.27	0.15	1.20	0.21	2.17	0.02	0.04	8.05
Wetice/ Meltwater	4.00	0.00	0.33	1.72	0.07	1.38	0.02	0.05	7.58
Deep/ LowSSWater	0.39	0.63	0.00	0.17	0.02	0.18	0.03	0.02	1.43
Coarse Sediment	5.64	3.53	0.12	0.00	5.96	12.88	5.25	1.50	34.87
Fine Sediment	0.34	0.06	0.00	0.49	0.00	0.49	0.23	0.13	1.74
Bedrock	4.22	2.66	0.23	11.11	3.74	0.00	16.19	1.93	40.09
Tundra Vegetation	0.15	0.21	0.16	0.30	0.42	1.35	0.00	3.40	5.99
Wet/ DenseVeg	0.04	0.03	0.01	0.03	0.01	0.06	0.04	0.00	0.24
	14.78	11.40	1.00	15.02	10.42	18.50	21.79	7.08	

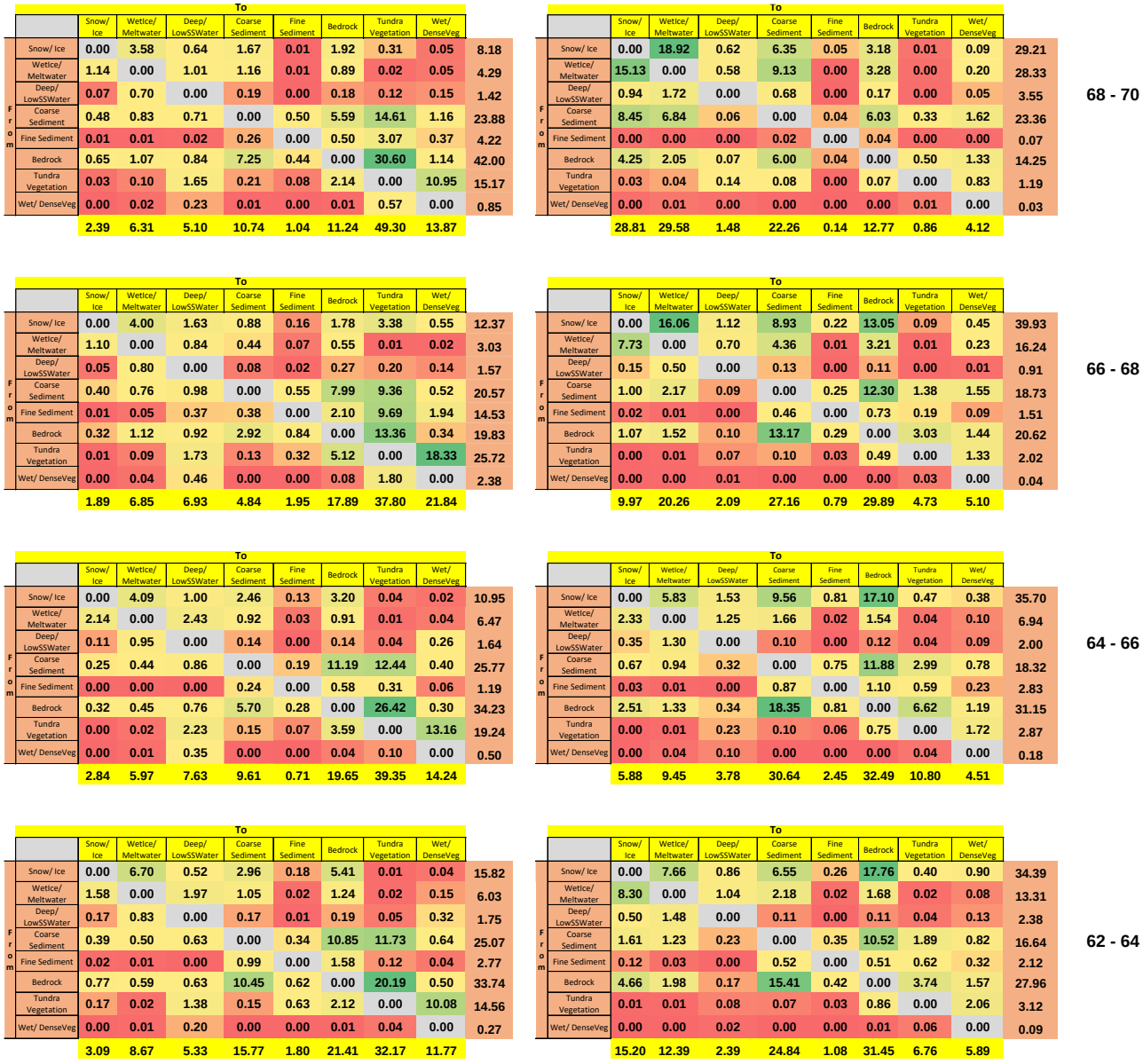

From \ To	Snow/ Ice	Wetice/ Meltwater	Deep/ LowSSWater	Coarse Sediment	Fine Sediment	Bedrock	Tundra Vegetation	Wet/ DenseVeg		
Snow/ Ice	0.00	3.58	0.64	1.67	0.01	1.92	0.31	0.05	8.18	
Wetice/ Meltwater	1.14	0.00	1.01	1.16	0.01	0.89	0.02	0.05	4.29	
Deep/ LowSSWater	0.07	0.70	0.00	0.19	0.00	0.18	0.12	0.15	1.42	
Coarse Sediment	0.48	0.83	0.71	0.00	0.50	5.59	14.61	1.16	23.88	
Fine Sediment	0.01	0.01	0.02	0.26	0.00	0.50	3.07	0.37	4.22	
Bedrock	0.65	1.07	0.84	7.25	0.44	0.00	30.60	1.14	42.00	
Tundra Vegetation	0.03	0.10	1.65	0.21	0.08	2.14	0.00	10.95	15.17	
Wet/ DenseVeg	0.00	0.02	0.23	0.01	0.00	0.01	0.57	0.00	0.85	
	2.39	6.31	5.10	10.74	1.04	11.24	49.30	13.87		

From \ To	Snow/ Ice	Wetice/ Meltwater	Deep/ LowSSWater	Coarse Sediment	Fine Sediment	Bedrock	Tundra Vegetation	Wet/ DenseVeg		
Snow/ Ice	0.00	18.92	0.62	6.35	0.05	3.18	0.01	0.09	29.21	
Wetice/ Meltwater	15.13	0.00	0.58	9.13	0.00	3.28	0.00	0.20	28.33	
Deep/ LowSSWater	0.94	1.72	0.00	0.68	0.00	0.17	0.00	0.05	3.55	68 - 70
Coarse Sediment	8.45	6.84	0.06	0.00	0.04	6.03	0.33	1.62	23.36	
Fine Sediment	0.00	0.00	0.00	0.02	0.00	0.04	0.00	0.00	0.07	
Bedrock	4.25	2.05	0.07	6.00	0.04	0.00	0.50	1.33	14.25	
Tundra Vegetation	0.03	0.04	0.14	0.08	0.00	0.07	0.00	0.83	1.19	
Wet/ DenseVeg	0.00	0.01	0.00	0.00	0.00	0.00	0.01	0.00	0.03	
	28.81	29.58	1.48	22.26	0.14	12.77	0.86	4.12		

From \ To	Snow/ Ice	Wetice/ Meltwater	Deep/ LowSSWater	Coarse Sediment	Fine Sediment	Bedrock	Tundra Vegetation	Wet/ DenseVeg		
Snow/ Ice	0.00	4.00	1.63	0.88	0.16	1.78	3.38	0.55	12.37	
Wetice/ Meltwater	1.10	0.00	0.84	0.44	0.07	0.55	0.01	0.02	3.03	
Deep/ LowSSWater	0.05	0.80	0.00	0.08	0.02	0.27	0.20	0.14	1.57	
Coarse Sediment	0.40	0.76	0.98	0.00	0.55	7.99	9.36	0.52	20.57	
Fine Sediment	0.01	0.05	0.37	0.38	0.00	2.10	9.69	1.94	14.53	
Bedrock	0.32	1.12	0.92	2.92	0.84	0.00	13.36	0.34	19.83	
Tundra Vegetation	0.01	0.09	1.73	0.13	0.32	5.12	0.00	18.33	25.72	
Wet/ DenseVeg	0.00	0.04	0.46	0.00	0.00	0.08	1.80	0.00	2.38	
	1.89	6.85	6.93	4.84	1.95	17.89	37.80	21.84		

From \ To	Snow/ Ice	Wetice/ Meltwater	Deep/ LowSSWater	Coarse Sediment	Fine Sediment	Bedrock	Tundra Vegetation	Wet/ DenseVeg		
Snow/ Ice	0.00	16.06	1.12	8.93	0.22	13.05	0.09	0.45	39.93	
Wetice/ Meltwater	7.73	0.00	0.70	4.36	0.01	3.21	0.01	0.23	16.24	
Deep/ LowSSWater	0.15	0.50	0.00	0.13	0.00	0.11	0.00	0.01	0.91	66 - 68
Coarse Sediment	1.00	2.17	0.09	0.00	0.25	12.30	1.38	1.55	18.73	
Fine Sediment	0.02	0.01	0.00	0.46	0.00	0.73	0.19	0.09	1.51	
Bedrock	1.07	1.52	0.10	13.17	0.29	0.00	3.03	1.44	20.62	
Tundra Vegetation	0.00	0.01	0.07	0.10	0.03	0.49	0.00	1.33	2.02	
Wet/ DenseVeg	0.00	0.00	0.01	0.00	0.00	0.00	0.03	0.00	0.04	
	9.97	20.26	2.09	27.16	0.79	29.89	4.73	5.10		

From \ To	Snow/ Ice	Wetice/ Meltwater	Deep/ LowSSWater	Coarse Sediment	Fine Sediment	Bedrock	Tundra Vegetation	Wet/ DenseVeg		
Snow/ Ice	0.00	4.09	1.00	2.46	0.13	3.20	0.04	0.02	10.95	
Wetice/ Meltwater	2.14	0.00	2.43	0.92	0.03	0.91	0.01	0.04	6.47	
Deep/ LowSSWater	0.11	0.95	0.00	0.14	0.00	0.14	0.04	0.26	1.64	
Coarse Sediment	0.25	0.44	0.86	0.00	0.19	11.19	12.44	0.40	25.77	
Fine Sediment	0.00	0.00	0.00	0.24	0.00	0.58	0.31	0.06	1.19	
Bedrock	0.32	0.45	0.76	5.70	0.28	0.00	26.42	0.30	34.23	
Tundra Vegetation	0.00	0.02	2.23	0.15	0.07	3.59	0.00	13.16	19.24	
Wet/ DenseVeg	0.00	0.01	0.35	0.00	0.00	0.04	0.10	0.00	0.50	
	2.84	5.97	7.63	9.61	0.71	19.65	39.35	14.24		

From \ To	Snow/ Ice	Wetice/ Meltwater	Deep/ LowSSWater	Coarse Sediment	Fine Sediment	Bedrock	Tundra Vegetation	Wet/ DenseVeg		
Snow/ Ice	0.00	5.83	1.53	9.56	0.81	17.10	0.47	0.38	35.70	
Wetice/ Meltwater	2.33	0.00	1.25	1.66	0.02	1.54	0.04	0.10	6.94	
Deep/ LowSSWater	0.35	1.30	0.00	0.10	0.00	0.12	0.04	0.09	2.00	64 - 66
Coarse Sediment	0.67	0.94	0.32	0.00	0.75	11.88	2.99	0.78	18.32	
Fine Sediment	0.03	0.01	0.00	0.87	0.00	1.10	0.59	0.23	2.83	
Bedrock	2.51	1.33	0.34	18.35	0.81	0.00	6.62	1.19	31.15	
Tundra Vegetation	0.00	0.01	0.23	0.10	0.06	0.75	0.00	1.72	2.87	
Wet/ DenseVeg	0.00	0.04	0.10	0.00	0.00	0.00	0.04	0.00	0.18	
	5.88	9.45	3.78	30.64	2.45	32.49	10.80	4.51		

From \ To	Snow/ Ice	Wetice/ Meltwater	Deep/ LowSSWater	Coarse Sediment	Fine Sediment	Bedrock	Tundra Vegetation	Wet/ DenseVeg		
Snow/ Ice	0.00	6.70	0.52	2.96	0.18	5.41	0.01	0.04	15.82	
Wetice/ Meltwater	1.58	0.00	1.97	1.05	0.02	1.24	0.02	0.15	6.03	
Deep/ LowSSWater	0.17	0.83	0.00	0.17	0.01	0.19	0.05	0.32	1.75	
Coarse Sediment	0.39	0.50	0.63	0.00	0.34	10.85	11.73	0.64	25.07	
Fine Sediment	0.02	0.01	0.00	0.99	0.00	1.58	0.12	0.04	2.77	
Bedrock	0.77	0.59	0.63	10.45	0.62	0.00	20.19	0.50	33.74	
Tundra Vegetation	0.17	0.02	1.38	0.15	0.63	2.12	0.00	10.08	14.56	
Wet/ DenseVeg	0.00	0.01	0.20	0.00	0.00	0.01	0.04	0.00	0.27	
	3.09	8.67	5.33	15.77	1.80	21.41	32.17	11.77		

From \ To	Snow/ Ice	Wetice/ Meltwater	Deep/ LowSSWater	Coarse Sediment	Fine Sediment	Bedrock	Tundra Vegetation	Wet/ DenseVeg		
Snow/ Ice	0.00	7.66	0.86	6.55	0.26	17.76	0.40	0.90	34.39	
Wetice/ Meltwater	8.30	0.00	1.04	2.18	0.02	1.68	0.02	0.08	13.31	
Deep/ LowSSWater	0.50	1.48	0.00	0.11	0.00	0.11	0.04	0.13	2.38	
Coarse Sediment	1.61	1.23	0.23	0.00	0.35	10.52	1.89	0.82	16.64	62 - 64
Fine Sediment	0.12	0.03	0.00	0.52	0.00	0.51	0.62	0.32	2.12	
Bedrock	4.66	1.98	0.17	15.41	0.42	0.00	3.74	1.57	27.96	
Tundra Vegetation	0.01	0.01	0.08	0.07	0.03	0.86	0.00	2.06	3.12	
Wet/ DenseVeg	0.00	0.00	0.02	0.00	0.00	0.01	0.06	0.00	0.09	
	15.20	12.39	2.39	24.84	1.08	31.45	6.76	5.89		

Figure 7.1 Matrices of class transition. Cell values represent percentage of latitudinal band area covered by this transition. Static surfaces in the diagonals are removed and not considered in percentages as we are only concerned with defining class transitions here. Numbers on the right represent latitudinal band (degrees) and the columns denote coast (i.e. left: west, right: east). Colour coding is per-matrix, i.e. colour scaled from red (low occurrence) to green (high occurrence) within that latitudinal band.

80 - 82

From \ To	Snow/ Ice	Wetice/ Meltwater	Deep/ LowSSWater	Coarse Sediment	Fine Sediment	Bedrock	Tundra Vegetation	Wet/ DenseVeg	
Snow/ Ice	0.00	2.68	0.77	8.18	15.31	8.29	0.04	0.07	35.33
Wetice/ Meltwater	0.31	0.00	0.71	0.41	0.42	0.55	0.01	0.01	2.42
Deep/ LowSSWater	0.04	0.25	0.00	0.07	0.05	0.09	0.00	0.00	0.51
Coarse Sediment	0.10	0.41	0.14	0.00	8.23	7.57	0.68	0.14	17.26
Fine Sediment	0.07	0.25	0.04	16.57	0.00	15.07	0.12	0.05	32.17
Bedrock	0.15	0.88	0.26	5.42	4.13	0.00	1.22	0.15	12.21
Tundra Vegetation	0.00	0.00	0.01	0.00	0.00	0.02	0.00	0.05	0.08
Wet/ DenseVeg	0.00	0.00	0.00	0.00	0.00	0.00	0.00	0.00	0.01
	0.68	4.46	1.93	30.66	28.14	31.60	2.07	0.46	

From \ To	Snow/ Ice	Wetice/ Meltwater	Deep/ LowSSWater	Coarse Sediment	Fine Sediment	Bedrock	Tundra Vegetation	Wet/ DenseVeg	
Snow/ Ice	0.00	3.96	0.28	4.19	1.45	3.67	0.00	0.03	13.59
Wetice/ Meltwater	1.51	0.00	0.46	1.87	0.03	1.80	0.01	0.02	5.69
Deep/ LowSSWater	0.50	1.34	0.00	0.24	0.01	0.27	0.02	0.03	2.40
Coarse Sediment	0.83	1.80	0.17	0.00	6.23	23.20	2.09	0.98	35.28
Fine Sediment	0.11	0.14	0.00	8.45	0.00	2.26	0.28	0.19	11.43
Bedrock	0.92	1.80	0.26	18.51	2.63	0.00	5.99	0.91	31.03
Tundra Vegetation	0.00	0.01	0.05	0.04	0.03	0.06	0.00	0.37	0.56
Wet/ DenseVeg	0.00	0.00	0.00	0.00	0.00	0.00	0.00	0.00	0.01
	3.87	9.06	1.22	33.30	10.38	31.26	8.39	2.53	

78 - 80

From \ To	Snow/ Ice	Wetice/ Meltwater	Deep/ LowSSWater	Coarse Sediment	Fine Sediment	Bedrock	Tundra Vegetation	Wet/ DenseVeg	
Snow/ Ice	0.00	1.53	0.57	1.09	3.01	0.81	0.01	0.01	7.01
Wetice/ Meltwater	0.69	0.00	0.84	0.72	0.07	1.67	0.05	0.02	4.06
Deep/ LowSSWater	0.82	1.58	0.00	0.28	0.12	1.82	0.44	0.11	5.16
Coarse Sediment	0.19	0.59	0.68	0.00	5.13	33.38	2.33	0.30	42.60
Fine Sediment	0.14	0.04	0.05	4.76	0.00	7.51	0.23	0.02	12.74
Bedrock	0.33	0.66	0.69	9.97	3.68	0.00	5.77	0.39	21.48
Tundra Vegetation	0.00	0.02	0.23	0.02	0.07	5.94	0.00	0.42	6.70
Wet/ DenseVeg	0.00	0.01	0.02	0.00	0.00	0.07	0.14	0.00	0.24
	2.17	4.42	3.08	16.84	12.07	51.20	8.95	1.27	

From \ To	Snow/ Ice	Wetice/ Meltwater	Deep/ LowSSWater	Coarse Sediment	Fine Sediment	Bedrock	Tundra Vegetation	Wet/ DenseVeg	
Snow/ Ice	0.00	4.14	0.73	3.14	0.56	4.98	0.01	0.06	13.62
Wetice/ Meltwater	4.18	0.00	0.53	1.87	0.01	1.68	0.01	0.04	8.31
Deep/ LowSSWater	0.46	0.57	0.00	0.15	0.00	0.17	0.05	0.07	1.46
Coarse Sediment	2.36	1.78	0.22	0.00	4.11	15.17	2.25	1.33	27.23
Fine Sediment	0.09	0.06	0.00	4.30	0.00	0.82	0.09	0.09	5.45
Bedrock	3.98	2.57	0.35	29.07	1.65	0.00	3.18	2.38	43.20
Tundra Vegetation	0.01	0.01	0.05	0.03	0.05	0.08	0.00	0.48	0.72
Wet/ DenseVeg	0.00	0.00	0.00	0.00	0.00	0.00	0.01	0.00	0.02
	11.08	9.13	1.90	38.56	6.39	22.90	5.60	4.46	

76 - 78

From \ To	Snow/ Ice	Wetice/ Meltwater	Deep/ LowSSWater	Coarse Sediment	Fine Sediment	Bedrock	Tundra Vegetation	Wet/ DenseVeg	
Snow/ Ice	0.00	6.70	2.15	16.54	3.95	38.12	1.53	0.43	69.43
Wetice/ Meltwater	0.62	0.00	0.37	0.70	0.06	1.55	0.10	0.03	3.43
Deep/ LowSSWater	0.08	0.18	0.00	0.06	0.01	0.11	0.02	0.01	0.48
Coarse Sediment	0.17	0.33	0.08	0.00	0.29	11.24	0.53	0.13	12.76
Fine Sediment	0.00	0.00	0.00	0.64	0.00	1.50	0.07	0.02	2.24
Bedrock	0.56	0.66	0.12	7.61	0.22	0.00	1.82	0.24	11.24
Tundra Vegetation	0.00	0.00	0.02	0.01	0.00	0.20	0.00	0.17	0.40
Wet/ DenseVeg	0.00	0.00	0.00	0.00	0.00	0.01	0.01	0.00	0.02
	1.43	7.88	2.74	25.57	4.54	52.74	4.07	1.03	

From \ To	Snow/ Ice	Wetice/ Meltwater	Deep/ LowSSWater	Coarse Sediment	Fine Sediment	Bedrock	Tundra Vegetation	Wet/ DenseVeg	
Snow/ Ice	0.00	3.11	0.24	1.55	0.15	2.32	0.00	0.02	7.39
Wetice/ Meltwater	3.46	0.00	0.91	1.42	0.01	1.02	0.01	0.02	6.86
Deep/ LowSSWater	0.73	1.06	0.00	0.14	0.00	0.13	0.03	0.05	2.15
Coarse Sediment	3.41	2.12	0.29	0.00	2.07	18.26	2.76	0.86	29.77
Fine Sediment	0.14	0.06	0.00	2.96	0.00	0.80	0.29	0.07	4.32
Bedrock	5.56	3.11	0.56	25.25	1.41	0.00	9.87	1.31	47.06
Tundra Vegetation	0.01	0.04	0.21	0.08	0.09	1.28	0.00	0.66	2.38
Wet/ DenseVeg	0.00	0.01	0.03	0.00	0.00	0.03	0.02	0.00	0.08
	13.31	9.51	2.24	31.40	3.74	23.84	12.98	2.98	

74 - 76

From \ To	Snow/ Ice	Wetice/ Meltwater	Deep/ LowSSWater	Coarse Sediment	Fine Sediment	Bedrock	Tundra Vegetation	Wet/ DenseVeg	
Snow/ Ice	0.00	13.90	5.17	3.87	0.42	12.49	0.04	0.02	35.91
Wetice/ Meltwater	2.46	0.00	2.71	1.02	0.00	1.51	0.00	0.01	7.72
Deep/ LowSSWater	0.21	0.94	0.00	0.07	0.00	0.07	0.00	0.00	1.29
Coarse Sediment	0.51	0.92	0.53	0.00	0.18	17.45	1.26	0.14	21.00
Fine Sediment	0.01	0.00	0.00	0.43	0.00	0.85	0.04	0.01	1.35
Bedrock	1.24	1.55	0.56	22.61	0.15	0.00	5.57	0.26	31.95
Tundra Vegetation	0.00	0.00	0.07	0.01	0.00	0.54	0.00	0.15	0.78
Wet/ DenseVeg	0.00	0.00	0.00	0.00	0.00	0.00	0.00	0.00	0.00
	4.44	17.32	9.05	28.01	0.76	32.92	6.92	0.59	

From \ To	Snow/ Ice	Wetice/ Meltwater	Deep/ LowSSWater	Coarse Sediment	Fine Sediment	Bedrock	Tundra Vegetation	Wet/ DenseVeg	
Snow/ Ice	0.00	2.74	0.15	1.65	0.33	3.14	0.06	0.11	8.19
Wetice/ Meltwater	2.29	0.00	0.46	1.65	0.01	1.46	0.05	0.12	6.05
Deep/ LowSSWater	0.44	0.92	0.00	0.15	0.00	0.19	0.06	0.19	1.95
Coarse Sediment	3.66	2.27	0.36	0.00	3.29	16.62	4.05	1.08	31.33
Fine Sediment	0.42	0.06	0.00	2.79	0.00	1.16	0.37	0.14	4.95
Bedrock	4.89	2.82	0.54	17.83	2.24	0.00	12.96	1.70	42.98
Tundra Vegetation	0.05	0.09	0.38	0.11	0.10	1.23	0.00	2.44	4.40
Wet/ DenseVeg	0.01	0.02	0.03	0.00	0.00	0.02	0.06	0.00	0.14
	11.77	8.91	1.94	24.19	5.96	23.83	17.62	5.79	

72 - 74

From \ To	Snow/ Ice	Wetice/ Meltwater	Deep/ LowSSWater	Coarse Sediment	Fine Sediment	Bedrock	Tundra Vegetation	Wet/ DenseVeg	
Snow/ Ice	0.00	7.30	1.30	3.67	0.29	3.91	0.08	0.26	16.81
Wetice/ Meltwater	1.00	0.00	1.67	2.03	0.02	1.06	0.03	0.07	5.89
Deep/ LowSSWater	0.07	1.10	0.00	0.14	0.00	0.09	0.01	0.04	1.46
Coarse Sediment	0.28	1.12	0.64	0.00	0.54	13.05	9.64	1.29	26.57
Fine Sediment	0.00	0.00	0.00	0.38	0.00	0.59	0.07	0.02	1.06
Bedrock	0.18	0.73	0.81	14.08	0.52	0.00	24.49	1.57	42.38
Tundra Vegetation	0.00	0.02	0.75	0.24	0.06	1.60	0.00	3.08	5.76
Wet/ DenseVeg	0.00	0.01	0.04	0.00	0.00	0.00	0.01	0.00	0.06
	1.53	10.29	5.22	20.54	1.43	20.31	34.34	6.33	

From \ To	Snow/ Ice	Wetice/ Meltwater	Deep/ LowSSWater	Coarse Sediment	Fine Sediment	Bedrock	Tundra Vegetation	Wet/ DenseVeg	
Snow/ Ice	0.00	3.93	0.10	1.52	0.39	2.50	0.06	0.10	8.60
Wetice/ Meltwater	3.88	0.00	0.22	1.51	0.04	1.51	0.06	0.10	7.33
Deep/ LowSSWater	0.39	0.47	0.00	0.14	0.01	0.16	0.02	0.03	1.22
Coarse Sediment	5.13	3.48	0.18	0.00	4.69	13.52	5.15	1.38	33.53
Fine Sediment	0.62	0.13	0.05	1.84	0.00	0.88	0.29	0.13	3.95
Bedrock	5.26	2.97	0.32	14.26	4.40	0.00	12.23	1.73	41.17
Tundra Vegetation	0.14	0.17	0.17	0.26	0.31	1.19	0.00	1.74	3.97
Wet/ DenseVeg	0.04	0.03	0.01	0.03	0.01	0.06	0.05	0.00	0.22
	15.45	11.19	1.06	19.57	9.84	19.82	17.85	5.21	

70 - 72

From \ To	Snow/ Ice	Wetice/ Meltwater	Deep/ LowSSWater	Coarse Sediment	Fine Sediment	Bedrock	Tundra Vegetation	Wet/ DenseVeg	
Snow/ Ice	0.00	7.18	0.38	4.35	0.32	5.12	0.76	0.13	18.23
Wetice/ Meltwater	1.40	0.00	0.82	2.98	0.00	2.09	0.03	0.06	7.38
Deep/ LowSSWater	0.08	0.84	0.00	0.16	0.00	0.16	0.01	0.05	1.30
Coarse Sediment	0.72	1.51	0.25	0.00	0.45	11.19	7.53	2.24	23.89
Fine Sediment	0.00	0.00	0.00	0.20	0.00	0.21	0.17	0.05	0.65
Bedrock	0.19	1.05	0.34	16.61	0.72	0.00	22.38	2.45	43.73
Tundra Vegetation	0.00	0.04	0.28	0.27	0.08	0.89	0.00	3.23	4.80
Wet/ DenseVeg	0.00	0.01	0.01	0.00	0.00	0.00	0.01	0.00	0.02
	2.39	10.63	2.07	24.57	1.57	19.67	30.89	8.21	

From \ To	Snow/ Ice	Wetice/ Meltwater	Deep/ LowSSWater	Coarse Sediment	Fine Sediment	Bedrock	Tundra Vegetation	Wet/ DenseVeg	
Snow/ Ice	0.00	4.27	0.15	1.20	0.21	2.17	0.02	0.04	8.05
Wetice/ Meltwater	4.00	0.00	0.33	1.72	0.07	1.38	0.02	0.05	7.58
Deep/ LowSSWater	0.39	0.63	0.00	0.17	0.02	0.18	0.03	0.02	1.43
Coarse Sediment	5.64	3.53	0.12	0.00	5.96	12.88	5.25	1.50	34.87
Fine Sediment	0.34	0.06	0.00	0.49	0.00	0.49	0.23	0.13	1.74
Bedrock	4.22	2.66	0.23	11.11	3.74	0.00	16.19	1.93	40.09
Tundra Vegetation	0.15	0.21	0.16	0.30	0.42	1.35	0.00	3.40	5.99
Wet/ DenseVeg	0.04	0.03	0.01	0.03	0.01	0.06	0.04	0.00	0.24
	14.78	11.40	1.00	15.02	10.42	18.50	21.79	7.08	

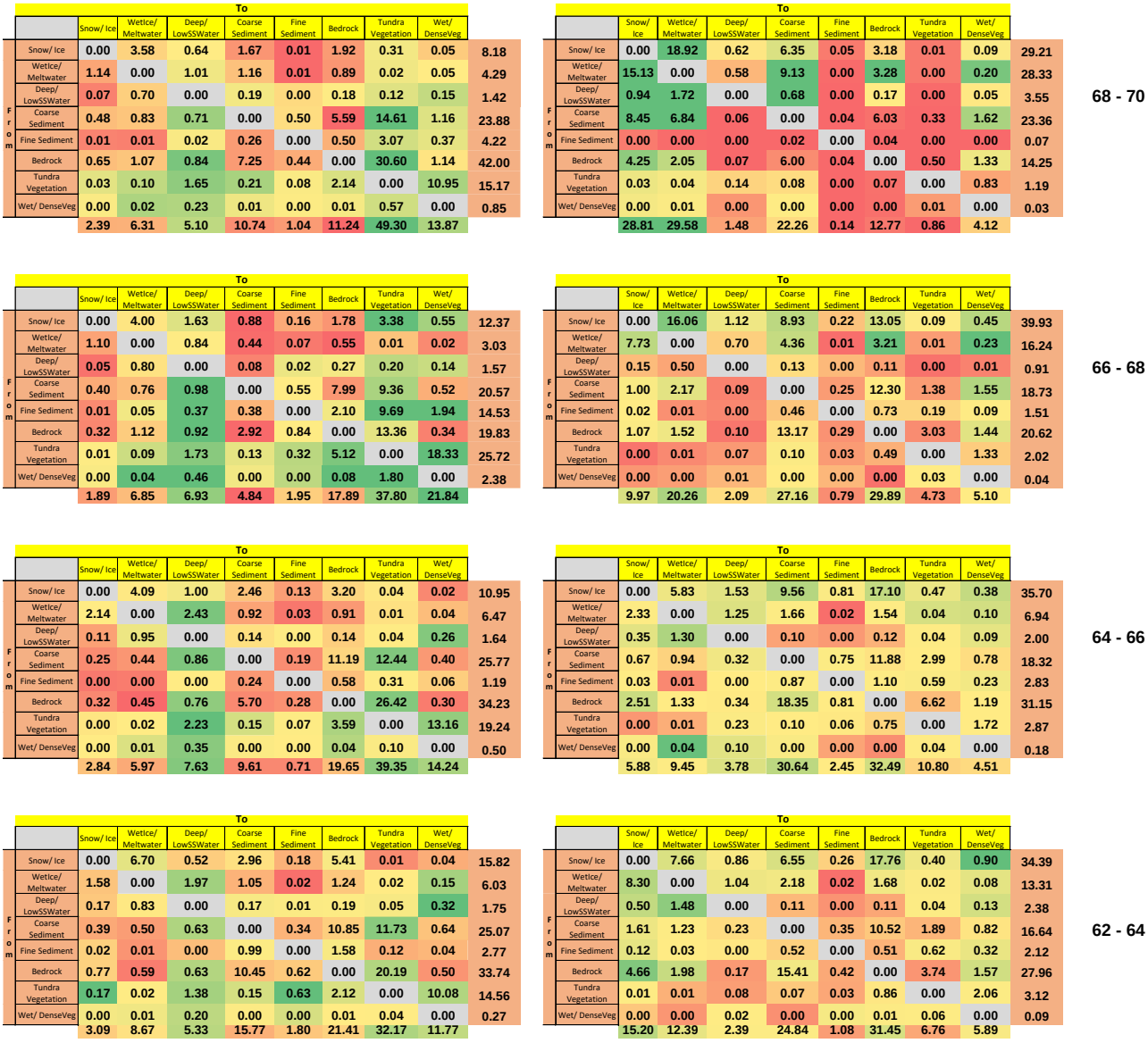

From \ To	Snow/ Ice	Wetice/ Meltwater	Deep/ LowSSWater	Coarse Sediment	Fine Sediment	Bedrock	Tundra Vegetation	Wet/ DenseVeg	
Snow/ Ice	0.00	3.58	0.64	1.67	0.01	1.92	0.31	0.05	8.18
Wetice/ Meltwater	1.14	0.00	1.01	1.16	0.01	0.89	0.02	0.05	4.29
Deep/ LowSSWater	0.07	0.70	0.00	0.19	0.00	0.18	0.12	0.15	1.42
Coarse Sediment	0.48	0.83	0.71	0.00	0.50	5.59	14.61	1.16	23.88
Fine Sediment	0.01	0.01	0.02	0.26	0.00	0.50	3.07	0.37	4.22
Bedrock	0.65	1.07	0.84	7.25	0.44	0.00	30.60	1.14	42.00
Tundra Vegetation	0.03	0.10	1.65	0.21	0.08	2.14	0.00	10.95	15.17
Wet/ DenseVeg	0.00	0.02	0.23	0.01	0.00	0.01	0.57	0.00	0.85
	2.39	6.31	5.10	10.74	1.04	11.24	49.30	13.87	

From \ To	Snow/ Ice	Wetice/ Meltwater	Deep/ LowSSWater	Coarse Sediment	Fine Sediment	Bedrock	Tundra Vegetation	Wet/ DenseVeg	
Snow/ Ice	0.00	18.92	0.62	6.35	0.05	3.18	0.01	0.09	29.21
Wetice/ Meltwater	15.13	0.00	0.58	9.13	0.00	3.28	0.00	0.20	28.33
Deep/ LowSSWater	0.94	1.72	0.00	0.68	0.00	0.17	0.00	0.05	3.55
Coarse Sediment	8.45	6.84	0.06	0.00	0.04	6.03	0.33	1.62	23.36
Fine Sediment	0.00	0.00	0.00	0.02	0.00	0.04	0.00	0.00	0.07
Bedrock	4.25	2.05	0.07	6.00	0.04	0.00	0.50	1.33	14.25
Tundra Vegetation	0.03	0.04	0.14	0.08	0.00	0.07	0.00	0.83	1.19
Wet/ DenseVeg	0.00	0.01	0.00	0.00	0.00	0.00	0.01	0.00	0.03
	28.81	29.58	1.48	22.26	0.14	12.77	0.86	4.12	

68 - 70

From \ To	Snow/ Ice	Wetice/ Meltwater	Deep/ LowSSWater	Coarse Sediment	Fine Sediment	Bedrock	Tundra Vegetation	Wet/ DenseVeg	
Snow/ Ice	0.00	4.00	1.63	0.88	0.16	1.78	3.38	0.55	12.37
Wetice/ Meltwater	1.10	0.00	0.84	0.44	0.07	0.55	0.01	0.02	3.03
Deep/ LowSSWater	0.05	0.80	0.00	0.08	0.02	0.27	0.20	0.14	1.57
Coarse Sediment	0.40	0.76	0.98	0.00	0.55	7.99	9.36	0.52	20.57
Fine Sediment	0.01	0.05	0.37	0.38	0.00	2.10	9.69	1.94	14.53
Bedrock	0.32	1.12	0.92	2.92	0.84	0.00	13.36	0.34	19.83
Tundra Vegetation	0.01	0.09	1.73	0.13	0.32	5.12	0.00	18.33	25.72
Wet/ DenseVeg	0.00	0.04	0.46	0.00	0.00	0.08	1.80	0.00	2.38
	1.89	6.85	6.93	4.84	1.95	17.89	37.80	21.84	

From \ To	Snow/ Ice	Wetice/ Meltwater	Deep/ LowSSWater	Coarse Sediment	Fine Sediment	Bedrock	Tundra Vegetation	Wet/ DenseVeg	
Snow/ Ice	0.00	16.06	1.12	8.93	0.22	13.05	0.09	0.45	39.93
Wetice/ Meltwater	7.73	0.00	0.70	4.36	0.01	3.21	0.01	0.23	16.24
Deep/ LowSSWater	0.15	0.50	0.00	0.13	0.00	0.11	0.00	0.01	0.91
Coarse Sediment	1.00	2.17	0.09	0.00	0.25	12.30	1.38	1.55	18.73
Fine Sediment	0.02	0.01	0.00	0.46	0.00	0.73	0.19	0.09	1.51
Bedrock	1.07	1.52	0.10	13.17	0.29	0.00	3.03	1.44	20.62
Tundra Vegetation	0.00	0.01	0.07	0.10	0.03	0.49	0.00	1.33	2.02
Wet/ DenseVeg	0.00	0.00	0.01	0.00	0.00	0.00	0.03	0.00	0.04
	9.97	20.26	2.09	27.16	0.79	29.89	4.73	5.10	

66 - 68

From \ To	Snow/ Ice	Wetice/ Meltwater	Deep/ LowSSWater	Coarse Sediment	Fine Sediment	Bedrock	Tundra Vegetation	Wet/ DenseVeg	
Snow/ Ice	0.00	4.09	1.00	2.46	0.13	3.20	0.04	0.02	10.95
Wetice/ Meltwater	2.14	0.00	2.43	0.92	0.03	0.91	0.01	0.04	6.47
Deep/ LowSSWater	0.11	0.95	0.00	0.14	0.00	0.14	0.04	0.26	1.64
Coarse Sediment	0.25	0.44	0.86	0.00	0.19	11.19	12.44	0.40	25.77
Fine Sediment	0.00	0.00	0.00	0.24	0.00	0.58	0.31	0.06	1.19
Bedrock	0.32	0.45	0.76	5.70	0.28	0.00	26.42	0.30	34.23
Tundra Vegetation	0.00	0.02	2.23	0.15	0.07	3.59	0.00	13.16	19.24
Wet/ DenseVeg	0.00	0.01	0.35	0.00	0.00	0.04	0.10	0.00	0.50
	2.84	5.97	7.63	9.61	0.71	19.65	39.35	14.24	

From \ To	Snow/ Ice	Wetice/ Meltwater	Deep/ LowSSWater	Coarse Sediment	Fine Sediment	Bedrock	Tundra Vegetation	Wet/ DenseVeg	
Snow/ Ice	0.00	5.83	1.53	9.56	0.81	17.10	0.47	0.38	35.70
Wetice/ Meltwater	2.33	0.00	1.25	1.66	0.02	1.54	0.04	0.10	6.94
Deep/ LowSSWater	0.35	1.30	0.00	0.10	0.00	0.12	0.04	0.09	2.00
Coarse Sediment	0.67	0.94	0.32	0.00	0.75	11.88	2.99	0.78	18.32
Fine Sediment	0.03	0.01	0.00	0.87	0.00	1.10	0.59	0.23	2.83
Bedrock	2.51	1.33	0.34	18.35	0.81	0.00	6.62	1.19	31.15
Tundra Vegetation	0.00	0.01	0.23	0.10	0.06	0.75	0.00	1.72	2.87
Wet/ DenseVeg	0.00	0.04	0.10	0.00	0.00	0.00	0.04	0.00	0.18
	5.88	9.45	3.78	30.64	2.45	32.49	10.80	4.51	

64 - 66

From \ To	Snow/ Ice	Wetice/ Meltwater	Deep/ LowSSWater	Coarse Sediment	Fine Sediment	Bedrock	Tundra Vegetation	Wet/ DenseVeg	
Snow/ Ice	0.00	6.70	0.52	2.96	0.18	5.41	0.01	0.04	15.82
Wetice/ Meltwater	1.58	0.00	1.97	1.05	0.02	1.24	0.02	0.15	6.03
Deep/ LowSSWater	0.17	0.83	0.00	0.17	0.01	0.19	0.05	0.32	1.75
Coarse Sediment	0.39	0.50	0.63	0.00	0.34	10.85	11.73	0.64	25.07
Fine Sediment	0.02	0.01	0.00	0.99	0.00	1.58	0.12	0.04	2.77
Bedrock	0.77	0.59	0.63	10.45	0.62	0.00	20.19	0.50	33.74
Tundra Vegetation	0.17	0.02	1.38	0.15	0.63	2.12	0.00	10.08	14.56
Wet/ DenseVeg	0.00	0.01	0.20	0.00	0.00	0.01	0.04	0.00	0.27
	3.09	8.67	5.33	15.77	1.80	21.41	32.17	11.77	

From \ To	Snow/ Ice	Wetice/ Meltwater	Deep/ LowSSWater	Coarse Sediment	Fine Sediment	Bedrock	Tundra Vegetation	Wet/ DenseVeg	
Snow/ Ice	0.00	7.66	0.86	6.55	0.26	17.76	0.40	0.90	34.39
Wetice/ Meltwater	8.30	0.00	1.04	2.18	0.02	1.68	0.02	0.08	13.31
Deep/ LowSSWater	0.50	1.48	0.00	0.11	0.00	0.11	0.04	0.13	2.38
Coarse Sediment	1.61	1.23	0.23	0.00	0.35	10.52	1.89	0.82	16.64
Fine Sediment	0.12	0.03	0.00	0.52	0.00	0.51	0.62	0.32	2.12
Bedrock	4.66	1.98	0.17	15.41	0.42	0.00	3.74	1.57	27.96
Tundra Vegetation	0.01	0.01	0.08	0.07	0.03	0.86	0.00	2.06	3.12
Wet/ DenseVeg	0.00	0.00	0.02	0.00	0.00	0.01	0.06	0.00	0.09
	15.20	12.39	2.39	24.84	1.08	31.45	6.76	5.89	

62 - 64

Figure 7.2 Matrices of class transition where cell values represent percentage of latitudinal band area covered by this transition. Static surfaces in the diagonals are removed and not considered in percentages as we are only concerned with defining class transitions here. Numbers on the right represent latitudinal band (degrees) and the columns denote coast (i.e. left: west, right: east). Colour coding is relative to that cell transition in each of the other matrixes, i.e. colour scaled from red (low occurrence) to green (high occurrence) for that exact transition across all matrices.

Appendix B: Results of DEM Co-registration

A) 1978 Area

AeroDEM to ArcticDEM

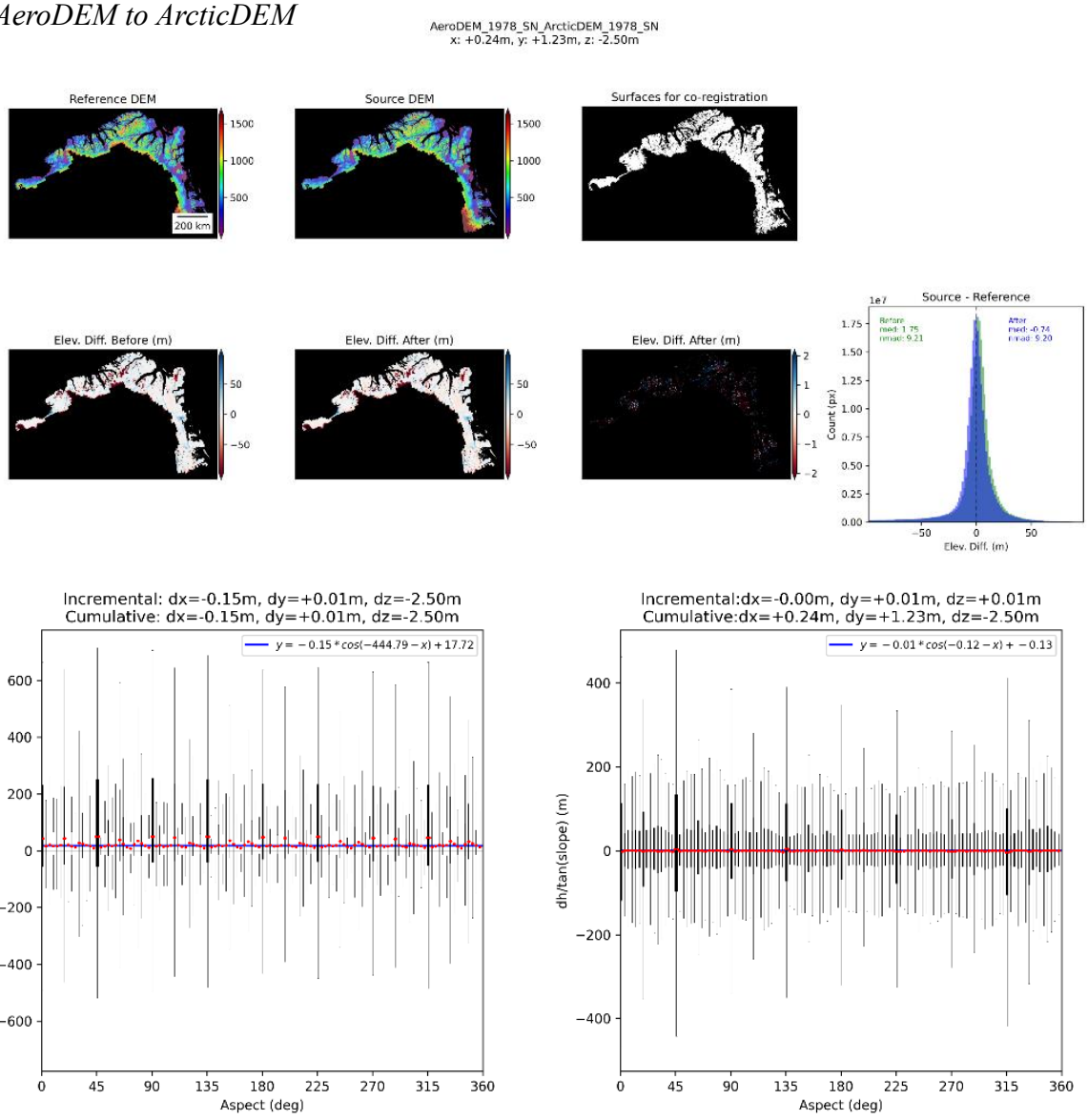

B) 1978 Area

GIMP to ArcticDEM

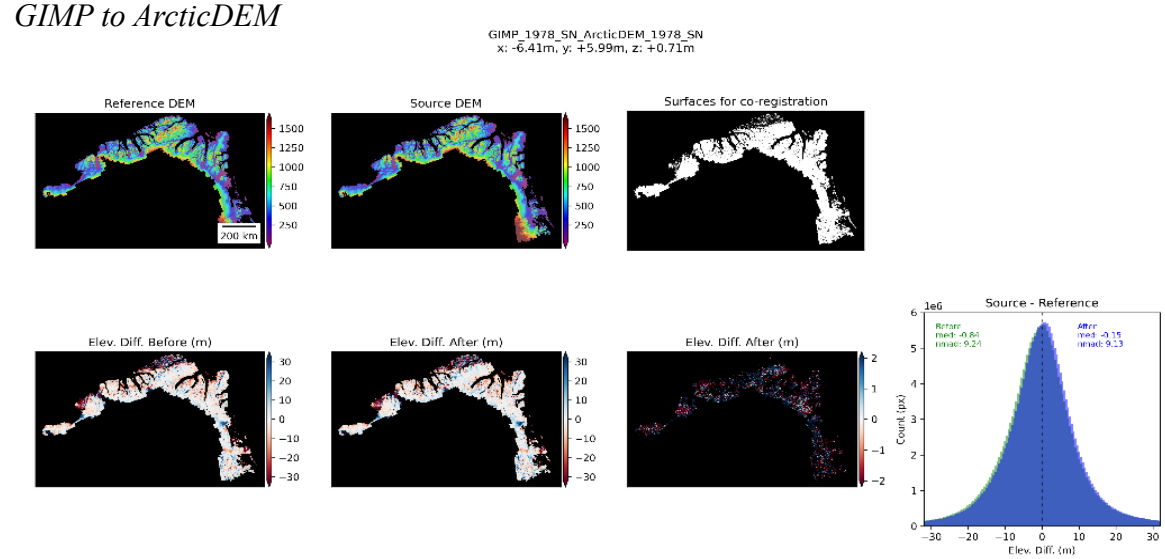

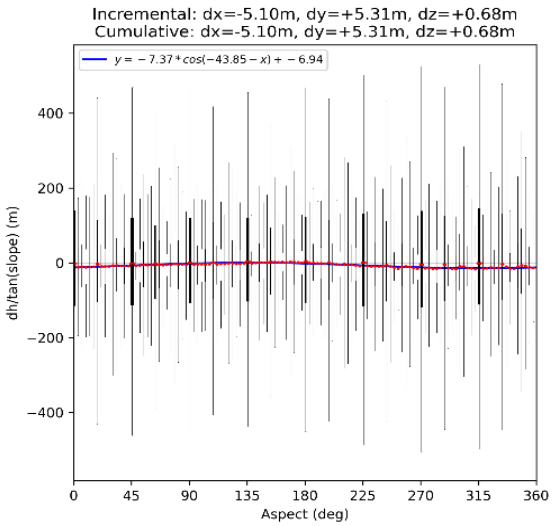

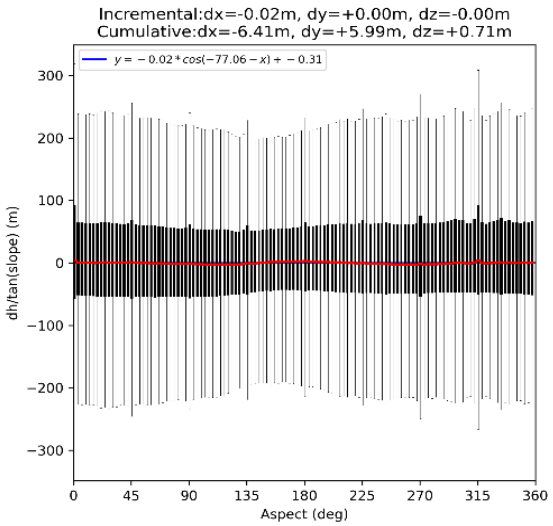

C) 1981 Area

AeroDEM to ArcticDEM

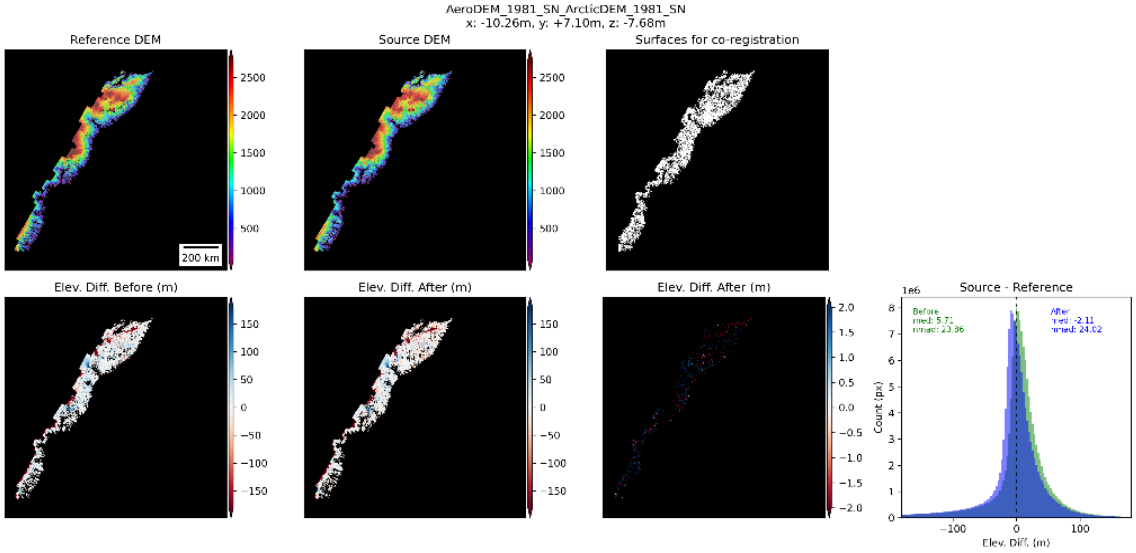

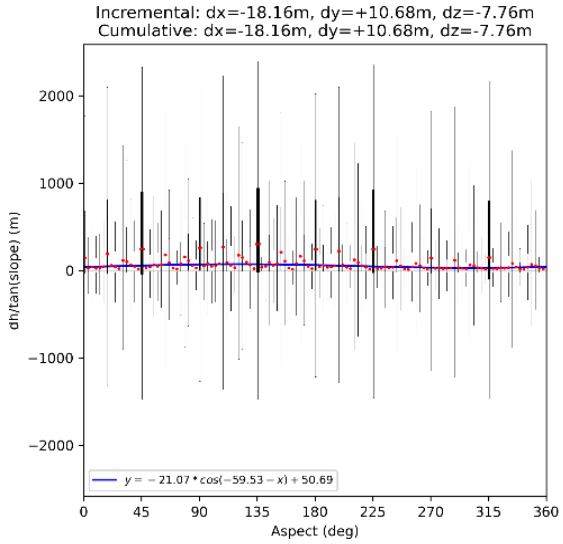

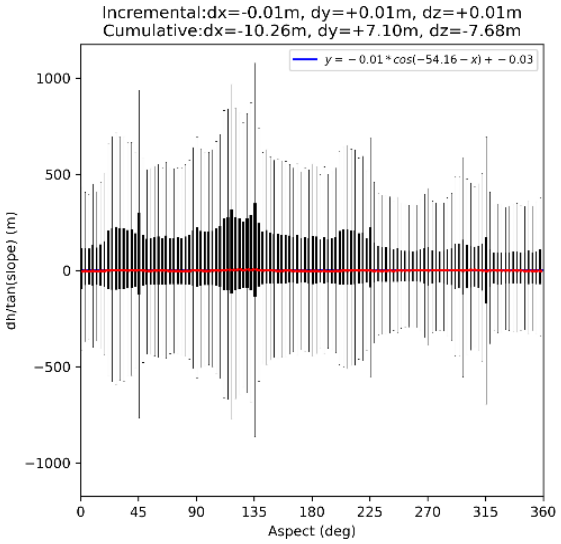

D) 1981 Area

GIMP to ArcticDEM

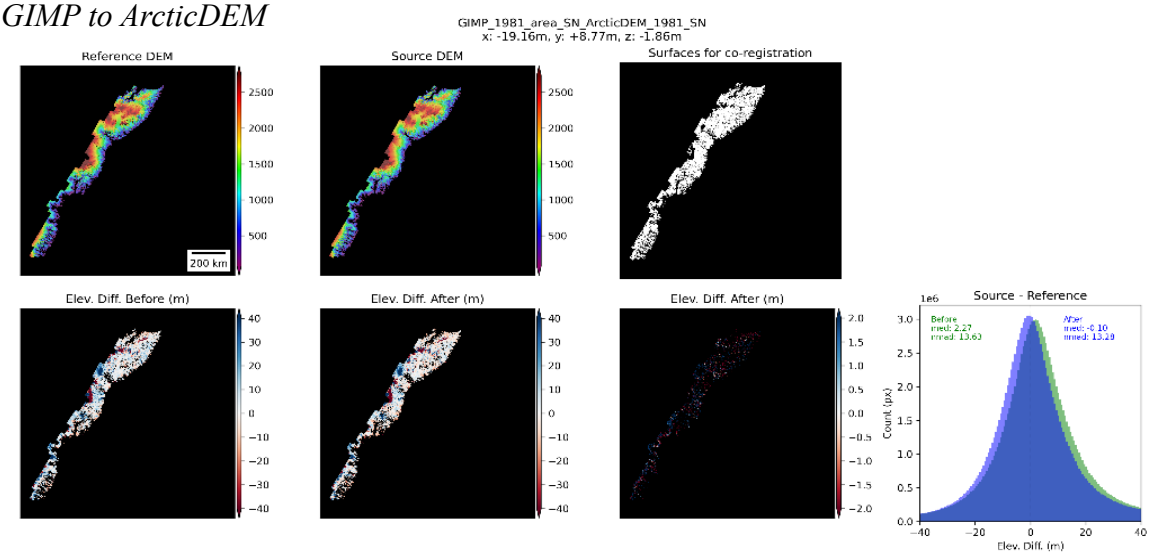

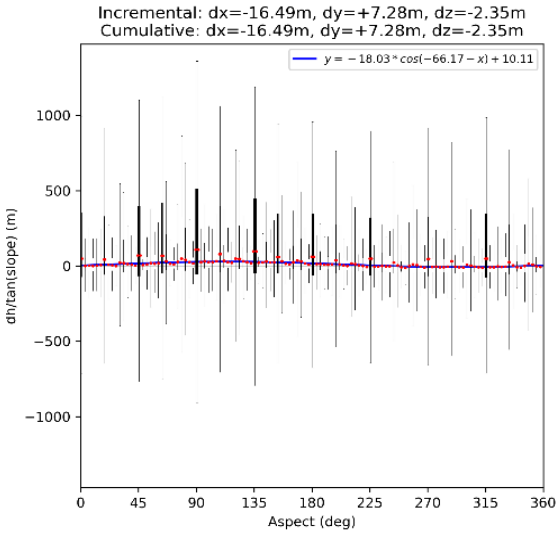

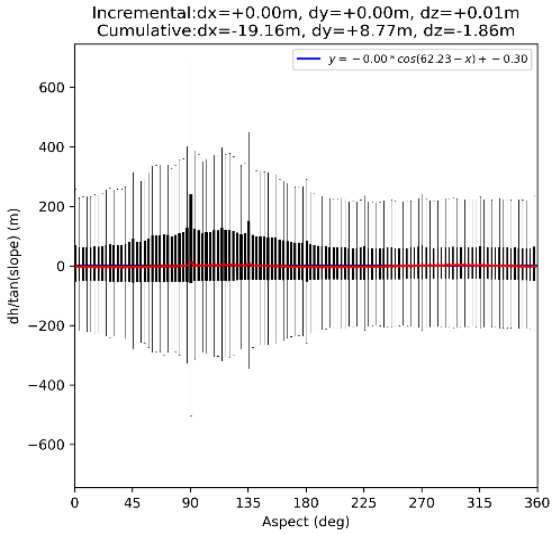

E) 1985 Area

AeroDEM to ArcticDEM

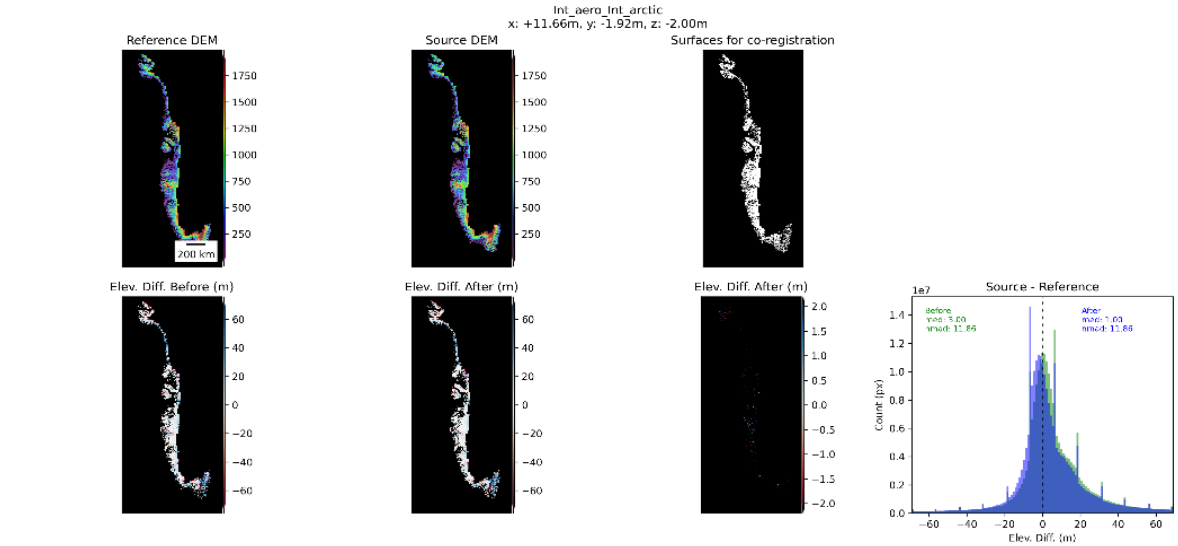

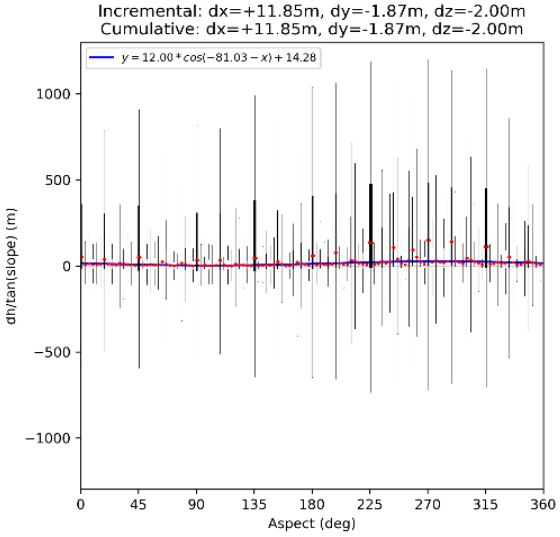

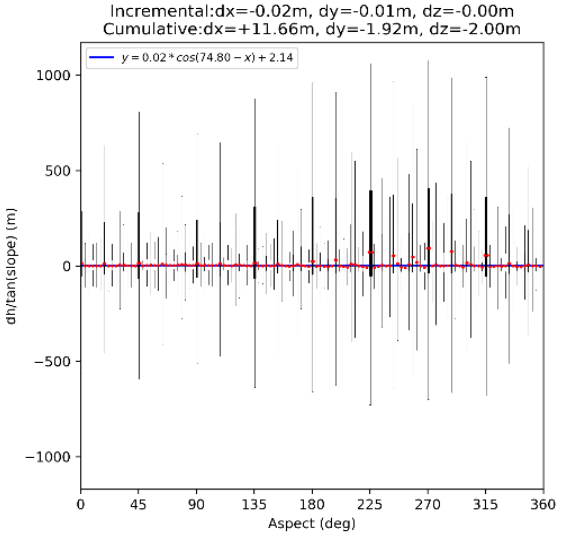

F) 1985 Area

GIMP to ArcticDEM

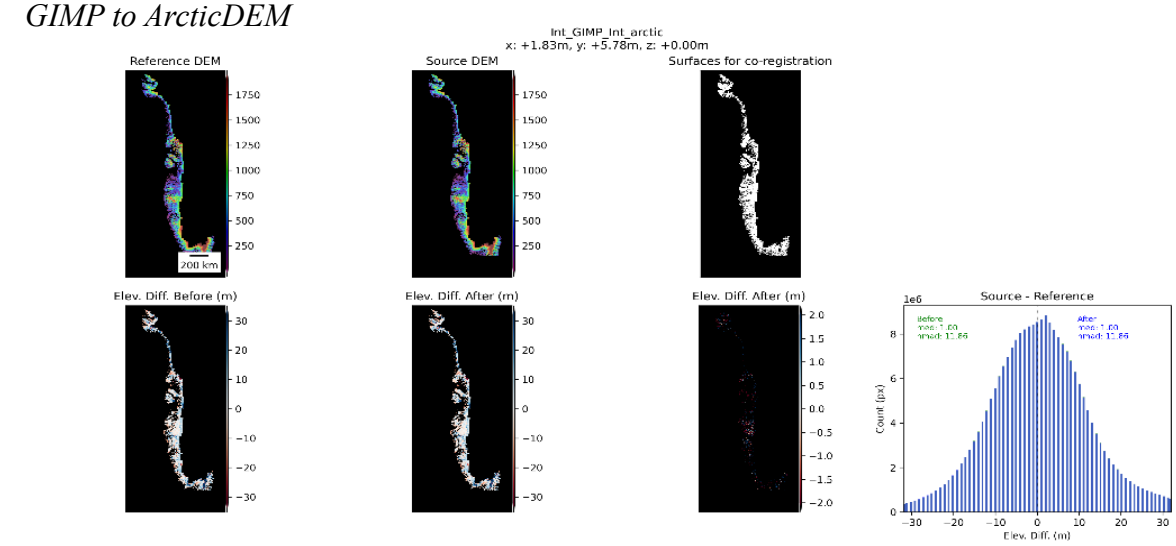

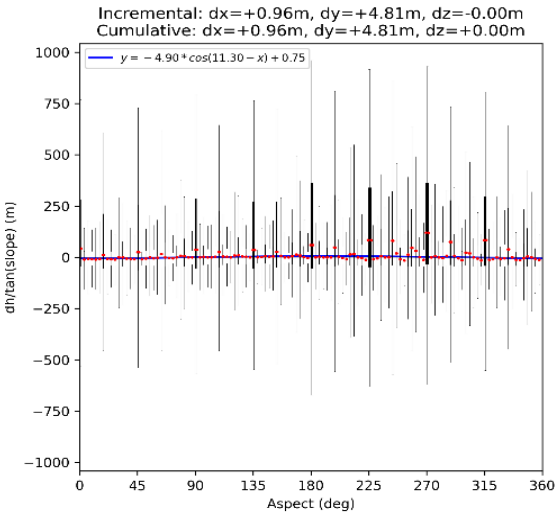

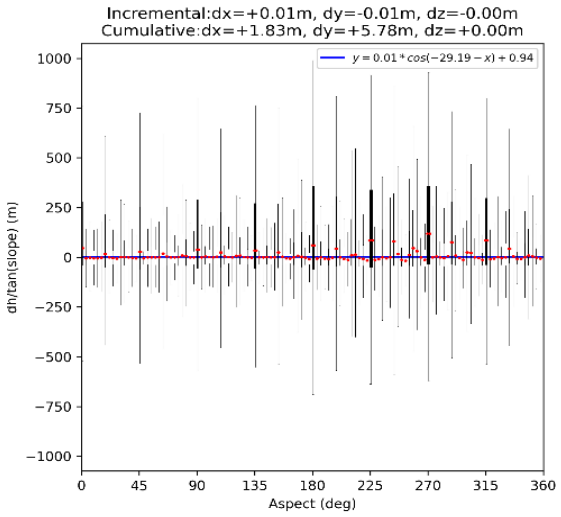

G) 1987 Area

AeroDEM to ArcticDEM

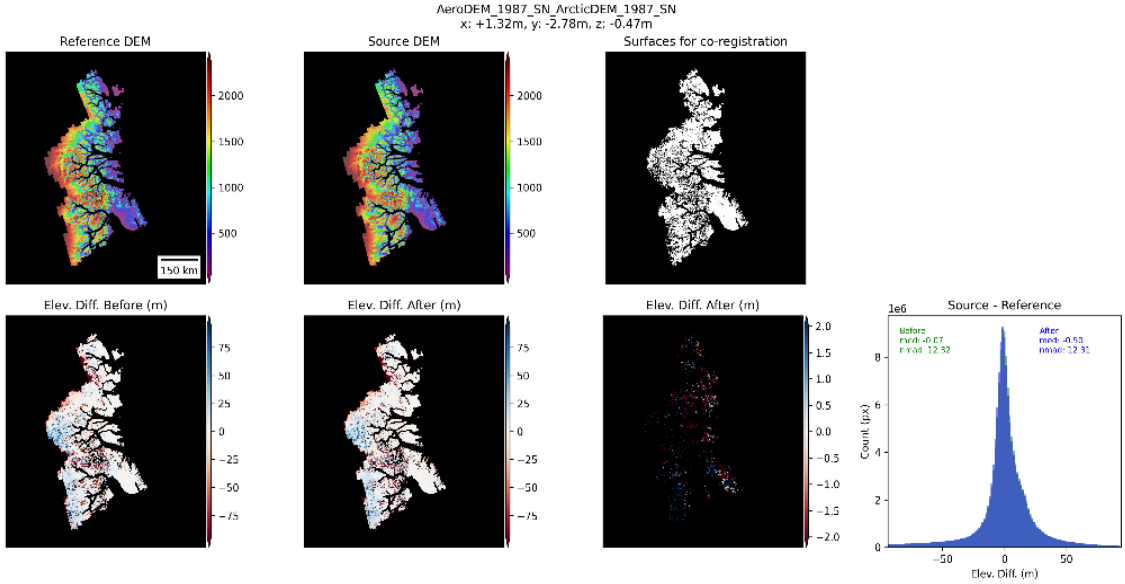

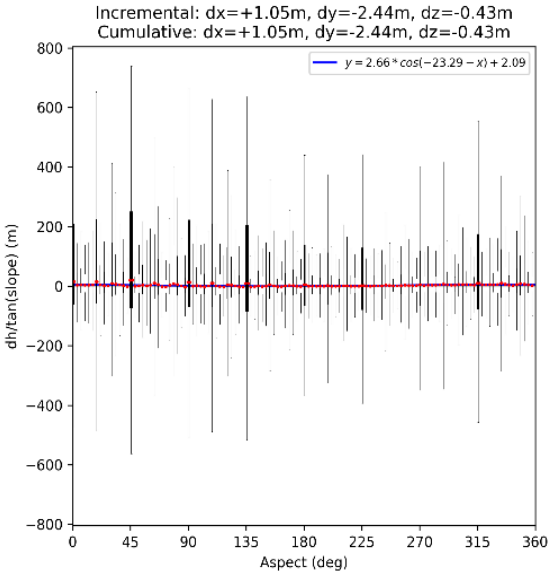

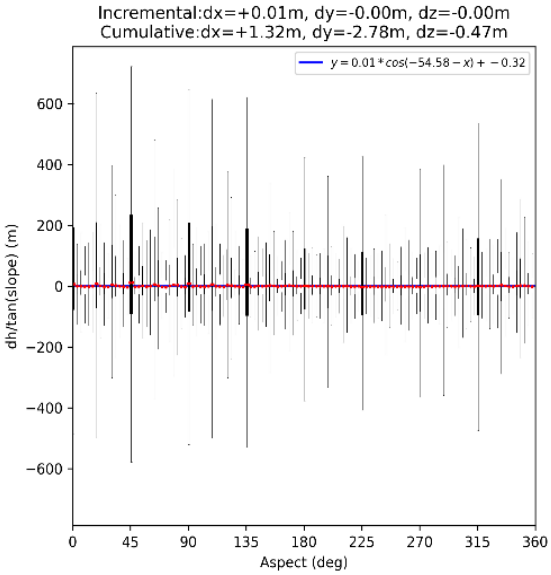

H) 1987 Area

GIMP to ArcticDEM

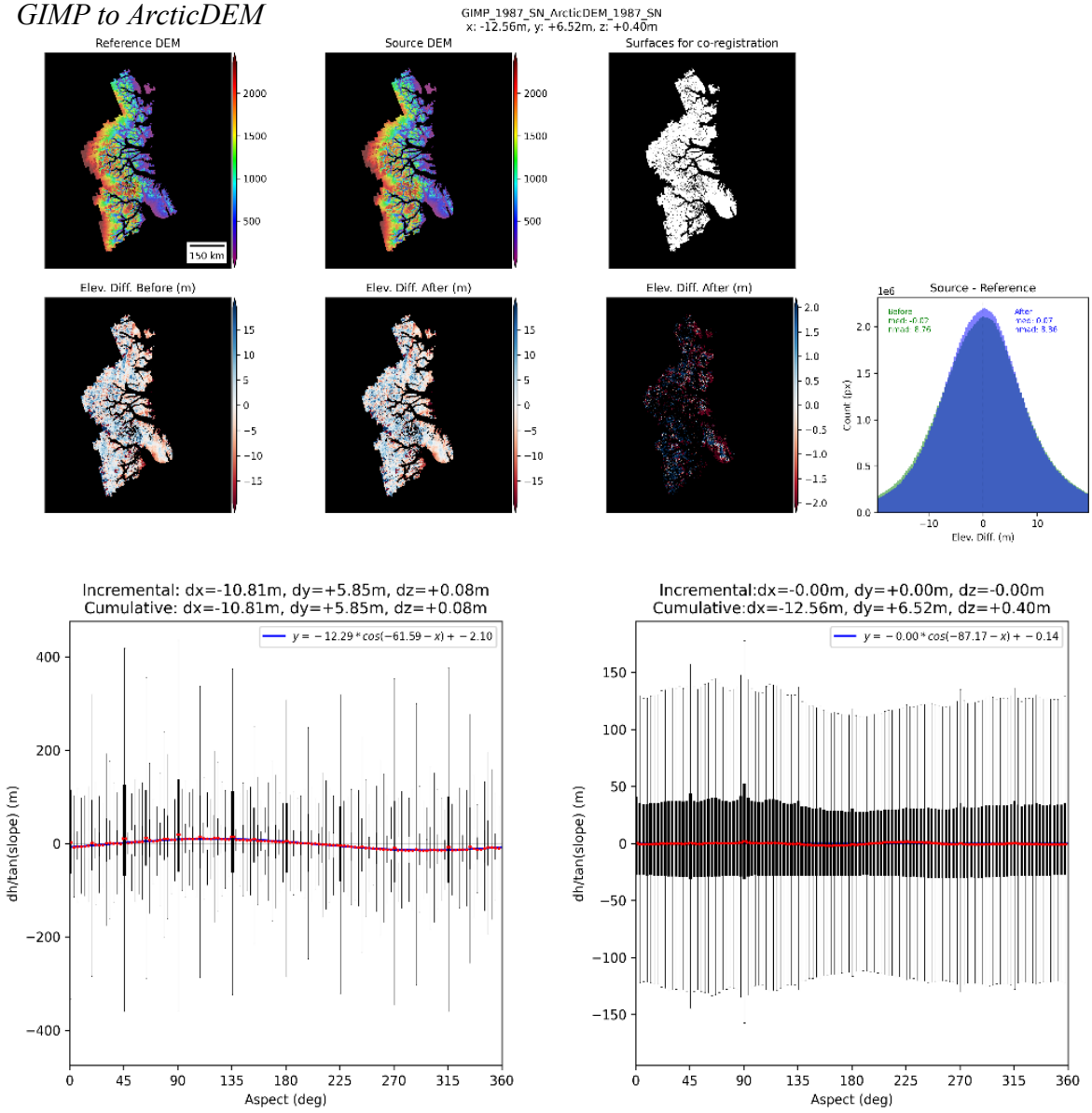

Figure 7.3. Co-registration results including pre- and post-alignment graphs and statistics of elevation differences over static surfaces as output from the DEM co-registration scripts of David Shean (Shean et al., 2016). Panels A – G are labelled as to the region and DEMs being coregistered.